The Dissertation Committee for Şeyma Keskin
Certifies that this is the approved version of the following dissertation:

Conducting Metallopolymers with Tridentate Ligands and Coordination Chemistry with Corresponding Model Compounds

APPROVED BY
SUPERVISING COMMITTEE:

Supervisor:

Richard A. Jones

Eric V. Anslyn

Ananth Dodabalapur

Emily Que

Conducting Metallopolymers with Tridentate Ligands and Coordination Chemistry with Corresponding Model Compounds

by

Şeyma Keskin

Dissertation

Presented to the Faculty of the Graduate School of

The University of Texas at Austin

in Partial Fulfillment

of the Requirements

for the Degree of

Doctor of Philosophy

The University of Texas at Austin

May 2018

Dedication

To my son,

for accompanying me during the first nine months of his life in a chemistry laboratory.

Acknowledgements

I would like to express my sincere gratitude and appreciation to my supervisor Professor Richard A. Jones for his knowledge, help, support and guidance. In addition, I am deeply grateful to my committee: Professor Eric V. Anslyn, Professor Ananth Dodabalapur and Professor Emily Que for their time, help and support. Lastly, I greatly appreciate Professor Alan H. Cowley for his valuable corrections in my manuscripts and I would like to thank Professor Jennifer S. Brodbelt and Associate Dean of Graduate Studies Professor Dean P. Neikirk for their help and guidance.

I would like to thank my co-workers for their help in my measurements: Michelle L. Mejia, Julie M. Wilkerson and Lauren Avery Mitchell for diffracting my crystals and solving my crystal structures, Travis W. Hesterberg for XPS measurements, Dr. XunJin Zhu for his contribution in chapter four, Sarah Stranahan (Willets research group) for Raman spectroscopy measurements, Lauren J. De Pue (Jones research group) for teaching me how to use ATR-IR instrument and regenerating the glove box catalyst, Jeff McCarty (Jones research group) for teaching me the Casa-XPS peak extrapolating technique, Drew Lewis for orbital composition calculations and Nicholas Delone (Stevenson research group) for specular reflectance IR measurements.

I would like to thank my dear parents, my husband, my siblings and my son for their never-ending love, support, patience, understanding, and more importantly for their prayers. This work would not be possible without my family's support.

Abstract

Conducting Metallopolymers with Tridentate Ligands and Coordination Chemistry with Corresponding Model Compounds

Şeyma Keskin, Ph.D.

The University of Texas at Austin, 2018

Supervisor: Richard A. Jones

Conducting polymers that contain metals are remarkable materials, because they have the properties of both organic backbones and metals. Depending on the position of the metal relative to the conjugated backbone, i.e. attached to or directly in the backbone, these two can couple resulting in advancement of the functionality and therefore potential applications of these types of materials. Complexes of tridentate ligands with donor atoms such as phosphorus, nitrogen, and sulfur also have a wide variety of applications. In addition, complexes of tridentate ligands have advantages of stability and control of electron density by variation of donor atoms. Therefore, conjugated polymers with tridentate ligand units will have promise for various applications and advantages in their designs.

Many types of PNP ligands have been studied in the literature because the hemilabile property of the nitrogen atom promotes some catalytic reactions and gives different coordination geometries. Complexes of a PNP ligand with molybdenum and

carbonyl ancillary ligands were synthesized and characterized. Isomerization and conversion reactions between them were investigated as well as the coordination modes.

Conducting polymers can be used as redox-active ligands and they can be used to control electron density on the metal attached to them. Synthesis and characterization of a novel polymerizable ligand 3,5-bis-EDOT-N,N-bis[2-diphenylphosphinoethyl]aniline was achieved. Related molybdenum complexes with ancillary ligands as carbonyls were also synthesized and characterized. Monomer complexes and the free ligand were electropolymerized and studied.

Tris(bipyridine)ruthenium(II) chloride and analogous complexes have been studied extensively in the literature due to their luminescent and photochemical properties, and excited state lifetimes. Conducting polymers with similar ruthenium groups have been investigated for various applications. Synthesis of ruthenium complexes with 2,6-Bis[4-[2-(3,4-diethylenedioxy)thiophene]pyrazol-1-yl]pyridine and four different bidentate ligands were reproduced; electropolymerizations of the complexes were achieved; electrochemical, UV-Vis and luminescence studies were performed and discussed.

Various complexes of copper, silver, platinum, and palladium with nitrogen and phosphorus donors have been reported for their luminescence behavior as well as their interesting structures. Model complexes of these metals with a PNP ligand have been synthesized and characterized. Absorption and luminescence behaviors as well as the coordination modes were investigated.

Table of Contents

List of Tables

List of Figures

List of Schemes

Chapter 1: An Introduction to Conducting Metallopolymers for Device Applications

CONDUCTING METALLOPOLYMERS

The discovery of conducting polymers dates back to the 1970s. The intrinsically insulating organic polymer polyacetylene was reported to be conducting upon oxidation with chlorine, bromine, or iodine in 1977 by Shirakawa *et al.*[1, 2] The discovery and development of conductive polymers was a major breakthrough, resulting in the awarding of the 2000 Nobel Prize in Chemistry to Alan J. Heeger, Alan G. MacDiarmid, and Hideki Shirakawa. Since then, tremendous progress has been made in developing functional organic materials that conduct electricity.

Systems that are highly conjugated through π electrons are essential to conducting polymers. Polymers are intrinsically insulating, and the electrons in these delocalized orbitals have high mobility only when the material is "doped" through reaction with either oxidizing or reducing agents. Although the process is a redox reaction, it is often referred to as “doping” by analogy with inorganic semiconductors. Adding electrons to the π system or removing them is relatively easy. Chemical or electrochemical doping produces charged species within the polymer backbone. The mobility of these charges defines the bulk conductivity of a given material. Oxidation removes some of these delocalized electrons and results in p-type doping. The radical cation formed is charge neutralized by the reduced form of the oxidizing agent. Thus, the conjugated p-orbitals form a one-dimensional electronic band, and the electrons within this band become mobile when it is partially emptied. On the other hand, n-type doping is achieved by treating the neutral polymer with a reducing agent. Common π-conjugated polymers are presented in **Figure 1**.

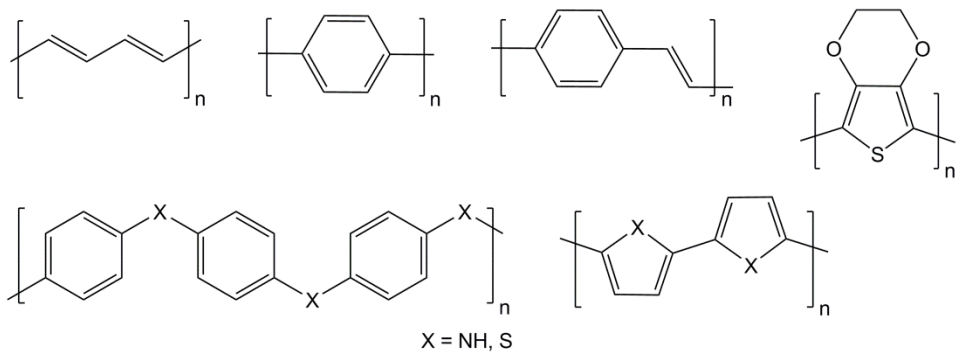

Figure 1. Structures of some conducting polymers. From top left clockwise: polyacetylene, poly(p-phenylene), polyphenylene vinylene, poly(3,4-ethylenedioxythiophene), polypyrrole (X = NH) and polythiophene (X = S), polyaniline (X = NH/N) and polyphenylene sulfide (X = S).

Incorporating transition metals either attached to or directly in a π-conjugated polymer backbone has the potential to greatly increase the function and applications of conducting polymer systems.[3] Conducting metallopolymers are of particular interest since they allow scientists to exploit properties of both metal complexes and organic polymers. Polymer films that can be deposited on specific surfaces are suitable for applications such as chemical sensors, electroluminescent devices, electrocatalysis, batteries, and memory devices.[3,4]

Metals can be incorporated into conducting polymer systems in a variety of different architectures. Wolf has classified conducting metallopolymers into three groups according to the location of the metal relative to the polymer backbone.[5] For all types of conducting metallopolymers, metals can bind to the organic backbone by coordinating to ligand sites or by covalent bonding. Type I are the polymers that have a metal tethered to the backbone by a link such as an alkyl group. Since the metal is not in electronic communication with the backbone, properties of the metal group are similar to those of the untethered complex. In type II conducting metallopolymers, metal complexes are next to the polymer backbone. Therefore, it is possible to have an electronic

interaction/coupling between the metal and the backbone. Type III conducting metallopolymers are obtained when the metal located directly in the conjugated backbone (**Figure 2**) and metal centers are part of the polymer backbone. Therefore, there is a strong electronic interaction between the metal centers and the polymer backbone.

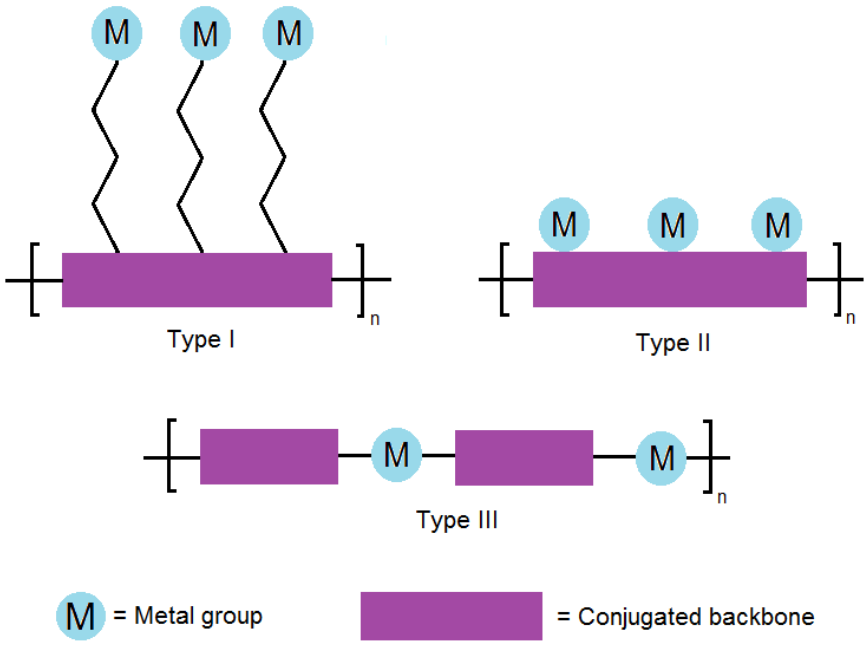

Figure 2. Classification of metal incorporation into conducting polymers. Illustration adapted from reference [5].

Examples of Wolf Type I-III conducting metallopolymers from the literature are presented in **Figure 3** for polymer light-emitting diode and photodetector applications. In the first example, Balamurugan *et al*. prepared a Type I Wolf conducting metallopolymer that contained a terbiyumiridium complex. They reported that the carboxylic functionalized polymeric material with incorporated Tb^{3+}-diketonate complexes showed bright sky-blue emission.[6] Zhang *et al*. synthesized a Type II Wolf conducting metallopolymer that has electrophosphorescent conjugated polyfluorenes (PFOPPyIr)

based on (4,4'-dibromophenylpyridinato-*N*,*C*2)bis(2-phenylpyridinato-*N*,*C*2)iridium(III).[7] They reported a luminance efficiency of 3.80 cd/A and a luminance of 1248 cd/m^2. In the third example, an alternating layer-by-layer deposition of a conducting polymer that has ruthenium and SPAN (SPAN structure is illustrated in the figure below) has been made to create a photodetector. This particular example belongs to the Type III Wolf conducting metallopolymer. Functioning devices have exhibited short circuit currents and open circuit voltages in the 8.9–15.0 μA/cm^2 and 0.76–0.84 V ranges, under simulated solar illumination.[8]

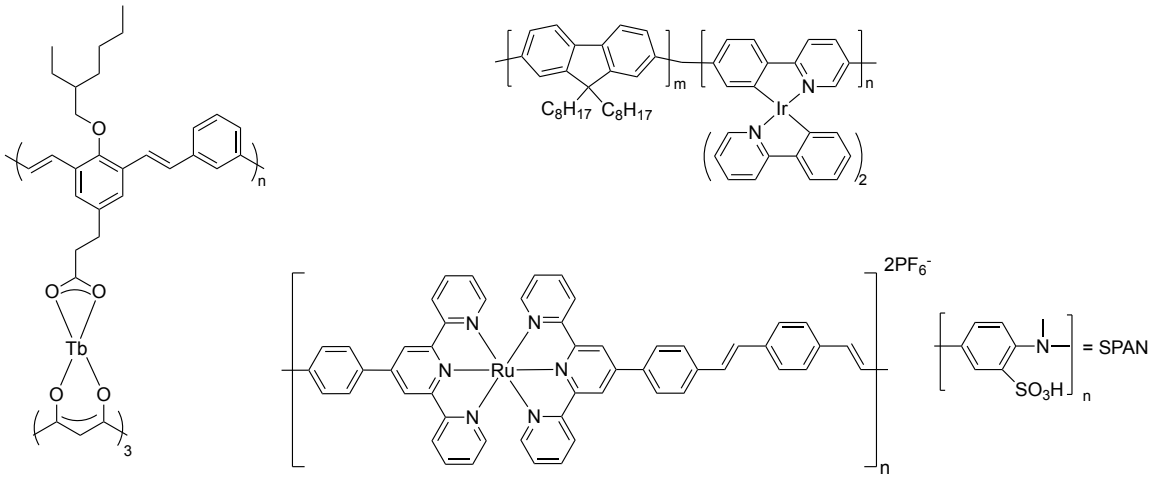

Figure 3. Examples of the Wolf Type I-III conducting metallopolymer systems reported in the literature.[6-8] Top left is a Wolf Type I, top right is a Wolf Type II, bottom is a Wolf Type III conducting metallopolymer.

Conducting metallopolymers can be synthesized via chemical coupling polymerization, electropolymerization, coordination polymerization or polymer metalation (**Figure 4**).[9] In the chemical coupling polymerization, a monomer that is a metal complex with an aromatic system is chemically reacted to other aromatic moieties by coupling reactions such as Stille or Suzuki couplings. In the electropolymerization, an

external polential is applied to the solution containing monomers that are metal comlexes. This technique is particularly convenient for bithiophene (BT) or 3,4-ethylenedioxythiophene (EDOT) groups and preferred, since there is no need to purify the polymer formed at the anode and there are no byproducts. Furthermore, the thickness of the film can be controlled by varying either the potential or the current during the electropolymerization process. An applied potential electrochemically oxidizes thiophene sites and forms radical cations, which couple to form a dication dimer that subsequently becomes a neutral dimer through the loss of two protons. This process continues until a polymer is deposited at the anode (coupling of thiophenes are represented for simplicity in **Figure 5**).[10] After polymerization, abstracting electrons from the polymer backbone by electrochemical techniques results in a p-doped (or positively charged) semiconductor. The third method of conducting metallopolymer synthesis is carried out via coordination polymerization in which the ligands that have at least two coordination sites have been used to metallate. The last method of conducting metallopolymer synthesis is the polymer metalation. In this method, the polymer is synthesized first and then the ligand sites in the polymer are metallated. The drawback of this method is that the metalation process may not complete.

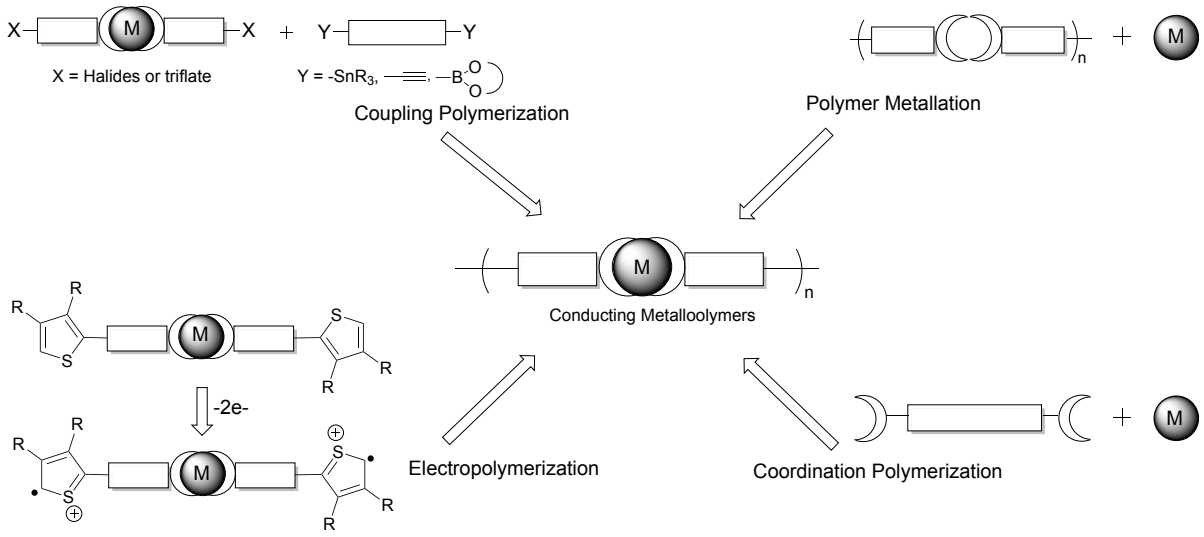

Figure 4. Methods of synthesizing conducting metallopolymers. Illustration is adapted from reference [9]

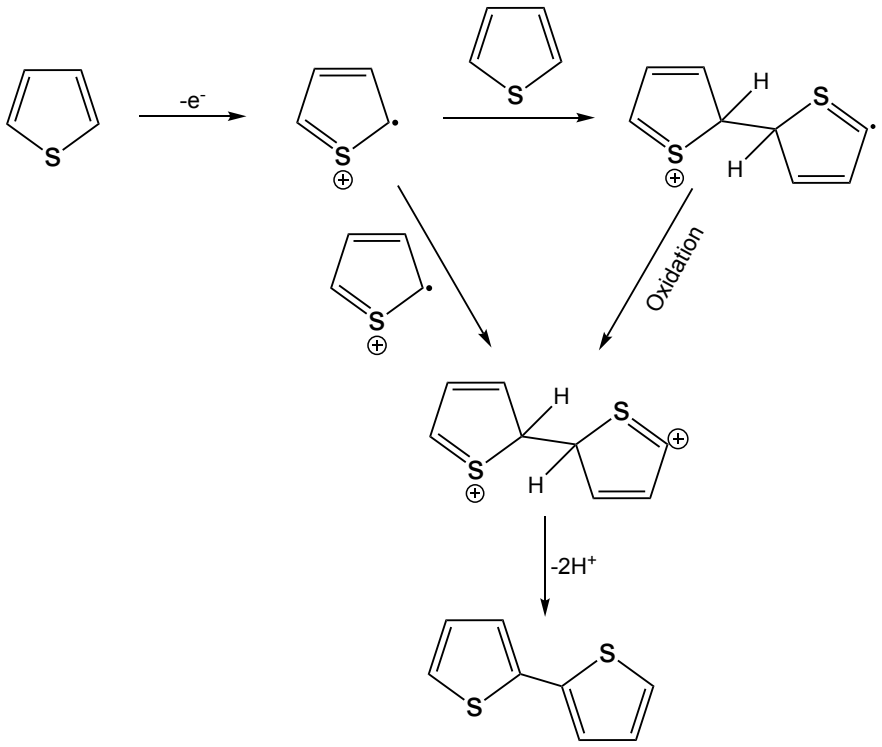

Figure 5. Initial steps in the electropolymerization of thiophenes.

Two different redox conductivity mechanisms are observed in conducting metallopolymers: outer and inner sphere electron transfer mechanisms.[3] In the outer sphere mechanism, metal orbitals do not mix. On the contrary, in the inner sphere mechanism, two metal centers communicate by orbital overlap via a mutually bridging ligand. The rate of electron transfer by this mechanism depends on the nature of the bridging ligand and its orbital overlap with the two metal centers. In the outer sphere arrangement, there are redox-active metal centers or complexes that have no direct interaction with the delocalized orbitals of the conducting organic polymer backbone and they can still provide important charge transfer mechanisms. Inner sphere architectures involve transition metal centers with strong coupling between the metal orbitals and the polymer strand. Additional charge transport pathways can be achieved when the energies of the orbitals are equivalent (same redox potential or redox matched) provided by strong coupling between the metal and the polymer. Highly conductive materials can therefore be obtained.

DEVICE APPLICATIONS

Conductivity is not the only interesting property in these materials. Electrochromism, electroluminescence, and high charge-carrier mobilities are some of the other useful properties of conducting metallopolymers.[11] These materials could therefore be used in energy harvesting devices such as solar cells or polymer-based light emitting devices. Properties of light-absorbing or emitting metal groups and high charge-carrier mobilities of the conjugated material may be combined, possibly resulting in enhanced device performance.[12] Consequently, the photophysics, specifically the singlet and triplet excited states of these materials, are of particular interest.

Many transition metal complexes have strong UV-Vis absorptions in charge transfer character such as, metal to ligand charge transfer (MLCT) or ligand to metal charge transfer (LMCT) that result in colorful emissions. When those metal complexes are incorporated in a π-conjugated system that has an efficient charge transfer, applications of these materials in photo electronic devices becomes very promising. Before designing such systems, one should know the luminescent properties of metal complexes and requirements for materials applications.

Luminescence

Luminescence is a generic name for the emission of light from a substance whose electrons have been excited. It is a cold-body radiation and different from incandescence, which is the emission of light by a substance as a result of heating. Types of luminescence are named according to how the phenomenon is generated. For example, electroluminescence is the emission of light as a result of the flow of an electric current through a substance; photoluminescence occurs as a result of the excitation of an electron by irradiation of light; piezoluminescence is produced by the action of pressure on certain solids, etc.

Although there are various methods to induce excitation and subsequent emission, and therefore corresponding prefixes are used for luminescencewhich is the generic term, it is sometimes used instead of photoluminescence. There are two forms of luminescence, which are fluorescence and phosphorescence. They differ both in spin state of the excited state from which the emission occurs and in luminescence lifetime. Fluorescence is a radiative relaxation of an electron from the singlet excited state to the singlet ground state and occurs in nanoseconds, but phosphorescence is a radiative relaxation from a triplet

excited state to a singlet ground state, with a lifetime in microseconds. Because spin is not conserved in phosphorescence, it is a spin-forbidden transition, and relaxation takes longer than in fluorescence.

A Jablonski diagram summarizing the photophysical processes that an electron can undergo is illustrated in **Figure 6**.[13] Each column represents a specific spin multiplicity for a particular species. Within each column, horizontal lines represent the limits of electronic energy states (S_0, S_1, S_2…). Within each electronic energy state, there are multiple vibronic energy states. Each of these vibrational energy states can be subdivided even further into rotational energy levels, but that level of detail has been omitted. As electronic energy states increase, the difference in energy decreases, eventually becoming a continuum.

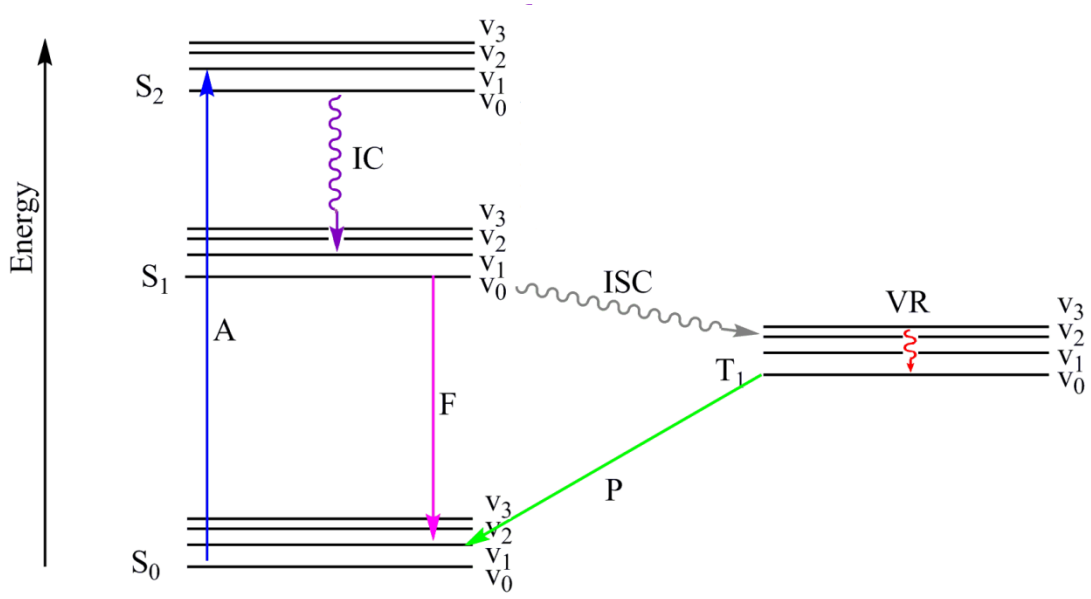

Figure 6. Jablonski diagram showing the photophysical processes in a molecule. Diagram is adapted from reference [13].

The first transition is the absorption (A) of a photon. During absorption, the energy of the photon is transferred to a particular electron, resulting in the excitation of the electron to a higher energy level. The difference of energy levels corresponds to the energy of the photon and therefore to the wavelength of the light absorbed. Absorption generally occurs in ~ 10^{-15} seconds from the ground state since, as statistical mechanical calculations have shown, most electrons occupy the ground state at reasonable temperatures.

Once an electron is excited, there are different ways for it to return from the unstable excited state to the ground state.[13] Return processes can be referred to as relaxation, decay, or deactivation. If the relaxation is in the form of a photon -in other words, if a photon is released- then it is called emission or radiative relaxation, which can either be fluorescence (F) or phosphorescence (P), as described above. According to Kasha's rule, photon emission occurs in significant yield only from the lowest excited state of a given multiplicity.[14] So, an excited electron in a higher state relaxes to the first excited state before emitting light; even within the same excited state, the electron relaxes from the higher vibrational states to the ground vibrational state of an electronically excited state. Consequently, the emitted light has a lower energy than that of the absorbed light, and the emission wavelength is longer than the excitation wavelength. The difference between the positions of absorption and emission maxima is known as the Stokes shift.

Nonradiative decays happen through different mechanisms. Relaxation of an electron from the excited state to its lowest vibrational level is called vibrational relaxation, labeled VR in the diagram. In this process, energy dissipates from the molecule to its surroundings; therefore, it does not occur in isolated molecules. A second type of nonradiative decay is internal conversion (IC), which occurs when an electron in

the ground vibrational state of an electronically excited state passes into a high vibrational state of a lower electronic state without changing its spin. The third nonradiative process is called intersystem crossing (ISC), which occurs when an electron in the ground vibrational state of an electronically excited state passes into a high vibrational state of a lower electronic state in a different spin state. Intersystem crossing is most commonly observed in molecules with large spin-orbit coupling. This type of nonradiative transition leads to phosphorescence if the relaxation from T_1 to S_0 is radiative. The presence of a heavy metal atom that especially facilitates high spin orbit coupling, phosphorescence is observed.

There are four types of electronic transitions in transition metal complexes. For all of these transitions, if the spin is conserved during emission, it is a fluorescence emission; if the spin changes, then the emission becomes phosphorescence (**Figure 7**).[15]

a) dd states (metal-centered (MC) transition): Metal d orbitals are split upon ligand coordination. Promotion of an electron within d orbitals results in excited dd states.

b) dπ* states (metal-to-ligand charge transfer (MLCT)): This transition is observed when an electron is promoted from a metal-centered d orbital to a ligand-centered π* antibonding orbital.

c) π, π* or n, π* states (intraligand (IL) transition): In this type of transition, an electron is promoted from a bonding π or a nonbonding n orbital to an antibonding π* orbital. All are ligand-based orbitals.

d) πd states (ligand-to-metal charge transfer (LMCT)): This transition involves transfer of an electron from the ligand-based π orbital to a metal-based d orbital.

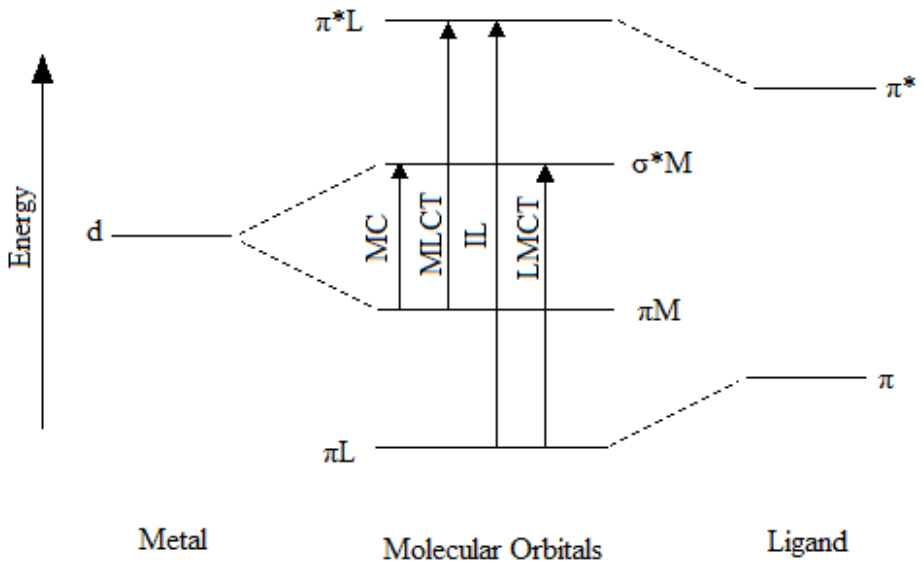

Figure 7. Electronic transitions in transition metal complexes.

The ordering of these four states depends on the metal, ligands, and geometry of the complex and can therefore be changed.[16] By a careful design of new complexes, the identity of the emitting state is predetermined for material applications, especially in organic light emitting diodes, cell imaging, and photocatalysis.[16,17]

Organic Light-Emitting Diodes (OLED)

After the first practical visible-spectrum LED (light-emitting diode) had been developed in 1962 by Nick Holonyak Jr. of General Electric, the first commercial LEDs were commonly used as replacements for incandescent and neon indicator lamps, and in seven-segment displays.[18] The commercial potential of OLEDs, in which the emissive electroluminescent layer is an organic-compound film that emits light in response to an electric current, was realized in 1987, when it was reported by Tang and VanSlyke of Kodak.[19]

OLEDs have many advantages over the silicon-based or inorganic technology both in solid state lighting and in displays. OLEDs illuminate a large area, since they constitute a surface light source. However, incandescent light bulbs and inorganic LEDs are point sources and illuminate small areas. Unlike in incandescent light bulbs, heat generation in OLEDs is minimal, making them energy efficient. The organic layers of an OLED are thinner, lighter, and more flexible than the crystalline layers in an LED or LCD (liquid crystalline display). OLEDs can be fabricated on flexible surfaces such as plastic, fabric, or clothing as well as on glass. Having flexible substrates, creates possibility of new applications, such as roll-up displays.[20] OLEDs generate light themselves, obviating the need for backlighting. For this reason, they consume much less power than LCDs. Reducing power consumption is especially important in battery operated devices, such as cell phones. OLEDs can easily be produced in large thin films. Growing sufficient quantities of liquid crystals to make LCDs is difficult by comparison. For providing large viewing angle (about 170 degrees), brighter colors with higher contrast ratios, and faster response time and higher refresh rates, OLEDs are considered aesthetically superior to standard LCDs.

Although OLEDs have so many advantages over the silicon-based or inorganic technology, they do have some drawbacks, the most important one being a limited lifetime. Blue organics have considerably shorter lifetimes than red and green ones. This difference creates another problem, which is color balancing. Materials that produce blue light degrade more rapidly than the materials that produce green and red. Therefore, the color output of blue decreases, causing a change in the color balance of the display, which is more noticeable than a decrease in overall luminance. Efficiency of blue OLEDs are also low, reported as around 4 to 6%.[21] Cost is another drawback, as manufacturing processes are still expensive. Lastly, OLED displays are susceptible to water damage.

In a typical OLED device, thin organic films consisting of an electron-transport layer, an emissive layer, and a hole-transport layer are situated in between the anode, which is generally made up of transparent ITO (indium tin oxide)and the metallic cathode which uses a low work-function metal, such as magnesium, calcium, aluminum or lithium – aluminum (**Figure 8**).[15] During operation, the anode is positive with respect to the cathode. Under an applied electric field, electrons from the cathode are injected into the LUMO (lowest unoccupied molecular orbital) of the electron-transport layer, and electrons are withdrawn from the anode; in other words, holes from the anode are injected into the HOMO (highest occupied molecular orbital) of the hole-transport layer. Carriers are made to drift and approach each other by electrostatic forces. They finally meet in the emissive layer to form the exciton which is the bound state of an electron and a hole. Both charges may arrive on a single molecule, or two molecules may form excited states. The radiative decay of this excited state results in the emission of light. The frequency of this radiation depends on the energy difference between the HOMO and LUMO levels of the emissive material.

Theoretically, an OLED can function by having only an emissive layer between the electrodes.[22] In order to work efficiently by this configuration, the emissive layer should have a high quantum yield as well as assist in the injection and transportation of charges. Fulfilling all of these requirements with a single material is difficult. Thus, single-layer OLEDs have poor efficiency and brightness.[23] OLEDs with a multilayer configuration, in which each layer fulfills a purpose, significantly improves the performance.[24]

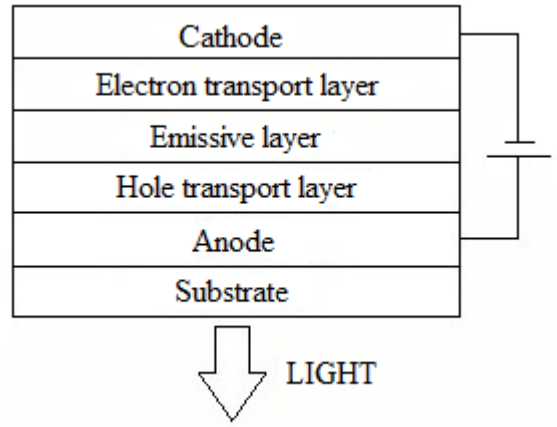

Figure 8. Set up of a typical OLED. Illustration is adapted from reference [14].

The electron-transport layer (ETL) in OLEDs is used to remove electrons from the metal cathode and transport them. In addition, it plays a role in blocking holes. To serve as an efficient hole blocker, the material should have a wide band-gap energy with high ionization potential.[25] Furthermore, the cathodic reduction processes of ETL should be reversible to form stable radical anions.[26] The ability to form homogeneous thin films with morphological and thermal stability is the other requirement for ETL materials. ETL materials contain electron-withdrawing groups on the molecule. Heteroaromatic rings such as pyridine, triazine, 1,3,4-oxadiazole and benzothiadiazole are some examples of ETL materials.[25] Current examples include electron-withdrawing groups at the o-, m-, or p-positions of a centraltriphenylbenzene core, or at the 2,4,6-positions of a triazine or triphenyltriazine core to form nonplanar molecules.[27]

The hole-transport layer facilitates hole injection and transport from the anode into the emissive layer, as well as blocking escape of electrons from the emissive layer. Typical materials for HTL have low electron affinities and ionization potentials to promote electron removal, in addition to a reversible anode oxidation that yields a stable

cationic radical.[25] The most impressive hole-transport materials are those with a truxene core consisting of three fluorenyl moieties fused together.[22]

There are two main classes of organic light emitting diodes: SMOLEDs (small-molecule based organic light-emitting diodes) and PLEDs (polymer light emitting diodes). PLEDs have advantages over the small molecule OLEDs, such as high charge carrier mobility, ease of fabrication, ability to cover a large area, and stability.[4,28]

Both singlet and triplet excitons are formed during electrical excitation. When an exciton is generated, there are four possible ways to combine the half integer spins of two charge carriers. Three of them are triplets; only one of them is a singlet state. As was mentioned in the previous section, fluorescence is the emission of light during relaxation from the singlet excited state to the singlet ground state; in other words, spin multiplicity does not change during the process. On the other hand, phosphorescence involves relaxation from the triplet excited state to the singlet ground state. The first OLED devices used fluorescent organic compounds.[15, 19] Devices using fluorescent materials benefit only from singlet excitons, so the luminescence efficiency is limited. It has been found that luminous efficiency may be improved by a factor of four if phosphorescent materials are used as emitters. Although the decay of a triplet state is forbidden by the conservation of spin symmetry, complexes containing heavy metal atoms have spin orbit coupling, which mixes the singlet and triplet excited states, and both singlet and triplet states are utilized in emission; as a result, internal quantum efficiency is increased.

Efficient phosphorescence is rare at room temperature. In addition, few materials exhibit luminescence due to the quenching of emission by surrounding molecules. To solve the problem, luminescent materials are doped into the charge transport hosts.[19] There are three mechanisms for energy transfer from the host to the dopant molecule: Förster, Dexter, and charge trapping. Förster transfer[29] is a long-range (~ 40 – 100 Å),

non-radiative, dipole-dipole coupling of donor (D) and acceptor (A) molecules. This mechanism transfers energy only to the singlet state of the acceptor molecule via:

$$^1D^* + {}^1A \rightarrow {}^1D + {}^1A^* \quad (1)$$

$$^3D^* + {}^1A \rightarrow {}^1D + {}^1A^* \quad (2)$$

Dexter transfer is a short-range process in which excitons diffuse from D to A sites via intermolecular electron exchange.[30] In contrast to Förster transfer, Dexter processes require only that the total spin of the D-A pair be conserved.

$$^1D^* + {}^1A \rightarrow {}^1D + {}^1A^* \quad (3)$$

$$^3D^* + {}^1A \rightarrow {}^1D + {}^3A^* \quad (4)$$

As a result, Dexter transfer permits both singlet-singlet and triplet-triplet transfers. Yet, due to the fact that Förster transfer is faster over long distances, it dominates singlet-singlet transfer at low acceptor concentrations. In charge trapping, the guest molecule traps the charge and generates an exciton by recombination with an opposite charge on a neighboring molecule.[31] The relative competition among these mechanisms of energy transfer depends on the lifetime of the exciton, its mobility within the film, and the thickness of the emissive film layer. For singlet–singlet modes, Förster energy transfer generally dominates, while all three mechanisms operate to some extent. Dexter and charge trapping mechanisms are the major modes for triplet exciton energy transfer, though all three energy transfer mechanisms are available.

External quantum efficiency Φ(ext) is one of the most important critical traits of OLEDs.[32] It is the ratio of the number of photons emitted through the glass substrate to the

number of injected electrons. As shown in equation 1, the Φ(ext) is the product of the OLEDs' internal quantum efficiency Φ(int) and out-coupling efficiency ξ.

$$\Phi(\text{ext}) = \xi\, \Phi(\text{int}) \qquad (1)$$

Internal quantum efficiency is the fraction of excitons that create photons. It is a maximum of 0.25 for fluorescence and 1 for phosphorescence. It can also be described as the ratio of electrons and holes injected from the electrode (electron hole balance). In standard OLED architecture, the out-coupling efficiency is approximately 20%, due to the mismatch of refractive indices between the emissive layer, HTL, indium-tin oxide (ITO) anode, and the glass substrate.[33,34]

In order to obtain novel, high-quality triplet emitters for OLED applications, requirements for emission wavelength (λem), lifetimes (τ), and quantum yields (Φ) must be fulfilled. For full color displays, efficient OLEDs emitting the three primary colors, blue (~450–470 nm), green (~500–550 nm), and red (~650–700 nm), are required. As was mentioned above, blue emitters remain more challenging due to the large energy gap required between the excited triplet and ground states to obtain this emission wavelength. Long emission lifetimes are also a problem. They severely decrease the OLED saturation threshold. If a molecule remains in the triplet state for an extended period, conversion of electrical to photon energy is limited by inhibiting the rapid repopulation of excited states. The ideal phosphorescence lifetime has been reported in the region of 5–50 μs at 298 K.[15] Internal quantum efficiency should approach unity at 298 K. This is difficult to achieve, but to obtain any advantage over fluorescence emitters, internal quantum efficiency should be at least 0.25 at 298 K. In addition, suitable triplet emitters should ideally be stable under high operating temperatures and exhibit reversible redox behavior.

Solar cells (photovoltaics)

A photovoltaic cell is a semiconductor diode that absorbs light and converts the absorbed photons to the electric current. The first photovoltaic effect was experimentally demonstrated by Edmond Becquerel in 1839.[35] Albert Einstein proposed the photoelectric effect (in 1905) for which he received the Nobel Prize in Physics in 1921. The first practical photovoltaic cell was publicly demonstrated on April 25, 1954 at Bell Laboratories.[36] Since then, the research has been focused on developing new materials for solar cell applications.

Due to the fact that petroleum based energy sources are limited and have been depleting, finding renewable energy sources have been a crucial. Primarily, silicon based technology both crystalline and amorphous forms have been improved and used since then. The use of silicon based photovoltaic cells has been limited because of high processing cost of high purity single crystal material and the lack of effective mass production techniques. Materials such as galium-arsenide, cadmium-telluride and copper-indium-diselenide have been considered to replace the silicon technology. However, those were unstable and unreliable. Alternative to the silicon and inorganic solar cell technology, organic and polymer based solar cell materials have been improved. Although the organic solar cells have not been as efficient as the silicon based technology and lifetimes of organics are short, they have many advantages over the silicon based solar cells such as easy processing, low cost, having flexible surface and large surface areas, tunable band gaps through molecular design, etc. The organic materials used in fabricating solar cells have common characteristics of having extended conjugation. Incorporating metals to the conducting polymer systems have further advantages such as facilitating the formation of triplet state excitons.[37]

Four steps are necessary in order to operate solar cells: 1) the absorption of light, generation of excitons, i.e., electron-hole pairs. 2) exciton dissociation, i.e., the separation of charge carriers of opposite types. 3) charge transport to contacts. 4) transport of electrons and holes to the electrodes or current in external circuit.[9] The band gap and charge mobility of the materials in active layers are important for the exciton generation and charge transport processes. Furthermore, the structures of organic solar cell devices affect the exciton diffusion and charge separation. The structure of devices must allow the generated excitons to reach the interface, where charge separation occurs, within this diffusion-length limit. An alternative way to reduce the recombination of the generated excitons is to facilitate the formation of triplet-state excitons, which can be achieved by the incorporation of metals.[38] Metal complexes could help increasing the efficiency of polymer solar cells by extending exciton lifetimes, reducing charge recombination and increasing free-charge-carrier separation. Furthermore, the polymer backbone and metal complexes result in the formation of donor-acceptor (D-A) polymers. Conducting metallopolymers are discovered to have low band gaps due to the orbital mixing of the donor and acceptor units.[37]

There are several types of polymer solar cell set ups. Two examples of set ups are illustrated in **Figure 9**. In the bilayer heterojunction cell, the electrons and holes are separated at the interface of the material. Therefore, electron-hole recombination is happening less than the bulk heterojunction cells. The bilayer only has one active zone, and therefore, energy conversion is low; the excitons have to diffuse to the interface and only a few of the excitons go the distance. Bulk-heterojunction cells solve this problem by having the donor and acceptor materials mixed throughout the active layer. Therefore, active zone is larger and energy conversion is better. The disadvantage of the bulk heterojunction structure is that a penetrating pathway of the hole and electron

transporting phase to the electrodes is needed for the separated charges in order to reach their corresponding electrodes.[37]

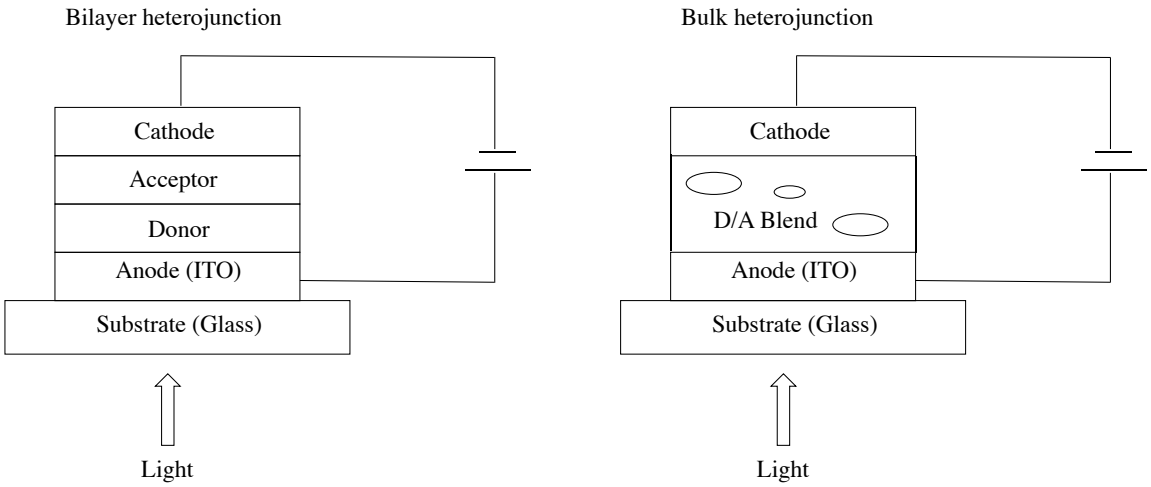

Figure 9. Examples of organic solar cell structures. Illustration is adapted from refrence [37].

Chemical structures of selected conducting metallopolymers from the literature are illustrated in **Figure 10**.[39, 40] Metallopolyyne and metalloporphyrin polymers have been extensively studied and produced promising results for polymer photovoltaic applications.[39, 40]

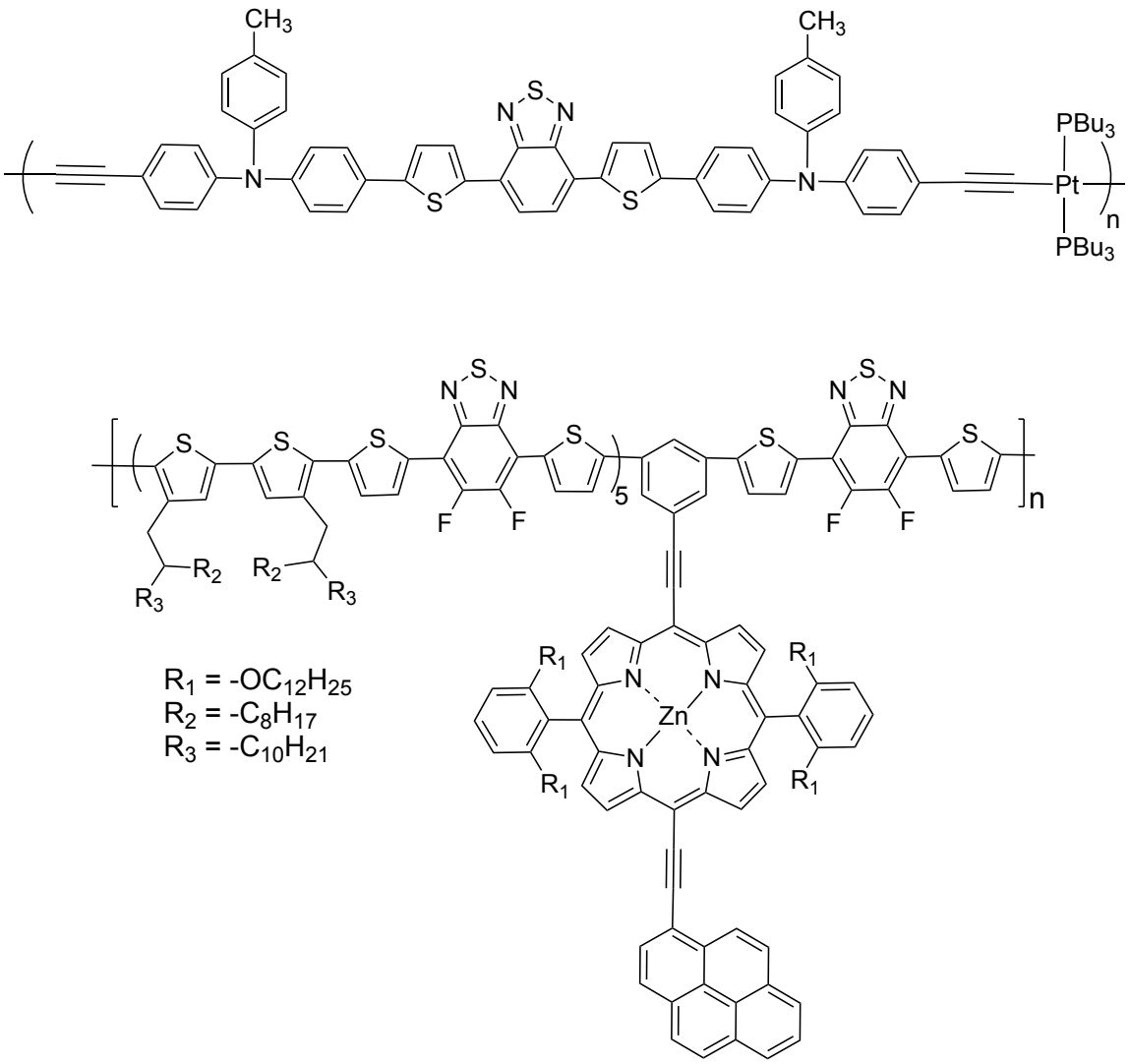

Figure 10. Examples of metallopolyyne and metalloporphyrin polymers for the photovoltaic applications reported in the literature.

Memory Devices

Conducting polymers are good candidates for memory devices or data storage applications due to the fact that they have two stable states: non-conducting or high resistance in their neutral state and conducting upon chemical or electrochemical doping.

This property can be used to store data by switching between the two states, in other words, switching between "on" (1) and "off" (2) modes. Furthermore, incorporation of metals into the conducting polymers provides further advantages in data storage devices by having redox and magnetic properties of metal centers contained in the polymer systems.

Different types of categorizations for the memory devices have been reported in the literature regarding the initiation of stimulus, maintaining of modes, and device structure, etc. Memory devices can be classified into two main groups according to how the stimulus initiated the switching: resistive memory devices and magnetic memory devices. An applied potential is needed for the resistive memory devices in order to switch between the conducting and neutral modes. Examples of the conducting metallopolymers reported in the literature for the resistive memory materials applications are presented in **Figure 11**.[41-43] The initiation of the stimulus is different in magnetic memory devices than in resistive memory devices. In the magnetic storage devices, magnetization of the material is detected and modified by a read-and-write head. The two magnetic polarities of the material represent the "on" and "off" states. Transition metals with d^4-d^7 electron configurations can exist in either low-spin or high-spin states. The electronic transition between the two states is known as the spin crossover.[44] As a result of the spin cross over, changes in the material are observed, such as change in color, or magnetic property of the material.[45] The spin cross over property can be utilized for developing memory devices, with the low-spin state representing the "0" mode and the high-spin state representing the "1" mode.

Memory devices can also be classified as volatile and non-volatile devices according to how to on/off modes are maintained. In volatile devices, in order to keep the "on" mode, the external stimulus needs be maintained. If the stimulus is not maintained,

the “on” state will relax to the “off” state. Example of this class are DRAM (dynamic random access memory) and SRAM (static random access memory). In the non-volatile memory devices, “on” mode is maintained even after the stimulus has been removed. Examples of this type of memory devices are WORM (write-one read- many-time) and flash (rewritable) memory devices.[46]

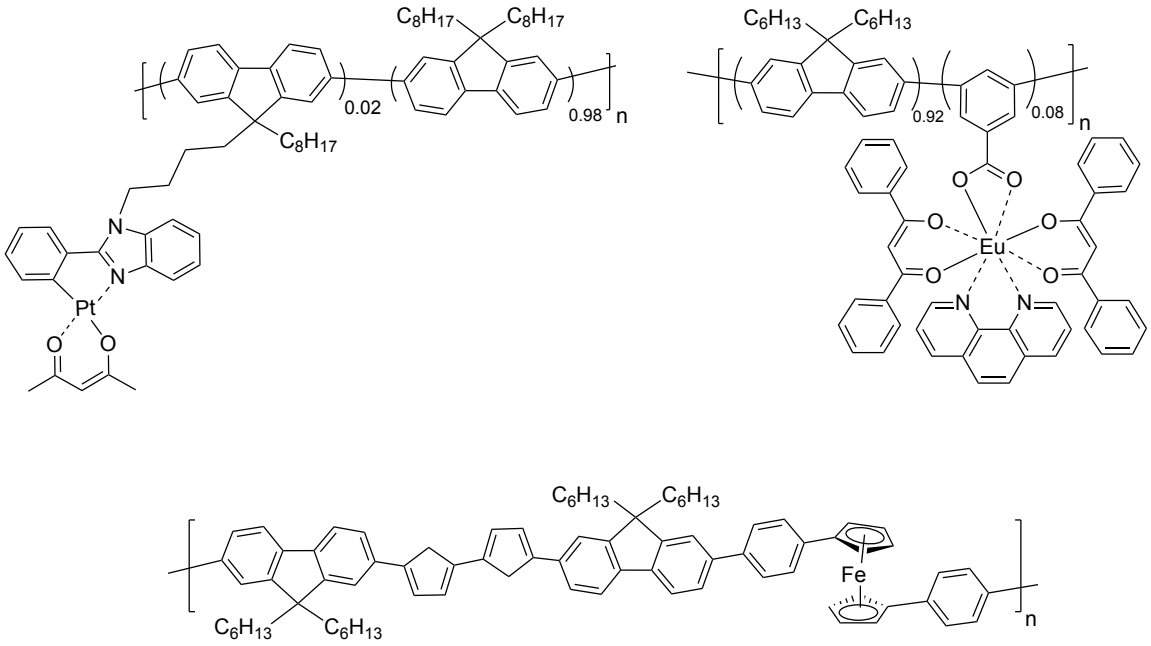

Figure 11. Examples of metallopolymers for resistive memory devices reported in the literature.[41-43]

In summary, conducting metallopolymers are promising materials to be used in memory devices for both building resistive devices and for building magnetic devices, in spite of the fact that there still remain some challenges to overcome before commercial devices can be made.

Sensors

In addition to the application in polymer based memory devices, metal complexes may be used to geometrically orient π-conjugated materials in specific three-dimensional arrangements in the solid state. Dramatic color shifts occur in response to changes in solvent, temperature, applied potential, and binding to other molecules. Both color changes and conductivity changes are induced by the same mechanism, which consists of twisting the polymer backbone and disrupting conjugation. This mutability makes conjugated polymers attractive as sensors that can provide a range of optical and electronic responses. The number of coplanar rings determines the conjugation length. The longer the conjugation length, the lower the separation between adjacent energy levels, and the longer the absorption wavelength becomes.

The binding of an analyte will affect the redox potential of coordinatively unsaturated transition metals. Therefore, overlap of the metal and the conjugated polymer will also be affected, resulting in a measurable response in conductivity. The redox potential of the metal center and the conjugated polymer can match to a greater or lesser extent depending on the binding. If the redox potential of the metal and the conjugated polymer match perfectly, the binding to the analyte will result in a poorer overlap, resulting in a very sensitive response exhibited as a severe decrease in conductivity. If the redox potential of the metal and the polymer display partial or no redox matching, then a single binding event can create a favorable redox matching that enhances local transport. The sensitivity of this case is best suited to the detection of target analytes at intermediate concentrations.[3]

Sensory systems based on conducting metallopolymers are given in the following examples. Lippard *et al*. synthesized and studied families of conducting polymers, incorporating elements from the most studied conducting polymers in conjunction with

bipyridyl or terpyridyl units for metal binding (**Figure 12:** eight polymers: CP1a, CP1b, CP1c, CP2a, CP2b, CP2c, CP3b, CP3c).[47] They observed that the emission in the materials was quenched by 75-100% in the presence of copper(II) ions. The quenching efficiency depends on the metal-ligating group and the identity of the spacer between these units. Main-chain bipyridyl binding units allow more efficient quenching than do minor side-chain terpyridyl units. Decreasing the electron-donating ability of spacers between binding units increases the quenching efficiency.

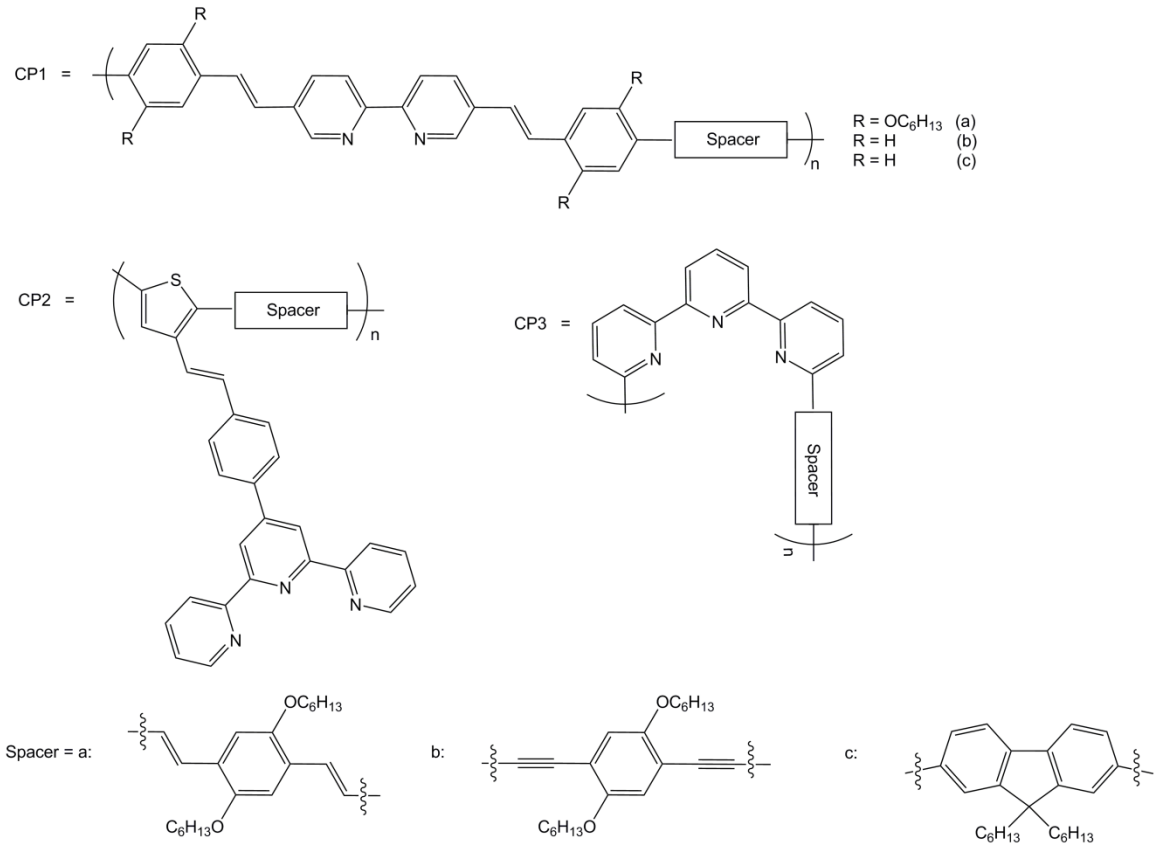

Figure 12. Series of ligand substituted conjugated polymers for nitric oxide detection.

Swager *et al*. reported an example of the sensor that is based on the polymetallorotaxane, which takes advantage of its reversible metal ion-binding rotaxane

structure (**Figure 13**).[48] The materials displayed changes in both their optical and electrical properties with metal coordination. In particular, the addition of copper or zinc ions resulted in a 34 nm red-shift in the UV-Vis spectrum from the metal-free polymer.

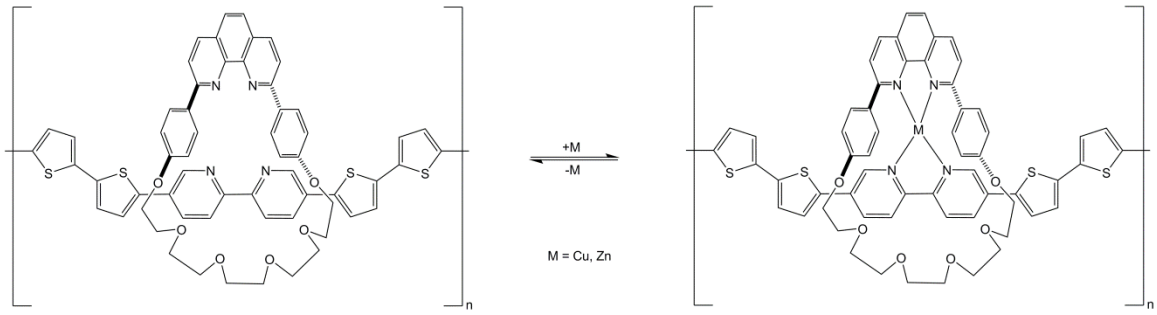

Figure 13. Reversible metal-ion binding to rotaxane structure.[48]

Swager *et al*. also reported a cobalt-based salen polymer that detects nitric oxide both in solution and in the gas phase.[49,50]

Electrocatalysis

Conducting polymers with coordinated transition metals have a potential use in catalysis: the reactivity of the catalyst can be tuned by applying a voltage, or the polymers can deliver multiple electrons to the reaction site. A recent example, a precursor to fabricate palladium nanoparticle (NP)/polymer hybrids for oxygen reduction, has been published.[51] First, an electropolymerizable palladium(II) metal complex was synthesized. Electropolymerization of the complex allowed for the palladium(II) metal centers to act as seed points for size-controlled palladium NP growth (**Figure 14**). A thin film of the polymer was exposed to a nitrogen-sparged mixture of $PdCl_2$ in water and a $Na_2CO_3/NaHCO_3$ buffer solution. Then, a nitrogen-sparged aqueous ascorbic acid solution was added to the vessel with the films and left to sit for a few minutes. The

electropolymerized films were then removed from the nanoparticle growth solution and rinsed. The palladium nanoparticle/conducting metallopolymer hybrid material demonstrated electrocatalytic behavior toward oxygen reduction, with peak current densities around 400 μA/ cm^2 in acidic aqueous conditions.[51]

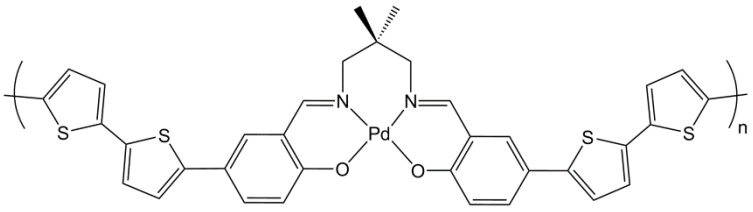

Figure 14. Palladium-containing conducting metallopolymer for electrocatalysis applications.[51]

Another example is the four-electron reduction of oxygen to water electrocatalytically. The polymer material has been shown to reduce oxygen to water efficiently (**Figure 15**). The redox matching allows the rapid delivery of electrons to the cobalt and the complete conversion of the oxygen to water. Almost no trace of hydrogen peroxide formation was detected by rotating disk voltammetry.[52]

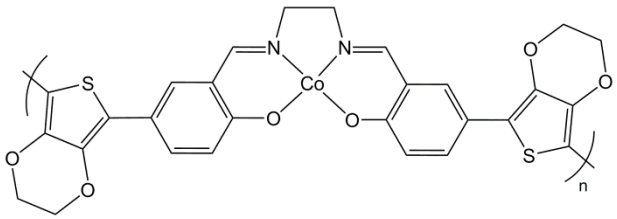

Figure 15. Cobalt-containing conducting metallopolymer for electrocatalysis applications.[52]

TRIDENTATE LIGANDS IN CONDUCTING POLYMERS

Complexes of tridentate ligands have a broad range of functionalization, which allows them to be tuned for specific application needs such as catalysis (hydroformylation, aldol condensation, reductive deamination and Heck arylation),[53,54] molecular materials (synthesis of oligomeric and polymeric coordination compounds, light-emitting diodes and solar cells),[55,56] biomimics (active sites of metalloenzymes),[57,58] and chemosensors (Hg detection)[59] (**Figure 16**). Tridentate ligands provide enhanced stability to complexes, due to the well-known chelate effect. They can be used as a redox-active component and therefore can affect the binding of ancillary ligands.[60]

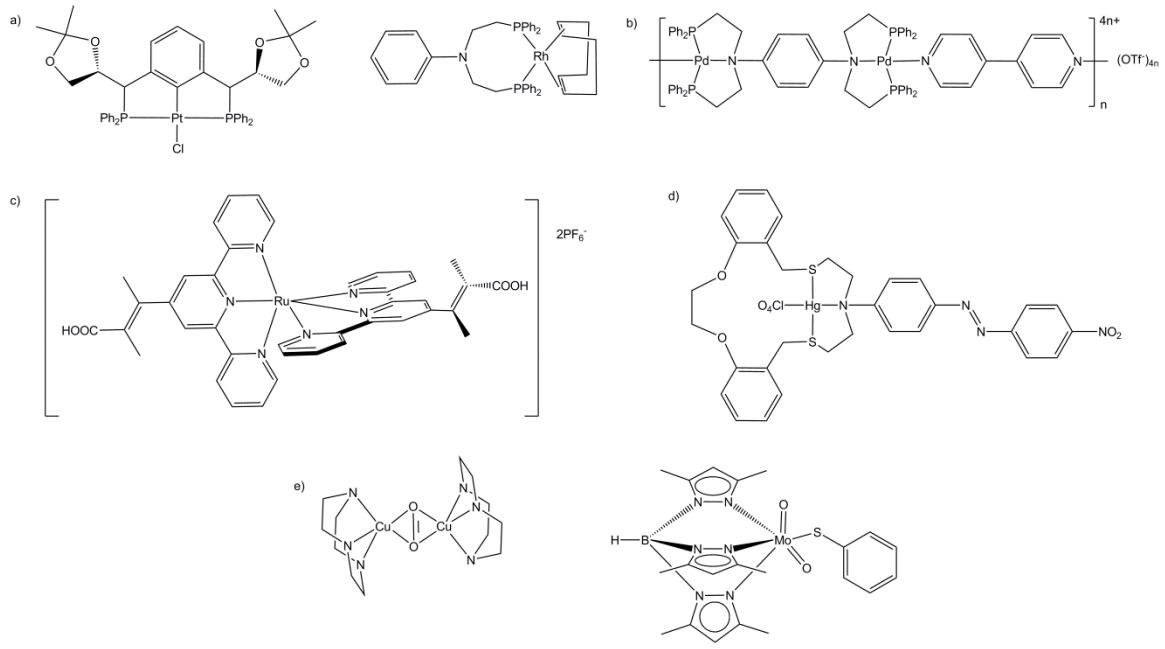

Figure 16. Examples of the applications of complexes with tridentate ligands: (a) catalysts, (b) coordination polymer, (c) solar cell material, (d) chemosensor, (e) biomimics.

These ligands can also be incorporated into polymer systems. Many types of tridentate ligands have been studied widely because the hemilabile property of the central atom

promotes some catalytic reactions and gives different coordination geometries, such as tridentate monomeric, bidentate monomeric, and bidentate dimeric modes. Binding modes can be controlled by the strength of the central donor atom by having different R groups attached.[55]

In *octahedral* complexes, tridentate ligands can occupy either two coplanar edges in a *meridional* conformation, or a face of the octahedron in the *facial* conformation. It is obvious that some ligands coordinate in only one of the two modes (*facial* or *meridional*), whereas others are flexible enough to adapt to either type of coordination. Tridentate ligands are classified into four groups (**Figure 17**)[61]: (a) crown ligands such as triazacyclononane, in which the three donor atoms are held together by a cyclic system, and which can coordinate in a *facial* mode only; (b) triskelion ligands such as tris(pyrazolyl)borate (*triskelion* from the Greek *skelos*, leg: a symbolic figure of three legs or lines that come from a common center), which have a larger flexibility than the crown ligands but cannot adapt to the *meridional* conformation because of their radial topology; (c) clamp ligands, such as terpyridines, in which the three donor atoms are forced to be nearly coplanar and adapt to only the *meridional* coordination mode, and (d) open chain ligands or ribbons, such as diethylenetriamine, that are flexible enough to adapt to either the *facial* or the *meridional* conformation. It should be noted that crown and triskelion ligands form three chelate rings upon complexation, whereas clamp and ribbon ligands form only two such rings.

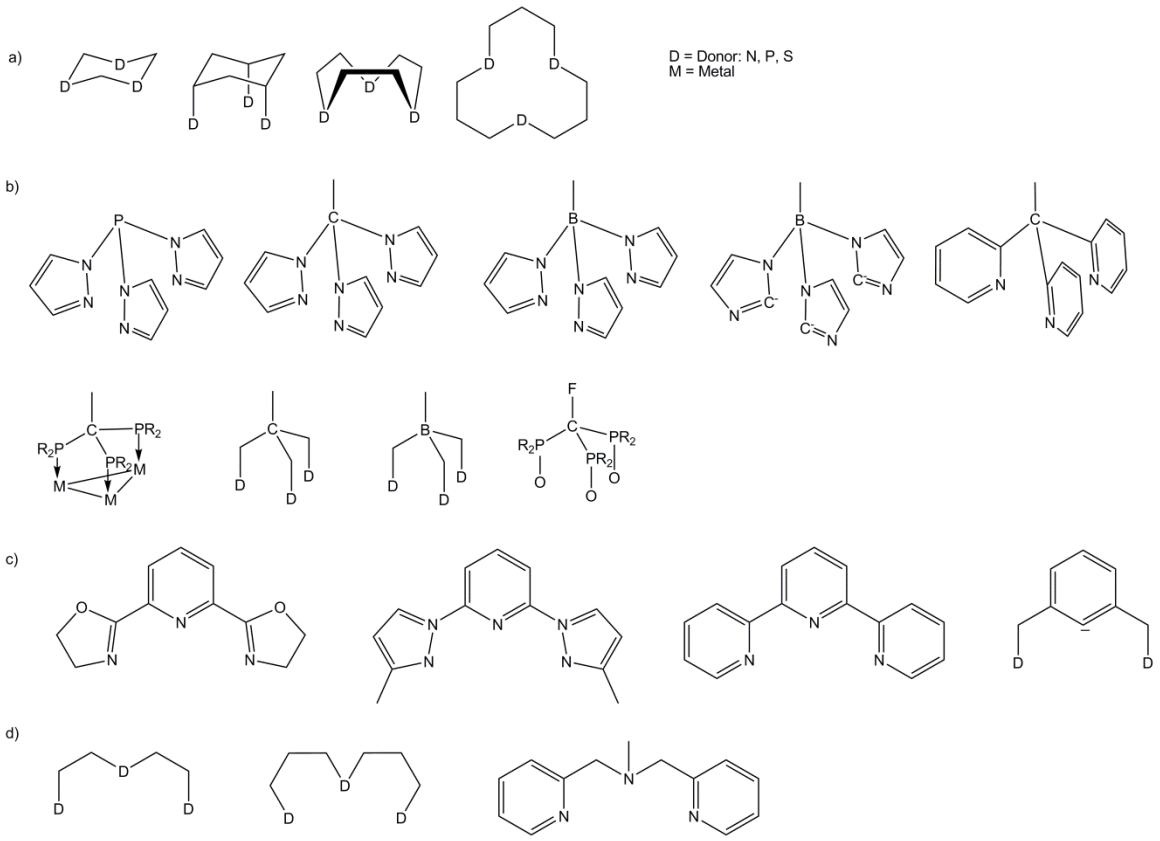

Figure 17. Classes of tridentate ligands: (a) crowns (b) triskelions (c) clamps (d) ribbons.

The triskelion ligand tris(pyrazolyl)borate (Tp) known as a "scorpionate" ligand, was first reported by DuPont chemist Swiatoslaw Trofimenko in 1966.[62] The name scorpionate comes from the fact that the ligand can bind a metal with two donor sites, like the pincers of a scorpion, and the third donor site reaches over the plane to bind to the metal. The binding can be thought of as a scorpion grabbing the metal with two pincers before stinging it. Many different scorpionate ligands with a central atom different from boron and with different donor atoms are known. An additional specific class of tridentate ligands are called pincer ligands, a type of chelating agent that binds tightly to three adjacent coplanar sites, usually on a transition metal in a *meridional*

configuration. Synthesis of pincer complexes dates back to 1970s. Shaw and Moulton reported on a pincer–nickel compound with the nickel atom held in place by a monoanionic, terdentate PCP ligand.[63] Pincer ligands generally contain an *ortho*-disubstituted, monoanionic aryl ring (or corresponding alkyl chain). They are covalently bound via a central M–C σ bond to the metal center and two *ortho* substituents, each bearing a heteroatom E providing the tridentate bonding of the pincer ligand with two E–M dative bonds.[54] Pincer ligands are a subgroup of clamp ligands. The inflexibility of the pincer-metal interaction confers high thermal stability to the resulting complexes. The structure and synthetic variability of these ligands are shown in **Figure 18**.[64]

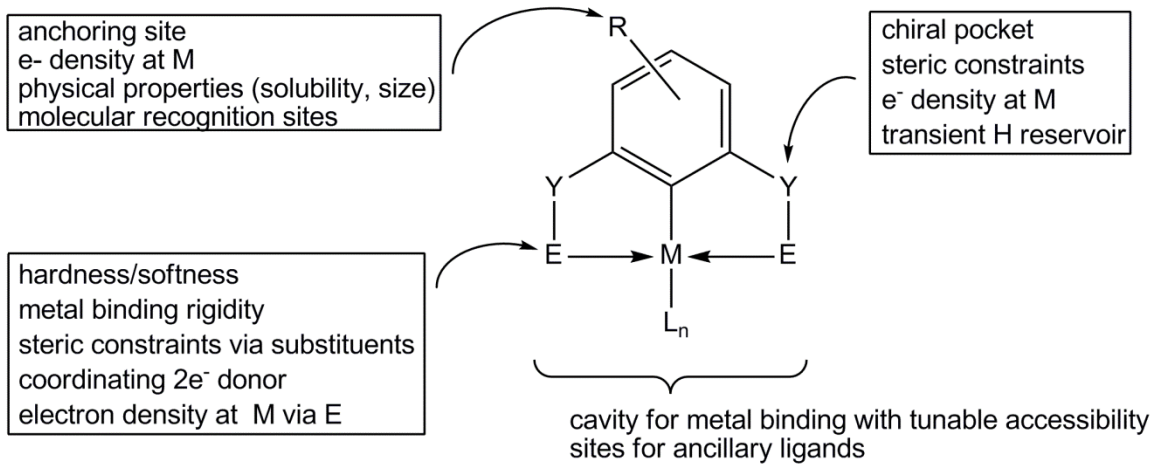

Figure 18. Structure and synthetic variability of pincer complexes. Illustration adapted from reference [64].

SCOPE OF THESIS

Several groups have reported conducting metallopolymers for various applications. For example, Wolf *et al*. coordinated transition metals to substituted thiophenes, thiophene-functionalized ferrocene and acetylides,[4, 5, 65] Swager *et al*. used bithiophene functionalized salen, crown ether, and bipyridine ligands.[48, 50, 52, 66, 67] Furthermore,

Reynolds *et al*. attached metal complexes to a polythiophene backbone.[68] A conducting polymer matrix itself can be a redox-active ligand due to available oxidation states. Transition metals also have multiple oxidation states and are therefore redox active. Electron density on the metal can be tuned by using redox-active conducting polymers as ligands. Also, electron density on the metal can be monitored by using ancillary ligands that can be detected spectroscopically, as in the examples of carbonyl, nitrosyl, and isocyanide detection in IR spectroscopy. Resulting polymer complexes are especially attractive for applications in sensing, and small-molecule storage and release.

In the present study, the design, synthesis, and characterization of novel electropolymerizable PNP ligand, which is a ribbon type tridentate ligand, and related to molybdenum complexes in two different coordination modes have been reported. Functionalization of the PNP ligand by EDOT groups allows for the electropolymerization of the complexes (Wolf type I and II). Electron-donating ether groups of EDOT act to reduce the oxidation potential of the polymer. Metallopolymers are obtained by potentiodynamic anodic polymerization. Electropolymerization is the preferred technique due to its convenience, having no byproducts and no need for purification. Moreover, film thickness can be controlled. Another designing feature is the use of a ribbon-type PNP ligand, which allows flexible coordination modes, stable complexes by chelate effect, and ancillary ligands for the metal. Carbonyls are used as ancillary ligands both because they can be monitored spectroscopically and because commercially available metal carbonyls can readily be coordinated into the ligand. furthermore, they are less expensive than nitric oxide gas for coordination.

$Ru(bpy)_3Cl_2$ has been one of the most widely studied molecules due to its unique properties, especially in luminescence emission and excited-state lifetimes.[69] There are various derivatives of $[Ru(bipy)_3]^{2+}$ in the literature for applications in biodiagnostics,

photovoltaics, and organic light-emitting diodes, but no derivative has been commercialized.[70] Ruthenium(II) complexes are incorporated into the conjugated-polymer main chain, because of their promising luminescence properties for materials applications. Ruthenium-containing conjugated polymers reported in the literature are generally based on ligands in which nitrogen is the donor such as 2,2'-bipyridine (bpy), 1,10-phenanthroline (phen), 2,2',6',2"-terpyridine (terpy) and dipyridophenazine.[71-74] In luminescent conducting metallopolymers, both the complex and the polymer can function as independent light emitters[71] and conjugated polymers enhance charge carrier mobility.[4]

In this study, 2,6-bis(pyrazol-1-yl)pyridines which is a clamp type tridentate ligand with three nitrogen donors were used. The synthesis, characterization, electrochemistry/electropolymerization, absorbance, luminescence and photophysical measurements of 2,6-bis[4-[2-(3,4-diethylenedioxy)thiophene]pyrazol-1-yl]pyridine-Ru(L')Cl complexes were reported in the present study. The ligand is functionalized by EDOT in order to be electropolymerized. Subsequently, two anionic and two neutral ruthenium(II) complexes were synthesized with the following ligands (L') = 1,1,1,5,5,5-hexafluoro-2,4-pentanedione (hfac), dibenzoylmethane (dbm), 2,2'-bipyridine (bpy), 1,10-phenanthroline (phen). Further electropolymerization of the ruthenium complexes formed polymers in which the metal group was located directly in the conjugated backbone (Wolf type III) and strong electronic interactions between the organic bridge and metal group are possible. Furthermore, the conducting metallopolymer should serve as a better charge-carrier mobility than small molecules and the presence of ruthenium should facilitate phosphoresce emission. Such polymers have potential applications in OLED and photovoltaic devices.[75]

The coordination chemistry, isomerization, and luminescence properties of model complexes with N,N-bis[2-(diphenylphosphino)ethyl]phenylamine, which is the PNP

ligand without polymerizable groups were also investigated. Molybdenum, silver, copper, platinum, and palladium complexes of the ligand were synthesized and characterized. In one part of the study, complexes of PNP with molybdenum, isomers and coordination modes were studied. In the other part of the study, PNP complexes of various metals were synthesized, characterized, and luminescence properties were investigated. Because, complexes of copper, silver, gold, platinum, and palladium with nitrogen and phosphorous donors have been reported for their luminescence behavior as well as their interesting structures.

Chapter 2: Synthesis and Characterization of Molybdenum Carbonyl Complexes with Phosphorus/Nitrogen/Phosphorus Ligand as Bidentate and Tridentate Modes[1]

INTRODUCTION

Molybdenum complexes with low oxidation states have been investigated extensively due to the role of these complexes play in the contexts of both chemical and biological nitrogen fixation.[76] Currently, more than fifty molybdenum containing enzymes known,[77, 78] and the presence of molybdenum in these is required by eukaryotes.[77] Molybdenum complexes also play important roles in organometallic chemistry. For example, molybdenum carbonyls have been used in Pauson – Khand reactions, i.e. [2+2+1] cycloaddition in which an alkene, an alkyne, and carbon monoxide combine to form a α,β-cyclopentenone. Pauson–Khand reactions are mediated both by bimetallic and monometallic transition metal complexes.[79] The coordination chemistry of molybdenum complexes has also been studied under thermal or photolytic conditions.

Many types of PNP (phosphorus/nitrogen/phosphorus) ligands have been studied widely because the hemilabile property of the nitrogen atom promotes some catalytic reactions and provides different coordination geometries, such as tridentate monomeric (PNP), bidentate monomeric (PP), and bidentate dimeric (PP) modes (**Figure 19**).[55, 80] Binding modes can be controlled by donor strength of N by having different R groups to it (**Figure 20**).[55,80]

---

[1] This chapter has been published as a journal article: Keskin, G. S.; Stanley, J. M.; Cowley, A. H. Synthesis, Characterization and Theoretical Investigations of Molybdenum Carbonyl Complexes with Phosphorus/Nitrogen/Phosphorus Ligand as Bidentate and Tridentate Modes. *Polyhedron* **2017**, *138*, 206-217.
The syntheses, purifications, characterizations were carried out by Seyma Keskin; crystals were diffracted by Michelle L. Mejia; crystal data were completed by Julie M. Stanley; the article was written by Seyma Keskin; the article was edited by Alan H. Cowley; orbital composition calculations were performed by Drew Lewis. The principal investigator at the time of the study was Bradley J. Holliday.

The tridentate PNP ligand N,N-bis[2-(diphenylphosphino)ethyl] phenylamine that is used in the present study was synthesized previously and coordinated to Mn, Co, Ni, Rh, Pd, Re and Pt[53, 80-84] metals as well as one example of a Mo complex (which has an N_2 monodentate ligand and no carbonyls).[85]

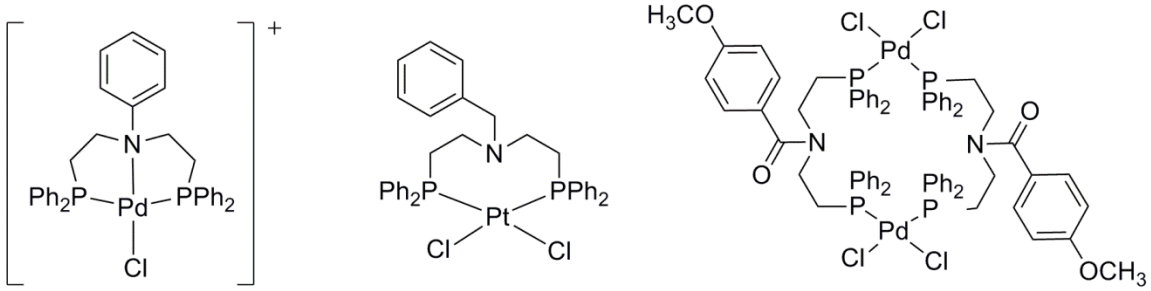

Figure 19. Possible coordination geometries of PNP ligand: PNP – monomeric, PP – monomeric, PP – dimeric. Illustration adapted from reference [55].

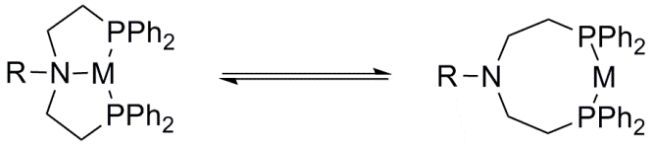

Figure 20. Coordination change by change in donor strength of hemilabile N. Illustration adapted from reference [80].

Previously, complexes of PNP ligand with molybdenum (*cis*-PNP-Mo(CO)$_4$, *facial* and *meridional* isomers of PNP-Mo(CO)$_3$) with different R groups on the nitrogen atom than our ligand were reported (**Figure 21**).[86-88] Similar crystal structures for the *cis*-PNP-Mo(CO)$_4$ and *fac*-PNP-Mo(CO)$_3$ complexes (with different R groups on the N compared with our complexes) were also shown.[88, 89] The crystal structures for the *meridional* isomer of the type PNP-Mo(CO)$_3$ have not been reported previously. Furthermore, Sicloan *et al*. reported that they could synthesize and purify the *facial*

isomer, but they were not able to isolate the *meridional* isomer.[86] The crystal structure for a *meridional* complex of Mo of the type PNP-Mo(CO)$_n$ with the PNP ligand in which N is an amine, the Mo is neutral and the monodentate ligands are all carbonyls have not been reported previously. There are examples of *meridional* complexes of Mo that have ionic Mo, or a Mo that has six monodentate ligands, or a PNP ligand that has an imine N in the literature.[90-93]

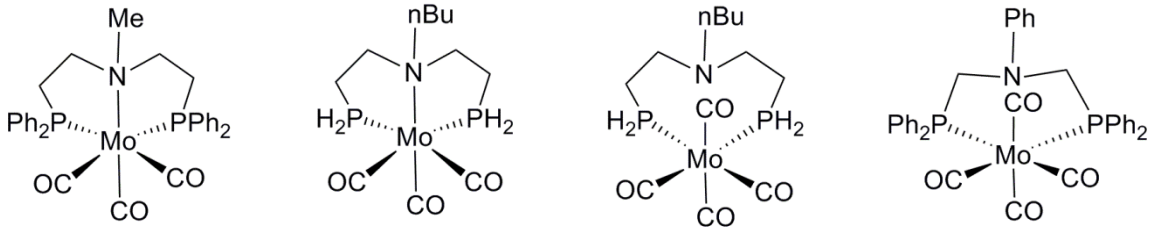

Figure 21. PNP-Mo(CO)$_n$, n = 3-4 complexes previously reported. Illustration adapted from references [86-88].

In the present study, molybdenum carbonyl complexes with an N,N-bis[2-(diphenylphosphino)ethyl]phenylamine ligand have been synthesized and fully characterized. Two isomers for the PNP-Mo(CO)$_3$, i.e. *facial* and *meridional* isomers, and one tetracarbonyl complex, *cis*-PNP-Mo(CO)$_4$, were obtained along with their crystal structures. Ligand binding modes, conversions between the three complexes and the preferred geometry of the *facial* over the *meridional* isomer were also investigated. The explanation for the preferred geometry of the *facial* isomer is based on the *trans* effect and π-back donation, Jahn–Teller effect, bond angles and bond distances. However, the choice of the *facial* or the *meridional* isomer was explained on the basis of electronics rather than sterics as in other journal articles.[76, 94, 95]

EXPERIMENTAL

Instrumentation

NMR spectra were recorded with a Varian Unity + 300 spectrometer with an Oxford Instruments Ltd. superconducting magnet, using a 5 mm auto-switchable probe ($^{1}H/^{19}F/^{13}C/^{31}P$) and a Sun Ultra 5 workstation. ^{1}H NMR signals were referenced to residual proton resonances in deuterated solvents. $^{13}C\{^{1}H\}$ NMR spectra were referenced relative to solvent peaks. $^{31}P\{^{1}H\}$ NMR spectra were referenced to a H_3PO_4 external standard. All peak positions are listed in ppm, and all coupling constants are listed in Hertz (Hz). The mass spectrometry was carried out using a Thermo Finnegan TSQ 700 spectrometer. Melting points were recorded on a Mel-Temp II melting temperature apparatus made by Laboratory Devices of Holliston, MA. Elemental analysis was performed by Quantitative Technologies Inc. (Whitehouse, NJ). Samples were freshly prepared prior to analysis.

Spectroscopy

IR spectra were recorded with a Nicolet Avatar 330 FT-IR spectrophotometer. The solid-state IR measurements were carried out using an ATR accessory. The solution IR data was recorded using DCM solutions ($\sim 10^{-2}$ M).

The Raman spectra were recorded with a Princeton Instruments Acton SpectraPro 2500i spectrophotometer, using epi-illumination through an X20 air objective in an Olympus IX-71 inverted microscope with a 0.5 mW 532 nm excitation. Each spectrum was carried out using an average of 10 acquisitions, each of which had an exposure time of 5s. All samples were in the solid-state and placed on glass substrates.

X-ray Crystal Structure Analysis

The single-crystal diffraction data were collected on a Nonius Kappa CCD diffractometer using a graphite monochromator with Mo Kα radiation (λ = 0.71073Å) and an Oxford Cryostream low temperature device. Absorption corrections were applied using Multi-scan.[96] Data reductions were performed using DENZO-SMN.[97] The structure was solved by direct methods using the program SIR97[98] and refined by full-matrix least-squares on F^2 with anisotropic displacement parameters for the non-H atoms using SHELXL-97.[99] The hydrogen atoms were calculated in ideal positions with isotropic displacement parameters set to 1.2xUeq of the attached atom (1.5xUeq for methyl hydrogen atoms). Neutral atom scattering factors and values used to calculate the linear absorption coefficient are taken from the International Tables for X-ray Crystallography (1992).[100]

Synthesis

General Methods

All chemicals were purchased from commercial suppliers and were used as received, except trimethylamine N-oxide dihydrate was purified by sublimation prior to use to remove the water of hydration.[101] Air- and moisture-sensitive reactions were carried out in oven-dried glassware using standard Schlenk techniques either under an inert nitrogen atmosphere or in a glove box with an argon atmosphere. The dry solvents were obtained from an Innovative Technologies Pure-Solv 400 solvent purification system. The target ligand, N,N-bis[2-(diphenylphosphino)ethyl]phenylamine **3**, was prepared according to Kostas' method.[53] The syntheses of *cis*-PNP-$Mo(CO)_4$ **4** and *fac*-PNP-

$Mo(CO)_3$ **5** were carried out using techniques similar to those of Blower[102] and Ainscough.[90]

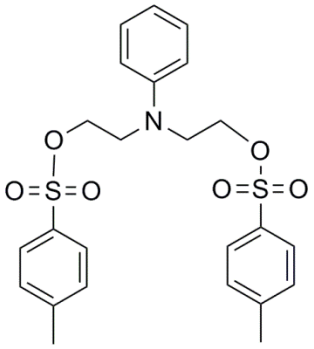

***N,N-bis*[2-(*p*-tolylsulfonyl)ethyl]phenylamine [1].** *N*-phenyldiethanolamine (2.7855 g, 15.37 mmol) was dissolved in dry pyridine and then cooled to 0 °C. *p*-Toluenesulfonylchloride (7.4134 g, 38.89 mmol) was also dissolved in dry pyridine separately and then added into the N-phenyldiethanolamine solution dropwise while stirring at 0 °C. After complete addition, the mixture was allowed to warm to room temperature and stirred overnight. The reaction contents were poured into a rapidly stirred water/ice bath. The resulting precipitate was collected via vacuum filtration. The precipitate was then recrystallized using a hot mixture of toluene/ethanol (1:1) (crystallized at 0 °C). The white crystalline product was collected by filtration (75%, 5.6438 g, 11.53 mmol). ^{1}H NMR (300 MHz, $CDCl_3$): 7.69 (d, 4H, J = 8.4), 7.25 (d, 4H, J = 8.1), 7.11 (dd, 2H, J = 8.7), 6.68 (t, 1H, J = 8.1), 6.40 (d, 2H, J = 8.1), 4.06 (t, 4H, J = 6.0), 3.53 (t, 4H, J = 6.0), 2.40 (s, 6H). ^{1}H NMR, ^{13}C{^{1}H} NMR and ESI MS were previously reported.[53]

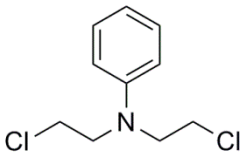

***N,N-bis*(2-chloroethyl)phenylamine [2].** *N*-Phenyldiethanolamine (0.5 g, 2.759 mmol) was dissolved in dry benzene and then cooled to 0 °C. Phosphorus oxychloride (0.9 mL, 96.56 mmol) was added dropwise. When the addition was complete, the resulting mixture was refluxed at 90 °C for 1 hour, then cooled to room temperature and stirred overnight. The resulting reaction mixture was then poured into ice-water, stirred for 1 hour, following which the mixture was transferred into a separatory funnel. The aqueous phase was then washed twice with benzene. The organic phases were then combined, washed twice with brine, dried over $MgSO_4$, and vacuum filtered, and the filtrate was evaporated. The crude product was then purified by column chromatography (silica gel). The eluent was a mixture of hexanes/CH_2Cl_2 (2:1). The first fraction was the product. The solvent was then evaporated to obtain the pure product as a yellowish oil (66%, 0.399g, 1.829 mmol). ^{1}H NMR (300 MHz, $CDCl_3$): 7.34 (t, 2H, J = 7.5), 6.86 (t, 1H, J = 7.5), 6.76 (d, 2H, J = 8.7), 3.8–3.66 (m, 8H).

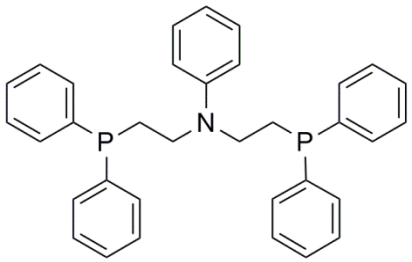

***N,N-bis*[2-(diphenylphosphino)ethyl]–phenylamine (PNP) [3].** The ditosylate starting material **1** (2.058 g, 4.2 mmol), was dissolved in dry THF under nitrogen in a Schlenk flask. $KPPh_2$ (17.23 ml, 8.6 mmol, 0.5 M in THF) was added via a glass airtight syringe. The resulting mixture was stirred for 2 hours at room temperature then quenched

with ~3.4 mL of dry methanol and stirred for 30 minutes. The solvents were evaporated and the resulting Schlenk flask was then transferred into the glove box. The residue was washed/suspended in toluene, and the resulting washings were passed through a frit in which there were celite/silica gel/celite layers. The filtrate was evaporated to dryness and the resulting residue was washed with ether and dried again. The analytically pure product was recovered as white precipitate (1.9 g, 3.67 mmol, 88 %). ^{1}H NMR (300 MHz, CD_2Cl_2): 7.45–7.32 (m, 20H), 7.07 (t, 2H, *J* = 7.8), 6.60 (t, 1H, *J* = 6.6), 6.37 (d, 2H, *J* = 8.1) 3.35 (m, 4H), 2.29 (t, 4H, *J* = 7.8). ^{31}P{^{1}H} NMR (121 MHz, CD_2Cl_2): -20 (s). ^{1}H NMR, ^{13}C{^{1}H} NMR and MS data were reported previously and match our data.[53]

Another approach to synthesizing the ligand, using *N,N-bis*(2-chloroethyl)phenylamine as the starting material instead of *N,N-bis*[2-(*p*-tolylsulfonyl)ethyl] phenylamine, was also used and resulting in a ~60%yield.

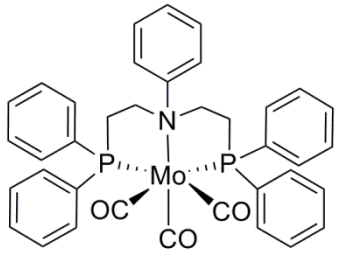

***fac-N,N-bis*[2-(diphenylphosphino)ethyl]phenylamine(tricarbonyl) molybdenum(0)**

***fac*-PNP-Mo(CO)$_3$ [4].** Both the ligand **3** (0.1g, 0.0001932 mole) and cycloheptatriene tricarbonylmolybdenum(0) (CHT-Mo(CO)$_3$) (0.053g, 0.0001937 mole) were dissolved in toluene separately in the glove box and then the metal solution was added to the ligand solution via a pipette. The resulting mixture was stirred overnight in a glove box which afforded a precipitate. The resulting precipitate was filtered through a frit containing Celite. The resulting solid was washed twice with toluene then dissolved

in dry CH_2Cl_2 and then dried in vacuo to give **4** as a yellow solid (59%, 0.08g, 0.0001147 mole).^{1}H NMR (300 MHz, CD_2Cl_2): 7-8 ppm (m, 25H), 3.67 (m, 4H), 3.16 (m, 4H). ^{31}P{^{1}H} NMR (121 MHz, CD_2Cl_2): 40 (s). HRMS (CI) calculated for *fac*-PNP-Mo(CO)$_3$ (M^+) 671.1041, found 671.1052. Hexanes were layered on a CH_2Cl_2 solution of the product to obtain a crystal suitable for X-ray analysis. Both solution state and solid state IR data were obtained. Solid state IR: 1923 cm^{-1}, 1836 cm^{-1}, 1784 cm^{-1}. Solution state IR (solution in CH_2Cl_2): 1932 cm^{-1}, 1838 cm^{-1}, 1802 cm^{-1}. Raman Spectrum: 1917 cm^{-1}, 1828 cm^{-1}, 1796 cm^{-1} and shoulder at 1782 cm^{-1}. Elemental Analysis: calculated for *fac*-PNP-Mo(CO)$_3$.2H$_2$O %C: 60.58, %H: 5.08, %N: 1.91; found %C: 61.08, %H:4.81, %N: 1.88. Mp: decomposed around 240 °C.

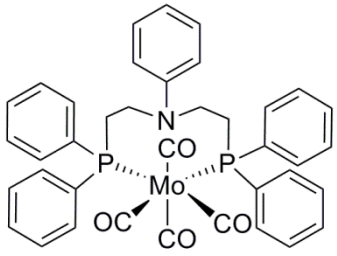

***cis-N,N-bis*[2-(diphenylphosphino)ethyl]phenylamine(tetracarbonyl) molybdenum(0)**

***(cis*-PNP-Mo(CO)$_4$) [5].** Ligand **3**, (0.15 g, 0.29 mmol), was dissolved in toluene in the glovebox following which (2,5-norbornadiene)tetracarbonylmolybdenum(0) (NBD-Mo(CO)$_4$) (0.087 g, 0.29 mmol), was added to the solution and stirred overnight at room temperature. The solvent was evaporated and the resulting residue was dissolved in CH_2Cl_2 and subsequently precipitated by the addition of hexanes. The resulting suspension was filtered through a frit. The filtrate was evaporated to afford a yellow solid (54%, 0.113 g, 0.156 mmol). ^{1}H NMR (300MHz, CD_2Cl_2): 7.53–7.25 (m, 20H), 7.08 (t, 2H, J = 8.4–6.9), 6.73 (t, 1H, J = 7.2), 6.38 (d, 2H, J = 8.4), 3.32 (m, 4H), 2.65 (m, 4H).

$^{13}C\{^{1}H\}$ NMR (75MHz, CD_2Cl_2): 148.9 (s), 138.9 (m), 132.6 (m), 129.8 (s), 129 (s), 128.7 (m), 118.6 (s), 114.9 (s), 48.8 (s), 30.26 (t, J = 15). $^{31}P\{^{1}H\}$ NMR (121 MHz, CH_2Cl_2): 25.8 (s). Low resolution MS (ESI): calculated for *cis*-PNP-Mo(CO)$_4$ (M^+) 724.11, found 727.5. Both the solution state and solid-state IR data were obtained. (Solid state, in ATR) IR: 2016 cm^{-1}, 1898 cm^{-1} (combination of two peaks), 1863 cm^{-1}. (Solution in CH_2Cl_2 in between KBr discs) IR: 2020 cm^{-1} and 1903 cm^{-1} (combination of 3 bands). Raman spectrum: 2014 cm^{-1}, 1899 cm^{-1} (combination of two bands), 1865 cm^{-1}. Elemental analysis: calculated for *cis*-PNP-Mo(CO)$_4$ C: 62.90, H: 4.58, N: 1.93; found% C: 62.92%, H: 4.45%, N: 1.80. Mp: decomposed approximately at 240 °C. Hexanes were layered on a concentrated CH_2Cl_2 solution of **5** thereby generating an X-ray diffraction quality single crystal.

As a second approach, Mo(CO)$_6$ (0.0963 g, 0.3648 mmol) was dissolved in acetonitrile (ACN) and refluxed under nitrogen for 1–2 hours until a clear yellow solution was obtained. The ligand, **3**, (0.1879 g, 0.363 mmol) was dissolved in CH_2Cl_2 and cannula transferred into the metal solution. The resulting mixture was stirred for 2 days in the dark. The removal of solvent resulted in the yellow-gray solid, **5** as a crude product mixture in low yield. Hexanes were layered onto a concentrated CH_2Cl_2 solution of **5** thereby generating an X-ray diffraction quality single crystal that was identical to the one described above.

A third way to synthesize compound **5** was developed by simply loading CO gas into a solution of **4**. For this purpose, 35 mg of compound **4** was dissolved in THF in a screw top NMR tube in a glove box, then the tube of which was connected to the Schlenk line. The line was vacuumed/N_2 three times. Meanwhile, the NMR tube was cooled down to 0 °C. The screw top was slightly opened and quickly vacuumed, then CO gas was loaded for 15 minutes while the CO tank was open. The reaction solution was kept under

a positive pressure of CO (the tank was closed) for 50 minutes. The $^{31}P\{^{1}H\}$ NMR was taken and the major product was found to be compound **5**. The NMR tube was then connected to the Schlenk line. The same steps were followed and CO was loaded again this time 15 minutes with open tank and 45 minutes with closed tank. The conversion of **4** to **5** was quantitative by $^{31}P\{^{1}H\}$ NMR spectra.

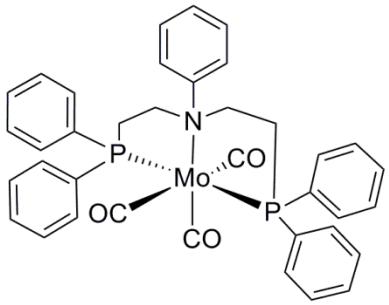

***mer-N,N-bis*[2-(diphenylphosphino)ethyl]phenylamine(tricarbonyl) molybdenum(0)**

***mer*-PNP-Mo(CO)$_3$ [6].** 50 mg (0.0689 mmol) of **5** was transferred into a 10 mL Schlenk flask and then dissolved in CH_2Cl_2 to get a clear, burnt orange solution. A stock solution of $(CH_3)_3NO$ was prepared by dissolving 49 mg (0.0006524 mol) material in 10 ml of CH_2Cl_2. 1 equivalence (1.06 mL) of the $(CH_3)_3NO$ solution was then transferred into the Schlenk flask via a syringe following which it was stirred overnight in the dark at room temperature. $^{31}P\{^{1}H\}$ NMR and ^{1}H NMR were obtained. However, there was no proof of the product formation. Accordingly, hexanes were layered on top of the NMR solution in order to grow crystals. **6** was obtained as a minor product (< 1%) of the reaction and observed in X-ray crystallography (**Figure 21**). The remainder of the product consisted of the unreacted starting material **5**.

As a second approach to the synthesis of the *meridional* isomer, the *facial* isomer **4** was dissolved in THF and stirred it for three weeks in the dark in a glove box. Some of

the *facial* isomer remained intact. However, some of the product decomposed to give the *meridional* isomer, and tetracarbonyl complex **5** in solution, and Mo(0) as a dark precipitate. $^{31}P\{^{1}H\}$ NMR (121 MHz, CD_2Cl_2): 57.6 (s) *meridional* product, 40 (s) *facial* product, 25 (s) tetracarbonyl complex.

RESULTS AND DISCUSSION

Synthesis

The PNP ligand, **3**, was prepared according to Kostas' method (**Scheme 1**).[53] It was obtained as a white solid. There were two synthetic routes to obtain **3**, i.e., by using **2** or by using **1**. Both were successful to prepare and used to synthesize **3**. The yield of **1** was higher than that of **2** by approximately 9%. The yield of **3** by using **1** as the starting material is 88%. The yield of **3** by using **2** as the starting material is ~60%.

Molybdenum reagents, ($Mo(ACN)_x(CO)_y$, $pip_2Mo(CO)_4$, NBD-$Mo(CO)_4$, and CHT-$Mo(CO)_3$) were allowed to react with one equivalent of the ligand in order to obtain the corresponding PNP-$Mo(CO)_n$ complexes (**Scheme 2**). Reaction of CHT-$Mo(CO)_3$ with the PNP ligand **3**, resulted in the generation of *fac*-PNP-$Mo(CO)_3$, **4**. The reactions of $Mo(ACN)_x(CO)_y$, $pip_2Mo(CO)_4$, and NBD-$Mo(CO)_4$ with the ligand **3**, resulted in the generation of *cis*-PNP-$Mo(CO)_4$, **5**. $Mo(ACN)_x(CO)_y$ reagent was obtained in situ by refluxing $Mo(CO)_6$ in ACN for 1-2 hours. However, the commercial NBD-$Mo(CO)_4$ reagent afforded the purest product for the synthesis of *cis*-PNP-$Mo(CO)_4$, which has been fully characterized. In order to obtain the *meridional* product *mer*-PNP-$Mo(CO)_3$, *cis*-PNP-$Mo(CO)_4$ was allowed to react with $(CH_3)_3NO$. $(CH_3)_3NO$ was prepared by sublimation of $(CH_3)_3NO \cdot 2H_2O$. The reaction mixtures of complex **5** and $(CH_3)_3NO$ resulted in a mixture of both the *meridional* product and the unreacted *cis*-PNP-$Mo(CO)_4$

as crystals. Only X-ray data of the *meridional* product was obtained from that reaction. Crystals of the *meridional* product was a few and can only be seen under the microscope.

The second approach to the synthesis of the *meridional* product involve the use of *fac*-PNP-Mo(CO)$_3$. For this purpose, the *facial* isomer was dissolved in THF. The resulting $^{31}P\{^1H\}$ NMR spectrum has a singlet peak initially at 40 ppm. The solution was stirred in the dark for three weeks, following which the $^{31}P\{^1H\}$ NMR spectrum of the solution was measured. Three singlets that were observed: the peak 57.6 ppm belonging to the *meridional* product **6**, the peak 40 ppm belonging to the *facial* product **4**, and the peak at 25 ppm belonging to the tetracarbonyl complex **5**. Refluxing of **4** in THF overnight resulted in the same outcome. An attempt was made to load PR_3 (R = Et_3, Ph_3, Et_2Ph, $EtPh_2$) into a solution of the *facial* isomer. However, the same results were evident: some of the *facial* isomer decomposed thereby generating the tetracarbonyl product **5**, the *meridional* isomer **6**, some unreacted *facial* isomer **4**, some free PNP ligand **3**, and a black precipitate of Mo(0).

Scheme 1. Synthesis of the PNP pincer ligand.

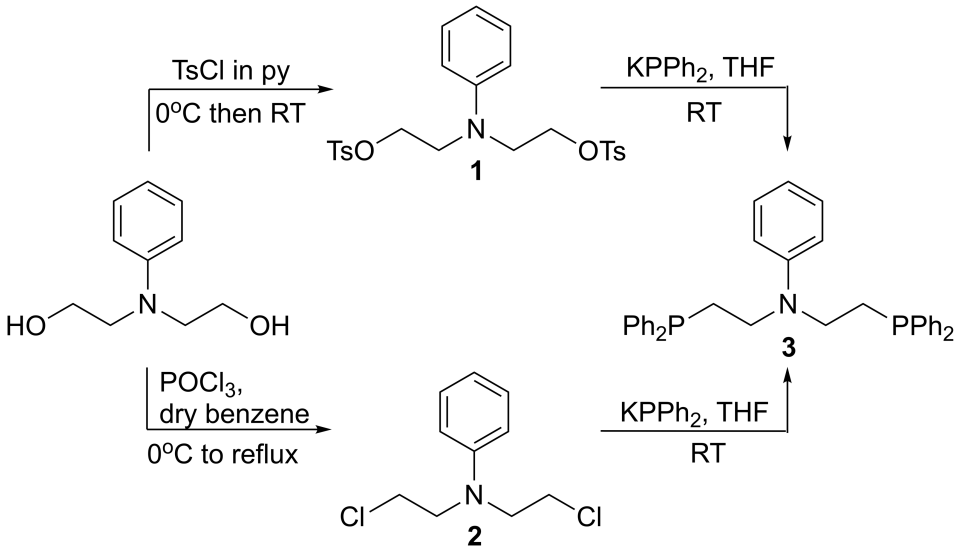

Scheme 2. Synthesis of PNP-Mo(CO)$_n$ complexes and isomers.

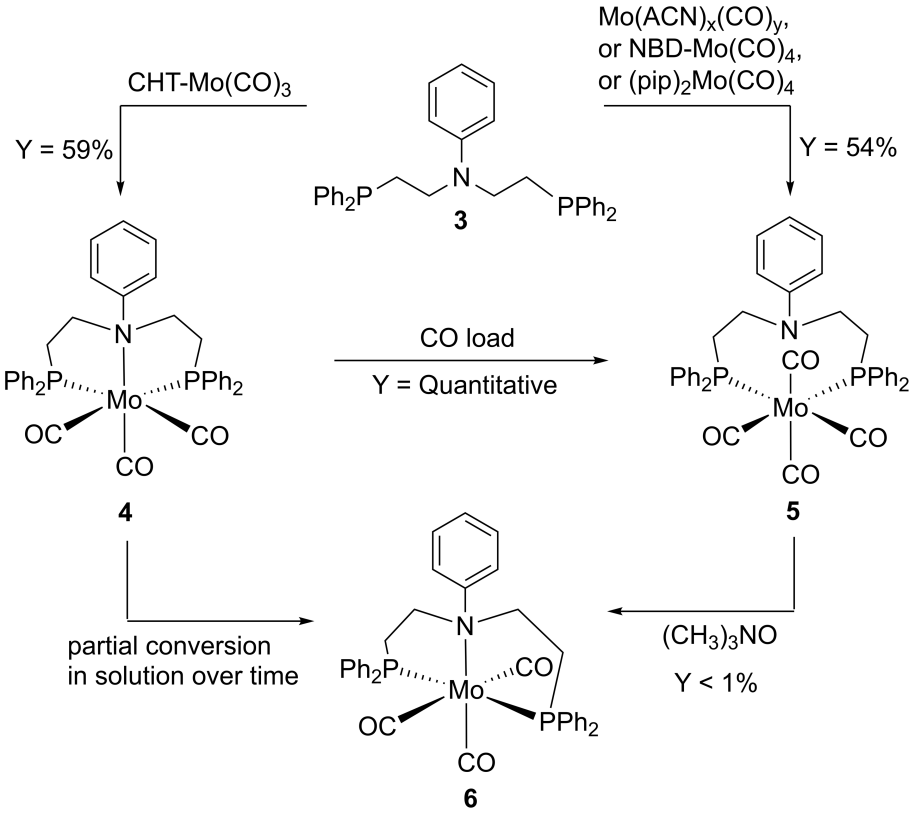

The experimental observations suggest that the conversion of the *facial* to the *meridional* isomer occurs via a dissociative mechanism. There is an equilibrium between the isomers and the *facial* isomer must be the thermodynamic product. Because, stirring a THF solution of pure *facial* isomer **4** gives a black precipitate Mo(0), *cis*-PNP-Mo(CO)$_4$ **5**, and *mer*-PNP-Mo(CO)$_3$ **6**, as well as intact *fac*-PNP-Mo(CO)$_3$ **4**. Some of the *fac*-PNP-Mo(CO)$_3$ must have decomposed to give Mo(0), and some of the excess carbonyls must have been picked up by other *fac*-PNP-Mo(CO)$_3$ to give *cis*-PNP-Mo(CO)$_4$; the rest of the free carbonyls must be picked up by the five-coordinate intermediate resulted from the dissociation of *fac*-PNP-Mo(CO)$_3$ thereby generating the *mer*-PNP-Mo(CO)$_3$ isomer. This opinion also explains why the *meridional* product is the minor product. Furthermore, this view is also supported bt the literature. Crabtree explained the reason that the ML$_3$(CO)$_3$ complexes undergo a dissociative mechanism. He also specifically provided the molybdenum complex MoL$_3$(CO)$_3$ as an example.[103]

Infrared and Raman Studies

All the complexes were found to be soluble in CH_2Cl_2. Solution and solid-state IR data and solid-state Raman data were obtained for the *fac*-PNP-Mo(CO)$_3$ and *cis*-PNP-Mo(CO)$_4$ (**Figure 22**) and found to be consistent with the proposed molecular structures. Each of the three complexes adopted the point group is C_s, which is as evident from each of the crystal structures. Group theory calculations of the CO stretches for the three complexes resulted in the following: $\Gamma = 2A' + A''$ for complex **4**, $\Gamma = 3A' + A''$ for complex **5**, and $\Gamma = 3A'$ for the complex **6**. All bands were fund to be both Raman and IR active.

The IR spectrum of **4** revealed three bands as expected from the above calculation. However, the Raman spectrum evidenced three bands and a shoulder (1782 cm^{-1}). The Raman and IR spectra for complex **5** resulted in three stretches in the measurements while the calculation afforded four stretches. But, one of the stretches (in both spectra) is broad and appears to look like a combination of two bands (1898 cm^{-1}). However, the solution state IR spectrum of **5** consusted of two stretches. It appears that the three bands between 1800 and 1900 cm^{-1} combined to resulted in a broad peak at 1903 cm^{-1}. The remaining peak was observed at 2020 cm^{-1}.

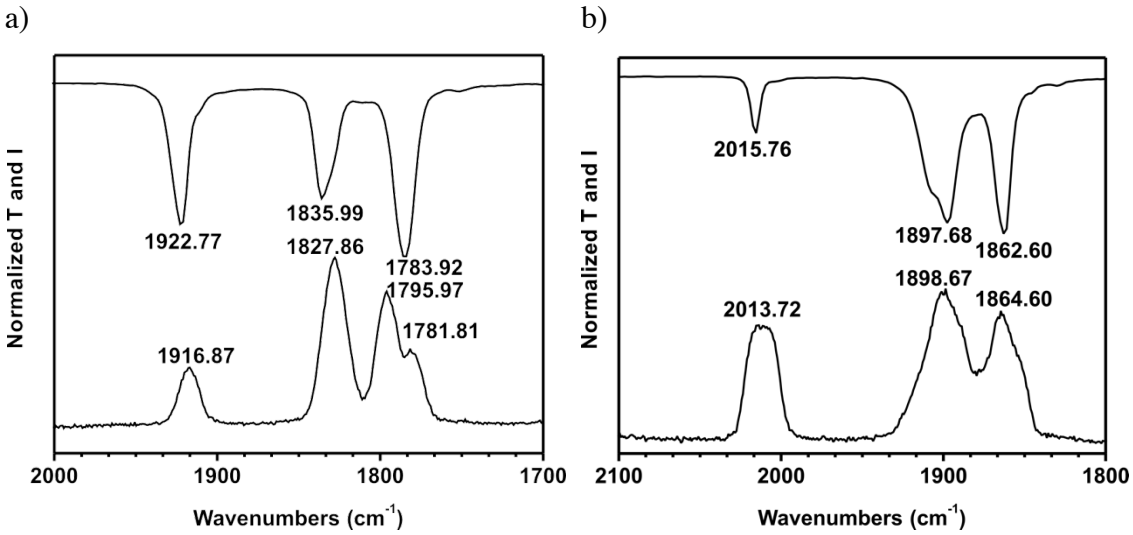

Figure 22. (a) Solid state IR and Raman spectra of *fac*-PNP-$Mo(CO)_3$. (b) Solid state IR and Raman spectra of *cis*-PNP-$Mo(CO)_4$.

Structure of the Complexes

The solid-state structure of complexes **4**, **5**, and **6** were determined by X-ray diffraction analysis and the resulting ORTEP representation can be seen in **Figures 23-25**, and crystallographic and structural refinement data are presented in **Table 1**. In the

crystal structure of complex **4** (**Figure 23**), the unit cell contains two *fac*-PNP-Mo(CO)$_3$ complexes, both of which have a six-coordinate Mo(0) that lies at the center of an *octahedral* environment. The coordination environment around the metal center is defined by two phosphorus atoms from the PNP ligand that are arranged *cis* to each other. Namely, one N atom from the PNP ligand, and three carbon atoms from the carbonyl ligands that have a *facial* arrangement. The difference between these two *facial* complexes depends on the orientation of the five membered rings that were formed upon chelation, which means that C16 and C17 in one structure have a different orientation than C53 and C54 in the other structure. In the case of complex **5**, the six-coordinate Mo(0) lies at the center of an *octahedral* environment. The coordination environment around the metal center is defined by two phosphorus atoms from the PNP ligand and four carbon atoms from the carbonyl ligands. The P atoms are arranged *cis* to each other. In the case of complex **6**, the six-coordinate Mo(0) also lies at the center of an *octahedral* environment. The coordination environment around the metal center is defined by two phosphorus atoms from the PNP ligand, one nitrogen atom from the PNP ligand and three carbon atoms from the carbonyl ligands. The phosphorus atoms are arraged *trans* to each other and the carbonyl ligands have the *meridional* arrangement.

Bond lengths and angles of **5**, and **6** were compared with similar complexes that can be found in the literature. The literature complexes that has a *facial* molybdenum tricarbonyl complex in [ref 87-complex 7a] has a consistent P-Mo-P angle compared to the complex **4**. However, all other values for the bond angles and bond distances are different from the complex **4**. The literature complexes similar to those **5** have slightly different angles. For example, the P-Mo-P angle for [ref 88] is 86.75° while that for [ref 87] is 88.1° (**Figure 21**, PNP-Mo(CO)$_4$ complex first from the right is from [ref 88] and the PNP-Mo(CO)$_4$ complex second from the right is from [ref 87]). Compound **5** has P1-

Mo-P2 angle of 94.78° but, bond lengths for the literature complexes and **5** are consistent. However, for the complex **6**, carbonyl carbons that are *trans* to each other (C35-Mo-C37) have a bond angle of 163°. On the other hand, the complex in the literature (ligand has an imine N) has an angle of 171.07°.[90] The *trans* phosphines of **6** and the literature values are consistent. However, the *trans* carbonyl carbons do not match those of the bond angles [ref 90] (the complex [ref 90] is abbreviated as *mer*-[$Mo(CO)_3$(PNCHP)] in the literature. The N-donor in the complex from [ref 90] is an imine nitrogen). All bond lengths are also consistent except for that of the Mo–N bond. **6** that has a Mo–N distance of 2.424 Å, while that of the literature complex has a value of 2.237 Å.

Table 1. Crystal data and structure refinement for molybdenum complexes.

Complex	**4**	**5**	**6**
CCDC	762872	762870	762871
Formula	$C_{37}H_{33}NO_3P_2Mo$	$C_{38}H_{33}NO_4P_2Mo$	$C_{37}H_{33}NO_3P_2Mo$
FW	697.52	725.53	697.52
T (K)	153(2)	153(2)	153(2)
Crystal system	Monoclinic	Monoclinic	Monoclinic
Space group	*C2*	*P2₁/n*	*P2₁/c*
a (Å)	19.456(4)	10.027(2)	17.620(4)
b (Å)	12.232(2)	19.158(4)	17.198(3)
c (Å)	13.608(3)	18.646(4)	20.971(4)
α (°)	90	90	90
β (°)	95.38(3)	102.853(1)	100.40(3)
γ (°)	90	90	90
V (Å^3)	3224.2(11)	3492.3(12)	3224.2(11)
Z	4	4	8
ϱ (g/cm^3)	1.437	1.38	1.482
μ (mm^{-1})	0.54	0.51	0.56
F(000)	1432	1488	2864
Crystal size (mm)	0.09 × 0.05 × 0.03	0.30 × 0.02 × 0.02	0.46 × 0.06 × 0.07
θ (°)	1.0 to 27.5	1.0 to 27.5	1.0 to 27.5
Index ranges	$-25 \le h \le 24$	$-13 \le h \le 13$	$-20 \le h \le 22$
	$-15 \le k \le 15$	$-24 \le k \le 23$	$-22 \le k \le 18$
	$-2 \le l \le 17$	$-24 \le l \le 24$	$-27 \le l \le 17$
Absorption correction	Multi-scan	Multi-scan	Multi-scan
Max. and min. transmission	0.953 and 0.984	0.990 and 0.863	0.994 and 0.896
GOF on F^2	1.16	1.02	1.15
R_1, R_2 I > 2σ (I)	0.0955, 0.1822	0.0640, 0.1452	0.0585, 0.1225
R_1, R_2 (all data)	0.1571, 0.2087	0.0758, 0.1487	0.0783, 0.1391
Largest diff. peak and hole (e Å^{-3})	1.70 and -1.45	0.66 and -0.63	0.94 and -0.93

Stability of the Complexes

A similar *mer*-PNP-Mo(CO)$_3$ product has also been reported by Siclovan *et al*. However, these authors also could not isolate the *meridional* isomer, despite the fact that they could successfully synthesize and purify the *facial* isomer.[86] The choice of the *facial*

or *meridional* isomer was explained on the basis of electronics rather than sterics in the literature: when the monodentate ligand is negatively charged, such as halogens, the preferred geometry becomes *meridional* due to the electrostatic repulsions between the halogens. In the case of neutral monodentate ligands such as the carbonyl ligand, the preferred geometry is *facial* in the complex.[76, 94] The explanation of the stability of the complexes of *meridional* and *facial* isomers -electronics of the monodentate ion plays a role rather than sterics- was not genuinely explaining experimental observations in the present study. Because in those journal articles, the only reason provided was repulsion of negative charges on halogens resulted in the *meridional* geometry. The reason for the *facial* geometry being the preferred geometry in PNP-Mo(CO)$_3$ complexes with neutral monodentate ligand i.e. carbonyls was not provided. Moreover, the Jahn–Teller effect, *trans* effect, π-back donation and sterics were not taken into account in those journal articles. In the present study, a variety of the aforementioned effects have been considered and discussions of each are provided.

The first argument concerns the *trans* effect, π-back donation and bond distances. The main reason for compound **4** being more stable than compound **6** is that all of the t_{2g}-type *d* orbitals in the *facial* geometry are effectively involved in Mo–CO π-back bonding. In the case of compound **6** which has a *meridional* geometry, the two CO ligands are located *trans* to each other compete each other as π acids and therefore one of the t_{2g}-type *d* orbitals are less effectively involved compared with the *facial* isomer. As a result, longer metal–carbon bond distances are observed for the *meridional* complex and therefore, the *facial* isomer is more stable. **Tables 5**, **6** and **7** show the distances of each atom to Mo center in the *octahedral* environment. The Mo–C distances are slightly shorter for complex **4** than those for complex **6**. The carbonyls that are located *trans* to the phosphines benefit from the π-back donation and are more tightly held by the metal,

as a result, the M–C distances are shorter than those for the carbonyls.[103] This is exactly what was observed for the *facial* complex **4** for which all the M–C distances are less than 2 Å (1.933–1.979 Å). In the case of complex **6**, phosphines that have less *trans* effect than the carbonyls, are *trans* to each other and the M–P bonds are shorter. As expected, the carbonyls that are located *trans* to each other have longer M–C distances (Mo–C35: 2.00 Å and Mo–C37: 1.99 Å) which results in a poor π-back donation. Furthermore, the M–C distances in which carbonyls are *trans* to the N atom for both complex **4** and **6** are shorter (for 4 Mo1–C2: 1.933 Å, Mo2–C39:1.937 Å; for 6 Mo– C36: 1.93 Å) than the other M–C distances (1.98 Å for 4, 1.99– 2.00 Å for 6) (*trans* to either phosphine or carbonyl). The reason for this is that there is a slight π-back donation from the metal to the phosphine; therefore, the N atom becomes a better electron donor than the phosphine and carbonyls *trans* to the N benefit from that electron donation.[44]

The second argument is whether having a less angle distortion is the reason for the *facial* complex being more stable than the *meridional* one or not; in other words, whether the Jahn–Teller effect plays a role in the stability between the *meridional* and *facial* isomers. The angles around the Mo atom were compared for each complex to determine if there is any angle distortion that could cause the difference in stability. The angles of the *meridional* isomer around the *octahedral* Mo atom are the most distorted of the three complexes. Furthermore, the angles between the Mo and the carbonyl groups that are supposed to be 180 are again the most distorted for the *meridional* isomer. The most distorted angles for the meridional isomer **6** are as follows; C35–Mo–C36: 78.8°, C35–Mo–C37: 163.1°, C35–Mo–N: 103.1°, N–Mo–P1: 79.1°, C36– Mo–P1: 101.4°, N–Mo–P2: 79.8°, P1–Mo–P2: 158.5°. The difference between the ideal angles changes between 10.2° and 21.5° (7 angles). The most distorted angles for the *facial* isomer **4** are as follows (angles greater than 10° distortions); C3–Mo1–N1: 100.4°, C3–Mo1–P1: 168.4°,

N1–Mo1–P1: 78.68°, C1–Mo1–P2: 169.0°, N1–Mo1–P2: 78.69°, C40–Mo2–N2: 100.9°, C40–Mo2–P3: 163.7°, N2–Mo2–P3: 77.66°, N2–Mo2–P4: 77.63°, P3–Mo2–P4: 100.84°. The difference between the ideal angles for Mo1 ranges between 10.4° and 11.32° (5 angles); for Mo2, changes between 10.84° and 16.3°. The most distorted angle for complex **5** was found to be only 7.3°. The less distorted the angles are the more stable the molecule should be. Moreover, the P–Mo–P angle for the *meridional* isomer **6** is distorted by 21.5°. While the C–Mo–C (*trans*) angle is distorted by 16.9°. The largest angle distortions between the C–Mo–C atoms in the *facial* isomer **4** are 8.8° for C38–Mo2– C40 and 3.03° for C1–Mo1–C3. P–Mo–P angle in complex **4** is distorted by 3.62° for P1–Mo1–P2 and 10.84° for P3–Mo2–P4. The distortions in bond angles for compound **4** are significantly smaller than those for compound **6**. **Tables 2**, **3** and **4** indicate the *octahedral* angles around the Mo atom and the Mo–C–O angles for each complex, as well as the deviation from the ideal angles. One can find the corresponding pictures for crystal structures to see the labeled atoms in the **Figures 23-25**.

The bond angles and bond distances for *mer*-PNP-$MoCl_3$ that were reported by Fernandez-Trujillo *et al*. was also studied in order to compare the data with **6**.[76] It was not surprising that the *mer*-PNP-$MoCl_3$ complex is more stable than *mer*-PNP-$Mo(CO)_3$ and can synthetically be made because Cl^- has a less *trans* effect than CO groups and also than phosphines; in addition, there are ionic bonds between Mo^{3+} and each Cl^- which should be stronger than the Mo–CO bonds. There are still angle distortions for *mer*-PNP-$MoCl_3$ compared to complexes **4** and **6**. The angle distortions which are greater than 10° around the Mo atom in the complex *mer*-PNP-$MoCl_3$ taken from the literature are P2–Mo–P3: 161.2° and P2– Mo–Cl7: 101.2° and their differences from ideality are 18.8° and 11.2°, respectively. The remaining angles and distortions can be found in **Table 8**. The

distances of the atoms to Mo in *octahedral* environment for *mer*-PNP-$MoCl_3$ are listed in **Table 9**.

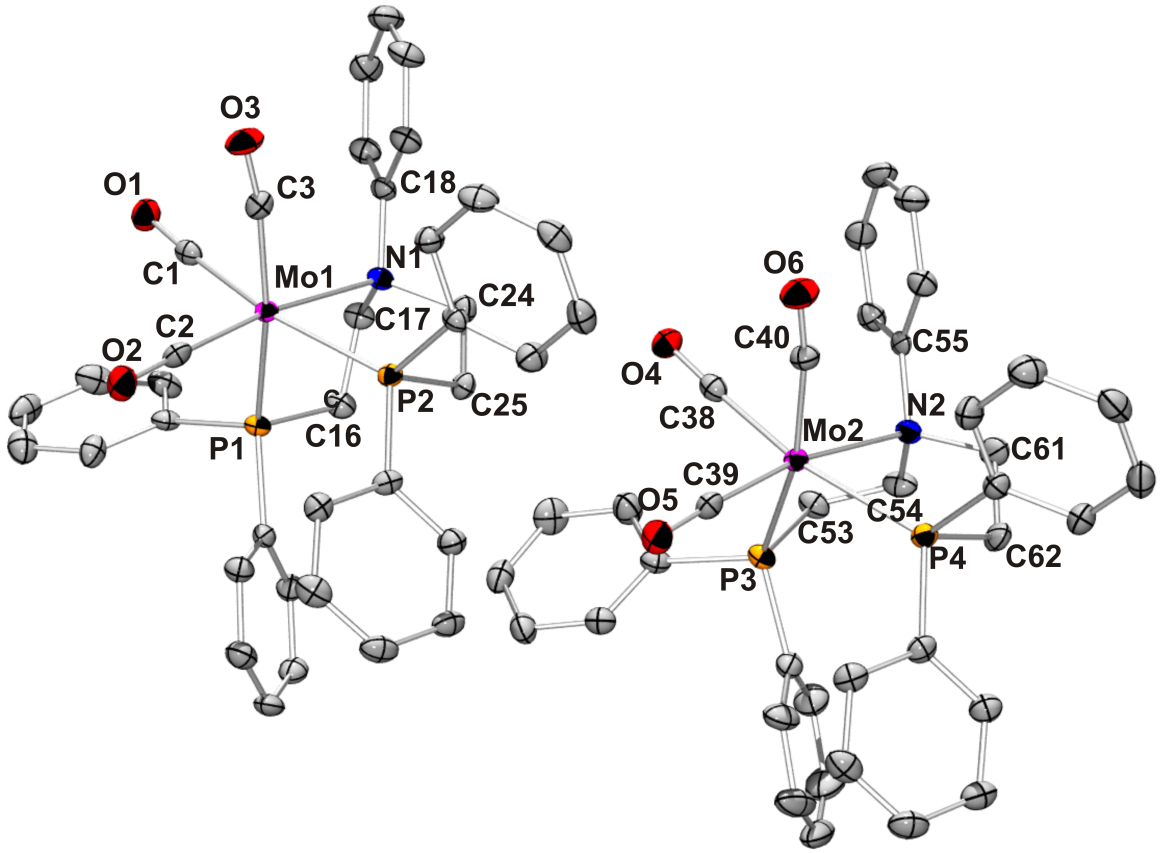

Figure 23. The crystal structure of *fac*-PNP-$Mo(CO)_3$ (**4**) showing the labeling of selected atoms. The hydrogen atoms have been omitted for clarity and the displacement ellipsoids are scaled to the 50% probability level.

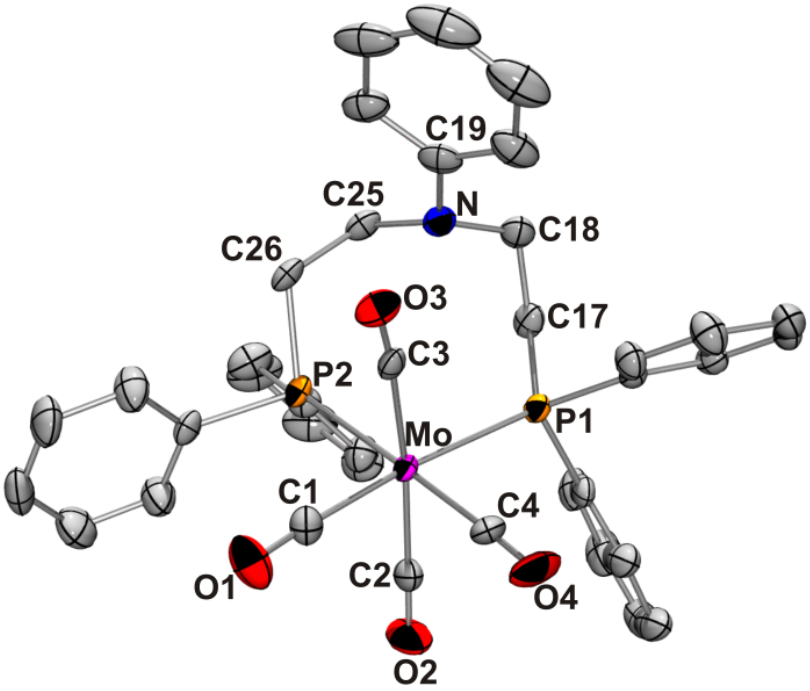

Figure 24. The crystal structure of *cis*-PNP-Mo(CO)$_4$ (**5**) showing the labeling of selected atoms. The hydrogen atoms have been omitted for clarity and the displacement ellipsoids are scaled to the 50% probability level.

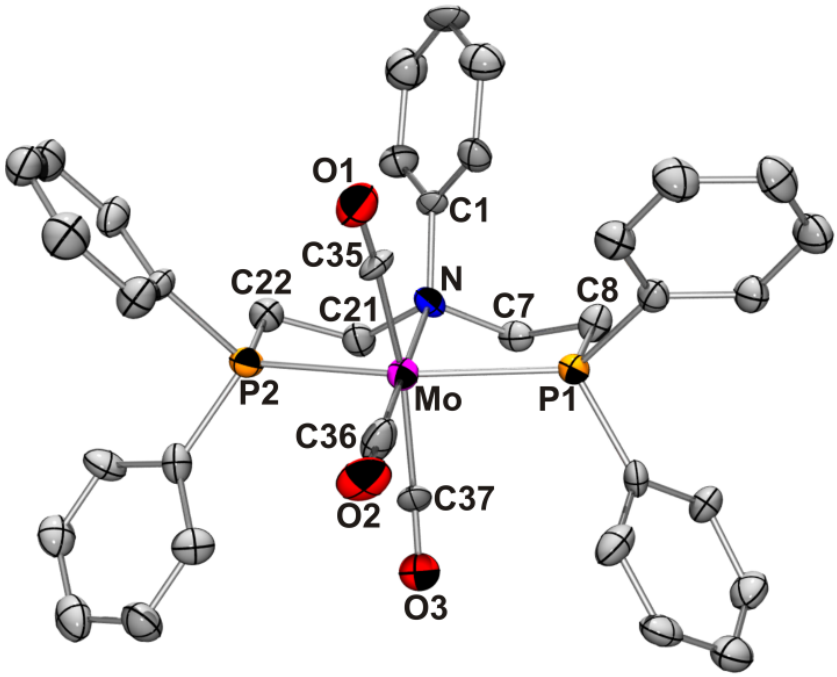

Figure 25. The crystal structure of *mer*-PNP-Mo(CO)$_3$ (**6**) showing the labeling of selected atoms. The hydrogen atoms have been omitted for clarity and the displacement ellipsoids are scaled to the 50% probability level.

Table 2. The bond angles around *octahedral* Mo atom and Mo-C-O for compound **4**.

fac-PNP-Mo(CO)$_3$	Angle	Ideal angle	Difference
C1-Mo1-C2	93.0(1)	90	-3
C1-Mo1-C3	82.3(1)	90	3.03
C1-Mo1-N1	90.5(1)	90	-0.5
C1-Mo1-P1	86.1(1)	90	-3.1
C1-Mo1-P2	169.0(1)	180	11
C2-Mo1-C3	87.5(1)	90	-2.5
C2-Mo1-N1	171.7(1)	180	-8.3
C2-Mo1-P1	94.1(1)	90	4.1
C2-Mo1-P2	98.0(1)	90	8
C3-Mo1-N1	100.4(1)	90	10.4
C3-Mo1-P1	168.4(1)	180	-11.6
C3-Mo1-P2	97.6(1)	90	7.6
N1-Mo1-P1	78.67(7)	90	-11.32
N1-Mo1-P2	78.68(7)	90	-11.31
P1-Mo1-P2	93.62(3)	90	3.62
C38-Mo2-C39	92.1(1)	90	2.1
C38-Mo2-C40	81.2(1)	90	-8.8
C38-Mo2-N2	94.3(1)	90	4.3
C38-Mo2-P3	82.8(1)	90	-7.2
C38-Mo2-P4	170.1(1)	180	-9.9
C39-Mo2-C40	88.9(1)	90	-1.1
C39-Mo2-N2	169.0(1)	180	-11
C39-Mo2-P3	94.3(1)	90	4.3
C39-Mo2-P24	96.9(1)	90	6.9
C40-Mo2-N2	100.9(1)	90	10.9
C40-Mo2-P3	163.7(1)	180	-16.3
C40-Mo2-P4	94.6(1)	90	4.6
N2-Mo2-P3	77.65(7)	90	-12.34
N2-Mo2-P4	77.62(7)	90	-12.37
P3-Mo2-P4	100.84(3)	90	10.84
Carbonyl groups			
O1-C1-Mo1	176.0(3)	180	-4
O2-C2-Mo1	178.7(3)	180	-1.3
O3-C3-Mo1	171.5(3)	180	-8.5
O4-C38-Mo2	176.2(3)	180	-3.8
O5-C39-Mo2	177.0(3)	180	-3
O6-C40-Mo2	171.4(3)	180	-8.6

Table 3. The bond angles around *octahedral* Mo atom and Mo-C-O for compound **5**.

cis-PNP-Mo(CO)$_4$	Angle	Ideal angle	Difference
C1-Mo-C2	87.4(1)	90	-2.6
C1-Mo-C3	85.4(1)	90	-4.6
C1-Mo-C4	86.1(1)	90	-3.9
C1-Mo-P1	174.5(1)	180	-5.5
C1-Mo-P2	90.5(1)	90	-0.5
C2-Mo-C3	172.7(1)	180	-7.3
C2-Mo-C4	88.3(2)	90	-1.7
C2-Mo-P1	90.7(1)	90	0.7
C2-Mo-P2	94.0(1)	90	4
C3-Mo-C4	90.0(1)	90	0
C3-Mo-P1	96.37(9)	90	6.37
C3-Mo-P2	87.25(9)	180	-2.74
C4-Mo-P1	88.7(1)	90	-1.3
C4-Mo-P2	175.8(1)	180	-4.2
P1-Mo-P2	94.78(3)	90	4.78
Carbonyl groups			
O1-C1-Mo	175.4(3)	180	-4.6
O2-C2-Mo	175.2(3)	180	-4.8
O3-C3-Mo	173.1(3)	180	-6.9
O4-C4-Mo	177.4(3)	180	-2.6

Table 4. The bond angles around *octahedral* Mo atom and Mo-C-O for compound **6**.

mer-PNP-Mo(CO)$_3$	Angle	Ideal angle	Difference
C35-Mo-C36	78.7(5)	90	-11.2
C35-Mo-C37	163.0(5)	180	-16.9
C35-Mo-P1	99.8(3)	90	9.8
C35-Mo-P2	89.0(3)	90	-1
C35-Mo-N	103.1(4)	90	13.1
C36-Mo-C37	84.5(5)	90	-5.4
C36-Mo-P1	101.4(4)	90	11.4
C36-Mo-P2	99.6(4)	90	9.6
C36-Mo-N	178.1(4)	180	-1.9
C37-Mo-P1	86.4(3)	90	-3.6
C37-MoP2	99.6(4)	90	9.6
C37-Mo-N	90.8(3)	90	0.8
N-Mo-P1	79.1(2)	90	-10.9
N-Mo-P2	79.8(2)	90	-10.2
P1-Mo-P2	158.5(1)	180	-21.5
Carbonyl groups			
O1-C35-Mo	173(1)	180	-7
O2-C36-Mo	177(1)	180	-3
O3-C37-Mo	175(1)	180	-5

Table 5. The bond lengths [Å] around Mo atom for compound **4**.

fac-PNP-Mo(CO)$_3$	Bond Lengths
Mo1-C1	1.979(4)
Mo1-C2	1.933(3)
Mo1-C3	1.977(3)
Mo1-N1	2.466(3)
Mo1-P1	2.496(1)
Mo1-P2	2.512(1)
Mo2-C38	1.977(4)
Mo2-C39	1.937(3)
Mo2-C40	1.977(3)
Mo2-N2	2.489(3)
Mo2-P3	2.495(1)
Mo2-P4	2.543(1)

Table 6. The bond lengths [Å] around Mo atom for compound **5**.

cis-PNP-Mo(CO)$_4$	Bond Lengths
Mo-C1	1.982(3)
Mo-C2	2.027(4)
Mo-C3	2.049(3)
Mo-C4	1.978(3)
Mo-P1	2.551(1)
Mo-P2	2.5404(9)

Table 7. The bond lengths [Å] around Mo atom for compound **6**.

mer-PNP-Mo(CO)$_3$	Bond Lengths
Mo-C35	2.00(1)
Mo-C36	1.93(1)
Mo-C37	1.99(1)
Mo-P1	2.458(3)
Mo-P2	2.442(3)
N-Mo	2.424(9)

Table 8. The bond angles around *octahedral* Mo atom for the compound *mer*-PNP-$MoCl_3$.[76]

mer-PNP-$MoCl_3$	Angle	Ideal angle	Difference
N1-Mo-P2	80.5	90	-9.5
N1-Mo-P3	81.1	90	-8.9
N1-Mo-Cl5	87	90	-3
N1-Mo-Cl6	91.1	90	1.1
N1-Mo-Cl7	177.2	180	-2.8
P2-Mo-Cl5	86.8	90	-3.2
P2-Mo-Cl6	88.9	90	-1.1
P2-Mo-Cl7	101.2	90	11.2
P2-Mo-P3	161.2	180	-18.8
P3-Mo-Cl5	88.5	90	-1.5
P3-Mo-Cl6	95.2	90	5.2
P3-Mo-Cl7	97	90	7
Cl5-Mo-Cl6	175.5	180	-4.5
Cl5-Mo-Cl7	91	90	1
Cl6-Mo-Cl7	91.1	90	1.1

Table 9. The bond lengths [Å] around Mo atom for compound *mer*-PNP-$MoCl_3$.[76]

mer-PNP-$MoCl_3$	Bond Lengths
Mo-N	2.332
Mo-P2	2.524
Mo-P3	2.541
Mo-Cl5	2.417
Mo-Cl6	2.395
Mo-Cl7	2.376

The third argument is whether composition of the molecular orbitals play a role in compound **4** being the more stable isomer than compound **6** or not. Some DFT calculations have been performed to determine the composition of the molecular orbitals. GaussSum version 2.1 has been used to find the orbital contributions. As it is indicated in **Tables 10**, **11** and **12**, the biggest contribution in the HOMO level of each complex is coming from the molybdenum atom. In the case of compound **5**, the percent contribution of the Mo atom (40%) to the HOMO is less than compound **4** and **6** (62% and 67% respectively). However, nitrogen group contributes more in **5** (35%), and interestingly there is no bond between N and Mo in this compound. The percent contribution from N for complexes **4** and **6** are 3% and 0% respectively. The lowest HOMO level (which should make the complex more stable) among all of the complexes also belongs to **5**. LUMO levels are mainly ligand based in all three complexes. It can be concluded that HOMO to HOMO-2 levels of complexes **4** and **6** are metal base. HOMO level of complex **4** is slightly more stable in which Mo is contributing 62% and two of the carbonyl groups are con- tributing 16% each. On the other hand, HOMO level of complex **6** is composed of 67% metal orbital and 23% is coming from one of the carbonyls. Contribution of the two carbonyl groups to the molecular orbital in complex **4** compared with complex **6** that has only one carbonyl overlap with the metal, should be the reason for the lower level HOMO for **4**. HOMO-1 of complexes **4** and **6** are not much different because the main contribution is coming from the metal and two of the carbonyls in both complexes.

Table 10. Composition of selected HOMOs and LUMOs of the complex **4**, expressed in terms of composing fragments.

MO	eV	P2	P1	Mo	C2 (CO)	C3 (CO)	N	C1 (CO)
L+6	-0.48	46	10	4	0	2	33	3
L+5	-0.56	8	81	2	1	0	7	1
L+4	-0.64	44	17	9	2	3	20	4
L+3	-0.75	29	59	4	2	3	1	1
L+2	-0.85	75	13	4	1	1	3	2
L+1	-1.05	8	90	0	0	0	1	0
LUMO	-1.11	81	14	1	0	1	1	1
HOMO	-4.86	0	1	62	16	2	3	16
H-1	-4.88	3	1	63	16	13	1	3
H-2	-4.98	4	5	61	2	15	1	12
H-3	-6.52	2	20	4	1	0	72	1
H-4	-6.68	5	71	3	0	0	19	1
H-5	-6.93	44	54	1	0	1	1	0
H-6	-6.96	49	48	1	0	0	2	0

Table 11. Composition of selected HOMOs and LUMOs of the complex **5**, expressed in terms of composing fragments.

MO	eV	P2	P1	C3 (CO)	Mo	C1 (CO)	C4 (CO)	N	C2 (CO)
L+6	-0.72	77	15	1	1	1	2	2	2
L+5	-0.82	92	1	1	2	3	0	1	1
L+4	-0.91	3	95	0	1	0	0	0	0
L+3	-1.01	87	4	3	1	1	1	0	3
L+2	-1.15	3	53	16	9	0	1	0	17
L+1	-1.2	10	19	29	12	1	0	0	29
LUMO	-1.33	5	37	21	11	1	2	0	22
HOMO	-5.32	3	3	1	40	9	9	35	1
H-1	-5.51	3	2	3	37	8	6	40	2
H-2	-5.66	3	1	10	56	8	5	6	11
H-3	-5.73	1	2	10	52	2	8	15	9
H-4	-6.79	6	22	0	1	0	0	71	0
H-5	-6.83	21	46	0	3	1	1	28	0
H-6	-6.92	67	25	0	2	1	0	3	0

Table 12. Composition of selected HOMOs and LUMOs of the complex **6**, expressed in terms of composing fragments.

MO	eV	P2	P1	C37 (CO)	Mo	C36 (CO)	N	C35 (CO)
L+6	-0.58	23	13	0	6	8	40	9
L+5	-0.62	4	86	1	1	0	7	1
L+4	-0.67	42	13	0	5	11	18	12
L+3	-0.79	16	9	0	2	3	68	3
L+2	-0.85	11	55	0	2	6	21	4
L+1	-0.93	10	17	0	8	17	32	17
LUMO	-0.98	51	3	0	9	16	4	17
HOMO	-4.65	3	3	23	67	2	0	1
H-1	-5.01	6	4	1	61	14	1	14
H-2	-5.11	0	2	12	56	14	1	14
H-3	-6.8	46	51	0	2	0	1	0
H-4	-6.82	63	34	0	1	0	1	0
H-5	-6.92	100	0	0	0	0	0	0
H-6	-7.04	4	94	0	0	0	1	0

CONCLUSIONS

Three different PNP-Mo(CO)$_n$ complexes where n = 3, 4 were synthesized, characterized, and the conversion conditions between them were investigated. The synthesis and purification of *fac*-PNP-Mo(CO)$_3$ and *cis*-PNP-Mo(CO)$_4$ were successfully achieved, but the synthesis and isolation of *mer*-PNP-Mo(CO)$_3$ could never be controlled. *mer*-PNP-Mo(CO)$_3$ was observed as a minor product in the syntheses reactions by $^{31}P\{^1H\}$ NMR and X-ray diffraction measurements. The solution of pure *fac*-PNP-Mo(CO)$_3$ underwent decomposition thereby generating *cis*-PNP-Mo(CO)$_4$, *mer*-PNP-Mo(CO)$_3$, and Mo(0) as a dark precipitate along with some *fac*-PNP-Mo(CO)$_3$ that was left intact in solution.

The *facial* isomer was favored compared with the *meridional* isomer mainly because of the *trans* effect and π-backdonation (effective involvement of all t_{2g} orbitals in

the *facial* geometry). Possible other effects such as Jahn-Teller effect (angle distortions) has been discussed. The reason for the preferred geometry being the *facial* arrangement was not electronics as it was reported in the literature.[76,94,95]

Chapter 3: Polymerizable Complexes of Molybdenum with Carbonyls as Ancillary Ligands and Corresponding Metallopolymers[2]

INTRODUCTION

The materials made from conjugated polymer systems have become very popular due to their easy preparation, mechanical processability and electrical conductivity upon doping.[11] Transition metals have been incorporated into these systems in order to impart interesting redox, magnetic, optical, or catalytic properties in the resulting materials.[104]

The conjugated polymers with redox-active ligand sites have been investigated to control the reactivity and binding of transition metal complexes. The conjugated polymer matrix has a large number of available oxidation states. In turn, this wide variety of oxidation states can be used to tune the amount of electron density on the metal center and consequently affect the binding of an additional ligand.[105-107] Reactivity of metal complexes which have redox active ligands can be modulated without changing the immediate coordination sphere. The compound can be interconverted between two useful states of reactivity in a turn on/turn off fashion by manipulation of these redox changes. These systems have potential applications such as small molecule storage and delivery,[108] electrochemical sensors,[109] and catalysis.[110]

Several redox active complexes have been reported in the literature thus far. Many of them used metallocene complexes with or without carbonyl ligands attached to them. Metal carbonyls are useful for monitoring the changes that takes place upon ligand oxidation and reduction due to the fact that M–CO stretches depend on the electron

---

[2] Complex **15** was part of a publication and ACS 2009 presentation: Milum, K. M.; Keskin, S.; Villa, M. I.; Mejia, M. L.; Holliday, B. J. Redox-Mediated Small Molecule Binding in Conducting Metallopolymers. *Abstracts of Papers of the American Chemical Society* **2009,** *238*.
Complex **15** was designed, synthesized, purified and characterized by Seyma Keskin. The rest of the publication included other molecules and measurements which were carried out by the other authors and not included in this dissertation. The principle investigator at the time of the work was Dr. Bradley J. Holliday.

density on the metal center and therefore can be monitored by IR spectroscopy. The carbonyl stretching frequencies for terminally bound carbonyl complexes are typically observed between ~1750–2100 cm^{-1} for electron-rich and electron-poor complexes, respectively. Free carbonmonoxide gas has a stretching frequency at 2143 cm^{-1}.[44]

Wolf *et al*. have carried out extensive research on the development of new materials by synthesizing novel conducting metallopolymers. In one of such studies, metallopolymers with redox active units were prepared in order to change the electron density at the metal center by a function of charge in the conducting polymer backbone. The resulting changes were demonstrated by peak frequencies of CO stretches in the IR spectrum of 4 and 6 cm^{-1} between neutral and oxidized systems.[107] Mirkin *et al*. worked with ruthenium and rhodium complexes and their polymer systems to make electrochemically tunable redox-active ligand systems. They found that the monothiophene rhodium complex was not suitable for redox-active ligand systems, because rhodium was oxidized before the monothiophene, and polymer growth was inhibited. The systems with terthiophene could easily be polymerized. They also reported a ruthenium-terthiophene based polymer with a reversible increase in CO stretching. However, no tunable change was observed, and these systems can utilize thiophene and polythiophene derivatives as redox-active ligand systems.[108, 111, 112] Milum *et al*. reported a conducting metallopolymer based on an electropolymerizable NCN pincer ligand containing platinum and 2,6-dimethylphenyl isocyanide. The amount of electron density on the platinum atom was probed by the isocyanide ligand. The IR stretching frequency was decreased by 9 cm^{-1} upon oxidation of the polymer film thus indicating that the Pt-C σ-bond was weakened due to the withdrawal of electrons from the conducting polymer backbone. They also showed redox attenuated metal–ligand interactions by monitoring with UV-Vis spectroelectrochemistry without the incorporation of a reporter ligand.[60]

Molybdenum-containing hybrid and coordination polymers have been reported to be useful for a variety of applications.[113-121] For example, Boruah *et al*. have reported polymer-anchored peroxo compounds of vanadium(V) and molybdenum(VI) for their activities with alkaline phosphatase (ALP) and catalase.[113] In another example of molybdenum containing polymers, Moreno *et al*., prepared (hydroxypropyl)-2-aminomethyl pyridine containing hybrid polymer–silica SBA-15 materials supporting Mo(VI) centers and they studied it for heterogeneous catalysts for oct-1-ene epoxidation. The materials they prepared displayed high catalytic activity, stability and reusability in the epoxidation of 1-octene with TBHP (tert-butyl hydroperoxide) as oxidant. The presence of mesoporosity in the final Mo(VI) containing hybrid materials improved the catalytic activity of metal centers.[114] Maurya *et al*. also used polymer-anchored hybrid materials of oxovanadium(IV), dioxomolybdenum(VI), and copper(II) complexes of the bidentate ligand 2-(2 -hydroxyphenyl)benzimidazole to investigate their catalytic activities in the oxidation of styrene and ethylbenzene.[115] Schrock and coworkers synthesized polymer-supported chiral Mo-based complexes as efficient catalysts for enantioselective olefin metathesis. They obtained optically enriched products through the use of the supported complexes. The products contained significantly lower levels of metal impurities compared to products synthesized with the corresponding homogeneous catalysts.[116] Shultz and coworkers reported the acyclic diene metathesis (ADMET) polymerization of an organometallic molybdenum-containing diene (*cis* - $Mo(CO)_4(Ph_2P(CH_2)_3CH=CH_2)_2$) and its copolymerization with an organic diene (**Figure 26a**).[117] Kim *et al*. synthesized terthiophenes bearing pendant organomolybdenum complexes and electropolymerized them to obtain electroactive films (**Figure 26b**).[122]

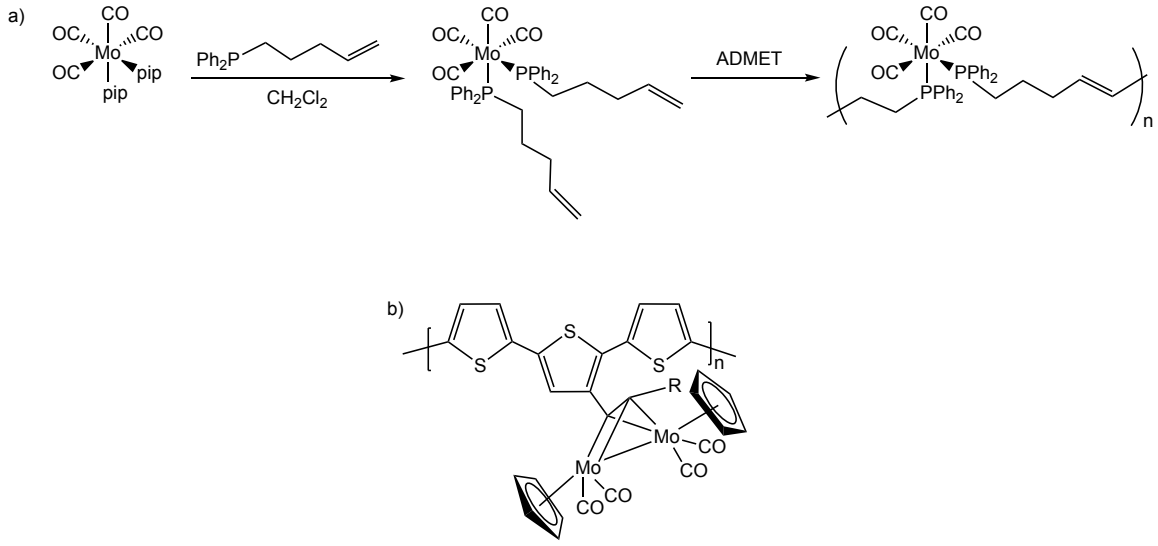

Figure 26. Molybdenum carbonyl-containing polymers.[117,122]

In addition to polymer-anchored molybdenum complexes, a number of coordination polymers of molybdenum have been reported. For example, Chelebaeva *et al*. synthesized one-dimensional cyano-bridged coordination polymers based on the luminescent lanthanide ion Nd^{3+} and the $[Mo(CN)_8]^{3-}$ building block, i.e. $Nd(phen)_n(DMF)_m[M(CN)_8]$ (M = Mo, W). Adjustment of the number of phenanthroline ligands in the coordination sphere of the lanthanide was reached by modulating the experimental conditions. These compounds displayed the Nd^{3+} typical NIR emission enhanced by the presence of the phenanthroline ligand and ferromagnetic interactions between Nd^{3+} and Mo^{3+} ions.[118] Another molybdenum-containing coordination polymer was obtained by Matsumoto *et al*. to study metal-dependent and redox-selective coordination behaviors of the metalloligand [MoV(1,2-benzenedithiolato)$_3$]- with Cu(I)/Ag(I) ions. They found that the complex with copper has a 1-D structure; the complex with silver had a 3-D structure due to additional π-π stacking interactions between adjacent [MoV(bdt)$_3$]- moieties.[119] Zhang *et al*. synthesized a non-interpenetrating 3-D $[MoOS_3Cu_3]$

based coordination polymer and found third-order nonlinear optical properties.[120] Das *et al*. also synthesized a molybdenum containing coordination polymer. They aimed to use the polymer for catalytic applications. Hexahydro-5-oxoquinoline-3-carboxylates and 1,4-dihydropyridine-3,5-dicarboxylates were synthesized efficiently and rapidly (2 minutes) in the presence of molybdenum- and tungsten-based coordination polymers $[M(Bu_3Sn)_2O_4)]_n$ (M = Mo or W) as catalyst. The products were formed at room temperature in excellent yields (90–98%). The catalysts worked under heterogeneous conditions and were recyclable.[121]

The purpose of this study is to synthesize and characterize an electropolymerizable tridentate ligand, and then corresponding molybdenum complexes with carbonyl groups, and electropolymerization of these compounds. Two different M–CO systems are targeted. In the first one, the metal is directly bound to a conjugated polymer backbone through N coordination and makes a Wolf type II[5] conducting metallopolymer. The second one has no bond between the M and N atoms, therefore forming a Wolf type I[5] conducting metallopolymer. The reason for designing two polymers is to determine if the applied potential exerts any control over the carbonyl release in these different types of metallopolymers. In other words, the metal-polymer backbone communication can be evaluated to determine whether it has any effect on carbonyl release.

Electropolymerization is used instead of chemical polymerization. An applied potential electrochemically oxidizes 3,4-ethylenedioxythiophene (EDOT) sites by forming radical cations that couple to form a dication dimer. The dication dimer subsequently becomes a neutral dimer due to the loss of two protons. This process continues until a polymer is deposited at the anode. Electropolymerization is convenient for the bithiophene (BT) or EDOT groups and is preferred, due to the fact that there is no

need to purify the polymer that is formed at the anode and there are no byproducts. After polymerization, the abstraction of electrons from the polymer backbone by electrochemical techniques results in a p-doped (or positively charged) semiconductor for such systems.[3, 11, 60, 104, 123, 124] Conduction in the polymer backbone may cause the metal centers to change in effective charge or may even be in the oxidation state of metal centers. This should result in the small molecule release due to the lack of electrons for the π-backdonation to the metal center. (**Figure 27**)

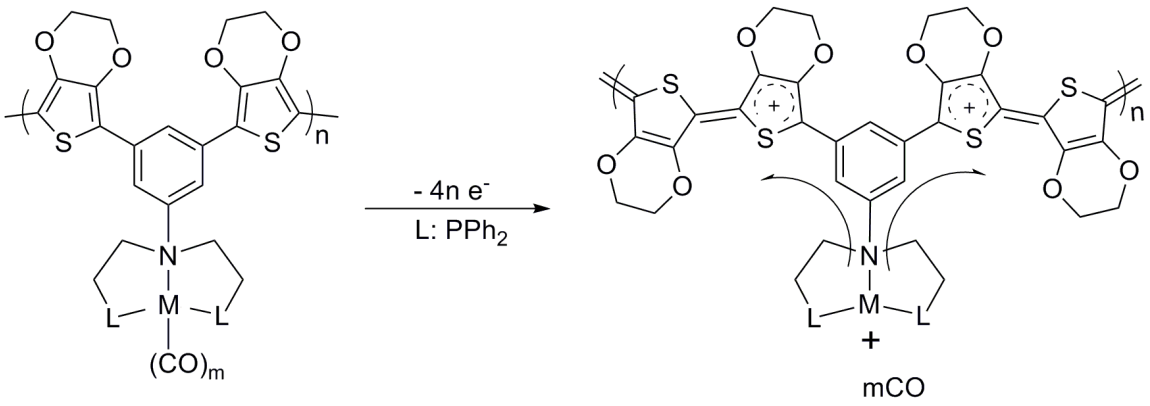

Figure 27. Change in electron density upon oxidation of the polymer.

EXPERIMENTAL

Instrumentation

^{1}H NMR spectra were recorded using a Varian Unity + 300 spectrometer and were referenced to the residual solvent peaks. The ^{31}P{^{1}H} NMR spectra were referenced to a H_3PO_4 external standard. The ^{13}C{^{1}H} NMR spectra were referenced relative to the solvent peaks. All peak positions are listed in ppm, and all coupling constants are listed in Hertz (Hz). Mass spectrometry was carried out using a Waters Autospec Ultima spectrometer

and the IR spectra were recorded with a Nicolet Avatar 330 FT-IR spectrophotometer. The solid state IR measurements were obtained by using an ATR accessory. The solution IR data was recorded using CH_2Cl_2 solutions (~ 10^{-2} M). The X-ray photoelectron spectroscopy (XPS) was carried out on by using a PHI 5700 XPS system that was equipped with dual Mg X-ray sources and a monochromatic Al X-ray source complete with depth profile and angle-resolved capabilities. The elemental analysis was performed by QTI, Whitehouse, NJ. The microwave assisted reaction was performed in a CEM Discover reactor. And all samples were freshly prepared prior to analysis.

X-ray Crystal Structure Analysis

The single–crystal diffraction data were collected on a Rigaku AFC12 diffractometer with a Saturn 724+ CCD, using a graphite monochromator with MoKα radiation (λ = 0.71073Å). All absorption corrections were applied using Multi-scan. The data reductions were performed using a Rigaku Americas Corporation Crystal Clear version 1.40.[125] The structures were solved by direct methods and refined anisotropically using full-matrix least-squares methods with the SHELX 97 program package.[98, 99] The coordinates of the non-hydrogen atoms were refined anisotropically. All the hydrogen atoms were included in the calculations isotropically but not refined. Neutral atom scattering factors and values that were used to calculate the linear absorption coefficient are taken from the International Tables for X-ray Crystallography (1992).[100] The crystal data collection and refinement details are presented in **Table 14** and selected bond lengths are available in **Table 15**.

Electrochemistry

The electrochemical syntheses and scan rate dependence studies were performed by using a GPES system from Eco. Chemie B.V. in a glove box under a nitrogen atmosphere. All electrochemical experiments were carried out in a three-electrode cell with $Ag/AgNO_3$ reference electrode, a Pt working electrode, and a Pt wire coil counter electrode. For the XPS and IR measurements of the polymers, ITO coated glass was used as a working electrode instead of a Pt button. For the reference electrode, an Ag wire was dipped in a 0.01 M $AgNO_3$ solution along with 0.1 M $[(n\text{-}Bu)_4N][PF_6]$ ($TBAPF_6$) in CH_3CN. The measured potentials were relative to the reference electrode and needed to be calibrated by ferrocene as an external reference. The calibrations were carried out before and after the experiments were performed. The average of the ferrocene measurements before and after the electrochemical experiment was calculated and used to correct the measured potentials. A solution of 0.1 M ($TBAPF_6$) in CH_2Cl_2 was used as the electrolyte. However, the $TBAPF_6$ needed to be purified. Hot ethanol was used to recrystallize the $TBAPF_6$ three times following which the white crystals were dried for 3 days approximately at 100-150°C under active vacuum. Polymer films were prepared by using Delta Technologies ITO-coated glass for spectroscopic measurement and for XPS. Electrochemical syntheses of the polymer films were preformed from ~1 x 10^{-3} M monomer solutions by continuous cycling between -1.4 V (or -0.25 V) and 1.5 V at v = 100 mVs^{-1} (potentials are before referencing with ferrocene). The polymer films were washed with dry CH_2Cl_2 in the glove box to remove any monomer or electrolyte left on the films before further experiments.

Synthesis

General Methods

All chemicals were purchased from commercial suppliers and were used as received. Dry solvents were obtained from an Innovative Technologies Pure-Solv 400 solvent purification system. The air- and moisture-sensitive reactions were carried out in oven-dried glassware using standard Schlenk techniques under an inert nitrogen atmosphere or in a glove box with an argon atmosphere. The syntheses of *fac*-$EDOT_2PNP\text{-}Mo(CO)_3$ **9** and *cis*-$EDOT_2PNP\text{-}Mo(CO)_4$ **10** were achieved by techniques similar to those used by Blower[102] and Ainscough.[90] The 2-(tributylstannyl)-3,4-(ethylenedioxy)thiophene was prepared by using the method described by Swager *et al*.[126]

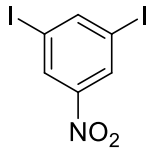

1-nitro-3,5-diiodobenzene [7]. 2,6-diiodo-4-nitroaniline (7g, 17.95 mmol) was dissolved in H_2SO_4 (98%, 27 ml) at 0 °C by adding small portions. After the dissolution was complete, $NaNO_2$ (2.693 g) was added to the solution in a portionwise fashion. After all of $NaNO_2$ had been added, the resulting mixture was stirred for 2 hours at 0 °C. A dark, viscous solution was obtained and then it was poured over crushed ice (180 g) which was being stirred. A burnt orange precipitate was generated and then it was filtered off. The filtrate was carefully added to the refluxed solution of $CuSO_4.5H_2O$ (0.6825 g) in C_2H_5OH (360 ml) and heated to 90 °C, then stirred at that temperature for 2 hours. The resulting mixture was cooled to 0 °C in order to promote precipitation. The precipitate was then collected by vacuum filtration and washed three times with a C_2H_5OH/H_2O (1:1) mixture (50 ml total). The product was dried under vacuum (65%, 4.374 g, 11.67 mmol). ^1H NMR

(300 MHz, $CDCl_3$): δ = 8.354 (t, *J* = 1.2 Hz, 1H), 8.499 (d, *J* = 1.2 Hz, 2H). The purity and composition was then confirmed by comparing the ^1H NMR data with those of the literature values.[127]

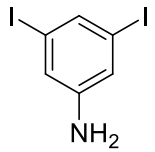

3,5-diiodoaniline [8]. $SnCl_2.2H_2O$ (15.1734 g) was added to a suspension of 1-nitro-3,5-diiodobenzene **7** (5g, 13.34 mmol) in C_2H_5OH (80 ml). The resulting mixture was then boiled, and a solution of $NaBH_4$ in C_2H_5OH was added dropwise. The reaction mixture was refluxed for 30 minutes, following which it was cooled to room temperature and quenched with H_2O, then neutralized with NaOH (aq). An intense white precipitate resulted and the mixture was extracted with CH_2Cl_2 three times. The organic phases were combined, dried over $MgSO_4$, and vacuum filtered, and the filtrate was evaporated to afford a cream-colored solid. The product was further dried under vacuum (88 %, 4.048 g, 11.736 mmol). ^1H NMR (300 MHz, $CDCl_3$): δ = 7.376 (t, *J* = 1.5 Hz, 1H), 6.96 (d, *J* = 1.5 Hz, 2H), 3.651 (broad s, 2H). The ^1H NMR data are consistent with the literature values.[128]

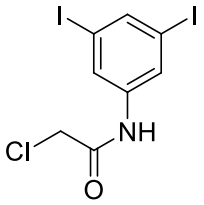

2-chloro-N-(3,5-diiodophenyl)-acetamide [9]. 3,5-diiodoaniline **8** (4.17 g, 12.09 mmol) and $N(C_2H_5)_3$ (8.7 ml) were dissolved in dry CH_2Cl_2 (130 ml) and cooled to 0 °C. Chloroacetylchloride (4.85 ml) solution in dry CH_2Cl_2 (120 ml) was added dropwise into

the mixture while stirring at that temperature. The resulting mixture was stirred overnight at room temperature and the solvent was then evaporated. The residue was redissolved in $CH_3COOC_2H_5$ and extracted with H_2O three times. The organic phase was dried over $MgSO_4$, then vacuum filtered, and the filtrate was evaporated. The residue was purified by using a silica-gel column in which the eluent was CH_2Cl_2. The resulting product was then collected as a white solid (90%, 4.5852g, 10.88 mmol). ^{1}H NMR (300 MHz, $CDCl_3$): δ = 7.9035 (d, *J* = 1.5 Hz, 2H), 7.837 (t, *J* = 1.5 Hz, 1H), 4.159 (s, 2H).

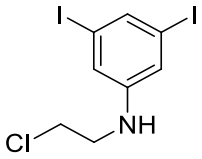

N-(2-chloroethyl)-3,5-diiodophenylamine [10]. 2-chloro-N-(3,5-diiodophenyl)-acetamide **9** (3.0855 g, 7.322 mmol) was dissolved in dry THF (250 ml) and then cooled down to 0 °C. The BH_3:THF (1M) (115 ml) reagent was added dropwise while the mixture was stirred at that temperature. After all the BH_3:THF had been added, the mixture was allowed to warm to room temperature and then stirred overnight. The product was monitored by TLC. The reaction mixture was quenched with CH_3OH that was added dropwise. The solvent was then evaporated and the oily residue was purified by using a silica-gel column in which the eluent was CH_2Cl_2/Hexanes (1:1). The product was then collected as a yellow oil (68%, 2.0285 g, 4.979 mmol). ^{1}H NMR (300 MHz, $CDCl_3$): δ = 7.360 (t, *J* = 1.5 Hz, 1H), 6.8905 (d, *J* = 1.5 Hz, 2H), 4.079 (broad s, 1H), 3.662 (m, 2H), 3.418 (m, 2H).

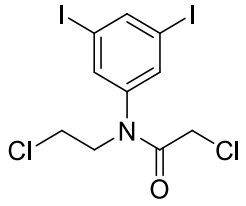

N-(2-chloroethyl)-(3,5-diiodophenyl)-2'-chloroacetamide [11]. N-(2-chloroethyl)-3,5-diiodophenylamine **10** (2.6187 g, 6.428 mmol) and $N(C_2H_5)_3$ (4.57 ml) were dissolved in dry CH_2Cl_2 (130 ml) and cooled to 0 °C. A chloroacetylchloride (2.60 ml) solution in dry CH_2Cl_2 (120 ml) was then added dropwise to the mixture while it was stirred at that temperature. The resulting mixture was allowed to warm to room temperature and stirred overnight. Formation of the product was checked with TLC. Some silica gel was added directly to the reaction mixture, and the solvent was evaporated to adsorb the product on silica gel. The product was purified by a silica-gel column in which the eluent was CH_2Cl_2/Hexanes (5:1). The product was then obtained as a brown viscous oil (90%, 2.794 g, 5.774 mmol). ^{1}H NMR (300 MHz, $CDCl_3$): δ = 8.104 (t, *J* = 1.5 Hz, 1H), 7.6425 (d, *J* = 1.5Hz, 2H), 3.973 (t, *J* = 6Hz, 2H), 3.826 (s, 2H), 3.652 (t, *J* = 6Hz, 2H).

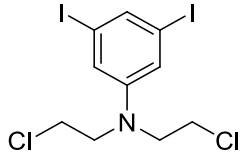

N,N-bis-[2-chloroethyl]-3,5-diiodo-phenylamine [12]. N-(2-chloroethyl)-(3,5-diiodophenyl)-2'-chloroacetamide **11** (3 g, 6.2 mmol) was dissolved in dry THF (250 ml) and cooled to 0 °C. The BH_3:THF (1M) (100 ml) reagent was added dropwise while the mixture was stirred at that temperature. After all the BH_3:THF had been added, the mixture was allowed to warm to room temperature and stirred overnight. The product was monitored by TLC. The reaction mixture was quenched with CH_3OH that was added dropwise. The solvent was evaporated, and the oily residue was purified by using a silica-

gel column in which the eluent was Hexanes/CH_2Cl_2 (3:1). The product was obtained as a crop of white crystals (69%, 2.0102 g, 4.278 mmol). ^{1}H NMR (300 MHz, $CDCl_3$): δ = 7.403 (t, J = 0.9 Hz, 1H), 6.9155 (d, J = 0.9Hz, 2H), 3.632 (symmetric multiplet, 8H). This compound had been reported previously, but only on the basis of elemental analysis data.[129] The ^{1}H NMR data are being reported for the first time in the present study.

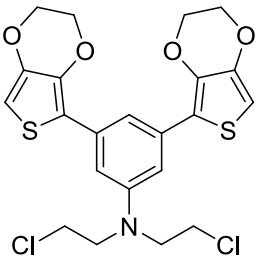

N,N-bis-(2-chloroethyl)-3,5-bis-(3,4-ethylenedioxythien-2-yl)-phenylamine [13]. N,N-bis-[2-chloroethyl]-3,5-diiodo-phenylamine **12** (47.9 mg, 0.102 mmol), $PdCl_2(PPh_3)_2$ (3.7 mg, 0.005271 mmol), and 5-tributylstannyl-EDOT (132.9 mg, 0.3082 mmol) were placed in a microwave reactor tube (8 ml tube) along with a small stirring bar. The tube was then sealed, and 4 ml of dry DMF was transferred by a cannula. The mixture was then sparged with Ar gas for approximately 5 minutes. The reaction mixture was placed in the reactor and irradiated with microwaves for 45 min at 105 $^\circ$C. After the reaction was complete, CH_2Cl_2 was added to the reaction mixture. The organic phase was extracted with saturated NH_4Cl solution three times. The organic phase was then dried over $MgSO_4$ and vacuum filtered, and the filtrate was evaporated. The residue was redissolved in $CH_3COOC_2H_5$ (~50 ml), and 40 ml of 10% KF solution was added. After approximately 1 hour of stirring, the precipitate was filtered off. The filtrate was then transferred into a separatory funnel, and the aqueous phase was separated. The organic phase was washed twice with fresh H_2O, then dried over $MgSO_4$, vacuum filtered, and the filtrate was evaporated. The residue was purified by using a silica gel column in which the eluent was CH_2Cl_2/Hexanes

(1:1) to afford a yellow solid (52%, 26.42 mg, 0.053 mmol). ^{1}H NMR (300 MHz, $CDCl_3$): δ = 7.269 (t, *J* = 1.2Hz, 1H), 7.012 (d, *J* = 1.2Hz, 2H), 6.286 (s, aromatic 2Hs of EDOT), 4.266 (symmetric m, 8Hs of EDOT), 3.714 (symmetric m, 8Hs of ethyl chloride group).

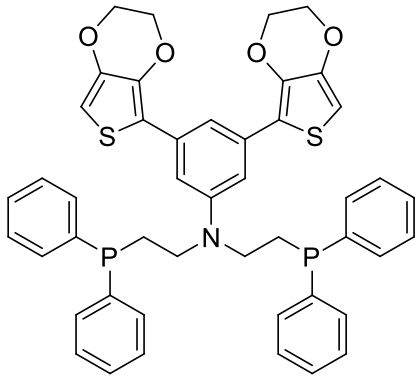

N,N-bis-[2-diphenylphosphinoethyl]-3,5-bis-(3,4-ethylenedioxythien-2-yl)-phenylamine [14] (EDOT$_2$PNP). N,N-bis-(2-chloroethyl)-3,5-bis-(3,4-ethylenedioxythien-2-yl)-phenylamine **13** (100 mg, 0.201 mmol) was dissolved in dry THF in a Schlenk flask under a Schlenk line. 3.25 mL of 0.5M $KPPh_2$ was added via a glass syringe under N_2. The resulting orange mixture was stirred for an hour. The mixture was then taken into the glove box, and filtered through a frit in which there were layers of celite/silica gel/celite. The filtrate was then collected into another Schlenk flask, and the solvent was evaporated under the Schlenk line. The residue was transferred back into the glove box where it was dissolved in a minimal amount of CH_2Cl_2, and then a copious amount of hexanes was layered. The Schlenk flask was placed into the freezer (-30 °C) to precipitate the product for a week. The resulting precipitate was decanted, washed with diethyl ether, and dried under the Schlenk line to afford a yellow product (76%, 121.66 mg, 0.152 mmol): mp 66.7°C; ^{1}H NMR (300 MHz, $CDCl_3$): δ = 7.43-7.30 (m, 20H), 7.26 (s, 1H), 6.91 (s, 2H), 6.30 (d, 2H, *J* = 2.1 Hz), 4.21 (s, 8H), 3.42 (dt, 4H, J_d = 8.1 Hz, J_t = 7.5 Hz), 2.39 (t, 4H, *J* = 8.7 Hz). ^{31}P{^{1}H} NMR (121 MHz, $CDCl_3$): δ = -18.11 (s). ^{13}C{^{1}H}

NMR (75 MHz, CD_2Cl_2): δ = 147.63 (s), 142.68 (s), 138.79 (s), 138.62 (s), 134.49 (s), 132.94 (d, *J* = 18.6 Hz), 128.91 (t, *J* = 6.83 Hz), 118.90 (s), 112.91 (s), 109.77 (s), 97.64 (s), 97.54 (s), 65.03 (d, *J* = 18.075 Hz), 48.75 (d, *J* = 25.125 Hz), 26.27 (d, *J* = 14.775 Hz), 15.49 (s). HRMS (CI^+) calculated for $[M+H]^+$ as 798.2, and found to be 798.2022.

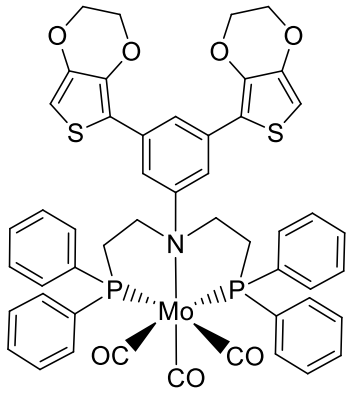

3,5-bis-(3,4-ethylenedioxythien-2-yl)-N,N-bis-[2-diphenylphosphinoethyl]-phenylamine-tricarbonylmolybdenum [15] ($EDOT_2PNP$-$Mo(CO)_3$). 14 (50 mg, 0.0627 mmol) was dissolved in dry THF/CH_2Cl_2 (3:1) in a glove box. CHT-$Mo(CO)_3$ (17 mg, 0.0625 mmol) was added to the solution and stirred overnight. The solvent was then evaporated under a Schlenk line. The residue was then dissolved in CH_2Cl_2 (filtered through alumina prior to use, in order to get rid of HCl that had formed in the solution) in the glove box, and hexanes were added to precipitate the product. The precipitate was then collected and dried (63%, 38.6 mg, 0.0395 mmol): mp 172-175°C (decomposed); $^{31}P\{^1H\}$ NMR (121 MHz, CD_2Cl_2): δ = 39.75 (s); ^1H NMR (300 MHz, CD_2Cl_2): δ = 7.49–7.36 (m, 21 H), 6.98 (s, 2H), 6.30 (s, 2H), 4.26 - 4.18 (m, 8H), 3.63 (bs, 4H), 2.81 (bs, 4H); HRMS (ESI) calculated for 979.09 and found to be 979.078. Both the solution state and the solid state IR data were obtained. Solid state IR (ATR): 1926 cm^{-1}, 1832 cm^{-1}, 1799 cm^{-1}. Solution state IR (solution in CH_2Cl_2): 1936 cm^{-1}, 1834 cm^{-1}, 1793 cm^{-1}. The

Raman Spectrum could not be obtained because it resulted in fluorescence of the complex. However, the crystal structure was obtained and will be discussed in the next section.

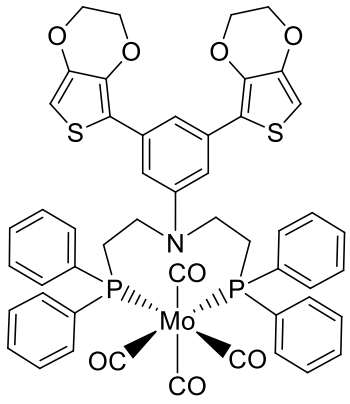

3,5-bis-(3,4-ethylenedioxythien-2-yl)-N,N-bis-[2-diphenylphosphinoethyl]-phenylamine-tetracarbonylmolybdenum [16] (EDOT$_2$PNP-Mo(CO)$_4$). 14 (49 mg, 0.0614 mmol) was dissolved in dry CH_2Cl_2 in a glove box. NBD-Mo(CO)$_4$ was dissolved in dry THF, and the metal solution was added to the ligand solution, and the resulting mixture was stirred overnight in a glove box. The solvent was then evaporated under a Schlenk line. The residue was transferred back into the glove box, where it was redissolved by using a minimal amount of CH_2Cl_2 (filtered through alumina prior to use, in order to get rid of any HCl that had formed in the solution). The hexanes were then layered on the solution in order to precipitate the product. The resulting precipitate was collected by celite filtration, then redissolved by using CH_2Cl_2. The resulting solution was then collected in a Schlenk flask. The solvent was evaporated to afford a yellow solid (68%, 61.8 mg, 0.0614mmol): mp 185-187 ^{o}C (decomposed); $^{31}P\{^{1}H\}$ NMR (121 MHz, CD_2Cl_2): δ = 22.92 (s); ^{1}H NMR (300 MHz, CD_2Cl_2): δ = 7.52 – 7.35 (m, 20 H), 7.27 (s, 1H), 6.63 (s, 2H), 6.31 (s, 2H), 4.26 - 4.21 (m, 8H), 3.51 (d, 4H, *J* = 10.2 Hz), 2.74 (bs,

4H). HRMS (ESI) calculated for 1005.08 and found to be 1005.88. Both the solution state and the solid state IR data were obtained. Solid state IR (ATR): 2030 cm^{-1}, 1900 cm^{-1} (broad, combination of 3 peaks). Solution state IR (solution in CH_2Cl_2): 2018 cm^{-1}, 1945 cm^{-1} (shoulder), 1921 cm^{-1} (the peaks at 1945 and 1921 cm^{-1} were combined as a broad peak with shoulder), 1897 cm^{-1}. The Raman Spectra could not be obtained due to the fact that it resulted in fluorescence of the complex.

RESULTS AND DISCUSSION

Synthesis

A PNP ligand with polymerizable EDOT groups has been synthesized by means of an eight-step organic synthesis in which four of the organic compounds (**10**, **11**, **13** and **14**) are new (**Scheme 3**). The ligand **14** was then allowed to react with CHT-$Mo(CO)_3$ and NBD-$Mo(CO)_4$ to obtain the corresponding metal complexes as monomers in which molybdenum tricarbonyl and tetracarbonyl are bound to the PNP ligand in *facial* and *cis* fashions respectively (**Scheme 4**). The monomer metal complexes **15** and **16** were characterized by solid state IR (ATR), solution state IR, ^1H, $^{31}P\{^1H\}$ NMR spectra and HRMS. The crystal structure data for only one complex (**15**) was obtained. The ^1H NMR data for **12** is being reported in the present study while the elemental analysis was reported previously.[129]

Scheme 3. Reagents and conditions: (a) i. $NaNO_2$, H_2SO_4, 0 °C, 2 hours ii. $CuSO_4$•$5H_2O$, EtOH, reflux, 2 hours (b) $SnCl_2$•$2H_2O$, $NaBH_4$, EtOH, reflux, 30 min (c) Chloroacetylchloride, NEt_3, CH_2Cl_2, 0°C→RT, 12 hours (d) BH_3:THF, 0°C→RT, 12 hours (e) Chloroacetylchloride, NEt_3, CH_2Cl_2, 0°C→RT, 12 hours (f) BH_3:THF, 0°C→RT, 12 hours; (g) 5-($SnBu_3$)-EDOT, $PdCl_2(PPh_3)_2$, DMF, 105°C microwave, 45 min (h) $KPPh_2$, THF, RT, 1 hour.

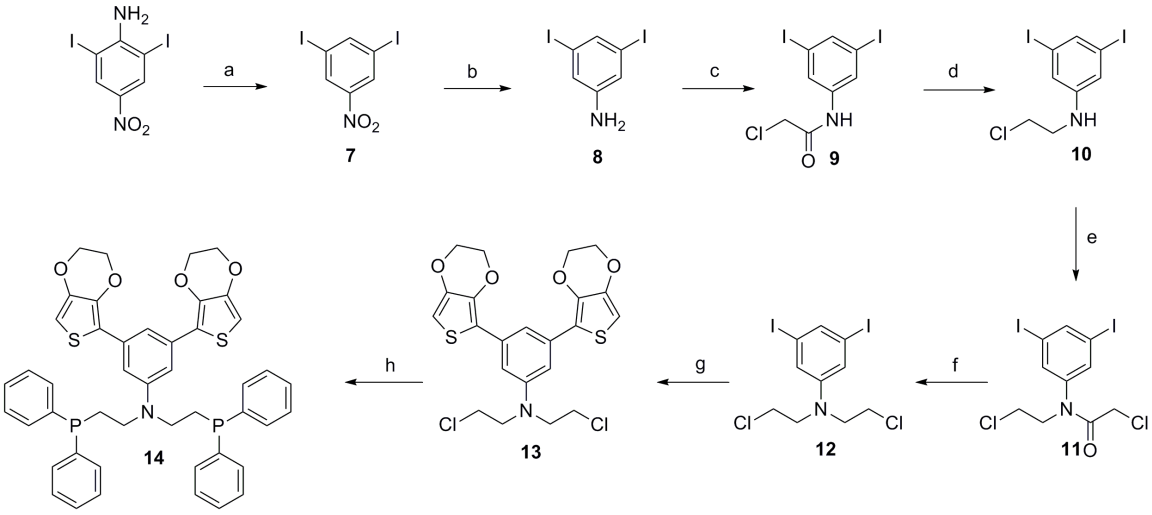

Scheme 4. Synthesis of $EDOT_2PNP$-$Mo(CO)_{3-4}$ complexes.

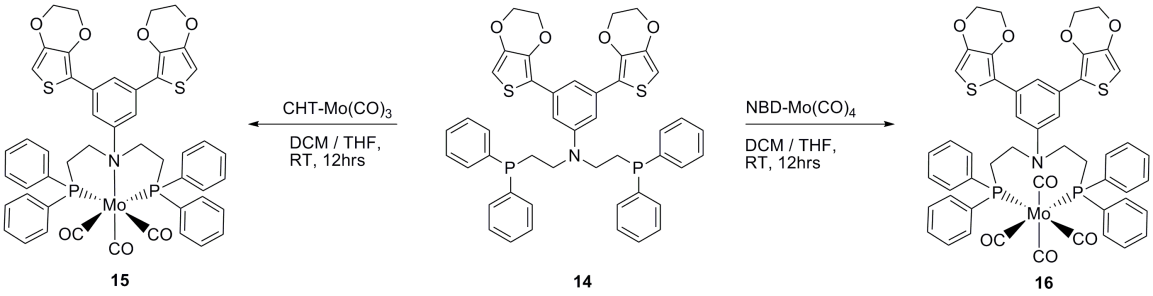

Spectroscopic Properties of Monomer Complexes

Complexes **15** and **16** are soluble in CH_2Cl_2 and the solution and solid state IR data were obtained. However, the Raman spectra could not be measured due to the fact

that the Raman beam caused sample fluorescence. The point group of complex **15** was identified as C_s based on its crystal structure (**Figure 29**). The crystal structure of compound **16** could not be obtained. Nevertheless, te point group of **16** was identified as C_s by comparison with complex **5** (**5** is in chapter 2). Based on the point group C_s, group theory calculations of CO stretches for the complexes resulted as follows: $\Gamma = 3A' + A''$ for complex **16** and $\Gamma = 2A' + A''$ for complex **15**. All bands were found to be both Raman and IR active and coincident.

Both the solid state and the solution state IR spectra of **15** resulted in three bands as expected from the calculation. However, there was an additional small peak at 2018 cm^{-1} and a shoulder at 1900 cm^{-1}; these values may come from the other parts of the molecule (non-carbonyl stretches) (**Figure 28a**). The solid state IR spectra of complex **16** revealed two bands (one of which was broad) in the measurements. On the other hand, the calculation predicted four stretches. The broad peak at 1900 cm^{-1} must be a combination of three peaks (**Figure 28b**). The solution state IR spectrum of **16** resuted in three stretches (2018 to 1897 cm^{-1}), and peaks were shifted in comparison with the solid state IR (2030 to 1900 cm^{-1}). The solution state IR of the complex **15** revealed three peaks (1936 to 1793 cm^{-1}). However, there was also a shift compared with that of the solid state data (1925 to 1798 cm^{-1}).

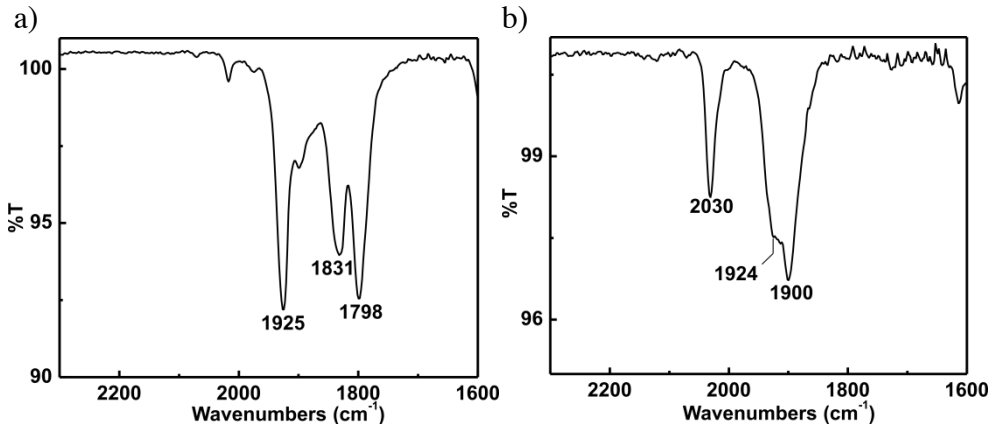

Figure 28. (a) ATR-IR spectra for monomer complex **15** (b) ATR-IR spectra for monomer complex **16**.

Structure of Complex 15

The solid state structure of monomer **15** was determined by single crystal X-ray diffraction analysis, and the resulting ORTEP representation can be seen in **Figure 29**. The crystallographic and structural refinement data are presented in **Table 13**; selected bond lengths and angles are listed in **Table 14.** The single crystals for X-ray diffraction measurement were grown by the slow diffusion of hexanes into a saturated solution of **15** in CH_2Cl_2. The coordination environment around the metal center was defined by two phosphorus and one nitrogen atom from the $EDOT_2PNP$ ligand and by three carbon atoms from the CO ligands. The carbonyl ligands adopted a *facial* arrangement, and phosphorus atoms were arranged in a *cis* fashion. The geometry around the molybdenum is slightly distorted from *octahedral*, having Mo–P and Mo–CO distances that are consistent with those of similar complex in the literature.[87] Due to the fact that the literature compound is a tetracarbonyl complex, carbonyls *trans* to phosphorus atoms are consistent with complex **15**. The other two carbonyls of the literature complex have longer M–C bonds

than **15**, due to the *trans* effect, and carbonyls *trans* to each other have poor π–backdonation.

Table 13. Crystal data and structure refinement for **15**.

CCDC	1547021
Formula	$C_{49}H_{41}NO_7P_2MoS_2$
FW	977.83
T (K)	100(2)
Crystal system	Triclinic
Space group	*P-1*
a (Å)	8.731(5)
b (Å)	10.333(6)
c (Å)	24.709(2)
α (deg)	84.016(2)
β (deg)	87.196(2)
γ (deg)	77.568(3)
V (Å^3)	2164.2(17)
Z	2
ρ (g/cm^3)	1.500
μ (mm^{-1})	0.53
F(000)	1004
Crystal size (mm)	0.16 × 0.07 × 0.07
θ (deg)	3.0 to 27.5
Index ranges	$-10 \leq h \leq 9$ $-12 \leq k \leq 11$ $-29 \leq l \leq 29$
Absorption correction	Multi-scan
Max. and min. transmission	1.000 and 0.453
GOF on F2	1.02
R1, R2 [I > 2σ (I)]	0.1061, 0.2184
R1, R2 (all data)	0.2003, 0.2781
Largest diff. peak and hole (e.Å^{-3})	0.89 and -1.01

Table 14. Selected bond lengths (Å) and angles (deg) of **15**.

Bond Lengths (Å)	
Mo – C(1)	1.910(10)
Mo – C(2)	1.990(10)
Mo – C(3)	1.980(10)
Mo – N	2.512(9)
Mo – P(1)	2.501(3)
Mo – P(2)	2.515(3)
Bond Angles (°)	
C(1) – Mo – C(2)	88.3(5)
C(1) – Mo – C(3)	90.1(5)
C(1) – Mo – N	170.6(4)
C(1) – Mo – P(1)	93.8(4)
C(1) – Mo – P(2)	97.9(4)
C(2) – Mo – C(3)	83.5(5)
C(2) – Mo – N	96.0(4)
C(2) – Mo – P(1)	88.3(4)
C(2) – Mo – P(2)	172.6(4)
C(3) – Mo – N	98.7(4)
C(3) – Mo – P(1)	170.9(4)
C(3) – Mo – P(2)	92.4(4)
N – Mo – P(1)	78.0(2)
N – Mo – P(2)	78.5(2)
P(1) – Mo – P(2)	95.2(1)
O(1) – C(1) – Mo	179(1)
O(2) – C(2) – Mo	173(1)
O(3) – C(3) – Mo	175(1)

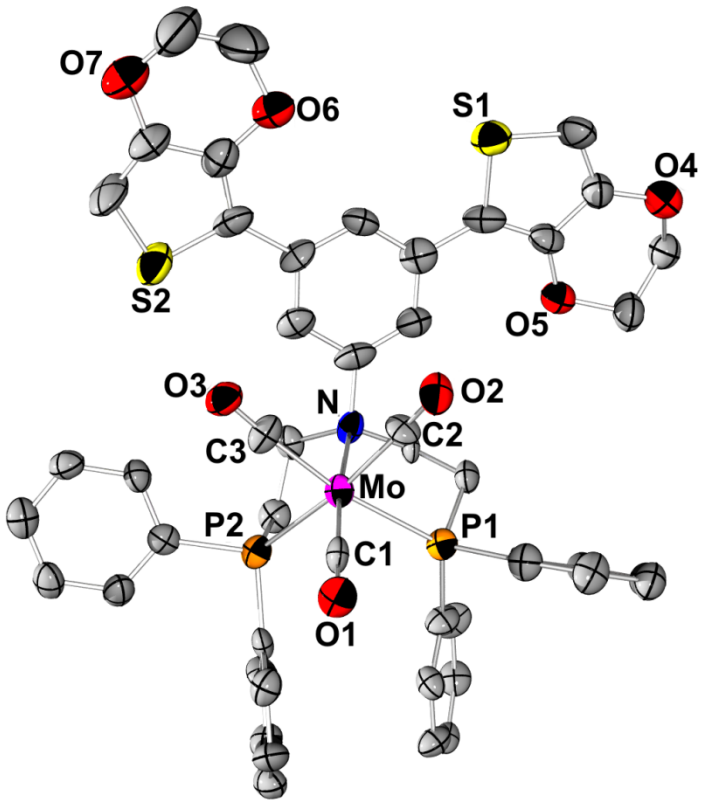

Figure 29. The crystal structure of **15** showing the labeling of selected atoms. The hydrogen atoms were omitted for clarity and the displacement ellipsoids were scaled to the 50% probability level.

Electrochemistry and Electropolymerization

The monomers **14**, **15**, and **16** were electropolymerized to form **poly-14**, **poly-15**, and **poly-16** on a working electrode, which is a platinum button, in order to obtain the corresponding polymerization profiles. The electropolymerization process was carried out by applying a potential throughout the solution containing the electrolyte (0.1M $TBAPF_6$ in CH_2Cl_2) and the monomers. The polymers are reddish-brown in color. Growth of a polymer film in all three monomers is indicated by a sequential growth in current.[3, 130] The polymerization profiles and the scan rate dependence of the polymerization

processes, which are very similar to each other, are illustrated in **Figures 30-32**. First scans are shown in red; all other scans are black in the graphs. Insets of **Figures 30-32** of polymerization profiles demonstrates a linear relationship between the current and the number of scans during polymerization. **Poly-14** indicates a uniform growth of the polymer up to 14 scans, after which the graph levels off. However, **Poly-15** and **poly-16** indicate a uniform growth up to 20 scans.

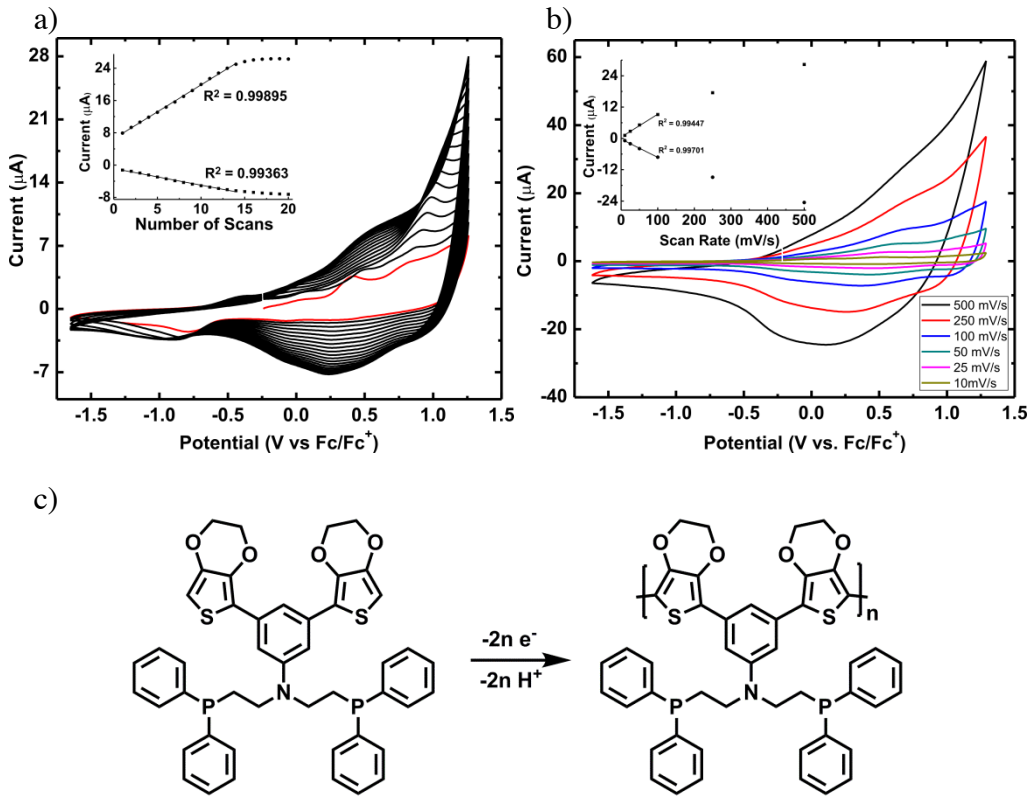

Figure 30. (a) Polymerization profile (b) scan rate dependence c) polymerization process for **poly-14**.

The first scan in the polymerization of ligand **14** started with an oxidation at 0.41 V and 0.81V whose positions became more positive with increasing scans. Reduction

occurs at 0.25 V (**Figure 30a**). Kvarnstrom *et al*. reported oxidation of EDOT as 1.1 V vs. Ag/AgCl. Therefore, the peak at 0.81 V may belong to monomer oxidation.[130]

The first scan of **15** started with an oxidation peak at around -0.07 V and 0.43 V (**Figure 31a**). The peak at 0.43 V became progressively more positive in subsequent scans. An irreversible reduction took place at around -0.85 V.

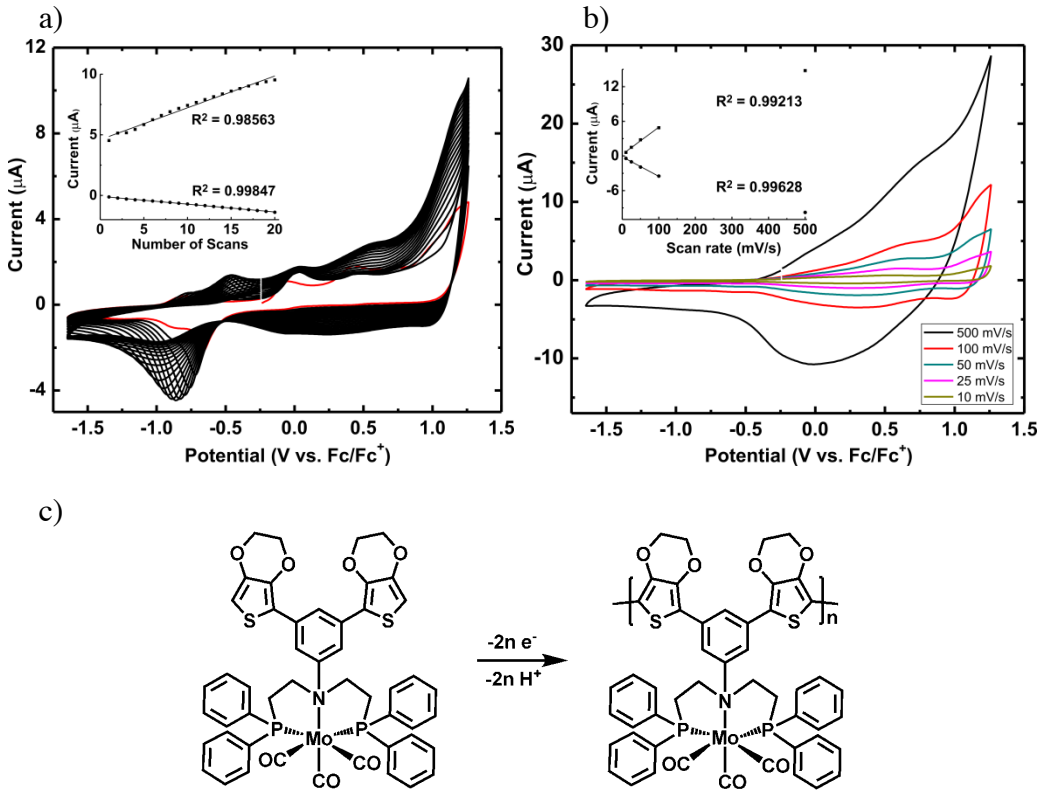

Figure 31. (a) Polymerization profile (b) scan rate dependence (c) polymerization process for **poly-15**.

First scan of **16** started with an oxidation peak at around 0.1 V, 0.43 V, and 0.73 V (**Figure 32a**). The latter two peaks were not observed in subsequent scans. However, a new peak appeared in the second scan at 1 V and became progressively more positive in

the following scans, most likely due to polymer oxidation. When compared with the electropolymerization of **15**, that peak is significantly clearer than that found in electropolymerization of **16**. An irreversible reduction occurred at approximately -0.85 V in the electropolymerization process of **16** similar to that of the electropolymerization process of **15**.

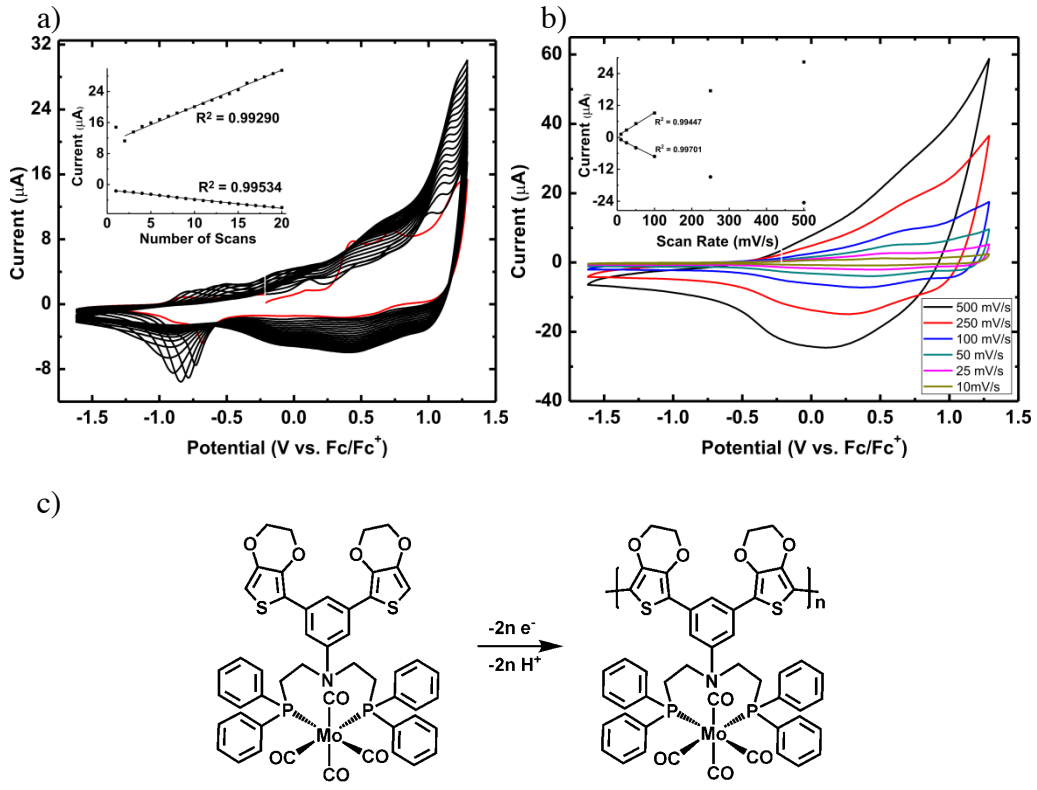

Figure 32. (a) Polymerization profile (b) scan rate dependence (c) polymerization process for **poly-16**.

15 and **16** were polymerized on different surfaces such as ITO to detect the carbonyl stretches in their IR Spectra. A variety of IR techniques have been used for that purpose. However, none of the polymers have shown CO stretches in any of the IR methods that were used. One can find the detailed discussion in the section of

Spectroscopic Properties of Polymers. An irreversible reduction at approximately -0.85 V can be seen for both **poly-15** and **poly-16** in **Figures 31** and **32**. In order to determine whether the carbonyl losses were due to the reduction around -0.85 V, an electropolymerization was performed in a narrower voltage window (~ -0.55 - +1.25V) by using complex **15** (**Figure 33**). Subsequent measurements indicated no carbonyl stretches in the IR spectra of the corresponding polymer. Evidently, the reduction occurred at approximately -0.85 V was not the reason of the loss of carbonyl groups because the reduction was not in the voltage window (**Figure 30**).

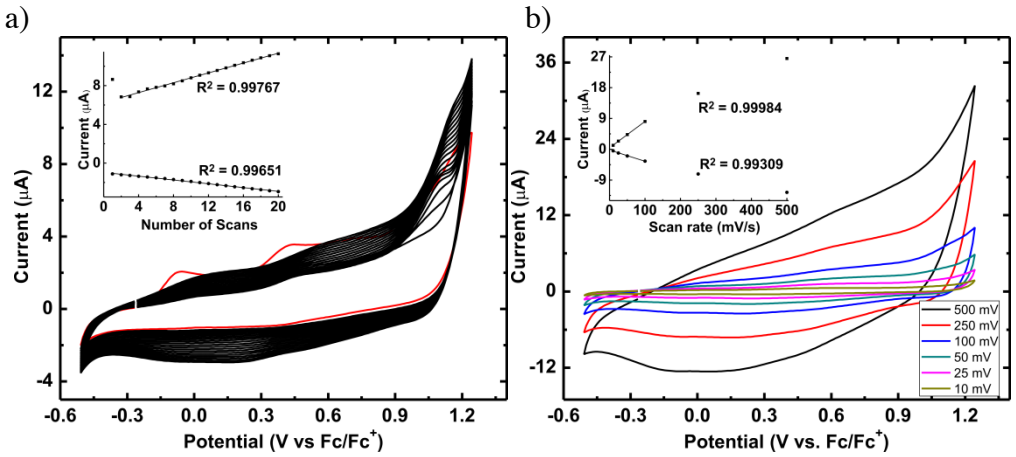

Figure 33. (a) Polymerization profile (b) scan rate of **poly-15** in a narrow window.

The reason for the carbonyl loss was further investigated. The polymerizations of complexes **15** and **16** were carried out in $TBAPF_6$. In some cases, the presence of PF_6^- causes HF production in the electrochemistry solution,[131] and the complexes are most likely to be unstable in the acidic media. As a consequence, the polymerization of **15** was also attempted in $TBAClO_4$. Surprisingly, however, the monomer did not polymerize as indicated by a decrease in the initial current. A brown residue was observed on the ITO-

coated glass working electrode and $(ClO_4)^-$ may be the cause of the dissociation of **15**. The residue was analyzed with XPS (**Figure 32e**) which indicated that the molybdenum was partially oxidized.

The CV data for the non-polymerizable model complex PNP-$Mo(CO)_3$ were obtained in order to find the Mo^0/Mo^{n+} oxidation potential (**Figure 34**). These data were compared with those of similar complexes in the literature to determine if the oxidation potential of Mo^0/Mo^{n+} falls in the polymerization window and could therefore cause the carbonyl loss. The Mo^0/Mo^+ oxidation was found to be -0.116 V, within the CV window for the polymerization (-1.65 to +1.29V vs Fc/Fc^+ in **Figure 31** and also -0.51 to 1.24V vs Fc/Fc^+ in **Figure 33**), and the literature value for that of a similar complex is 0.04 V.[132] Oxidation of Mo^0 might therefore play a role in the carbonyl loss during the electropolymerization.

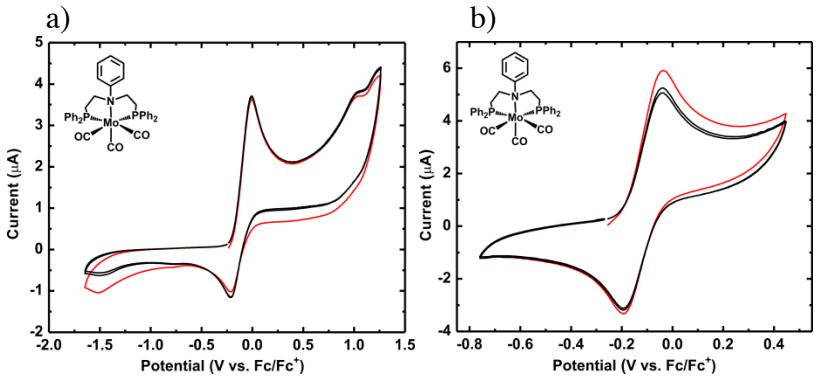

Figure 34. CV data for the model complex PNP-$Mo(CO)_3$.

Characterization of Polymers

XPS and scan-rate dependence were the characterization techniques that were used for the metallopolymers. The XPS data were used to determine the elemental composition of the polymer through survey scans of the film. The polymers were deposited on ITO surfaces for the XPS studies. Quantitative XPS analysis of **poly-15** indicated that the film has an atomic ratio of molybdenum:sulfur = 1:2.309 and molybdenum:phosphorus = 1:2.049, consistent with the stoichiometric molar ratio proposed for the film structure, 1:2. However, the molybdenum:nitrogen ratio found to be 1:4.13, inconsistent with the proposed ratio of 1:1. The extra nitrogen atoms most likely come from the electrolyte, which contained the tetrabutylammonium (TBA) cation, although the polymers were rinsed with CH_2Cl_2 after the polymerization process. Some TBA^+ must have remained in the polymer and is inaccessible to the rinsing solvent. Quantitative XPS analysis of **poly-16** indicated that the film has an atomic ratio of molybdenum:sulfur = 1:2.367 and molybdenum:phosphorus = 1:2.272, consistent with the stoichiometric molar ratio proposed for the film structure, 1:2. The molybdenum:nitrogen ratio found to be 1:1.728, also higher than the proposed ratio of 1:1.

The oxidation states of the molybdenum atoms in both monomers and polymers were determined by high resolution XPS and peak extrapolation of the data (**Figure 35**). Monomers have a zero oxidation state, and polymers are mostly oxidized to +6.[133]

The scan rate dependence is quite linear up to 100 mV for both of the polymerization processes, thus indicating that a strongly adsorbed electroactive material is not limited by the ionic flux of the counter ions. This arises because there is a decrease in the charge mobility through the polymer backbone at higher scan rates, less facile ion transport and a deviation from the linear relationship occurs.

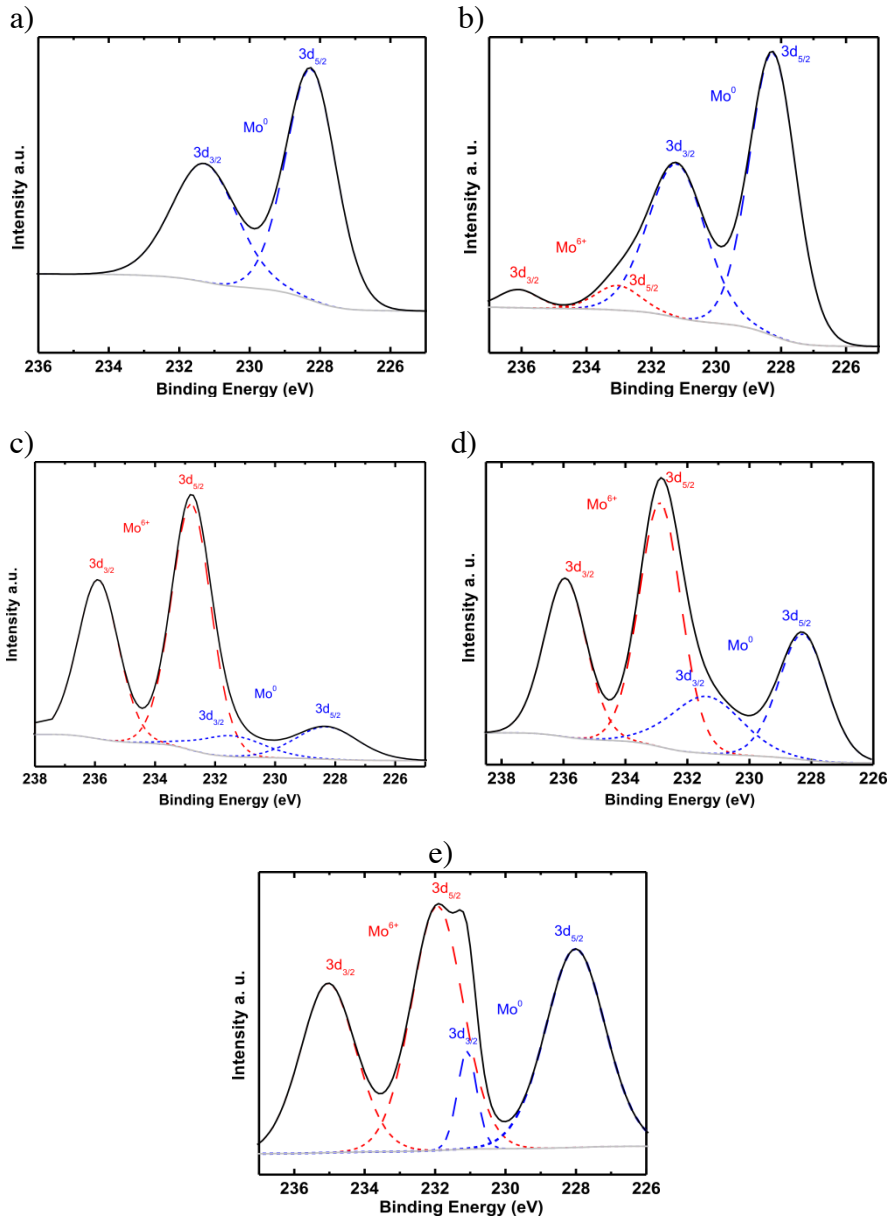

Figure 35. High resolution XPS data (solid line) and peak fitting technique (dashed and dotted lines). (a) **15** (b) **16** (c) **poly-15** (d) **poly 16** (e) attempt to make **poly 15** in $TBAClO_4$.

Spectroscopic Properties of Polymers

In order to measure the carbonyl stretches in the polymers, a variety of IR spectroscopic methods was employed. The complex could be polymerized by using $TBAPF_6$ as the electrolyte, on different surfaces such as Au-Cr on glass (for specular reflectance IR), Au-Ag-In_2O_3 on plastic (for ATR-IR), and indium tin oxide (ITO) to observe the carbonyl peaks in IR spectrum. The first method attempted was specular reflectance IR. In this method, the complexes were polymerized by using $TBAPF_6$ as the electrolyte, using an Au-Cr coated glass substrate as the working electrode. No CO stretches were detected by the specular reflectance IR technique. Subsequently, the monomers were polymerized on a plastic surface coated with Au-Ag-In_2O_3. The ATR-IR measurement was performed by placing the polymer on the plastic substrate directly onto the ATR apparatus. No carbonyl stretches were observed in the second method either. The last method employed was to isolate the polymer film from the substrate (working electrode) and measure the solid state IR data of the polymer film directly. After polymerizing the monomer on the ITO surface, the polymer was collected and separated by a razor blade from the ITO surface, and the ATR-IR spectrum of the collected film was obtained. The polymer film was also blended with some KBr (approximately 10 times more of the sample weight) to make a pellet for IR measurement. However, none of the IR studies indicated a carbonyl stretch, whereas the IR spectra of the monomers do otherwise.

Attempts were made to load CO gas on to the polymers that are on Au-Cr surface and also on the Au-Ag-In_2O_3 surface. The polymers on these surfaces were placed in a vial separately and covered by a septum. Following this, CO gas was blown in for 5 minutes and then the polymers were left under a positive pressure of CO gas for 30 minutes. Subsequently, IR measurements were carrired out. However, no CO stretch was

detected. Furthermore, the polymers were soaked in CH_2Cl_2 in a vial covered by a septum. The CO gas was bubbled for 5 minutes following which the polymers were left under a positive pressure of CO gas for an hour. The IR measurements indicated that no CO stretches were present.

Evidently, the carbonyl ligands must have been dissociated during the polymerization in which the molybdenum in the polymer was oxidized in the process. Therefore, the molybdenum atoms will not be able to donate its electrons to the carbonyls for π-backdonation. In order to prove this to be the case, the high resolution XPS data for the monomers **15**, **16** and polymers **poly-15**, **poly-16** were analyzed in order to find the oxidation state of the Mo. **Poly-15** and **poly-16** were deposited on an ITO-coated glass substrate that was used as the working electrode for studying the XPS data. The monomer complexes **15** and **16** contain Mo^0, i.e. complex **16** contains 92.3% Mo^0 and 7.7% Mo^{6+}. The polymers have mostly Mo^{6+} and some Mo^0 (**Figure 35**). Mo^0 has a binding energy value for 3d5/2 at 228 eV and 3d3/2 at 231 eV. Mo^{6+}. On the other hand, Mo^{6+} has 3d5/2 at 232.5 eV and 3d3/2 at 236 eV as reported in the literature.[133] The XPS data indicated that some of the Mo atoms on the polymer have been permanently oxidized and resulted in the disappearance of the carbonyl groups.

CONCLUSIONS

In conclusion, the design, syntheses and characterization of a novel polymerizable ligand **8** and the corresponding molybdenum carbonyl complexes **15** and **16** with this ligand have been reported in the present study. Both the ligand and the complexes were electropolymerizable. The conducting polymers **poly-14**, **poly-15** and **poly-16** have been produced and characterized by XPS and their scan rate dependences. The XPS

experiments proved that **poly-15** and **poly-16** contained Mo atoms by Mo/S and Mo/P ratios being consistent with the proposed ratios of ½. All three polymers were electroactive.

The monomer complexes indicated the presence of carbonyl stretches in their IR spectra. However, no carbonyl stretches were detected for the corresponding polymers in the various IR techniques that were used. The first oxidation of Mo in the CV data was found in the polymerization window. Carbonyl ligands were probably lost during the electropolymerization process. Another possibility for the carbonyl ligands to have been lost is that the presence of the PF_6^- anion might generate HF in the electrolyte and monomer complexes might not be stable in the acidic media.

The polymers were also exposed to CO gas with or without the solvent CH_2Cl_2. However, CO molecules did not coordinate to the metallopolymers.

In order to determine the oxidation states of the Mo atoms, an XPS analysis was performed both on the monomers and also on the polymers and results were compared. The XPS experiment indicated that the monomer complexes have Mo^0 atoms and the polymers that have Mo atoms were mostly oxidized. During the oxidation of Mo, carbonyl ligands must have been released due to the lack of electrons on Mo for π-backdonation. In fact, changing the oxidation state of the metal by using a redox active ligand caused the permanent release of the carbonyls.

Future efforts will be focused on the controlled release of carbonyl ligands by preparing metal complexes of the electropolymerizable PNP ligand, that have metal oxidation outside the polymerization window. As a consequence, when potential is applied to the complex, the carbonyl stretch in the IR spectra can be studied for controlled release. Since nitric oxide is isoelectronic and a similar molecule to carbon monooxide, electropolymerizable complexes with nitrosonium analogues of the

molybdenum polymers (and other metallopolymers) can also be prepared. The nitric oxide release can be probed by means of IR spectroscopy. It should also be noted that the controlled release of nitric oxide would likely to have clinical significance for implant applications.[134]

Chapter 4: Luminescent Electropolymerizable Ruthenium Complexes and Corresponding Conducting Metallopolymers

INTRODUCTION

$Ru(bpy)_3Cl_2$ has been thoroughly studied and frequently employed due to its unique properties, such as chemical stability, luminescence emission and excited state lifetime, redox properties, and excited state reactivity.[69] This red crystalline salt is obtained as the hexahydrate from the reaction of an aqueous solution of ruthenium trichloride with 2,2'-bipyridine. Ru(III) was reduced to Ru(II) in the process by hypophosphorous acid.[135] The complex is a chiral, d^6 system with D_3 symmetry, and its enantiomers are kinetically stable. All of the properties of interest were in the cation $[Ru(bipy)_3]^{2+}$ which has a noteworthy chemical stability. As a consequence, it can be stored in aqueous solutions for months. Furthermore, it is unaffected by boiling in concentrated HCl or 50% aqueous NaOH solutions.[136,137] Excited solutions of the cation emit photons with relatively long lifetimes both at room temperature (890 ns in CH_3CN, 650 ns in H_2O) and at 77 K (5 μs).[69, 138] When Ru(II)–polypyridine complexes undergo one electron oxidation, the process involves a metal centered orbital with the formation of Ru(III) complexes, which have a low spin $4d^5$ configuration and are inert to ligand substitution.[139] Single electron reduction of Ru(II)–polypyridine complexes generally takes place on a ligand orbital depending on either a sufficiently strong ligand field or easily reducible ligands. The reduced form in this case has a low spin $4d^6$ configuration and is usually quite inert.[140-142] Both single electron oxidation and reduction are reversible processes. The triplet excited state of $Ru(bipy)_3^{2+}$ has both oxidizing and reducing properties. This remarkable situation arises because the excited state can be described as a Ru^{3+} complex containing a $bipy^-$ ligand.[143] $Ru(bipy)_3^{2+}$ has been examined as a photosensitizer for both the oxidation and reduction of water.[144]

The excited states of Ru(II)–polypyridine complexes may involve three types of electronic transitions (**Figure 36a**).[16, 145-147] Polypyridine molecules possess σ–donor orbitals that are localized on the nitrogen atoms and the π–acceptor orbitals are delocalized on the aromatic rings. The promotion of an electron from a π_M metal orbital to π^*_L ligand orbitals results in metal-to-ligand charge transfer (MLCT) excited states, while promotion of an electron from π_M to σ^*_M orbitals results in metal centered (MC) excited states. The promotion of an electron from π_L to π^*_L generates ligand centered (LC) excited states. The presence of the heavy ruthenium atom causes spin-orbit coupling which leads to singlet-triplet mixing in the MC and MLCT excited states.[16, 145-147] Homotrischelated complexes of ruthenium with bidentate polypyridine ligands exhibit a D_3 symmetry; corresponding orbitals involved in electronic transitions are illustrated in **Figure 36b**.[148-150]

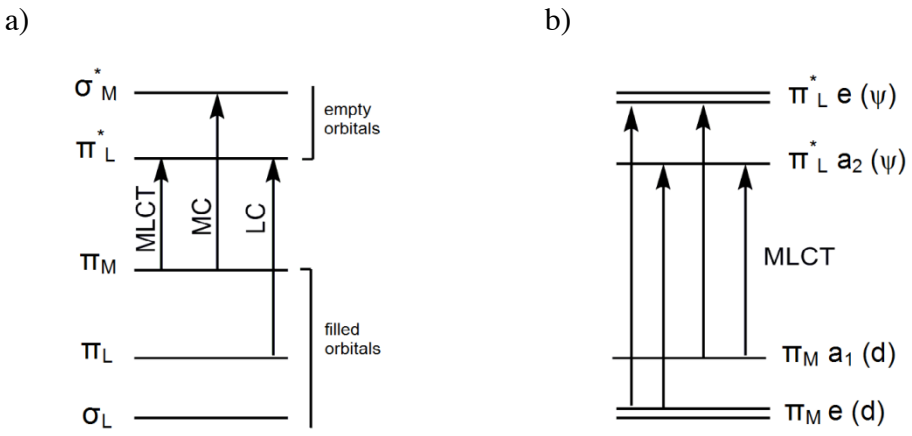

Figure 36. (a) The molecular orbital diagram for $Ru(LL)_3^{2+}$ showing types of electronic transitions that occur (b) detailed representation of the MLCT transition in D_3 symmetry. Diagram adapted from references [69].

Transition metal complexes in their high-energy excited states undergo fast nonradiative deactivation.[151] Therefore, the lowest excited state and the states populated

according to Boltzmann equilibrium law may result in luminescence emission and in bimolecular processes. The MC excited states of d^6 *octahedral* complexes are strongly displaced with respect to the ground state geometry; therefore, such molecules undergo rapid nonradiative deactivation or ligand dissociation reactions. Consequently, no luminescence can be observed at room temperature from the MC excited states.[152] Luminescence can generally be observed when the lowest excited states are LC and MLCT due to their small displacement from the ground state geometry; therefore, not undergo fast nonradiative decay.

Derivatives of $[Ru(bipy)_3]^{2+}$ are numerous and complexes of this type are being explored for applications in biodiagnostics, photovoltaics, and organic light-emitting diodes.[69, 70] Due to their promising luminescence properties for materials applications, ruthenium (II) complexes were incorporated into the conducting polymer backbones. The N-donating ligands with bidentate and tridentate coordination modes are typically used for such polymers (**Figure 37**).[71-74, 153] Electropolymerization of a series of Ru and Os bis-terpyridine complexes with bithienyl, quaterthienyl, or hexathienyl bridges has also been reported (**Figure 38**).[8, 66, 67, 154-162] Peng *et al*. reported a metallopolymer with increased photosensitivity upon incorporation of the metal complex that has a strong absorption in the visible region of the spectrum. They also showed that excitons formed during the excitation of the metal complexes are separated and transported by the conducting polymer backbone.[163, 164] In luminescent conducting metallopolymers, both the complex and the polymer can function as independent light emitters.[71] Ruthenium(II) polypyridine complexes can enhance the charge mobility of the resulting metallopolymer, and processing of the material is easy.[71]

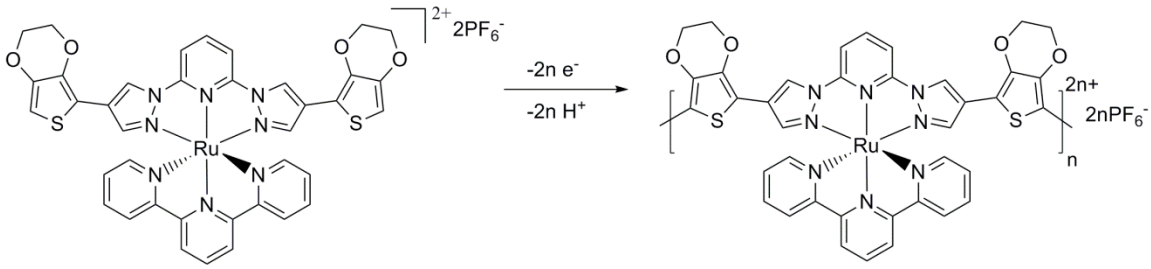

Figure 37. Electropolymerization of a ruthenium-containing polymer in which the donor atoms are N.[153]

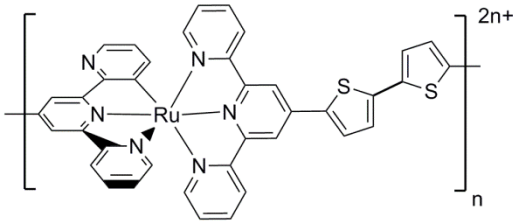

Figure 38. Ruthenium-containing rod-like conducting polymer with bithiophene units.[156]

In this study, the syntheses and characterization of four Ru(II) complexes with the polymerizable tridentate ligand *bis*[4-[2-(3,4-diethylenedioxy)thiophene]pyrazol-1-yl]pyridine (EDOT$_2$NNN) and the following bidentate ligands 1,1,1,5,5,5-hexafluoro-2,4-pentanedione (hfac), dibenzoylmethane (dbm), 2,2'-bipyridine (bpy), 1,10-phenanthroline (phen) are targeted. Subsequently, further studies of the complexes, i.e., electrochemistry/electropolymerization, UV-Vis spectroscopy of complexes and one of the polymers, luminescence studies of the monomer complexes in air free and aerated media as well as the luminesce study of one of the polymers are aimed. The reasons for selecting ruthenium containing polymers relates to their chemical stability, luminescence emission, ease of processibility and high charge carrier mobility compared with monomers as well as the electronic interactions between the organic backbone and the

ruthenium metals. Furthermore, having the bidentate ligands can enhance the light absorption. Possible application to these materials would be PLEDs.[75,165]

EXPERIMENTAL

Instrumentation

^{1}H and $^{13}C\{^{1}H\}$ NMR spectra were recorded with a Varian 400 MHz spectrometer. ^{1}H NMR signals were referenced to residual proton resonances in deuterated solvents. $^{13}C\{^{1}H\}$ NMR spectra were referenced relative to solvent peaks. All peak positions are listed in ppm and all coupling constants are listed in Hertz (Hz). Low-resolution and high-resolution mass spectra were carried out using a Thermo Finnegan TSQ 700 and Waters Autospec Ultima, respectively. Elemental analysis was performed by QTI, Whitehouse, NJ (www.qtionline.com). Absorption spectra were recorded on a Varian Cary 6000i UV-VIS-NIR spectrophotometer. Luminescence measurements were recorded on a Spex Fluorolog. X-ray photoelectron spectroscopy (XPS) was carried out on a PHI 5700 XPS system equipped with dual Mg X-ray sources and a monochromatic Al X-ray source, complete with depth profile and angle-resolved capabilities. Samples were freshly prepared prior to analysis.

Electrochemistry

Electrochemical syntheses and studies were performed in a dry box under a nitrogen atmosphere using a GPES system from Eco. Chemie B. V. All the electrochemical experiments were carried out in a three-electrode cell with a $Ag/AgNO_3$ reference electrode (silver wire dipped in a 0.01 M silver nitrate solution with 0.1 M $(n\text{-}Bu)_4N][PF_6]$ ($TBAPF_6$) in CH_3CN, a platinum-button working electrode, and a Pt wire coil

counter electrode. Potentials were relative to the 0.01 M $Ag/AgNO_3$ reference electrode. Ferrocene was used as an external standard to calibrate the reference electrode before and after experiments were performed, and that value was used to correct the measured potentials. The supporting electrolyte was 0.1 M $TBAPF_6$ that was purified by recrystallization three times from hot ethanol before being dried for 3 days at 100-150°C under active vacuum. Electrosyntheses of the films were performed from 0.01 mM monomer solutions by continuous cycling between -1.25 V and 1.25 V at a 100 mVs^{-1} scan rate. The films obtained were then washed with fresh CH_2Cl_2 several times before being used in further experiments.

Synthesis[3]

General Methods

All chemicals were purchased from commercial suppliers and were used as received. Air and moisture-sensitive reactions were carried out in oven dried glassware using standard Schlenk techniques under an inert atmosphere of dry N_2. All solvents were dried using a double-column anhydrous solvent system (Innovative Technologies, Newburyport, MA) and further degassed via nitrogen purge prior to use. 2-(tributylstannyl)-3,4-(ethylenedioxy)thiophene was prepared by Swager's method.[126]

[3] The syntheses of the ligand and the ruthenium complexes were first achieved by Dr. XunJin Zhu (Scheme 5-7). Seyma Keskin reproduced the syntheses and confirmed by the values of ^1H NMR data except complex **17** which is an insoluble black powder. $^{19}F\{^1H\}$ NMR and $^{13}C\{^1H\}$ NMR data of the ruthenium complexes were measured by Dr. Zhu. Samples were submitted to the UT Austin's MS facilities by Dr. Zhu and the technician of that time measured the MS data. UV-Vis data, electrochemistry/electropolymerization and complete photophysical measurements were carried out by Seyma Keskin. The principle investigator at the time of the work was Dr. Bradley J. Holliday.

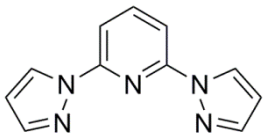

2,6-Bis(N-pyrazolyl)pyridine. 5.544g of pyrazole (81.44 mmol) was dissolved in 100 mL of dry THF. 1.9543 g NaH (81.44 mmol) was added portionwise under N_2. After all NaH has been added, the reaction mixture was stirred for 2 hours. 2,6-dibromopyridine was added and then the mixture was refluxed under N_2 for 4 days. THF was evaporated; the white residue was checked with C_2H_5OH to see if any NaH remained. The residue was dissolved in CH_2Cl_2 and extracted with H_2O three times. The combined aqueous phase was extracted with a fresh portion of CH_2Cl_2, and then the organic phases were combined, and dried over $MgSO_4$. $MgSO_4$ was vacuum filtered, and the filtrate was evaporated to afford the crude product which was redissolved in CH_2Cl_2. CH_3OH was added, and the mixture was cooled to 0°C. 5.81 g (yield = 68%) white crystals were collected via vacuum filtration. The structure was confirmed by comparing ^1H and $^{13}C\{^1H\}$ NMR spectroscopy data to literature values.[166]

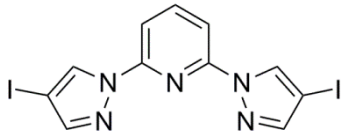

2,6-Bis(4-iodopyrazol-1-yl)pyridine. 2.935 g 2,6-bis(pyrazol-1-yl)pyridine (13.9 mmol), 0.9811 g HIO_3 (5.58 mmol), 39 mL CH_3COOH and 5 mL 30% H_2SO_4 were added into a Schlenk flask and then heated to 60 °C under N_2. Meanwhile, 2.8313 g I_2 (11.16 mmol) was dissolved in 98 mL CH_3COOH while sonicated for 45 minutes. 20 drops of H_2SO_4 was added into the I_2/ CH_3COOH solution and this solution was transferred into the addition flask which is connected to the Schlenk flask. I_2 solution was added into the reaction mixture dropwise. After all I_2 has been added, temperature was raised to 70°C and the reaction mixture

was stirred at this temperature under N_2 for three days. After the reaction mixture had cooled to room temperature, just enough $Na_2S_2O_3$ to quench the pale rose color was added. A $NaHCO_3/Na_2CO_3$ (1:1 in H_2O) solution was used to neutralize the CH_3COOH/H_2SO_4 mixture (pH = 7-8), and the product was extracted three times with CH_2Cl_2. The organic phase was dried over $MgSO_4$, and vacuum filtered, and the filtrate was evaporated, then dried under vacuum to afford a white solid **2** (6.173 g, yield 96%). The structure was confirmed by comparing ^1H and $^{13}C\{^1H\}$ NMR spectroscopy data to literature values.[167, 168]

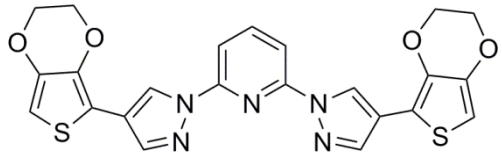

2,6-Bis[4-[2-(3,4-diethylenedioxy)thiophene]pyrazol-1-yl]pyridine [EDOT$_2$NNN]. 2,6-Bis(4-iodopyrazol-1-yl)pyridine (0.700 g, 1.511 mmol) and dichlorobis(triphenyl-phosphane)palladium(II) $Pd(PPh_3)_2Cl_2$, (0.053 g, 0.0756 mmol) were added into a Schlenk flask. About 60 mL of dry DMF was cannula-transferred into the Schlenk flask, and the mixture was stirred to dissolve while being heated to 120°C to give a clear yellow solution. Meanwhile, 2-(tributylstannyl)-3,4-(ethylenedioxy)thiophene was dissolved in about 20 mL of dry DMF, degassed by sparging with N_2, then cannula-transferred into the hot reaction mixture, and an immediate change to a dark color was observed. The reaction mixture was stirred at 120°C for two days. The reaction mixture was cooled to RT, and then DMF was evaporated under vacuum. The dark residue was redissolved in ethyl acetate and washed with H_2O three times. The organic phase was dried over $MgSO_4$; and vacuum filtered, and the filtrate was evaporated. The residue was further purified via column chromatography. The first fraction (impurities) was collected by CH_2Cl_2, then the second fraction (product) was collected via ethyl acetate. The product

was redissolved in CH_2Cl_2 with hexanes added to get rid of tributyl stannyl impurities. The tan precipitate was collected as 0.355 g (48% yield). ^{1}H NMR (400 MHz, δ ppm, $CDCl_3$, 298 K): 8.72 (s, 2H), 8.00 (s, 2H), 7.92-7.97 (dd, 1H, $^3J_{H,H}$ = 7.95 Hz, 1.80 Hz), 7.82-7.84 (d, 2H, $^3J_{H,H}$ = 7.9 Hz), 6.25 (s, 2H), 4.36 (m, 4H), 4.24(m, 4H). ^{13}C{^{1}H} NMR (100 MHz, δ ppm, $CDCl_3$, 298 K): δ = 149.9, 141.9, 141.2, 140.1, 137.8, 122.8, 116.8, 109.4, 108.3, 96.4, 64.9, 64.6. MS (ESI) calculated for $C_{23}H_{18}N_5O_4S_2$ *m/z* = 492.08 ([M + H]$^+$), found 492.12. UV-Vis (CH_2Cl_2, nm (ε)): 277 (21969), 315 (24507) sh, 335 (29034). The yield and the ε value are different than the literature values.[124]

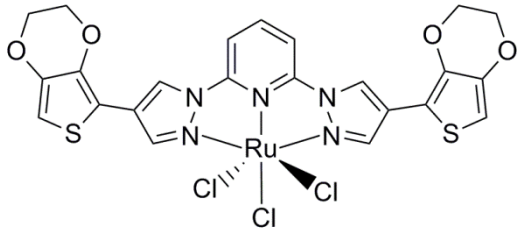

Ru(EDOT$_2$NNN)Cl$_3$ [17]. $RuCl_3$•XH_2O (167 mg, 0.805 mmol) and **3** (202 mg, 0.411 mmol) were heated to reflux in ethanol (60 mL) for 12 hours. After cooling, the precipitate was collected by filtration and washed with ethanol, then dried under high vacuum to afford a dark gray insoluble solid (250 mg, 81.4%).[122]

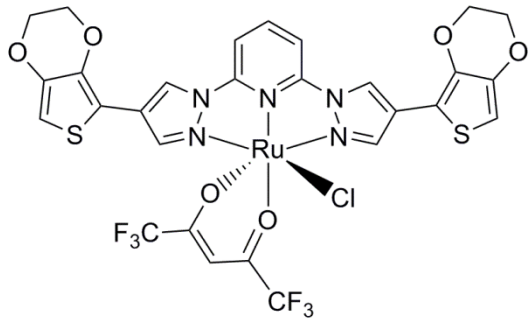

Ru(EDOT$_2$NNN)(hfac)(Cl) [18]. A mixture of **17** (101 mg, 0.144 mmol), triethylamine (0.81 mL, 5.81 mmol), and 1,1,1,5,5,5-hexafluoro-2,4-pentanedione (hfac)

(0.60 mL, 4.24 mmol) was dissolved in 100 mL of absolute ethanol and heated to reflux under Ar for 12 hours. The reaction mixture was allowed to cool, and the solvent was removed by rotary evaporation. The solid residue was redissolved in CH_2Cl_2 and filtered to remove insolubles. The product was then extracted between CH_2Cl_2 and H_2O once. The organic phase was dried over $MgSO_4$; and vacuum filtered, and the filtrate was evaporated and further dried under vacuum (81 mg, 67%). ^{1}H NMR (400 MHz, δ ppm, CD_2Cl_2, 298 K): 8.63 (s, 2 H), 8.24 (s, 2 H), 7.64 (t, 1H, *J* = 8.4 Hz), 7.47 (d, 2H, *J* = 8Hz,), 6.34 (s, 2H), 6.10 (s, 1H), 4.26-4.34 (m, 8H). ^{19}F NMR (376 MHz, δ ppm, CD_2Cl_2, 298 K): δ = -75.11, -75.62. MS (ESI) calculated for $C_{28}H_{18}ClF_6N_5O_6RuS_2$: *m/z* = 835.94 ([M + H]$^+$), 799.96 ([M –Cl]$^+$); found 836 ([M + H]$^+$), 799 ([M – Cl]$^+$). UV-Vis (CH_2Cl_2, nm (ε)): 281 (29011), 316 (21986) sh, 354 (12247), 497 (6896).

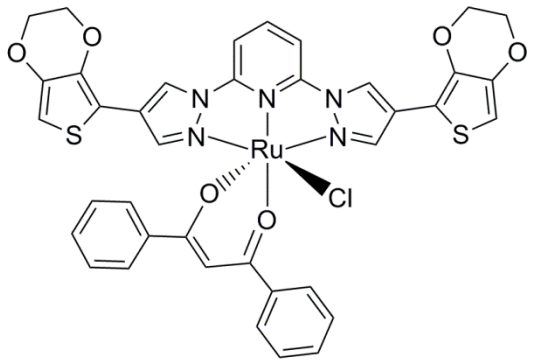

Ru(EDOT$_2$NNN)(dbm)(Cl) [19]: A mixture of **17**$_3$ (127 mg, 0.182 mmol), triethylamine (0.95 mL, 6.82 mmol), and dibenzoylmethane (dbm) (55.3 mg, 0.254 mmol) was dissolved in 127 mL of absolute ethanol and heated to reflux under Ar for 12 hours. The reaction mixture was allowed to cool, and the solvent was removed by rotary evaporation. The solid residue was redissolved in CH_2Cl_2 and filtered to remove insolubles. The filtrate was washed with NH_4Cl solution, and then dried over $MgSO_4$, then vacuum filtered. Hexanes were added to the filtrate to precipitate the product, which was

collected via vacuum filtration. The dark burgundy product was further dried under vacuum (97 mg, 63%). ^{1}H NMR (400 MHz, δ ppm, CD_2Cl_2, 298 K): 8.66 (s, 2 H), 8.34 (m, 2 H), 8.11 (s, 2H), 7.51-7.62 (6H), 7.17-7.14 (m, 3H), 7.06 (t, *J* = 8 Hz, 2H), 6.64 (s, 1H), 6.26 (s, 2H), 4.19-4.29 (m, 8H). MS (ESI) calculated for $C_{38}H_{28}ClN_5O_6RuS_2$ *m/z* =852.03 ($[M + H]^+$), 816.05 ($[M – Cl]^+$); found 852 ($[M + H]^+$), 815 ($[M – Cl]^+$). UV-Vis (CH_2Cl_2, nm (ε)): 256 (35714), 279 (38713), 326 (52803), 486 (8153).

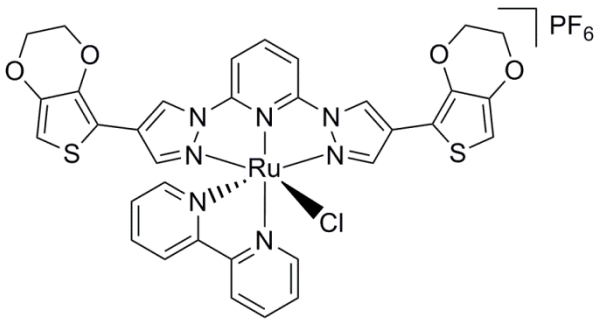

[Ru(EDOT$_2$NNN)(bpy)(Cl)](PF$_6$) [20]. 17 (100 mg, 0.143 mmol) and 2,2'-bipyridene (bpy) (26 mg, 0.166 mmol) were refluxed for 12 hours in 60 mL EtOH/H_2O (3/1 , v/v). The hot solution was filtered through celite and evaporated to dryness. After the crude product was dissolved in CH_2Cl_2, 26 mg of KPF_6 was added, and the mixture was stirred overnight. The resulting brown precipitate was collected via vacuum filtration. The product was redissolved in CH_2Cl_2 and a layer of pentane was added. The solid was collected 1 week later (60 mg, 45%). ^{1}H NMR (400 MHz, δ ppm, CD_3CN, 298 K): 10.25 (m, 1H), 8.92 (s, 2H), 8.56 (d, *J* = 8.0 Hz, 1H), 8.32 (d, *J* = 7.6 Hz, 1H), 8.23-8.27 (m, 1H), 8.18-8.22 (m, 1H), 8.01 (d, *J* = 8Hz, 2H), 7.89-7.92 (m, 1H), 7.70-7.74 (m, 1H), 7.5 (s, 2H), 7.38 (d, *J* = 8.0 Hz, 1H), 6.96-7.00 (m, 1H), 6.35 (s, 2H), 4.17-4.25 (m, 8H). ^{13}C{^{1}H} NMR (500 MHz, δ ppm, CD_3CN, 298 K): 207.4, 160.4, 158.4, 154.5, 153.9, 151.4, 143.1, 142.8, 140.3, 139.0, 137.6, 136.9, 127.3, 127.2, 126.6, 124.1, 123.8, 119.8, 108.2, 106.0, 99.0, 65.96, 65.58. Elemental analysis calculated for $C_{33}H_{25}ClF_6N_7O_4PRuS_2$:

C, 42.65; H, 2.71; N, 10.55; found: C, 42.11; H, 2.77; N, 10.62. MS (ESI) calculated for $C_{33}H_{25}ClN_7O_4RuS_2$ *m/z* = 784.01 ([M – PF_6]$^+$), found 784. UV-Vis (CH_2Cl_2, nm (ε)): 254 (30553), 290 (66486), 355 (21887), 455 (8894), 550 (4119).

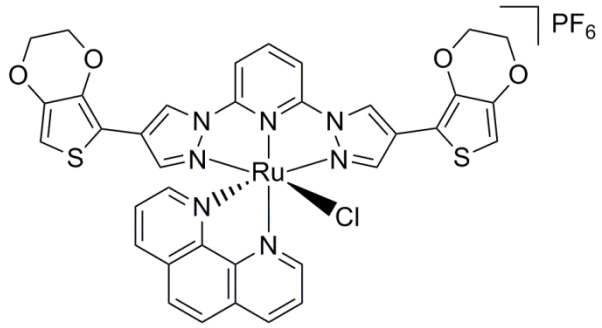

[Ru(L)(phen)(Cl)](PF$_6$) [21]. 17 (50 mg, 0.0713 mmol) and 1,10-phenanthroline (phen) (14.5 mg, 0.08 mmol) were refluxed for 12 hours in 30 mL EtOH/H_2O (3/1, v/v) under N_2. The reaction mixture was filtered through celite as hot. NH_4PF_6 (1g/10mL) was added to the filtrate and stirred for one hour. The solvent was then evaporated. The residue was redissolved in CH_2Cl_2 and then washed once with H_2O. The organic phase was dried over $MgSO_4$; and vacuum filtered, then the filtrate was evaporated and further dried under vacuum to afford a reddish brown solid (39 mg, 58%). ^{1}H NMR (400 MHz, δ ppm, CD_3CN, 298 K): 10.43 (dd, 1H), 8.90 (s, 2H), 8.78 (dd,1H), 8.23-8.29 (m, 4H), 8.04-8.08 (m, 3H), 7.74 (dd, 1H), 7.34 (s, 2H), 7.30 (dd, 1H), 6.28 (s, 2H), 4.11-4.19 (m, 8H). ^{13}C{^{1}H} NMR (500 MHz, δ ppm, CD_3CN, 298 K): 207.4, 155.2, 154.4, 151.7, 150.8, 149.8, 143.1, 140.2, 139.0, 136.5, 135.8, 131.7, 131.0, 128.7, 128.1, 127.3, 126.4, 125.3, 119.7, 108.2, 105.9, 98.9, 65.89, 65.54. MS (ESI) calculated for $C_{35}H_{25}ClN_7O_4RuS_2$ *m/z* ([M – PF_6]$^+$) = 808.01, found 808. UV-Vis (CH_3CN, nm (ε)): 223 (53267), 265 (66997), 349 (18970), 443 (11820), 549 (4033).

RESULTS AND DISCUSSION

Syntheses

The polymerizable $EDOT_2NNN$ ligand was prepared by using Zhu's technique in high yields as outlined in **Scheme 5**.[153, 168] First step was abstracting the hydrogen attached to the nitrogen of pyrazole by NaH. Subsequently, 2,6-dibromopyridine was added to synthesize 2,6-bis(N-pyrazolyl)pyridine in 68% yield. Then, 2,6-bis(N-pyrazolyl)pyridine was symmetrically iodinated in a hot, acidic medium to obtain 2,6-bis(4-iodopyrazol-1-yl)pyridine in 96% yield. The last step was the Stille coupling of 2-(tributylstannyl)-3,4-(ethylenedioxy)thiophene and 2,6-bis(4-iodopyrazol-1-yl)pyridine to obtain 2,6-bis(4-(3,4-ethylenedioxy)thien-2-yl)pyrazol-1-yl)pyridine ($EDOT_2NNN$) in 48% yield.

Scheme 5. Synthesis of the ligand. Illustration adapted from references [153 and 168].

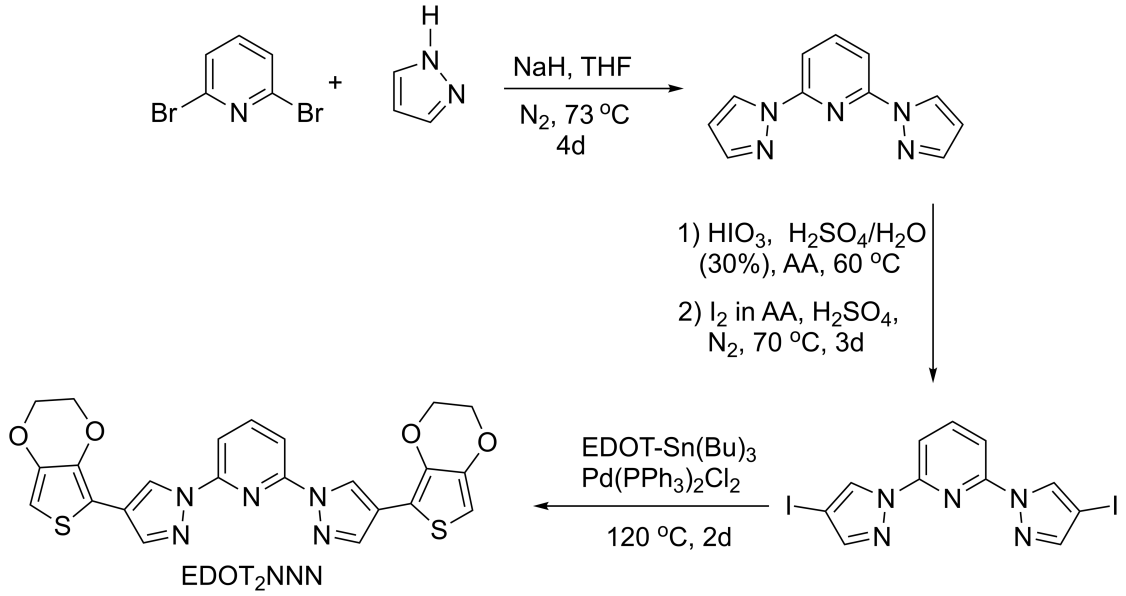

$EDOT_2NNN$ was allowed to react with $RuCl_3.XH_2O$ in boiling C_2H_5OH in order to obtain the $Ru(EDOT_2NNN)Cl_3$ precursor **17** as a dark powder in high yields (**Scheme 6**).[153]

Scheme 6. Synthesis of the ruthenium precursor.[153]

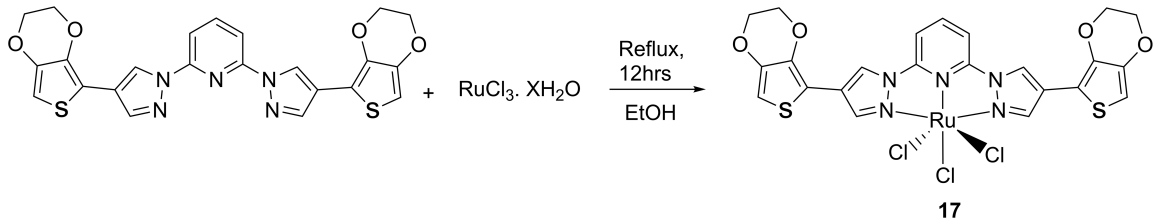

17

The ruthenium complexes **18** and **19** based on β-diketonate ligands and $EDOT_2NNN$, were synthesized according to methods reported by Jameson and coworkers[166] (**Scheme 7**). $Ru(EDOT_2NNN)(Cl)_3$ was placed in ethanol with excess β-diketonate and excess triethylamine used as a deprotonating agent. Ru(III) was reduced as the ethanol was oxidized. Complexes **20** and **21** were prepared as deep red salts by the reaction of **17** with 2,2'-bipyridine and 1,10- phenanthroline respectively in boiling $EtOH/H_2O$. While, Ru(III) was reduced, ethanol was oxidized and KPF_6 or NH_4PF_6 was added to the exchange the uncoordinating chloride with the the PF_6^- anion to obtain the complex salts.

Scheme 7. Complex synthesis.

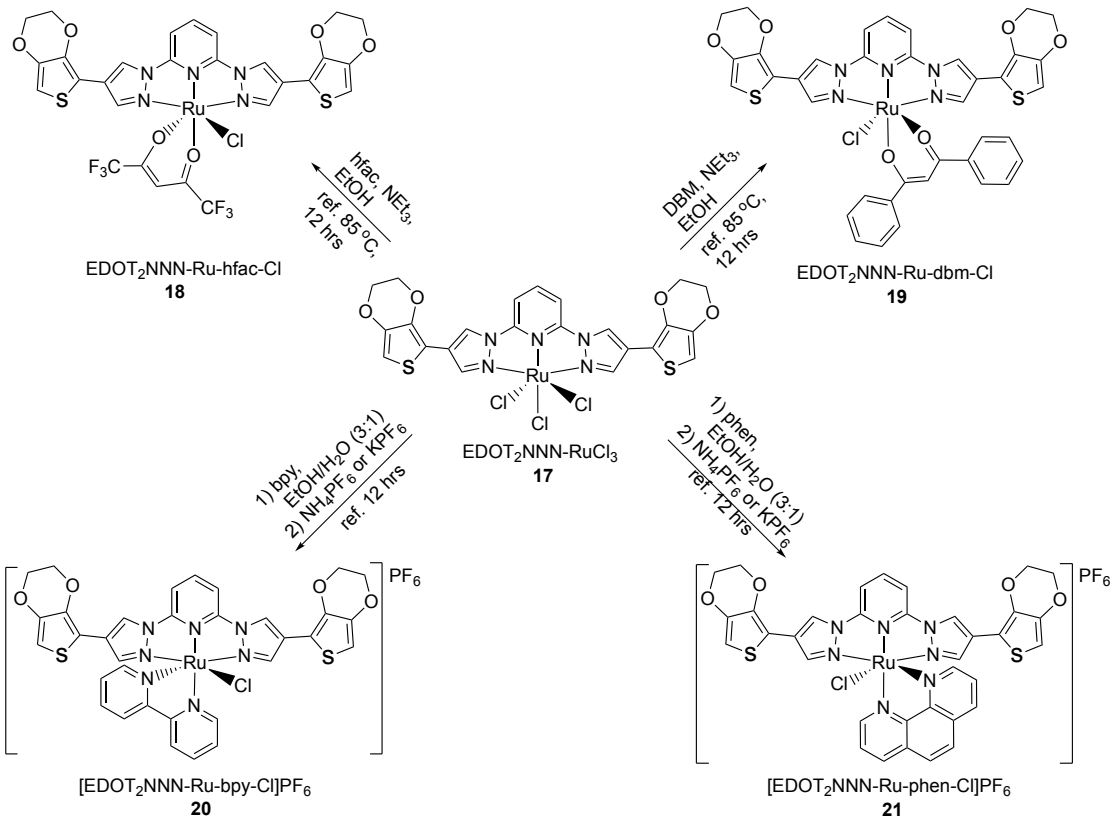

Electropolymerization of Ruthenium Complexes.

Solutions of monomers with a ~ $1x10^{-3}$ M concentration in CH_2Cl_2 including 0.1 M tetrabutylammoniumfluoride hexafluorophosphate ($TBAPF_6$) as the electrolyte were oxidatively and electrochemically polymerized while the potential of the electrode was swept between -1.75 V and +1.25 V versus ferrocene/ferrocenium (Fc/Fc^+) at a scan rate of 100mV/s (**Scheme 8**). The polymerization profiles for complexes **18**-**21** are presented in **Figure 39**. The polymerization profiles of all the complexes are similar to each other in terms of Ru(II)/Ru(III) redox couples and monomer oxidations. Although it is not practical or sufficient to compare the potentials reported in the literature, it should be

mentioned that the Ru(II)/Ru(III) potentials of the polypyridine complexes are around 1.25 V with respect to the normal hydrogen electrode NHE (0.62V vs Fc/Fc^+).[69, 153, 169] The substitution of polypyridine ligands can drastically change these potentials. For example, when one of the bpy ligands of $Ru(bpy)_3^{2+}$ is replaced by 2 Cl^- ligands, the potential is lowered by 0.35V.[69]

Scheme 8. Electropolymerization of $EDOT_2NNN$-Ru Complexes.

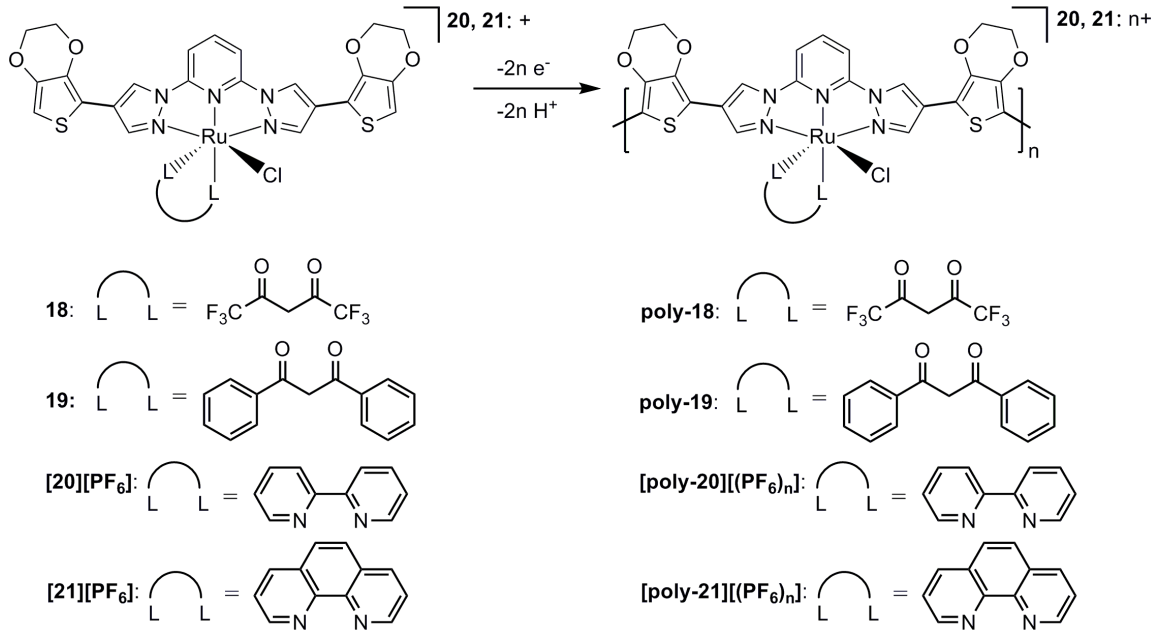

The first polymerization scan of complex **18** (**Figure 39a**) had a reversible oxidation at 0.30 V and an irreversible oxidation at 1.04 V. The peak at 0.30 V was assigned as the Ru(II)/Ru(III) oxidation, and the peak at 1.04 V was assigned as oxidation of the monomer. New oxidation and reduction peaks grew at -0.04 V and 0.71 V respectively. Complex **19** was polymerized on a stainless steel surface used as a working electrode. All other complexes were polymerized on platinum button as the working

electrode. Complex **19** had a Ru (II)/Ru(III) redox couple at 0.04 V and –0.40 V. The monomer oxidation was observed at 0.75 V (**Figure 39b**). Complex **20** had a Ru(II)/Ru(III) redox couple at 0.51 V and 0.41 V. The monomer oxidation was observed at approximately 1.04V, and new reduction (0.85 V) peaks were observed in subsequent scans (**Figure 39c**). Complex **21** had a Ru(II)/Ru(III) redox couple at 0.53 V and 0.46 V. The monomer oxidation was observed at 1.05 V and a reduction peak was observed at 0.96 V (**Figure 39d**). The peak around –0.75 V that appears during the polymerization of all complexes, may be due to the reduction of short oligomers that had not been incorporated into the polymer film.[153] Repeated cycling resulting in a linear increase of the peak currents with scan numbers (**Figure 39a-d**, insets), may be due to the accumulation of the redox-active polymer onto the electrode surface. Polymerization profiles of complexes **18** and **19** both have a linear increase of peak currents with number of scans up to sixteen and twenty scans, respectively (**Figure 39a** and **b**, insets). Polymerization profiles complexes **20** and **21** both have an increase in peak currents with number of scans; however the graphs start to level off at earlier scans (**Figure 39c** and **d**, insets).

The resulting polymer films of these complexes were then rinsed with fresh CH_2Cl_2 in a glove box in order to rinse any monomers and oligomers away from the polymers. Then the reddish brown films that were confined to the electrode were cycled in a monomer-free electrolyte solution of 0.1 M $TBAPF_6$ at scan rates that varied from 10 mV/s to 500 mV/s (**Figure 40**). **Poly-20** has reversible peaks at 0.53 V and 0.45 V; **poly-21** has reversible peaks at 0.60 V and 0.46V. Peak currents increase with increasing scan rate for both **poly-20** and **poly-21**. Scan rate dependence of the polymers was measured for characterization. It is quite linear up to 100 mV for both polymerization processes, indicating that the electroactive material is not limited by the ionic flux of counter ions. Because there is a decrease in charge mobility through the polymer backbone at higher

scan rates, less facile ion transport and a deviation from the linear relationship occur. A very similar ruthenium-containing conducting polymer has been reported in the literature and has results consistent results.[153]

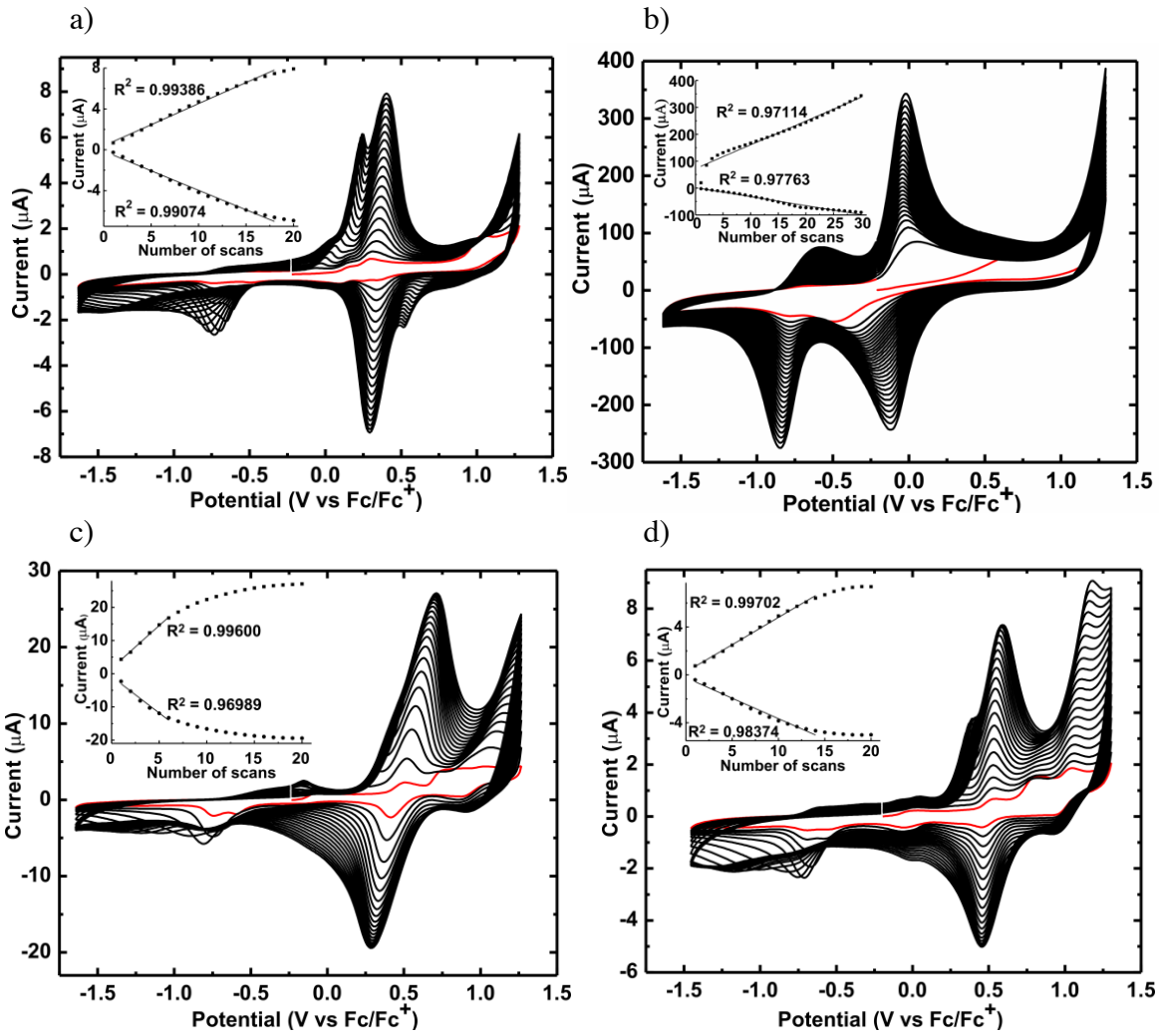

Figure 39. Electropolymerization of ruthenium complexes with initial scans shown in red. Insets: Current vs. number of scans. (a) **18** (b) **19** (c) **20** (d) **21**.

Complexes **18–21** have also been polymerized on a stainless steel surface as well as ITO on a glass substrate for XPS (X–ray photoelectron spectroscopy) measurement; however, the ruthenium peak coincides with the carbon peak in XPS, and the percentages

for the Ru atoms in the analysis were exaggerated. Another problem concerning the XPS data is that some of the $TBAPF_6$ (solution of which is the electrolyte) remained in the polymer film, despite the fact that the polymers were rinsed out with CH_2Cl_2 after the polymerization process was complete. As a consequence, the percentages of N, F, and P atoms were also difficult to interpret.

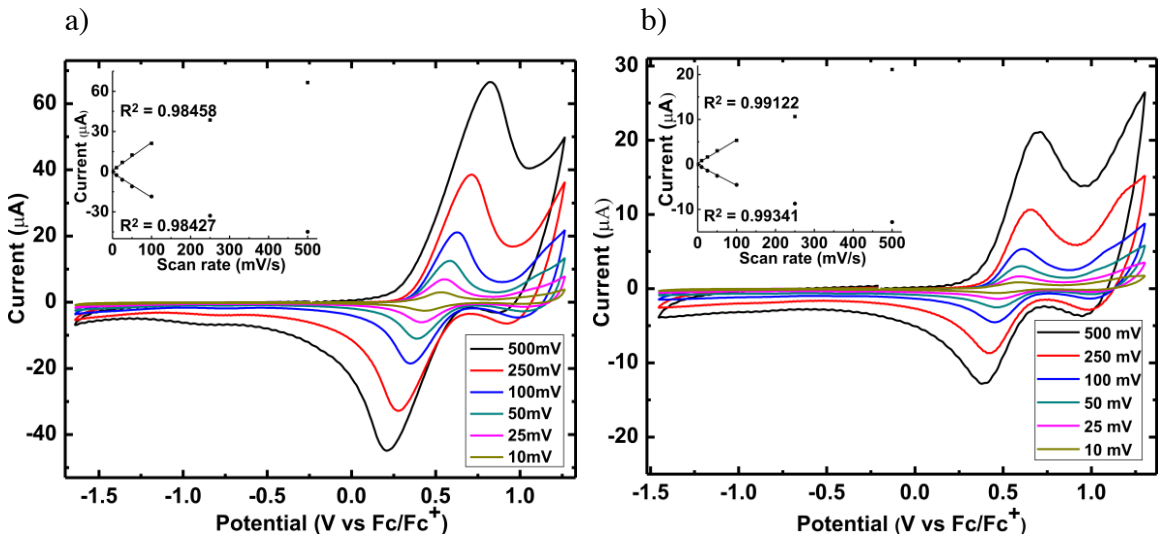

Figure 40. Electrochemical scan rate dependance of (a) **poly-20** (b) **poly-21**. Insets: Current vs scan rate.

UV-Visible Studies

All four complexes feature Ru^{2+}, which is a d^6 system. For most Ru(II) complexes in the literature, the lowest excited state is a ^{3}MLCT, which undergoes slow radiationless transitions and therefore exhibits long lifetimes and intense luminescence emissions.[69] UV-visible spectroscopic characterization of complexes **18**-**21** and the $EDOT_2NNN$ ligand were obtained. The complexes adopted a maroon to reddish brown color and the ligand adopted a tan color. The molar extinction coefficient values versus wavelength for

these complexes is displayed in **Figure 41**. Complexes **18**-**20** and the $EDOT_2NNN$ ligand were dissolved in CH_2Cl_2 and complex **21** was dissolved in CH_3CN (due to its lower solubility in CH_2Cl_2) to prepare stock solutions for UV-Vis absorption spectra. The maximum absorptions fall below 300 nm for complexes **18**, **20**, and **21**, and the maximum absorptions were found above 300 nm for complex **19** and the $EDOT_2NNN$ ligand due to LC (ligand centered) π to π^* transitions.[170,69] The $EDOT_2NNN$ ligand and complex **18** have relatively small molar extinction coefficient values (29034 and 29011, respectively), than complexes **19**-**21** which have molar extinction coefficient values of 52803, 66486, and 66997 $M^{-1}cm^{-1}$, respectively. Intense visible absorption bands around 450-600 nm were assigned as ^{1}MLCT for the complexes,[170] and clearly there is no such a band in the UV-Vis spectrum of the $EDOT_2NNN$ ligand. Furthermore, no peak was observed for the ^{3}MLCT absorption at room temperature. Overall, the results are consistent with those of the $Ru(bpy)_3^{2+}$ complex, which has reported values of LC transition at 285 nm, MLCT transitions at 240 and 450 nm, and MC transition at 344 nm (shoulder).

The ^{3}MLCT of the $Ru(bpy)_3^{2+}$ complex was observed at approximately 550 nm ($\varepsilon \sim$ 600) when the measurement was carried out in an ethanol–methanol glass at 77 K.[69]

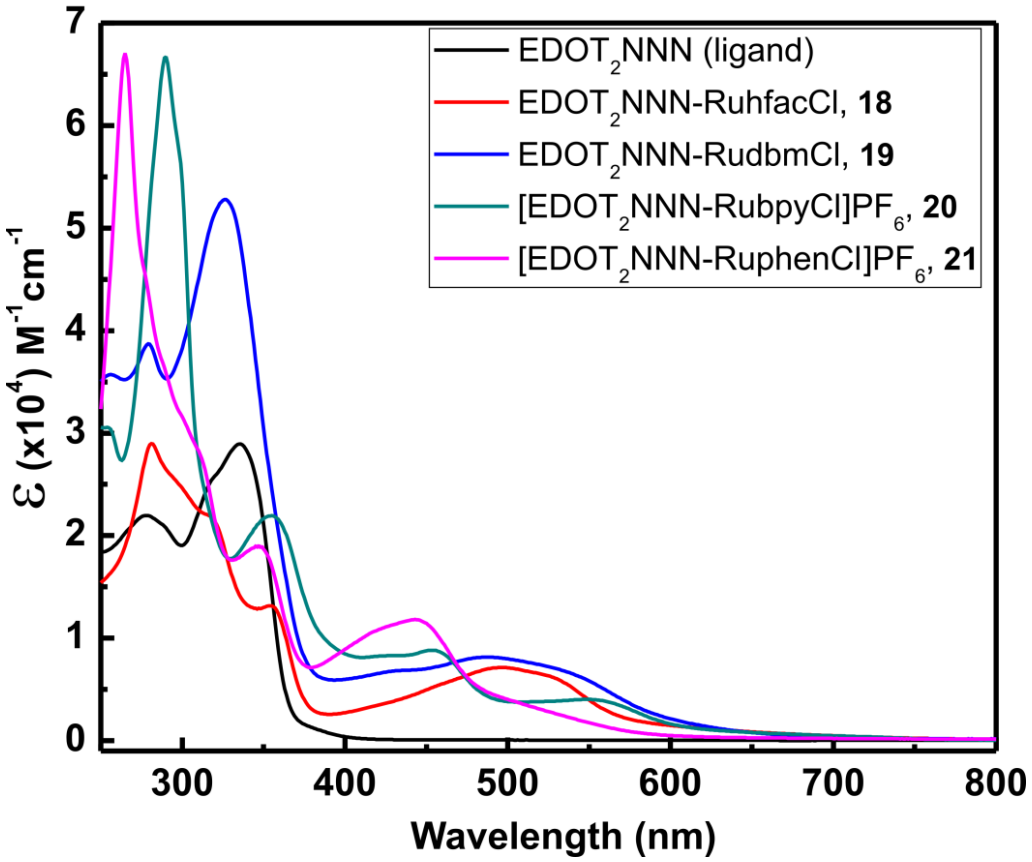

Figure 41. Molar extinction coefficient values vs wavelength for the complexes **18-21** and the ligand.

The $EDOT_2NNN$ ligand has an absorption maximum at 335 nm. The bidentate ligands, i.e. hfac, dbm, bpy, and phen have their absorption maxima and molar-extinction coefficients measured in CH_2Cl_2 as follows: for phen λ_{max} = 264 nm, ε = 31000[171]; bpy λmax = 302 nm, ε = 14125[172]; dbm λmax = 337 nm, ε = 26646[173]; hfac λmax = 275 nm[174]. For all the complexes, the absorption maxima were found to be blue shifted upon Ru^{2+} coordination with respect to the $EDOT_2NNN$ ligand. On the other hand, complex **19** has only a 9 nm blue shift, while other complexes typically have larger blue shifts (54 nm for complex **18**, and 45 nm for complex **20**, and 70 nm for complex **21**). When the absorption maxima of each complex are compared with the absorption maxima of the

corresponding bidentate ligand, the shift in λmax upon coordination is relatively small. For example, **18** is red shifted by 6 nm, **19** is blue shifted by 17 nm, and **20** is blue shifted by 12 nm. On the other hand, **21** is unchanged.

Complex **21** was electropolymerized on an ITO coated glass surface in order to obtain the solid-state absorption spectrum of the corresponding polymer (**Figure 42**). A plain ITO coated glass was used as a blank in a double beam instrument. The solid-state UV-Vis spectrum of **poly-21** revealed peaks at 289 and 355 nm, a shoulder at 441 nm. The absorbance measurement was performed up to 285 nm as a cut-off wavelength, due to the absorption coming from the substrate. The monomer complex **21** has peaks at 223 (not illustrated, measurement carried out in ACN. $\lambda_{\text{cutt-off ACN}}$ = 190 nm), 265, 349, and 443 nm. The peaks at 265 and 349 nm in the monomer **21** were slightly red shifted to 289 and 355 nm upon polymerization, due to the extended aromatic system that formed between the monomer units. The peak at 443 nm was shifted to 441 nm.

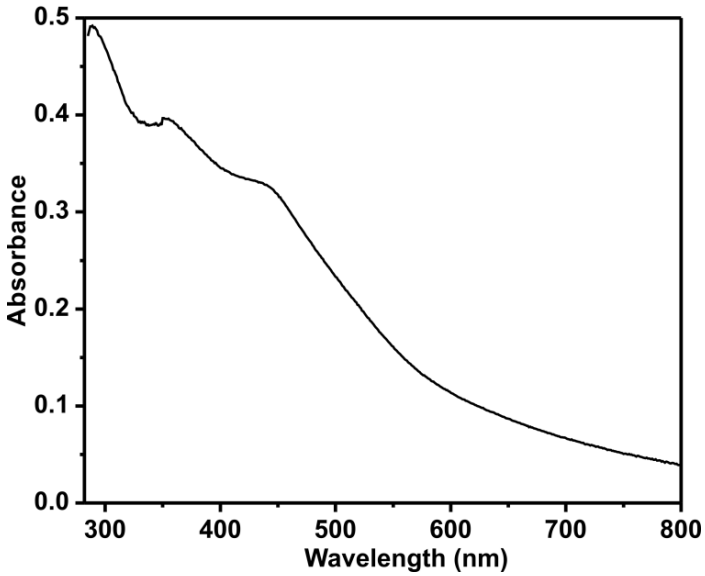

Figure 42. Absorption spectrum of **poly-21** electropolymerized on an ITO coated glass surface.

Luminescence Studies

Photophysical data for each complex, i.e. excitation and emission spectra at 77K and RT, in EtOH/MeOH (4:1) and in 2-MeTHF (dry, air-free and aerated), in cuvette and in EPR tube, quantum yield, luminescence lifetime, The radiative and nonradiative decay constants and oxygen quenching, has been obtained and listed in **Table 15**. The optical density of all complexes was about 0.1 absorbance unit to exclude the excimer formation and concentration quenching effect. Quantum yield measurements by using an integrating sphere did not provide any useful data. Therefore, measurements were carried out by the relative quantum yield technique in which previously reported values for a standard (or a reference) are needed. $Ru(bpy)_3Cl_2$ was selected as the reference. 2-MeTHF was used in the initial luminescence experiments, but later, EtOH/MeOH (4:1) was used to perform the measurements again, in order to compare the experimental results with the reference (measurements of the reference were carried out in EtOH/MeOH (4:1) in the literature). The relative quantum yield for each complex was calculated by using the following formula (2),[175] where the integration is the area under the emission peak. $\Phi_{reference}$ was reported as 0.35 and 0.328 in the literature, and the latter was used in the present calculations.[170, 176]

$$\Phi_{sample} = \Phi_{ref} \times \frac{\text{Integration sample}}{\text{Integration ref}} \times \frac{\text{Absorbance reference}}{\text{Absorbance sample}} \qquad (2)$$

The radiative (k_r) and nonradiative (k_{nr}) decay constants as well as the oxygen quenching rate coefficient (k_q) for each complex was calculated by using the following formulas (3-5).[123, 177] The oxygen concentration in the alcohol mixture was obtained from the literature.[178]

$$k_r = \Phi_{Em}/\tau_0 \quad (3)$$

$$k_{nr} = (1- \Phi_{Em})/\tau_0 \quad (4)$$

$$I/I' = 1+ (k_q. \tau_0.[O_2]) \quad (5)$$

Dry solvents of 2- MeTHF, EtOH and MeOH were degassed by the freeze-pump-thaw technique for 4-5 cycles and then transferred into the glove box which was filled with a N_2 atmosphere. Stock solutions for each complex were prepared in EtOH/MeOH (4:1). Subsequently, the optical density for sample solutions of each complex was measured by using the UV-Vis spectrophotometer (in order to confirm not to exceed 0.1 A). After reaching a proper range of optical density (0.05 – 0.1 A), fresh stock solutions were transferred into airtight quartz cuvettes in the glove box. Measurements with airtight cuvettes could only be carried out at room temperature, but samples in EPR tubes were suitable for measurements both at room temperature and at 77 K. A second set of measurements of each complex and the standard were carried out in an EPR tube in four different conditions, under the following order: air-free–RT, air-free–77 K, aerated–RT, aerated–77 K. The resulting luminescence spectra are presented in **Figure 43-46**. The luminescence spectra of all samples and the standard in airtight cuvettes were also obtained. Subsequently, the airtight cuvettes were aerated by bubbling air with a Pasteur pipette for the corresponding measurements (**Figure 47, 48**).

Table 15. Photophysical data for the ruthenium complexes.

Complex	**18**	**19**	**20**	**21**
λ_{Abs}/nm, (ε, $M^{-1}cm^{-1}$)	281 (29011), 316 (21986)sh, 354 (12247), 497 (6896)	256 (35714), 279 (3873), 326 (52803), 489 (8151)	254 (30553), 290 (66486), 355 (21887), 455 (8894), 550 (4119)	223 (53267), 265 (66997), 349 (18970), 443 (11820) 549 (4033)
$\lambda_{Em\,(Ex)}$/nm at 77 K	310, 400, 630, 750 (276); 450 (400)	306, 400, 635, 760 (278); 485 (450)	315, 400, 620, 750 (277); 581 (456)	312, 400, 618, 750 (278); 566 (453)
$\lambda_{Em\,(Ex)}$/nm at RT	318, 640 (276)	316, 650 (276)	327, 650 (277); 610 (450)	316, 618 (275); 580 (445)
τ_0/µsec (^{3}MLCT) in 2-MeTHF (air-free, dry)	6 +/- 3	7.2 +/- 0.4	11 +/- 1	14 +/- 1
τ_0/µsec (^{3}MLCT) in EtOH/MeOH (4:1) (air-free, dry)	6 +/- 2	8 +/- 3	10 +/- 3	14 +/- 1
τ_0/µsec (^{3}MLCT) in EtOH/MeOH (4:1) (aerated)	6 +/- 2	7 +/- 2	10 +/- 4	14 +/- 3
τ_0/µsec (^{3}MC) in EtOH/MeOH (4:1) (aerated)	5 +/- 1	4 +/- 2	9 +/- 6	7 +/- 3
Φ_{Em} (%) of phos. (^{3}MLCT) (air-free, dry)	1.07	1.4	7.94	10.6
Φ_{Em}(%) of phos. (^{3}MLCT) (aerated)	1.13	1.3	6.98	7.99
Φ_{Em} (%) of flurores. (air-free, dry)	35.8	14.4	19.3	22.5
Φ_{Em} (%) of flurorescence (aerated)	34.4	14.2	19.2	13.7
k_r (s^{-1}), air-free (aerated)	1783.33 (1883.33)	1750 (1857.14)	7940 (6980)	7571.43 (5707.1)
k_{nr} (s^{-1}), air-free (aerated)	164883.33 (164783.33)	123250 (141000)	92060 (93020)	63857.14 (65721.43)
k_q (M^{-1} s^{-1}) (O_2 quenching)	4.68×10^6	1.287×10^7	8.49×10^6	1.353×10^7

In order to find the excitation and emission spectra of complexes, solutions of each complex was excited at their UV–Vis absorption maxima. The resulting emission maxima were used to obtain the excitation maxima, and finally, samples were excited at the excitation maxima that was measured to obtain the maximized emission spectra. All complexes have excitation maxima at 276-278 nm both at room temperature and at 77 K, although all have different absorption maxima in their UV-Vis spectra (**Figure 41** and **43**). The resulting emission maxima are similar for all complexes, i.e. a peak located around 310-320 nm and a broad peak located approximately from 550 nm to 750 nm (**Figure 43**). Emissions around 310-320 nm correspond to ligand fluorescence, due to having both small Stokes shift and short excited-state lifetimes. Emissions around ~550-750 nm should come from ligand phosphorescence due to intersystem crossing after having a singlet excited state. The emission intensity was increased for all complexes and for the $Ru(bpy)_3^{2+}$ standard when the samples were cooled to 77 K in EtOH/MeOH (4:1) glass. The broad peak ~550-750 nm became slightly structured and blue shifted at 77 K. Furthermore, a new structured peak appeared around ~350-550 nm. These observations are due to the reduction of thermal nonradiative pathways available for energy loss.

The luminescent properties of a complex depend on the ordering of its low energy excited states and the orbital nature of its lowest excited state. As a consequence, the energy positions of MC, MLCT, and LC are important. The energies of the MC excited states depends on the ligand field strength, which is in turn related to the σ–donor and π–acceptor properties of the ligands, the steric crowding around the metal, and the bite angle of the polydentate ligands. The energy of the MLCT excited states depends on the reduction potential of the ligand that is involved in the MLCT, the oxidation potential of the metal in the complex, and the charge separation caused by the transition. The energy of the LC excited states depends on the intrinsic properties of the ligands, such as the

energy gap between the HOMO–LUMO levels and singlet–triplet splitting. Ru(II) polypyridine complexes generally have ^{3}MLCT as their lowest excited state and show long lifetimes and intense luminescence properties.[69]

In order to confirm that the orbital nature of the emission that occurred from ~350 to 550 nm appeared upon cooling to 77 K, emission spectra of all complexes and the standard were compared with the emission spectrum of the free ligand ($EDOT_2NNN$), which has been reported previously.[168] The room temperature absorption and the emission of $EDOT_2NNN$ have been reported as 339 nm and 378 nm respectively. These values are higher than the absorption and emission values for the complexes. Ligand phosphorescence of $EDOT_2NNN$ was observed between 484 and 650 nm. There is no peak around that region for the emission spectra of complexes. All complexes and the standard have the same structured emissions from ~375 to 550 nm upon cooling. However, the only common component among complexes **18** and **19** and the standard is Ru^{2+} ion, despite fact that emissions from ~350 to 550 nm overlap; the common components among complexes **20** and **21** and the standard are Ru^{2+} and the bpy ligand (phen is similar to bpy in complex **21**). Furthermore, the lifetimes of the emissions fall in the same range, i.e. a few microseconds (**Table 15**). Assignment of the peak is made as ^{3}MC emission. Literature supports the idea as follows: in d^6 *octahedral* complexes, MC excited states are strongly displaced with respect to the ground state geometry along metal–ligand vibration coordinates. As the lowest excited state is MC, it undergoes a fast nonradiative pathway to the ground state or ligand dissociation reactions. As a result, no luminescence can be observed at RT. Due to the fact that LC and MLCT excited states are not strongly displaced compared with the ground state, as a consequence the nonradiative pathways do not occur and luminescence can be observed. Luminescence coming from the ^{3}LC and ^{3}MLCT states is usually structured. The ^{3}LC emission typically

occurs close to the free ligand emission. On the other hand, the ^{3}MLCT emission occurs at lower energies. Moreover, the ^{3}LC emission is less influenced by the heavy metal ion, hence the emission lifetime is longer than that for ^{3}MLCT. Luminescence arising from a

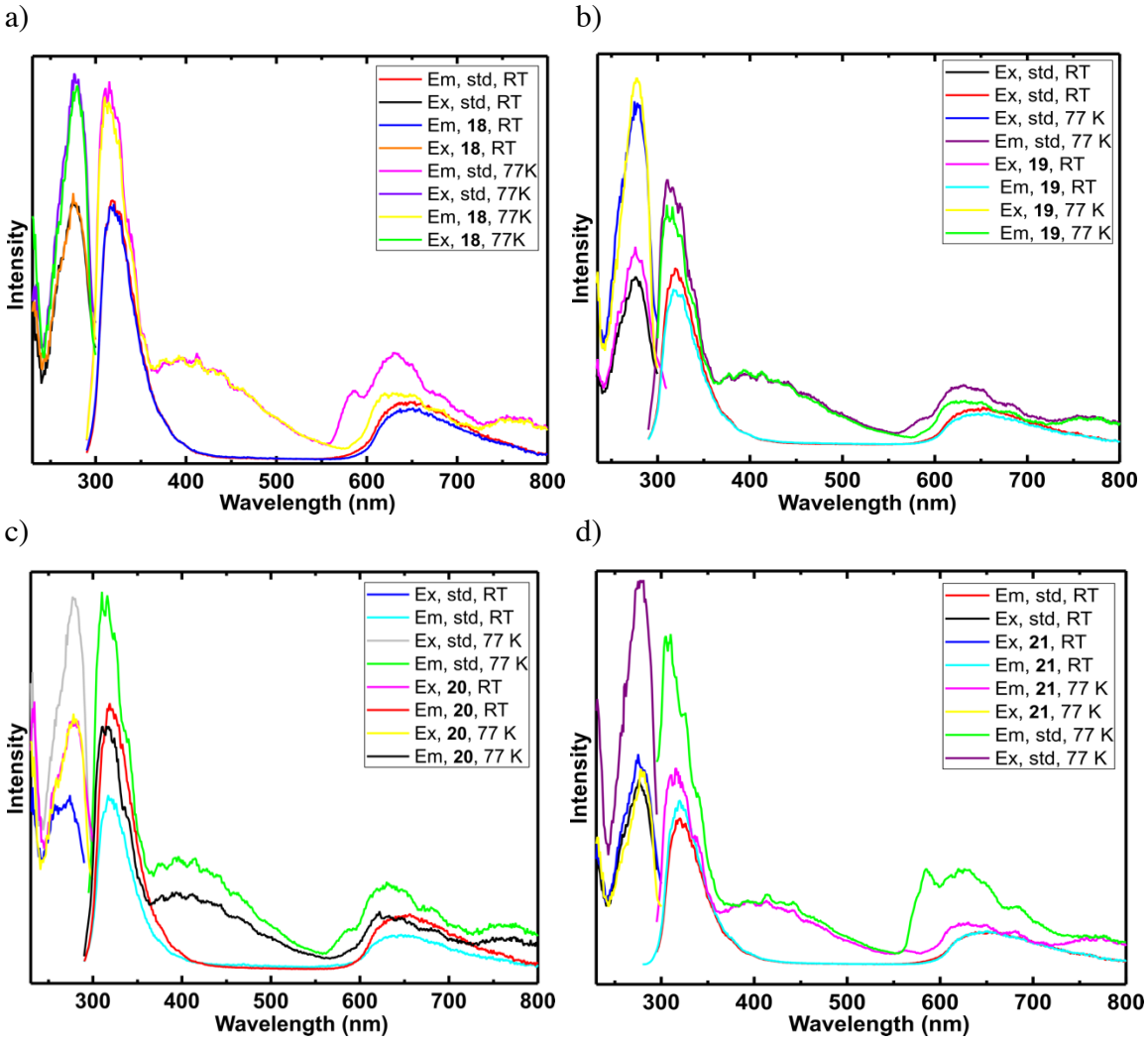

Figure 43. Excitation and emission spectra of the complexes (a) **18** (b) **19** (c) **20** (d) **21** and $Ru(bpy)_3^{2+}$ as the standard in dry, air-free EtOH/MeOH (4:1) solution at RT and at 77 K in a quartz EPR tube.

MC excited state appears as a Gaussian shaped emission band that is red shifted compared with the lowest energy absorption bands. The excited state lifetimes and the intensity decrease with increasing temperature. Furthermore, the ^{3}MC emissions cannot be observed in fluid solutions at RT.[69]

In order to find the luminescence originating from the MLCT transition, the excitation spectra of complexes were obtained by having the emission maxima at approximately 630 nm. The complexes were then excited at the excitation maxima found at ~ 450 nm. The resulting maximized emission spectra were assigned as the ^{3}MLCT emissions.[69, 170]

The luminescence measurements were performed initially at room temperature, then at 77 K in a quartz EPR tube (**Figure 44–46**). For complexes **18** and **19**, both excitation and emission peaks were found to be weak. In **Figure 44**, complex **18** did not even exhibit an emission peak at room temperature in an EPR tube (blue graph). However, upon cooling to 77 K, a shoulder appeared (green graph). Complex **19** yielded better results at both temperatures. Nevertheless, the peaks appeared still weak and noisy (black and red graphs). The emission of **19** was enhanced upon cooling and blue shifted. Neither complexes revealed good emission peaks for the measurements that were carried out at room temperature in a cuvette.

The ^{3}MLCT emissions of complexes **20** and **21** in an EPR tube at room temperature revealed small bumps (**Figure 45** and **46**). However, upon cooling to 77 K, both complexes revealed a highly structured excitation and emission bands as expected for a MLCT transition. Furthermore, the emission maxima for **20** and **21** were found to be blue shifted when cooled to 77 K. Having a broad, structureless spectra at room temperature and structured spectra upon cooling suggests that the thermal nonradiative pathways are reduced due to the energy loss.

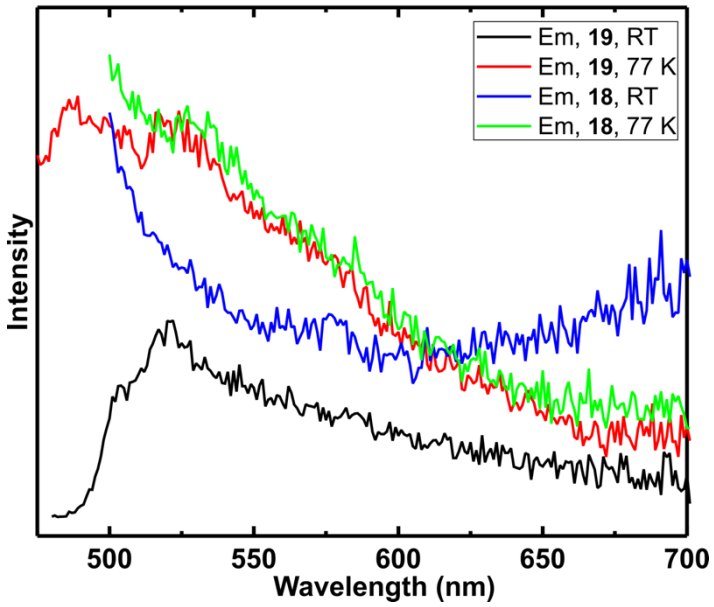

Figure 44. Emission spectra of ^{3}MLCT phosphorescence of complexes **18** and **19** at RT and at 77 K in a dry, air-free EtOH/MeOH (4:1) solution in a quartz EPR tube.

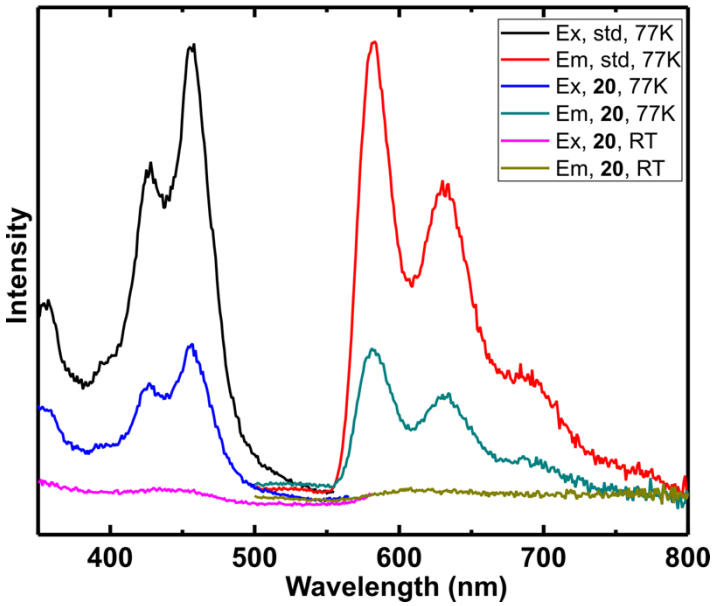

Figure 45. Excitation and emission spectra of ^{3}MLCT phosphorescence of complex **20** and $Ru(bpy)_3^{2+}$ as the standard at RT and at 77 K in a dry, air-free EtOH/MeOH (4:1) solution in a quartz EPR tube.

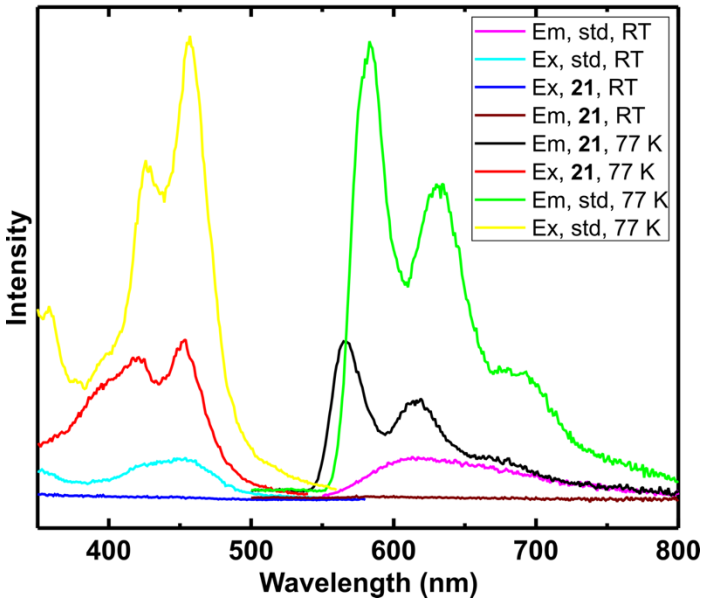

Figure 46. Excitation and emission spectra of ^{3}MLCT phosphorescence of complex **21** and $Ru(bpy)_3^{2+}$ as the standard at RT and at 77 K in a dry, air-free EtOH/MeOH (4:1) solution in a quartz EPR tube.

The excitation and emission spectra of complex **20** for the MLCT transition overlap with the excitation and emission spectra for the standard. On the other hand, the emission spectra for the MLCT transition of complex **21** is 15 nm blue shifted with respect to the standard.

The excitation and emission spectra for **20** and **21** in a quartz cuvette at RT showed broad, unstructured bands. This was true for the measurements that were carried out in an EPR tube at room temperature. The peak maxima for complex **21** were also blue shifted by 10–15 nm with respect to **20** and the standard (**Figure 47** and **48**).

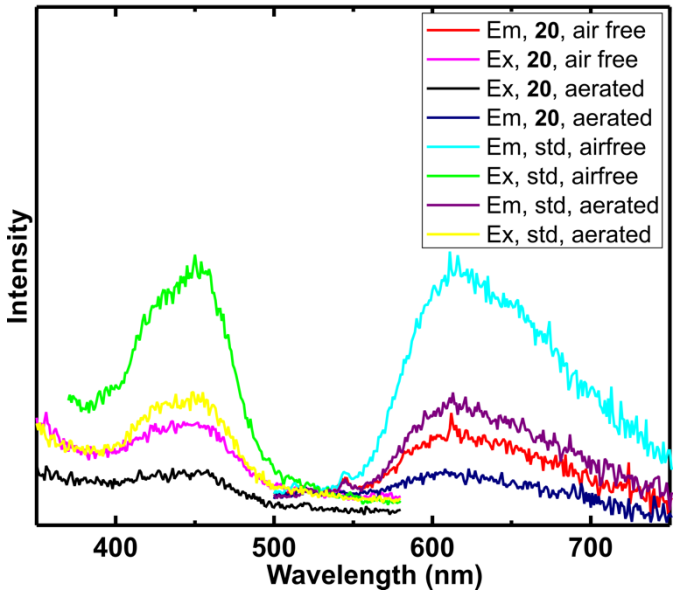

Figure 47. Excitation and emission spectra of ^{3}MLCT phosphorescence of complex **20** and $Ru(bpy)_3^{2+}$ as the standard at RT in air-free and aerated EtOH/MeOH (4:1) solution in an airtight quartz cuvette.

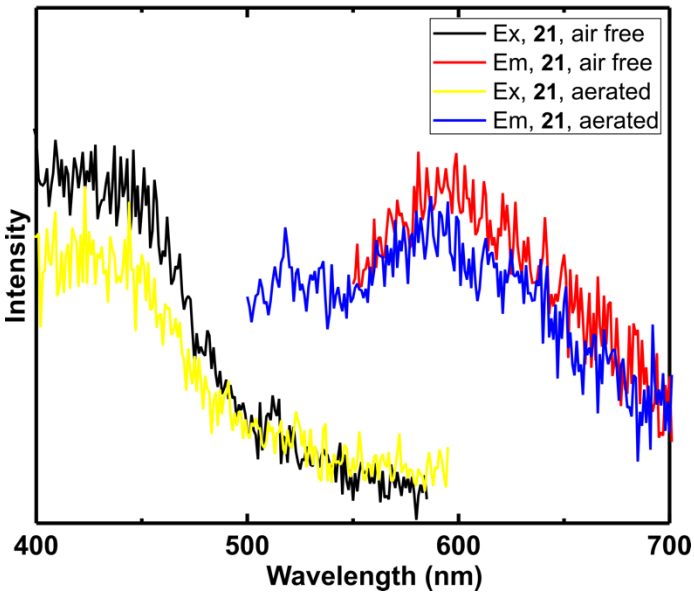

Figure 48. Excitation and emission spectra of ^{3}MLCT phosphorescence of complex **21** and $Ru(bpy)_3^{2+}$ as the standard at RT in air-free and aerated EtOH/MeOH (4:1) solution in an airtight quartz cuvette.

The emission lifetimes for all complexes in both air-free and aerated solutions were measured at 77 K and are presented in **Table 12**. The lifetime of the standard was also measured and found to be consistent with the literature value of 5 μs.[69] The complexes have mean lifetime values that range from 6 to 14 μs. Complex **18** has the shortest lifetime, and complex **21** has the longest lifetime. The lifetime values of complexes did not changed either by changing the solvent from 2-MeTHF to EtOH/MeOH (4:1) or by introducing air into the solutions. The lifetimes of phosphorescence due to the ^{3}MC transition of complexes were also measured. The corresponding values were almost the same as, but slightly lower than the ^{3}MLCT phosphorescence for all complexes.

The fluorescence and phosphorescence quantum yields of the complexes were calculated by using formula (1) for both dry, air-free and aerated solutions of the complexes. The quantum yield of ligand fluorescence was the highest for **18**. However, the quantum yield of phosphorescence due to ^{3}MLCT was the highest for **21**. The emission intensities of both fluorescence and phosphorescence values for all complexes decreased upon exposure to air. The corresponding quantum yield calculations were also decreased up to 2.61% for the phosphorescence and 8.8% for the fluorescence of **21**.

The quenching of the emission by dissolved molecular oxygen was also investigated. The preparation of degassed solution of complexes and introduction of air into samples has been described previously. Farley *et al*. reported a very efficient quenching of dissolved oxygen on their series of platinum complexes by the same technique that was used here, with the exception that the [O_2] was taken as 0.0022 M in their calculations, rather than the value used here as 0.0019099 M.[178, 179] In this study, oxygen quenching resulted in a slight decrease in the emission intensities and a k_q value on the order of 10^6–10^7 M^{-1} s^{-1}, in contrast to the values reported by Farley *et al*. as in the

order of 10^9 M^{-1} s^{-1}. The calculated values of the quantum yield also showed that the oxygen quenching is minimal (**Table 12**). The reason for having this much difference in the quenching might be due to the empty axial position of the metal in *square planar* platinum(II) complexes that Farley *et al*. reported, which are relatively accessible for interaction with a quencher. On the other hand, it is difficult to reach to metal center of an *octahedral* ruthenium complex, that is coordinatively saturated. Another technique for oxygen quenching has been reported by Rusak *et al*. In their technique, oxygen quenching of $Ru(bpy)_3^{2+}$ was studied by introducing SO_3^{2-} anions into the $Ru(bpy)_3^{2+}$ solution in order to adjust the O_2 concentration by the reaction:

$$2SO_3^{2-} + O_2 \rightarrow 2SO_4^{2-}$$

Subsequently, the measurements were carried out at room temperature, since the lifetimes are shorter than those at 77 K.[177] Measurements were carried out in an aqueous solution of $Ru(bpy)_3^{2+}$ without any degassing procedure. This is because the luminescence without SO_3^{2-} anions is measured first, and then added to decrease the O_2 concentration in order to obtain an enhanced luminescence.

Complex **21** was selected to be electropolymerized on an ITO coated glass surface in order to obtain the solid-state excitation and emission spectra of the corresponding polymer because **21** has the highest quantum yield of phosphorescence and the longest lifetime. Initially, **poly-21** was excited at 276 nm, which corresponds to be the excitation wavelength of monomer complexes that are mainly for the fluorescence emission. The corresponding emission spectra were recorded at 77 K (**Figure 49a**). The emission peaks were found at approximately 312 nm and 728 nm. The peak at 312 nm appeared in the same region as that of the monomer. However, the broad peak at ~728 nm had a

considerable red shift in comparison with that of the monomer emission that appeared at approximately 630 nm. The reason for this might be the extended π conjugation that occurred during the polymerization. The peak at 312 nm had a lower intensity than that of the broad peak at 747 nm. The emission spectrum of the monomer was the opposite in terms of the intensity, i.e. the peak at approximately 310 nm was significantly more intense than that of the MLCT emission peak at ~630 nm. The reason for this might be that the singlet excited state of the polymer encounters an efficient intersystem crossing that causes the triplet emission to be enhanced. **Poly-21** was also excited at the monomer excitation wavelength that is 453 nm in order to obtain a MLCT emission. However, the attempt did not result in any emission. Two excitation maxima were found in order to obtain the emission at 747 nm (531 and 639 nm, **Figure 49** in black). P**oly-21** was then excited at these two wavelengths in order to obtain the maximized emission spectra (**Figure 49b** red and blue).

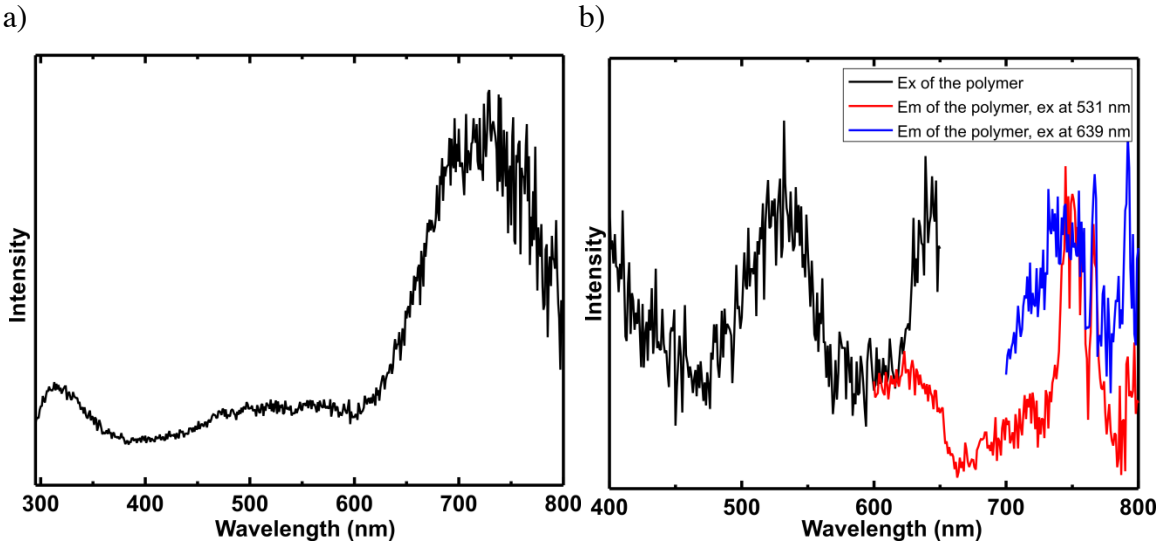

Figure 49. (a) The emission spectrum of **poly-21** that was excited at 276 nm. (b) The excitation (black) and emission spectra (red and blue) of **poly-21** in the visible region of the spectrum.

The lifetime of the 747 nm emission was measured as 13 +/- 8 μs. This value is very close to that of the monomer (14 +/- 1 μs) that has an emission at 566 nm at 77 K. However, the standard deviation is significantly higher than that of the monomer. The ITO coated glass substrate was also excited at 456 nm in order to determine if the emission originated from the ITO itself. The emission maximum of the ITO surface was found to be 730 nm which is a value fairly near, but different from the **poly-21** emission at 747 nm.

CONCLUSIONS

In summary, the syntheses, characterization, UV-Vis absorption, photophysical and luminescence properties and electrochemistry/electropolymerization of EDOT-functionalized (2,6-bis(pyrazol-1-yl)pyridine)Ru(II)(L)Cl complexes have been reported in the present study. The two of the L ligands were anionic (hfac and dbm), and the other two were neutral (bpy and phen) bidentate ligands for potential OLED/PLED applications. All of the complexes were electropolymerizable and the polymers were electroactive. Moreover, the complexes were emissive with relatively long lifetimes and the oxygen quenching of the emission was minimal. Complex **21** was polymerized on an ITO-coated glass substrate for the luminescence studies of the resulting polymer which has indicated promising results for photoluminescence. Future studies would be focused on the preparation of derivatives of the bidentate ligands in order to optimize and tune the emissions of the complexes of the corresponding polymers.

Chapter 5: Synthesis, Characterization, Coordination Chemistry, and Luminescence Studies of Copper, Silver, Palladium, and Platinum Complexes with Phosphorus/Nitrogen/Phosphorus Ligand[4]

INTRODUCTION

PNP ligands have been used widely in coordination chemistry since the 1960s.[180, 181] Complexes of these ligands to transition metals have been extensively reported since these types of ligands combine hard and soft donor atoms to provide flexible coordination modes.[80] The N-donor group in ligands of the type $RN(CH_2CH_2PR'_2)_2$ is hemilabile. When the R group is aromatic, for example, a phenyl group, the lone pair of electrons on the nitrogen is conjugated to the phenyl group. Consequently, the ligand is more hemilabile than similar ligands containing hydrogen or alkyl groups bound to the nitrogen. The preference for forming complexes as the monomeric tridentate ligands or as monomeric and dimeric bidentate ligands can be controlled by modifying the relative donor strength of the nitrogen donor via adjusting the electron donating or withdrawing ability of the substituent R and the anion X^- (**Figure 50**).[55, 182-184]

[4] Complex **22** has been published as a journal article/structure report: Keskin, S. G.; Stanley, J. M.; Mejia, M. L.; Holliday, B. J. {N,N-bis2-(diphenylphosphanyl)ethyl-aniline}(eta$_2$-dibenzylideneacetone)palladium(0). *Acta Cryst. Section E-Structure Reports Online* **2011,** *67*, M1327-U248.
Seyma Keskin carried out the synthesis, purification and characterization by $^{31}P\{^1H\}$ NMR and MS, and crystallization. The crystal was diffracted by Michelle L. Mejia; crystal data were completed by Julie M. Stanley. The experimental section, the related literature section and a part of comment section of the article were written by Seyma Keskin; the rest of the publication was written by Julie M. Stanley. The principle investigator at the time of the work was Dr. Bradley J. Holliday.

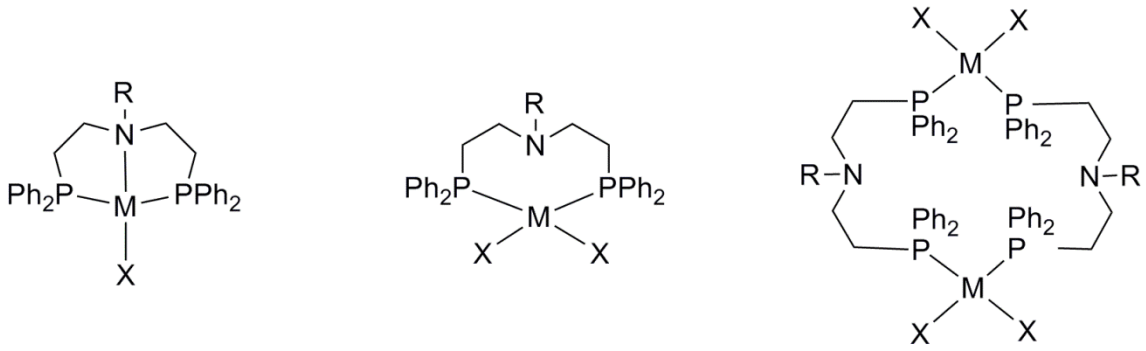

Figure 50. Binding modes of PNP ligand of the type $RN(CH_2CH_2PPh_2)_2$.

In addition to having different binding modes, a PNP ligand of the type $RN(CH_2CH_2PPh_2)_2$ can also be used to synthesize oligomeric and polymeric coordination compounds.[55] Complexes of these types of PNP ligand are suitable for many applications, such as molecular materials and catalysis.[185,186]

Various complexes of copper, silver, gold, platinum, and palladium with nitrogen and phosphorus donors have been reported for their luminescence behavior as well as their interesting structures (**Figure 51**).[187-191] Zhang *et al*. have reported copper and platinum complexes of the naphthyridine-phosphine ligand with their photophysical properties and different coordination modes. They reported that both mononuclear and binuclear copper complexes with distorted *tetrahedral* geometry, as well as a binuclear copper complex with distorted *trigonal planar* geometry, which has a Cu–Cu bond. Their platinum complexes, however, are mononuclear with *square planar* geometry. Spectroscopic investigations indicated that solution emissions of their compounds at room temperature resulted in ligand fluorescence, whereas solid state phosphorescence was obtained from a copper and a platinum complex.[187] Yam *et al*. also reported luminescent trinuclear copper(I) acetylides with PNP [bis(diphenylphosphino)-alkyl/-aryl amine] as bridging ligands. They changed the substituents on the

diphenylphosphinoamine for the design and study of donor-acceptor properties and substituent effects on the spectroscopic and electrochemical properties of the trinuclear copper complexes.[188] Harkins and Peters reported an exceptional luminophore based on an amido-bridged bimetallic copper system, $[(PNP)CuI]_2$, derived from a chelating bis(phosphine)amide ligand ($[PNP]^-$ = bis(2-(diisobutylphosphino)phenyl)amide). Its combined quantum yield is $\Phi > 0.65$, and its lifetime is $\tau > 10$ μs.[189] Catalano *et al*. reported luminescent gold(I) and silver(I) metallocryptates using a hybrid phosphine-phenanthroline ligand, 2,9-bis(diphenylphosphino)-1,10-phenanthroline (P_2phen).[190] Recently, Jin *et al*. reported palladium(II)–PPh_3 complexes with different heterocyclic-N/NS co-ligands, and found that the coexistence of PPh_3 and heterocyclic-N/NS ligands remarkably changed the luminescence property of d^8 palladium(II) complexes, although d^8 palladium(II) complexes were well known quenchers like platinum analogues.[191]

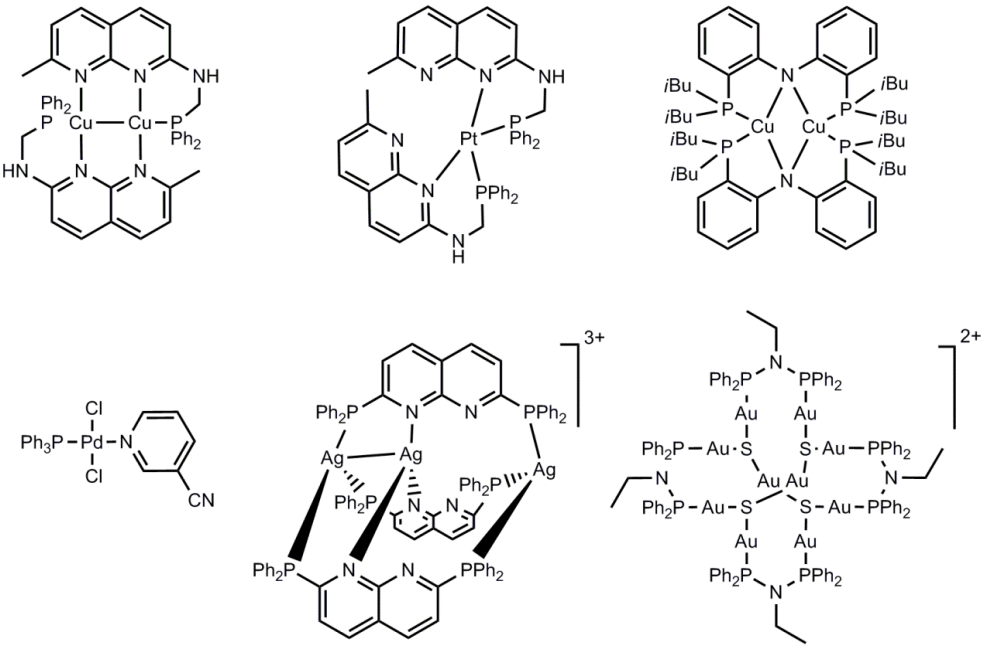

Figure 51. Examples of luminescent complexes of copper, silver, gold, platinum and palladium with phosphorus and nitrogen donating ligands.

Luminescent platinum(II) complexes can be divided into three groups: 1) mononuclear complexes, 2) dinuclear complexes with bridging ligands, and 3) linear chains comprising stacked complex units. Platinum(II) complexes with a d^8 electronic structure are often stacked in the solid state, which results in luminescence coming from metal–metal electronic interactions. The majority of the mononuclear platinum(II) complexes are non-luminescent in solution at room temperature, although they emit at low temperatures. The reasons can be that the *d-d* transition states may induce fast non-radiative deactivation, and solvent molecules can cause facile quenching of the excited state, because the *square planar* structures have open coordination sites, lastly, they can be quenched by triplet oxygen.[192] The metal-metal bond establishment results in the investigation of similar d^{10}-d^{10} complexes.

Luminescent properties of phosphine complexes of d^{10} metals such as Cu(I), Ag(I), Au(I), Ni(0), Pd(0), and Pt(0) have been reported.[193] Interestingly, in polynuclear d^{10} metal complexes, short metal–metal distances were observed. In theory, in the absence of metal *(n+1)s* and *(n+1)p* electrons, the interaction between the closed shell d^{10} metal centers would be expected to be repulsive. However, configuration mixing of the filled *nd* orbitals with the empty *(n+1)s* and *(n+1)p* orbitals turned this repulsion into a slight attraction between the metal centers, resulting in a weak metal-metal bonding interaction.[194]

In addition to their luminescent properties, some of the PNP complexes indicated catalytic activities, which first reported with iridium, rhodium, and palladium. Some of the complexes were chiral or have hydrophilic groups; in some cases, the nitrogen atom was tethered to solid supports.[195-197] Hii *et al*. reported PNP-Pd complexes with both 0 and +2 oxidation states and studied the rate of oxidative addition of Pd(0) to aryl iodides.[80] They indicated that the coordination behavior of PNP ligands with respect to palladium

was dependent on the nature of the nitrogen donor. They also found that nature of the nitrogen donor dramatically altered the reactivity of their palladium(0) complexes in oxidative addition reactions toward aryl halides which was an important first step in many palladium catalyzed reactions.

In the present study, synthesis, characterization and luminescence studies of copper, silver, platinum, and palladium complexes of N,N-bis[2-(diphenylphosphino)ethyl]phenylamine (PNP) ligand is targeted. Different coordination modes and different numbers of metal centers are possible with the title ligand. Consequently, the luminescence properties of the resulting complexes may be affected. Moreover, fluorescence spectra of the title ligand have not been reported previously.

EXPERIMENTAL

Instrumentation

NMR spectra were recorded with a Varian Unity + 300 or Varian 500 spectrometer with an Oxford Instruments Ltd. superconducting magnet using a 5 mm Auto-switchable probe ($^{1}H/^{19}F/^{13}C/^{31}P$) and Sun Ultra 5 workstation. ^{1}H NMR signals were referenced to residual proton resonances in deuterated solvents. $^{13}C\{^{1}H\}$ NMR spectra were referenced relative to solvent peaks. $^{31}P\{^{1}H\}$ NMR spectra were referenced to a H_3PO_4 external standard. All peak positions were listed in ppm, and all coupling constants were listed in Hertz (Hz). Mass spectrometry was carried out using a Thermo Finnegan TSQ 700 spectrometer. Melting points were recorded on a Mel-Temp II melting temperature apparatus made by Laboratory Devices of Holliston, MA. Elemental analysis was performed by Quantitative Technologies Inc. (Whitehouse, NJ). Luminescence

measurements were performed by a Photon Technology International QM 4 spectrophotometer. Samples were freshly prepared prior to analyses.

X-ray Crystal Structure Analysis

The single–crystal diffraction data of **25** were collected on a Nonius Kappa CCD diffractometer using a graphite monochromator with MoKα radiation (λ = 0.71073Å) and an Oxford Cryostream low temperature device. The single–crystal diffraction data of **26**, **27**, and **30** were collected on a Rigaku SCX-Mini diffractometer with a Mercury CCD using a graphite monochromator with MoKα radiation (λ = 0.71073Å). The single–crystal diffraction data of **28** and **29** were collected on a Rigaku AFC12 diffractometer with a Saturn 724+ CCD using a graphite monochromator with MoKα radiation (λ = 0.71073Å). Absorption corrections were applied by using Multi-scan. Data reductions were performed by using Rigaku Americas Corporation Crystal Clear version 1.40.[125] The structures were solved by direct methods and refined anisotropically using full-matrix least-square methods with the SHELX 97 program package.[99] The coordinates of the non-hydrogen atoms were refined anisotropically, while hydrogen atoms were included in the calculation isotropically but not refined. Neutral atom scattering factors and values used to calculate the linear absorption coefficient are from the International Tables for X-ray Crystallography (1992).[100] Crystal data collection and refinement details are presented in **Tables 18** and **19**. Selected bond lengths are given in **Tables 20–25**.

Synthesis

General Methods

All chemicals were purchased from commercial suppliers and were used as received. Air- and moisture-sensitive reactions were carried out in oven-dried glassware using standard Schlenk techniques under an inert nitrogen atmosphere or in a glove box with an argon atmosphere. Dry solvents were obtained from an Innovative Technologies Pure-Solv 400 solvent purification system. The PNP ligand, N,N-bis[2-(diphenylphosphino)ethyl]phenylamine **3**, was prepared according to Kostas' method[53] and the synthesis scheme was demonstrated in chapter 2 (**Scheme 1**). Bisbenzonitriledichloroplatinum(II) and bisbenzonitriledichloropalladium(II) were prepared according to literature methods.[198, 199] **Scheme 9** indicates the routes that were used to synthesize the metal complexes.

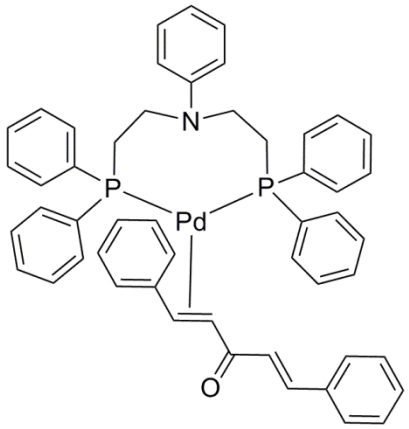

PNP-Pd-dba [22]. 3 (0.202 g, 0.39 mmol) was dissolved in 5 ml of THF in the glove box. Pd_2dba_3 (0.179 g, 0.205 mmol) was added to the ligand solution. The mixture was stirred overnight, then filtered through a piece of cotton and celite placed in a Pasteur pipette. The filtrate was dried under a Schlenk line. The residue was redissolved in DCM, on which hexanes were layered, and then the mixture was placed in the freezer to afford

orange crystals. Crystals were isolated (57.4%, 0.192 g, 0.22 mmol) and characterized by X-ray diffraction analysis for the first time.[200] $^{31}P\{^{1}H\}$ NMR and MS were match the reported values.[80]

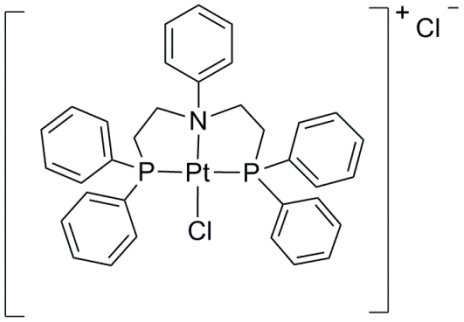

[PNP-PtCl]Cl [23]. The PNP ligand **3** (0.145 g, 0.28 mmol) and bis-benzonitriledichloroplatinum(II) (0.128 g, 0.28 mmol) were weighed into separate Schlenk flasks in the glove box, subsequently connected to a Schlenk line. Dry benzene was cannula-transferred into both flasks, which were then stirred. The mixture containing platinum did not dissolve, so it was refluxed to produce a light yellow solution. The ligand solution was cannula-transferred into the refluxing metal solution. The reaction mixture was refluxed for 1.5 hours to obtain a white precipitate and a colorless solution. The mixture was cooled to room temperature under N_2. The precipitate was cannula-filtered and then dried under vacuum to afford a white solid **23** (94.2%, 0.2067 g, 0.264 mmol). ^{1}H NMR (300 MHz, $CDCl_3$): 7.46 (dd, 8H, J = 8.1, J = 2.4), 7.26 – 7.35 (m, 6H), 7.13 (t, 8H, J = 7.2), 6.85 (t, 1H, J = 7.5), 6.56 (d, 2H, J = 8.4), 4.14 (d, 4H, J_{PH} = 19.8), 2.56 (bs, 4H). $^{31}P\{^{1}H\}$ NMR (121.498 MHz, $CDCl_3$): 10.32 (s) with satellites at 25.11 and -4.46 (J_{PtP} = 1796.96 Hz) (close to the literature value[84]). HRMS (ESI) data were calculated for $C_{34}H_{33}ClNP_2Pt$ $[M - Cl]^+$ 748.14, and found to be 748.11 (the literature value was calculated for $C_{34}H_{33}Cl_3NP_2Pt$ $[M + Cl]^-$ 817.0786 and found to be 817.0802[84]). Hexanes

were layered on a CH_2Cl_2 solution of the product in order to obtain a crystal suitable for X-ray analysis (crystal structure of a *trans*-PNP-Pt complex was obtained in the present study. However, the crystal structure of a cis-PP-Pt complex was reported in the literature.[84]) Elemental Analysis: calculated for $C_{34}H_{33}Cl_2NP_2Pt$ % C: 52.12, % H: 4.24, % N: 1.79 and found to be % C: 51.37, % H: 3.12, % N: 1.49. Mp: decomposed around 240°C.

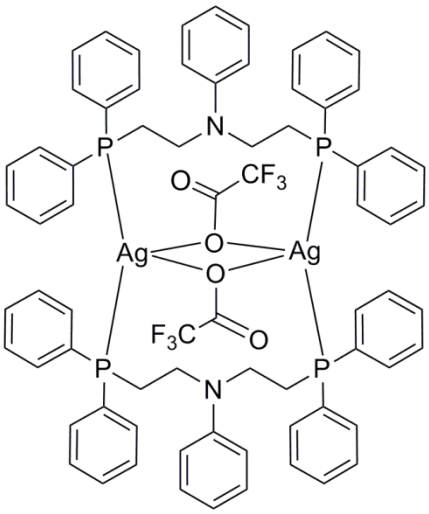

[PNP-AgCF$_3$COO]$_2$ [24]. 3 (0.030 g, 0.058 mmol) was dissolved in 5 ml of dry THF in the glove box. $AgCF_3COO$ (0.013 g, 0.058 mmol) was added to the ligand solution. The mixture was stirred for 3 hours in the dark (covered by aluminum foil in the glove box). Then, the reaction mixture was connected to a Schlenk line, and the solvent was pulled under a vacuum to obtain an off-white solid (88%, 0.038 g, 0.026 mmol). ^{1}H NMR (300 MHz, CD_2Cl_2): 7.44 – 7.24 (m, 40H), 7.04 (bs, 4H), 6.56 (bs, 2H), 6.12 (bs, 4H), 3.51 (bs, 8H), 2.58 (bs, 8H). ^{31}P{^{1}H} NMR (121.498 MHz, CD_2Cl_2): 2.153 (dd, ^1J(^{31}P, ^{109}Ag) = 520.257, ^1J (^{31}P, ^{107}Ag) = 450.516). HRMS (ESI) calculated for monomer $C_{34}H_{33}AgNP_2$ $[M - CF_3COO]^+$ 626.11 and found to be 626.1; HRMS (ESI) calculated for $C_{68}H_{66}Ag_2ClN_2P_4$ $[M–2(CF_3COO)+Cl]^+$ 1285.2 and found to be 1285.3; HRMS (ESI)

calculated for $C_{72}H_{66}Ag_2F_6N_2O_4P_4$ [M] 1476.2 and small peak found at 1474.8. Hexanes were layered on a CH_2Cl_2 solution of the product to obtain a crystal suitable for X-ray analysis. Elemental Analysis: calculated for $C_{36}H_{33}AgF_3NO_2P_2$ % C: 58.55, % H: 4.50, %N: 1.90 and found to be % C: 58.87, % H: 4.27, %N: 1.81. Mp: 200°C.

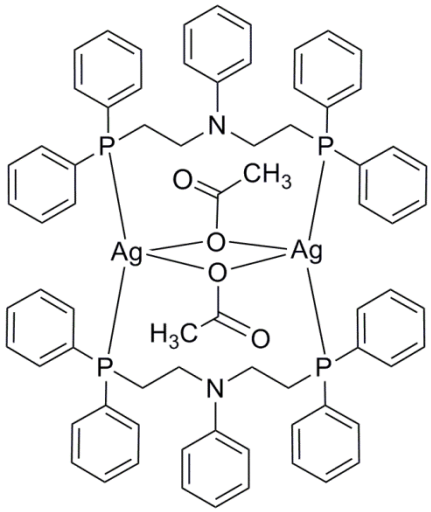

[PNP-AgCH$_3$COO]$_2$ [25]. Prepared the same way as **24**. Off-white solid was obtained (85%, 0.080 g, 0.058 mmol) ^{1}H NMR (300 MHz, CD_2Cl_2): 7.52–7.23 (m, 40H), 7.05 (t, 4H, J = 8.4), 6.61 (bs, 2H), 6.25 (bs, 4H), 3.54 (bs, 8H), 2.56 (bs, 8H), 1.91 (s, 6H). ^{31}P{^{1}H} NMR (121.498 MHz, CD_2Cl_2, 25°C): -2.386 (s). ^{31}P{^{1}H} NMR (202.348 MHz, CD_2Cl_2 27°C): -1.49 (s). ^{31}P{^{1}H} NMR (202.348 MHz, CD_2Cl_2, -40°C): -1.43 (dd, ^1J(^{31}P, ^{109}Ag) = 493.729, ^1J(^{31}P, ^{107}Ag) = 427.764). ^{31}P{^{1}H} NMR (202.348 MHz, CD_2Cl_2,-80°C): -2.44 (d, J = 467.829). HRMS (ESI) calculated for $C_{70}H_{69}Ag_2N_2O_2P_4$ [M – CH_3COO]$^+$ 1310.24 and found to be 1310.20. Hexanes were layered on a CH_2Cl_2 solution of the product to obtain a crystal suitable for X-ray analysis. During the crystal formation, CH_3COO^- anion replaced by Cl^- anion that was generated from the solvent CH_2Cl_2 and resulted in a crystal structure of $C_{68}H_{66}Ag_2Cl_2N_2P_4$ matching with the literature structure.[201] The literature complex contained an additional chloroform molecule in their unit cell.

The space group of the crystal (**25**) and the literature complex are different. Elemental Analysis: calculated for $C_{36}H_{36}AgNO_2P_2$ % C: 63.17, % H: 5.30, %N: 2.05 and found to be % C: 62.49, % H: 5.23, %N: 1.89. Mp: 183°C.

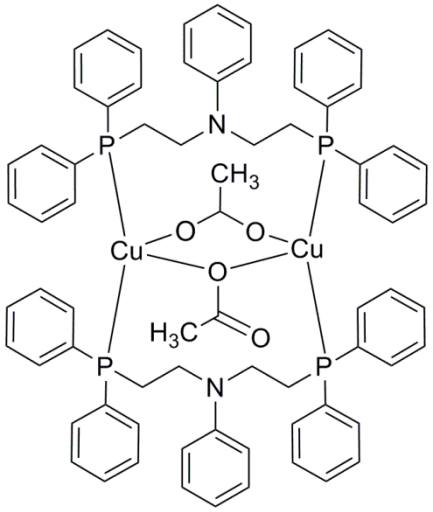

[PNP-CuCH$_3$COO]$_2$ [26]. Cu(CH$_3$COO)$_2$ (0.011 g, 0.058 mmol) was transferred into a Schlenk flask in the glove box. 5 ml of dry THF was added; the mixture was stirred but did not dissolve. **3** (0.030 g, 0.058 mmol) was added to the mixture, and the Schlenk flask was connected to a Schlenk line, then heated to reflux for 3 hours under N_2 to obtain a teal solution. The solvent was pulled under a vacuum to obtain a light teal solid (78%, 0.029 g, 0.023 mmol). ^{1}H NMR (300 MHz, CD_2Cl_2): 7.59 (bs, 4H), 7.19 - 7.04 (m, 40H), 6.73 (bs, 2H), 6.39 (bs, 4H), 3.41 (bs, 8H), 2.50 (bs, 8H), 1.88 (s, 6H). ^{31}P{^{1}H} NMR (121 MHz, CD_2Cl_2): -12.9 (s). HRMS (CI$^+$) calculated for monomer $C_{36}H_{37}CuNO_2P_2$ $[M + H]^+$ 640.16 and found to be 639.15. LRMS (ESI) calculated for $C_{68}H_{66}ClCu_2N_2P_4$ 1197.24 and found to be 1196.67. Hexanes were layered on a CH_2Cl_2 solution of the product to obtain a crystal suitable for X-ray analysis Elemental Analysis: calculated for $C_{36}H_{36}CuNO_2P_2$ % C: 67.54, % H: 5.67, %N: .2.19 and found to be % C: 64.96, % H: 4.90, %N: 1.92. Mp: 95°C.

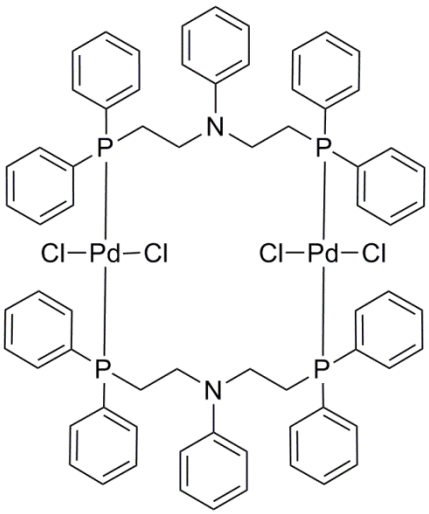

[PNP-PdCl$_2$]$_2$ [27]. The PNP ligand **3** (0.200 g, 0.386 mmol) and bis-benzonitriledichloropalladium(II) (0.148 g, 0.386 mmol) were weighed into separate Schlenk flasks in the glove box, then connected to a Schlenk line. Dry benzene was cannula-transferred into both flasks, which were then stirred. The solution containing palladium was refluxed to obtain a light orange solution. The ligand solution was cannula-transferred into the refluxing metal solution. Subsequently, the reaction mixture was refluxed for an hour to obtain a yellow precipitate and an orange solution. The mixture was cooled to room temperature under N_2 while being stirred. The precipitate and the solution were separated by cannula filtering, and then both were dried under vacuum. The yellow precipitate was mostly insoluble, thus it was not suitable for NMR studies (the precipitate may be a coordination polymer of Pd^{2+} and the PNP ligand). The dried orange solution was redissolved in CH_2Cl_2 and hexanes were layered to obtain large, prismatic, dark yellow, X-ray quality crystals (65%, 0.1745 g, 0.251 mmol). The X-ray diffraction experiment displayed the structure as a dimer. ^{1}H NMR (300 MHz, CD_2Cl_2): 7.77 (bs, 16H), 7.50 – 7.40 (m, 24H), 6.84 (m, 4H), 6.46 (m, 2H), 5.71 (m, 4H), 3.64 (bs, 8H), 2.73 (bs, 8H). ^{31}P{^{1}H} NMR (121 MHz, CD_2Cl_2): 10.92 (s). HRMS (ESI) calculated for monomer $C_{34}H_{33}ClNP_2Pd$ $[M - Cl]^+$ 660.08, and found to be 660.079. Elemental

Analysis: calculated for $C_{34}H_{33}Cl_2NP_2Pd$ % C: 58.77, % H: 4.79, %N: 2.02 and found to be % C: 58.52, % H: 4.02, %N: 1.88. Mp: decomposed around 165°C.

$PdCl_2$ was used as a second approach for the synthesis of **27**. 12 mL CH_2Cl_2 was added to $PdCl_2$ (0.030 g, 0.168 mmol). The mixture was stirred, but $PdCl_2$ was slightly soluble. Ligand **3** (0.087 g, 0.168 mmol) was added into the mixture, which was stirred for 3 hours in the glove box. The solvent was evaporated under a Schlenk line to afford a burnt orange residue. The residue was dissolved in CH_2Cl_2, and hexanes were layered to obtain large, prismatic, dark yellow crystals, which yielded the same crystal structure as the other method.

RESULTS AND DISCUSSION

Syntheses

The PNP ligand **3** was prepared according to the method reported by Kostas.[53] The title complexes of **3** with platinum, palladium, silver, and copper were synthesized as outlined in **Scheme 9** and characterized. Complexes of **3** with a variety of metals were reported [53, 80, 83] and molybdenum complexes of **3** was studied in chapter 2. In the syntheses of **23** – **27**, one equivalent of reacted with one equivalent of **3**, to afford good yields of the products (65–94.2%). However, in the synthesis of **22**, the metal to ligand ratio was 0.5, to give a 57.4% yield of the product. Crystallization was used as the purification technique for all complexes. Characterizations of complexes were achieved by ^{1}H NMR, ^{31}P{^{1}H} NMR, HRMS, EA, and X-ray crystallography. Both ^{1}H NMR and ^{31}P{^{1}H} NMR signals of **22** – **27** revealed different patterns and chemical shifts with respect to those found in the free ligand **3**, confirming the existence of complexes in the solution.

Complex **22** was previously reported, but no crystal structure has been previously reported. The synthesis of **22** was reproduced and it was crystallized as orange X-ray quality crystals. The attempt to make an electropolymerizable version of **22** for a heterogeneous catalyst application by using the ligand **14** (chapter 3) was not successful. In the syntheses of **22**–**27**, **22** was the only complex in which the metal has a zero oxidation state, and **23** was the only complex that is ionic. An oligomer has been reported with PNP-Pd coordination, in which dimeric and monomeric coordinations of Pd^{2+} were alternating.[55] The individual dimeric complexes were not prepared in that journal article. In the present study, the dimeric complex **27** was synthesized and characterized; its crystal structure was reported. Complexes **22** and **27** were both PNP-Pd complexes, yet Pd had different oxidation states and coordination modes. The synthesis of the monomeric complex in which the oxidation state of palladium is +2 was not obtained, although an example was previously reported.[185] Different reaction conditions and Pd starting materials resulted in the same complex **27**. Complex **26**, which had two Cu(I) centers, was obtained by using a Cu(II) source. When the same reaction was attempted by using $CuCH_3COO$ instead of $Cu(CH_3COO)_2$, the reaction was unsuccessful.

An exchange of the dba ligand of **22** was attempted with carbonyl ligands by bubbling CO (g) through a concentrated solution of **22** in a screw top NMR tube which was cooled to 0°C in order to increase the solubility of the gas. The reaction was monitored by $^{31}P\{^{1}H\}$ NMR. The identity of any resulting product was inconclusive, since the NMR spectrum of the reaction mixture was collapsed into a broad singlet, while $^{31}P\{^{1}H\}$ NMR spectrum of **22** displayed a doublet.

Ligand **3** resulted in all different coordination modes with different metals, i.e. monomeric tridendate (PNP) as in **23**, monomeric bidentate (PP) as in **22**, dimeric bidentate (PP) as in **27**, and dimeric bidentate (PP) with two bridges as in **24**, **25**, and **26**.

Bidentate versus tridentate coordination modes were determined by the donor strength of the hemilabile N atom of **3** as well as the anion. The donor strength of N can be tuned by attaching different R groups to the N for applications such as catalysis and molecular materials.[55] A result of bridged (*tetrahedral*) versus *square planar* coordination mode was due to crystal-field stabilization energy of the metal complex. The observed geometry was *square planar*, especially for platinum and palladium, because the crystal-field stabilization energy of a *square planar* geometry was the highest for platinum and palladium.[44] On the other hand, both *tetrahedral* and *square planar* geometries were observed for silver and copper in the literature, depending on the resulting crystal-field stabilization energy of the complex.[44]

Scheme 9. Synthesis of silver, copper, platinum, and palladium complexes of PNP ligand. (a) Pd_2dba_3, dry THF, RT, under N_2, 12 hours (b) $(PhCN)_2PtCl_2$, dry benzene, reflux, under N_2, 1.5 hours (c) $AgCF_3COO$, dry THF, RT, under N_2, 3 hours, in the dark (d) $AgCH_3COO$, dry THF, RT, under N_2, 3 hours, in the dark (e) $Cu(CH_3COO)_2$, dry THF, reflux, under N_2,3 hours (f) $(PhCN)_2PdCl_2$, dry benzene, reflux, under N_2, 1 hour, or $PdCl_2$, dry CH_2Cl_2, RT, under N_2, 3 hours.

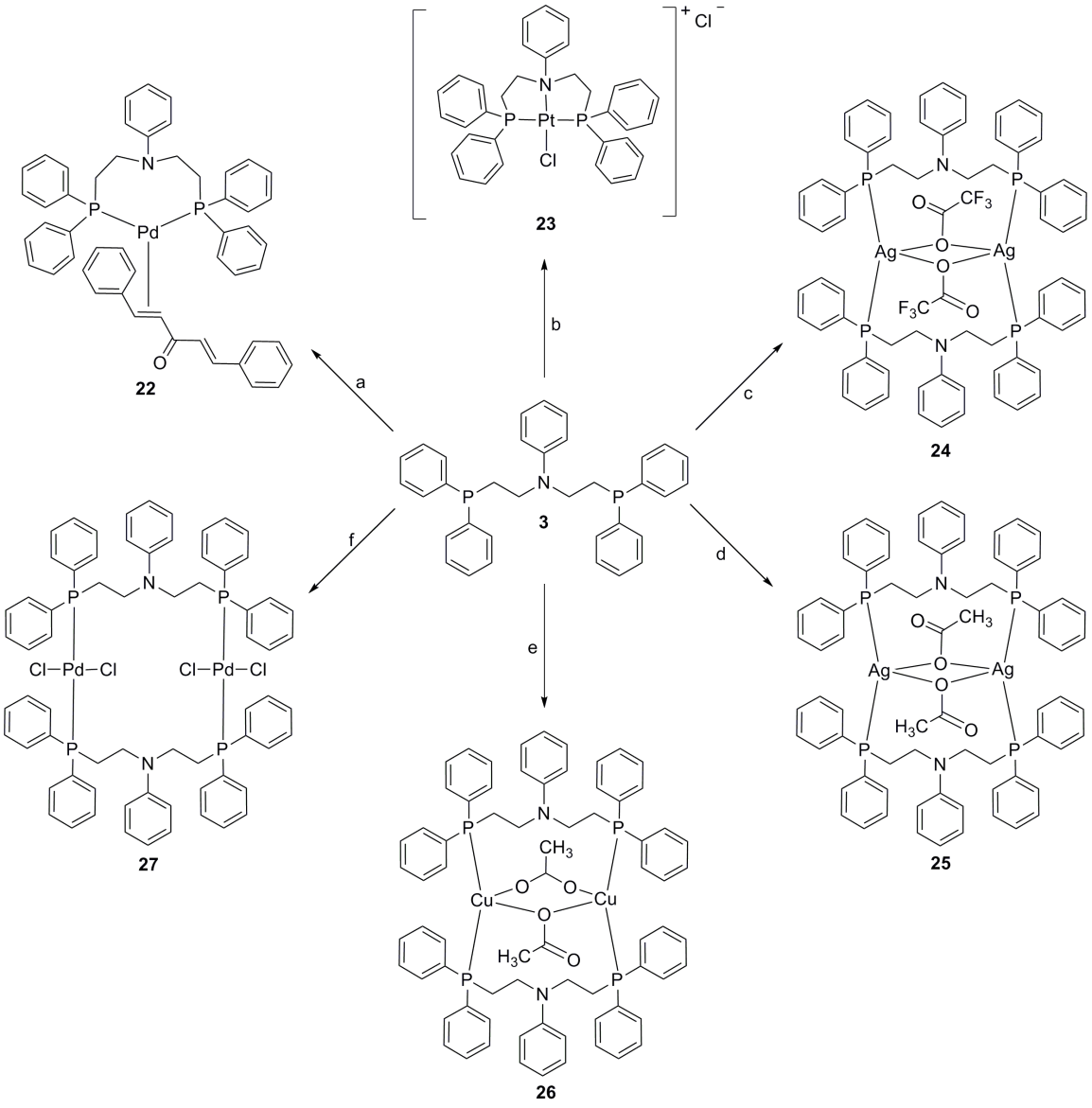

Both the solution of free ligand **3** in CH_2Cl_2 and **3** in solid state were exposed to air, in order to determine if the phosphorus atoms would oxidize or not. Surprisingly, phosphorus atoms did not oxidize, as traced by $^{31}P\{^1H\}$ NMR. On the other hand, during metallation reactions, phosphorus atoms of **3** oxidized. Therefore, metallation reactions were carried out in oxygen-free media, i.e. a glove box and a Schlenk line under nitrogen or argon.

An attempt has been made to synthesize a PNP-Au complex both with Au(I) and Au(III). However, the syntheses were not achieved. Syntheses of complexes containing Fe, Ru, Rh, Ir, Ni also were attempted, but the complexes were not isolated or identified (**Scheme 10-12**). PNP complexes of Fe(0) and Ru(0), which were dark green and orange respectively, were detected only in $^{31}P\{^1H\}$ NMR; reaction with iron resulted in a major peak at 56.67 ppm and a minor peak at 68.29 ppm, although the free ligand appears at –20 ppm. Reaction of **3** with $Ru_3(CO)_{12}$ resulted in 4 peaks: 40 ppm (main), 35 ppm, 28 ppm, and 23 ppm. Both Fe(0) and Ru(0) product mixtures were crystallized. Unfortunately, crystal qualities were not suitable for X-ray diffraction studies. PNP complexes of rhodium and iridium resulted in many products that could not be isolated, observed in $^{31}P\{^1H\}$ NMR as separate peaks. Finally, the reaction with nickel resulted in a red compound. $NiCl_2.6H_2O$ is green; when the ligand solution was added to the solution of Ni^{2+}, an immediate color change occurred, which was promising, but the product could not be identified. ^1H NMR in which peaks were concentrated in the aliphatic region as big broad peaks may have been caused by a paramagnetic product. Nonetheless, EPR did not reveal any peaks. Surprisingly, no peak was observed in $^{31}P\{^1H\}$ NMR spectrum. Crystallization attempts did not result in any crystals suitable for X-ray diffraction. Therefore attempted syntheses of complexes of these metals remain inconclusive (**Scheme 11**).

Scheme 10. Proposed structures for iron(0) and ruthenium(0) complexes of **3**.

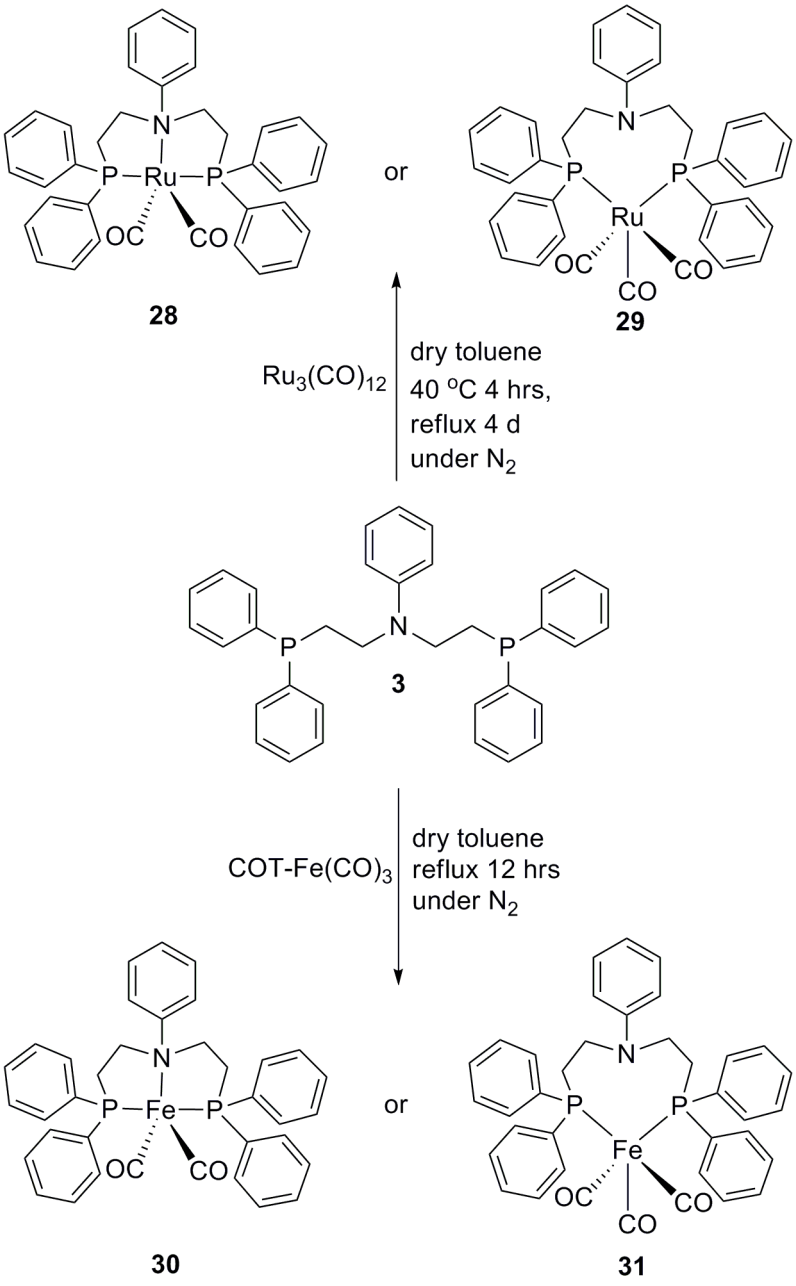

Scheme 11. Proposed structures for nickel(II) and ruthenium(II) complexes of **3**.

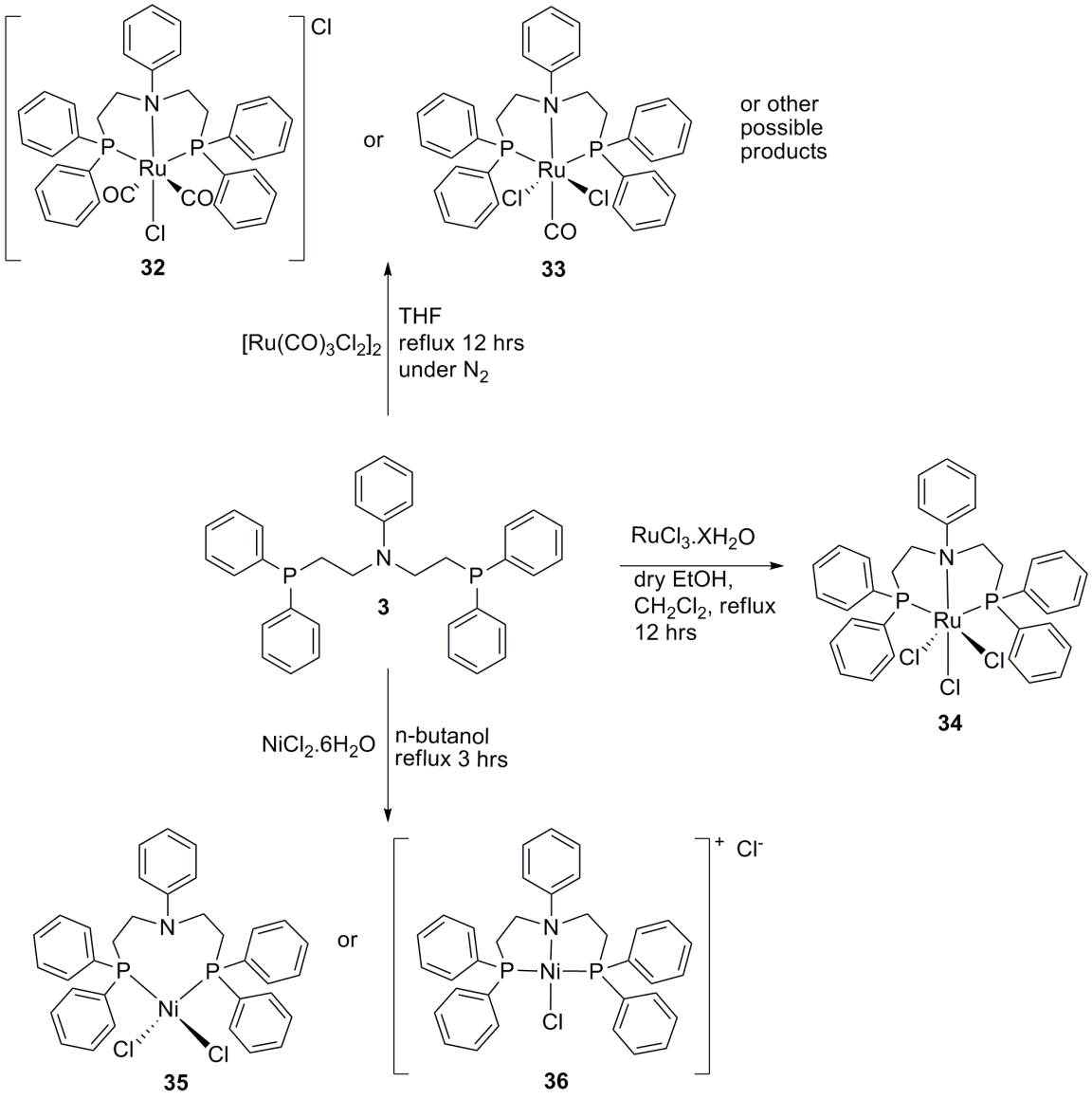

Scheme 12. Proposed structures for rhodium(I) and iridium(I) complexes of **3**.

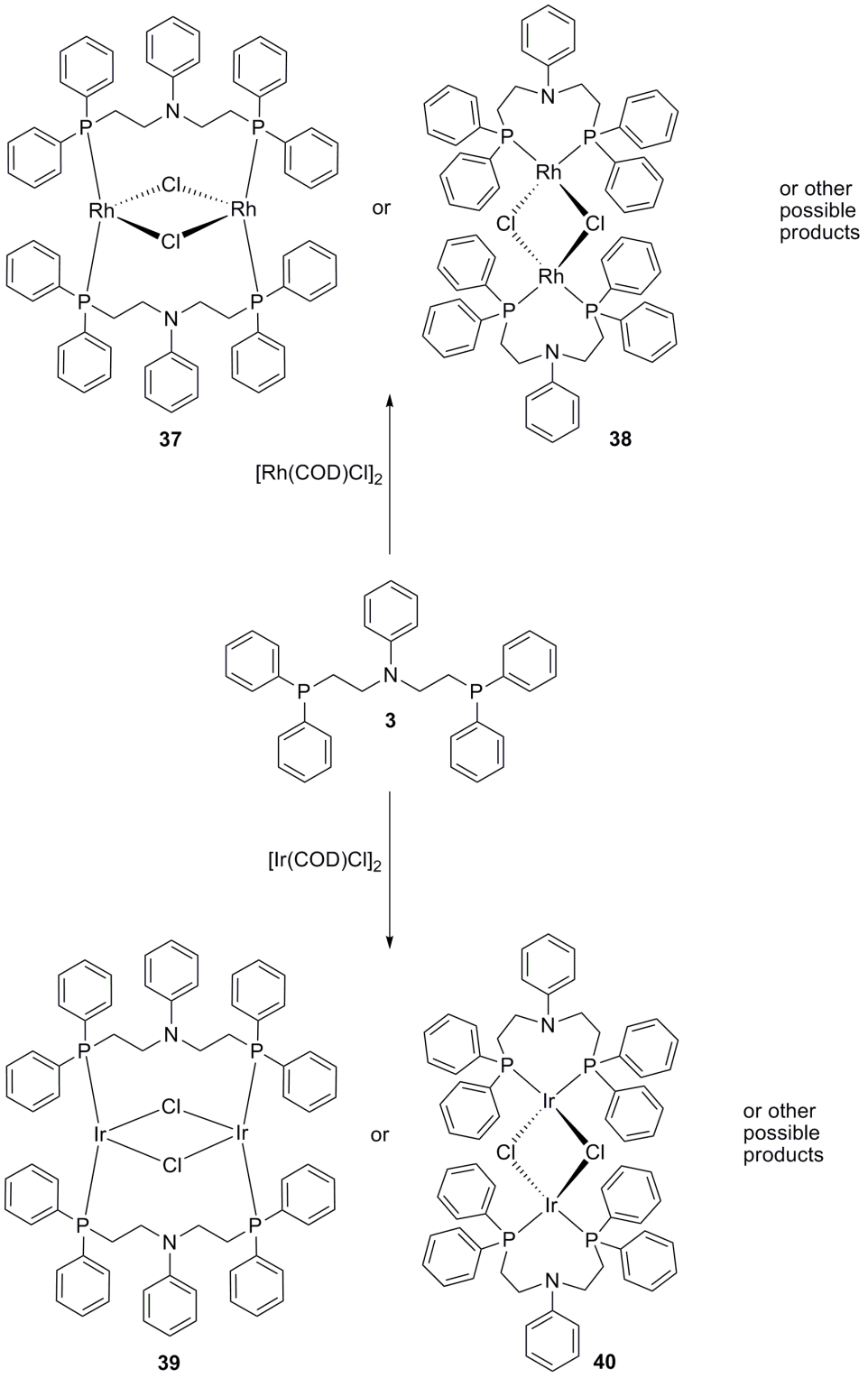

NMR Studies of the Complexes

The $^{31}P\{^{1}H\}$ NMR data for **22** revealed two singlets at 17.0 ppm and 18.7 ppm for each of two phosphorus atoms, since the phosphorus atoms are not equivalent due to symmetry of the molecule. Complexes **23** and **27** resulted in close $^{31}P\{^{1}H\}$ NMR chemical shifts, i.e. 10.32 ppm and 10.92 ppm respectively (**Figure 52**). $^{31}P\{^{1}H\}$ NMR spectra of **23** had platinum satellites as can be expected from a compound that has Pt-P bonds. Literature complex of *cis*-PNP-$PtCl_2$ was reported to have a $^{31}P\{^{1}H\}$ NMR chemical shift of 10.37 ppm and *trans*-[PNP-PtCl]Cl was reported to have a $^{31}P\{^{1}H\}$ NMR chemical shift of 27.20 ppm.[84] In the present study, **23** has a chemical shift of 10.32 ppm in its $^{31}P\{^{1}H\}$ NMR spectra. Subsequently, hexanes were slowly diffused to obtain crystals for X-ray diffraction experiment which resulted in a *trans*-[PNP-PtCl]Cl. If the *cis* complex in the present study has a chemical shift of 10.32 ppm in its $^{31}P\{^{1}H\}$ NMR spectra, it must have been converted into a *trans* isomer during crystallization. Otherwise, the literature value contradicted the present result.

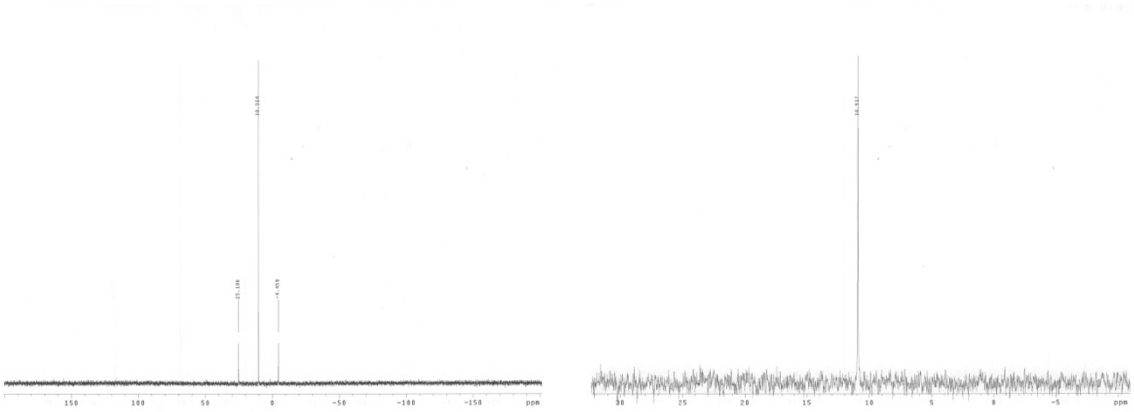

Figure 52. $^{31}P\{^{1}H\}$ NMR spectra of **23** (left) and **27** (right).

It is interesting that **27** which was a palladium complex had a $^{31}P\{^{1}H\}$ NMR chemical shift of 10.92 ppm (close to the value that of **23** which was a platinum complex) and it also

had phosphorus atoms *trans* to each other (*trans*-[PNP-PdCl]$_2$). $^{31}P\{^1H\}$ NMR chemical shift of **26** which was copper complex was also obtained as a singlet (-12.9 ppm).

Two different PNP-Ag complexes have been synthesized, i.e. **24** and **25**. These complexes differed only in the anions, which were CF_3COO^- and CH_3COO^-, respectively. Both complexes crystallized in a bridged dimer structure. In **25** (**Figure 53b**), acetate anions replaced by chloride anions, which probably occurred when the solution of **25** in CH_2Cl_2 was filtered through celite, prior to crystallization. HRMS and EA data of **25** proved that the compound has an acetate anion, and the $-CH_3$ group of the acetate was also observed in ^1H NMR.

The $^{31}P\{^1H\}$ NMR spectra of the two complexes are different at RT, as obtained by using a 300 MHz instrument. **24** has a doublet of doublets at 2.153 ppm at RT. However, **25** revealed a broad singlet at -2.39 ppm (**Figure 53**). $^{31}P\{^1H\}$ NMR of **24** supported that the dinuclear structure was also stable in solution, and the ^{31}P-Ag coupling constant was in the range typical to $[Ag(P_2 - donor)]_2X_2$ or $[Ag(\mu\text{-}X)_2(P_2 - donor)]_2$ systems, where X was the anion.[202] Reports of similar complexes in the literature, in which the phosphorus donors were linked by $CH_2\text{-}(CH_2)_n\text{-}CH_2$ groups, have indicated that when the anion was a perchloro or trifluoromethanesulfonate derivative, the *J* (^{31}P, Ag) coupling constant was in the range of 420 –580 Hz, and the chemical shifts were greater than for the halide or pseudohalide analogues; these observations demonstrated that the counter anion has an effect on the strength of the Ag–P bond. When the anion was a halide or acetate, a broad singlet has always been observed at room temperature in $^{31}P\{^1H\}$ NMR spectra, because the species were fluxional. Their low-temperature $^{31}P\{^1H\}$ NMR spectra resolved into a doublet or a doublet of doublets, which had coupling constants in the range of 350–450 Hz.[202] These findings were thoroughly consistent with the results of the present study.

When the $^{31}P\{^{1}H\}$ NMR spectra of **25** were obtained by using a 500 MHz instrument, a broad singlet was observed at RT. However, the spectrum displayed a well-resolved doublet of doublets, with large *J* values of 493.729 Hz and 427.764 Hz at low temperature (–40°C). $^{31}P\{^{1}H\}$ NMR coupling constants were smaller than that of **24**, with *J* values of 520.257 and 450.516 Hz. When the same sample of **25** was cooled further to –80°C , resolution of the peaks deteriorated and only a doublet was observed with a *J* value of 467.829 Hz (**Figure 54**). These large coupling constants and a coupling constant of **25** (X = CH_3COO^-) smaller than **24** (X = CF_3COO^-) were consistent with the literature.[202]

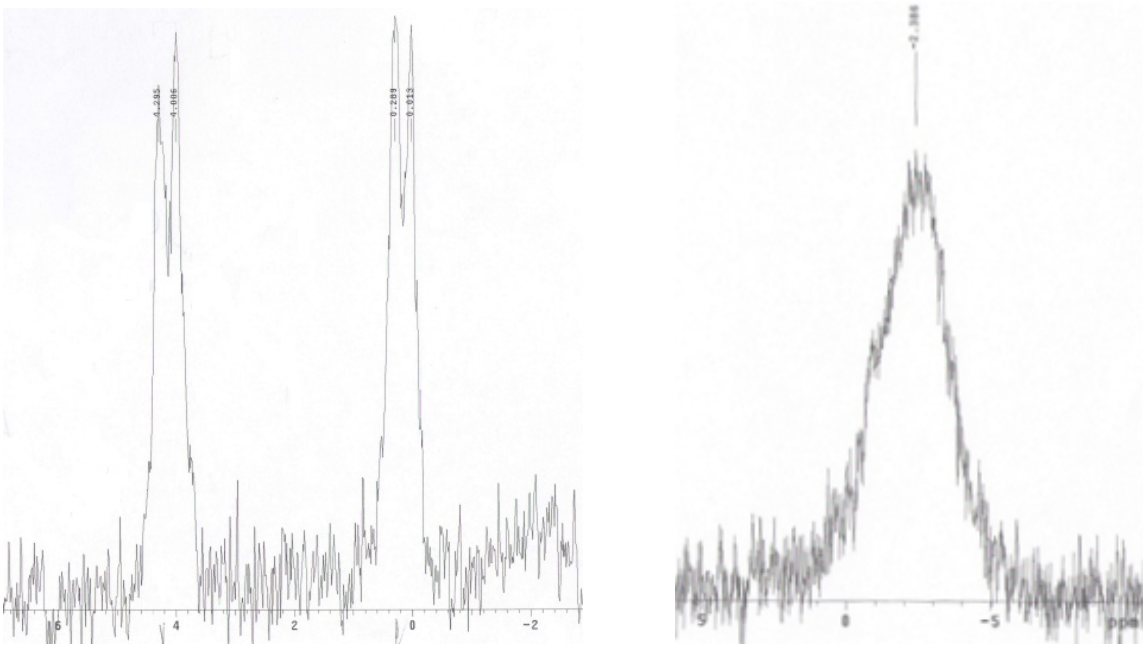

Figure 53. $^{31}P\{^{1}H\}$ NMR spectra of **24** (left) and **25** (right) obtained at RT using a 300 MHz instrument.

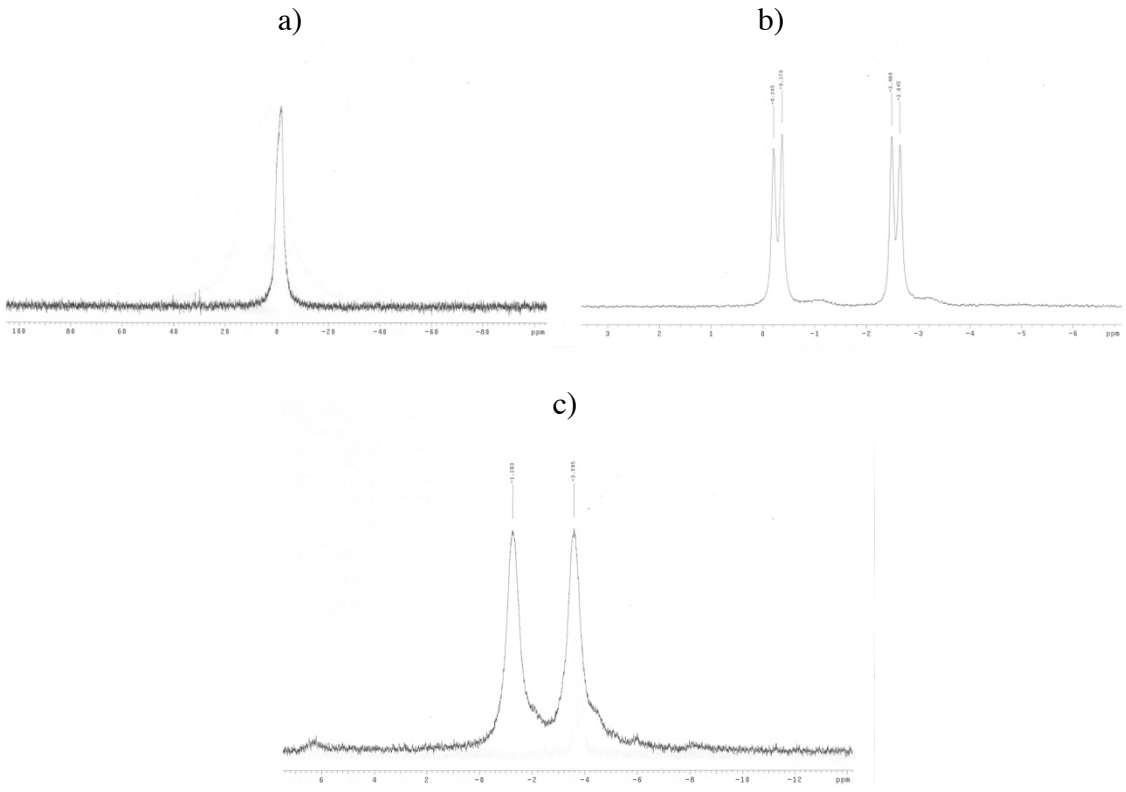

Figure 54. $^{31}P\{^{1}H\}$ NMR spectra of **25** (a) at RT (b) at -40 °C (c) at -80 °C obtained by using a 500 MHz instrument.

Mass Spectrometry of Complexes

The structure of dimers in the solution state was examined. Some journal articles reported similar structures as dimers in solution, identified by mass spectra as the main peak, but in the case of the present study, the m/z values of dimers did not correspond to the main peak. It was hard to prove with mass spectrometry if the solution structure was a dimer, because dimers could certainly split in the medium. For complex **24**, dimers split into monomers in MS medium, and the corresponding peak was dominant; the peak corresponding to the dimer exists, but was small. In addition, a peak at 1285.3 was

observed, corresponding to a dimer in which two trifluoroacetate groups have been replaced by only one chloride. The chloride might come from the solvent CH_2Cl_2. On the other hand, for complex **25**, a main peak that corresponded to a dimer that has lost only one acetate group was observed. High resolution CI^+ spectra for **26** indicated a main peak that corresponds to the monomer. The dimer that has lost two acetate groups and had two copper metals linked by a bridging chloride appeared in the LRMS (ESI). HRMS (ESI) of **27** revealed that the dimer was split and has lost one of its chlorides. No trace of the dimer was observed for **27**.

Complex **22** was well observed in the MS medium. Complex **23** is a cationic complex with a non-coordinating chloride anion. Both LRMS and HRMS revealed only the cation which is the *trans*-$[PNP\text{-}PtCl]^+$.

Crystal Structures of the Complexes

The solid state structures of complexes **22–27** were determined by X-ray crystallographic structure determination, and the resulting ORTEP representations were displayed in **Figures 55–58**. All crystals were obtained by slow diffusion of hexanes into saturated solutions of **22–27** in CH_2Cl_2. Crystallographic and structural refinement data were presented in **Tables 16** and **17**, and selected bond angles and distances around the metal centers were listed in **Tables 18–23**.

In complex **22**, the Pd(0) atom was coordinated in a *trigonal planar* geometry formed by two P atoms of ligand **3** and a C=C (η^2) bond involving the C atoms in the α,β positions relative to the central ketone of the dibenzylideneacetone ligand. The molecular structure of **22** was displayed in **Figure 55a**. The angle between the Pd–P1–P2 and Pd–C41–C42 planes was 1.40°. Ligand **3** was in a monomeric (PP) binding mode in which

the nitrogen atom of the ligand was not bound to the metal center (distance between N1 and Pd1 is 3.405 Å). The average Pd–P bond length was 2.326 Å, which was consistent with similar structures reported in the literature.[203, 204] Dibenzylideneacetone (dba) was bound to Pd via one of the carbon-carbon double bonds, with the C41=C42 bond (1.411 (3)Å) slightly elongated due to complexation when compared to C44=C45 (1.327 (3) Å), and the C41=C42 centroid-Pd distance was 2.044 Å. Similar Pd(0) coordination environments have been previously reported with chelating diphosphine and dba ligands, which also display the elongated carbon-carbon double bond (1.417 (3) Å).[203] This coordination mode was not unusual, since Pd_2dba_3 was the metal precursor that was used in the synthesis of **22** and included two palladium atoms with each metal bound η^2 to the three dba ligands.

In complex **23**, the four-coordinate Pt(II) lay in the center of a slightly distorted *square planar* environment (**Figure 55b**). The coordination environment around the metal center was defined by two phosphorus atoms from the PNP ligand, one nitrogen atom from the same ligand, and a chloride anion as a monodentate ligand. The other chloride anion was not coordinated to platinum and resulted in an ionic complex structure. Phosphorus atoms were *trans* to each other. Pt–P, Pt–N and Pt–Cl bonds were consistent with the reported values as well as the angles around the metal center.[205] The sole difference was that the literature complex had anionic nitrogen, thus the Pt–N distance was shorter. Another PNP-Pt complex that was the isomer of **23** was reported in the literature. The structure of the literature complex was *cis*-PNP-$PtCl_2$ in which phosphorus atoms were *cis* to each other; the platinum atom was not coordinated to the nitrogen atom and the two chlorides were bound to the platinum.[84]

a)

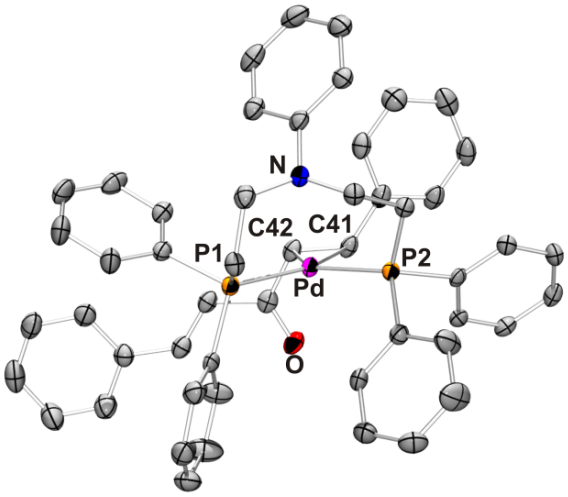

b)

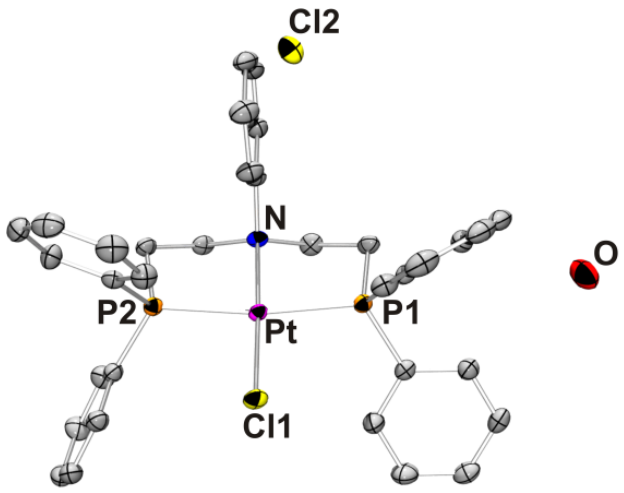

Figure 55. The crystal structure of (a) **22** (b) **23** showing the labeling of selected atoms. The hydrogen atoms were omitted for clarity and the displacement ellipsoids were scaled to the 50% probability level.

In complexes **24** and **25**, the four-coordinate Ag(I) centers formed bridged structures through trifluoroacetate and chloride anions, respectively. Two acetate groups of **25** replaced with two chloride anions during crystallization. The chloride anions might probably come from the solvent CH_2Cl_2 or from being filtered through celite. The geometries of Ag(I) centers in both **24** and **25** were distorted *tetrahedral*. The coordination environment around the metal center was defined by two phosphorus atoms from the separate PNP ligands and two bridging trifluoroacetate anions for **24** or two bridging chloride anions for **25** (**Figure 56**). In order to find if the solid state powder structure of **24** was a dimer or not, the powder X-ray data were examined together with the powder X-ray data predicted from the crystal structure. The fact that the two sets of data were matching was a proof of the dimeric structure in the solid state. The bond distances and the angles around the Ag atoms were consistent with the reported values for a similar structure to **24**.[202] A literature complex similar to **25** has consistent values for bond distances, yet there were some differences in bond angles due to structural differences in the ligand, i.e. ferrocene.[206] Another literature complex was compared with **25**. Ag(1)-Cl(1)-Ag(1*) and Ag(1)-Cl(1*)-Ag(1*) angles were 2.88 degrees different.[201]

In complex **26**, the four-coordinate Cu(I) centers formed bridged structures through acetate and/or chloride anions, i.e. a disorder in the crystal structure. The geometry of Cu(I) centers were distorted *tetrahedral*. The coordination environment around the metal center was defined by two phosphorus atoms from separate PNP ligands and two bridging acetate anions in bidentate and monodentate modes or a bridging chloride anion; half of the time one of the bridging ligands was observed as monodentate acetate, whereas half of the time it was observed as a bridging chloride (**Figure 57**). The bond distances and the angles around the Cu atoms were consistent with the reported values for the similar structures.[202,207]

a)

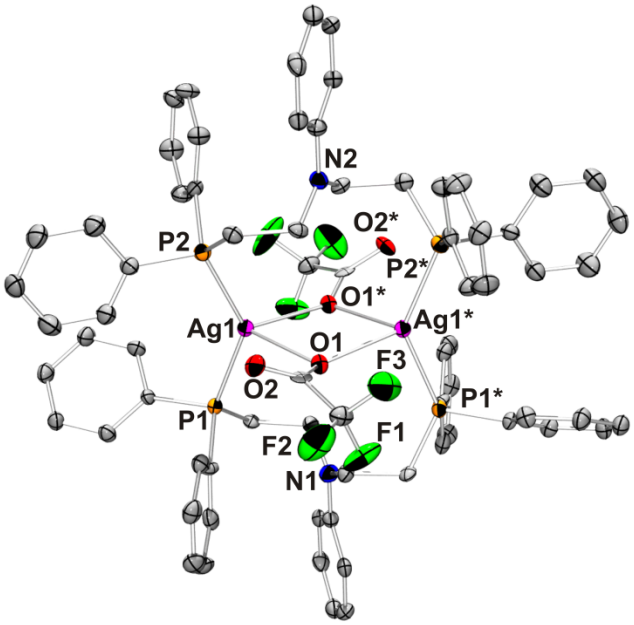

b)

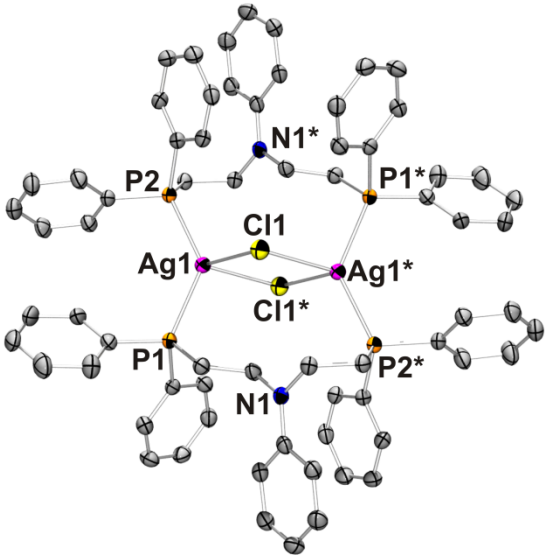

Figure 56. The crystal structure of (a) **24** (b) **25** showing the labeling of selected atoms. Hydrogen atoms were omitted for clarity. Displacement ellipsoids were scaled to the 50% probability level.

a)

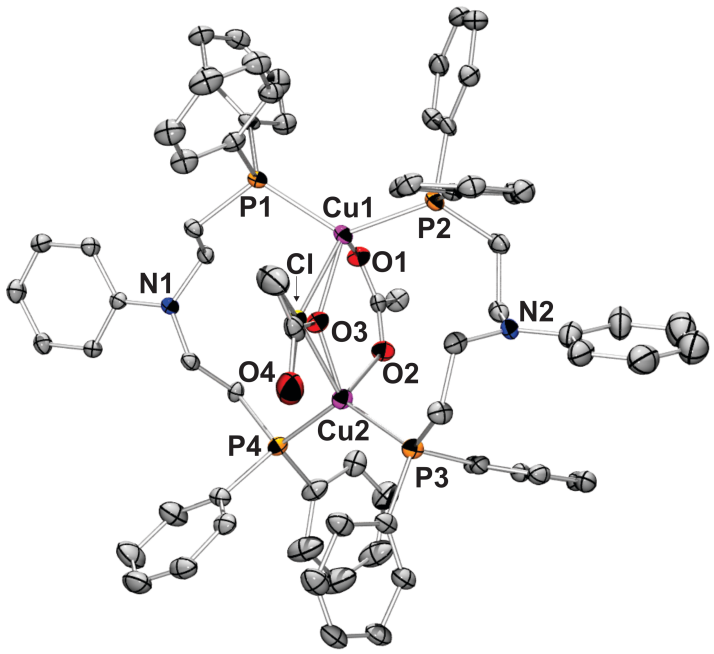

a)

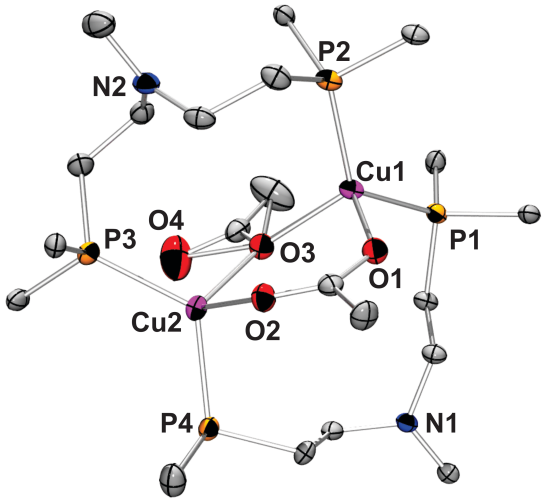

c)

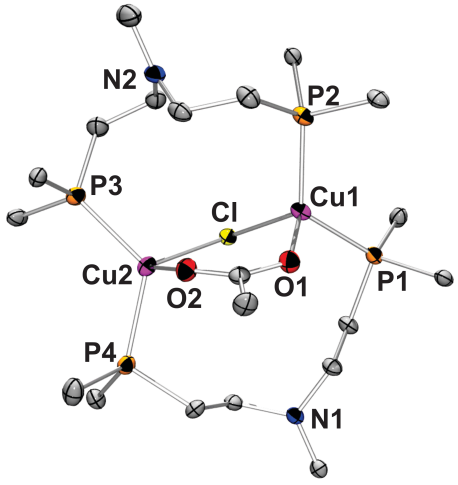

Figure 57. The crystal structure of **26** showing the labeling of selected atoms. Hydrogen atoms were omitted for clarity. (a) whole structure with two acetate groups (b) coordination environment only with two acetate groups (c) coordination environment only with one acetate and one chloride. Displacement ellipsoids were scaled to the 50% probability level.

In complex **27**, the four-coordinate Pd(II) centers formed a dimeric structure without any bridging ligands (**Figure 58**). The geometries of Pd(II) centers were distorted *square planar*, with a P(1)–Pd(1)–P(2) angle of 173.25(6)°. The coordination environment around the metal center was defined by two phosphorus atoms from the separate PNP ligands and chloride anions. The phosphorus atoms were *trans* to each other as were the chlorides. The Pd–P and Pd–Cl distances were very close to the reported average value, but the P–Pd–P angle was wider by 7.47° and the Cl–Pd–Cl angle was wider by 9.89° than the angle for the literature complex.[80]

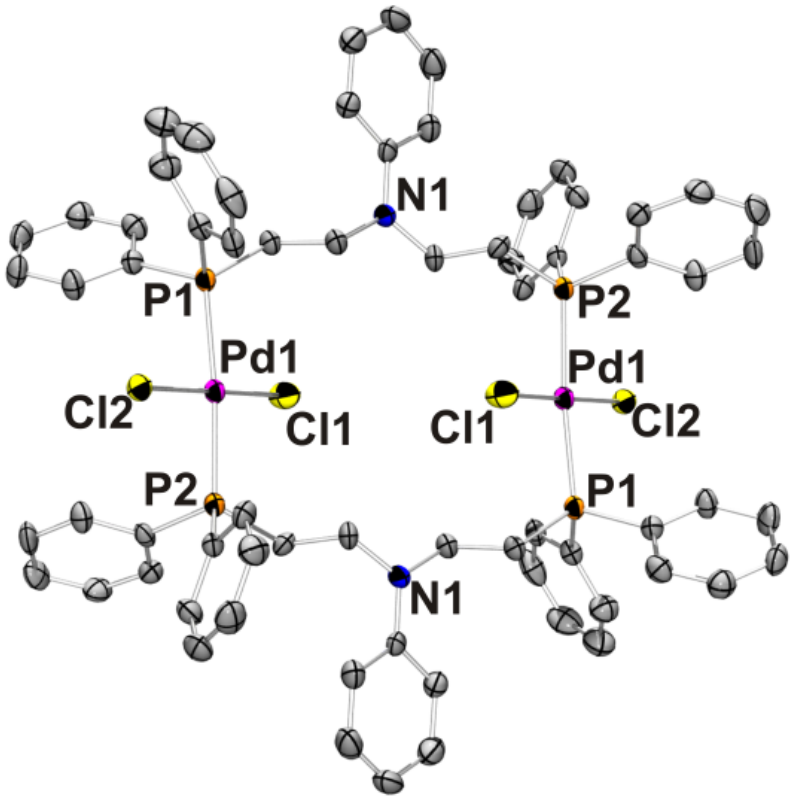

Figure 58. The crystal structure of **27** showing the labeling of selected atoms. Hydrogen atoms were omitted for clarity. Displacement ellipsoids were scaled to the 50% probability level.

Table 16. Crystal data and structure refinement for platinum and palladium complexes.

Complex	**22**	**23**	**27**
CCDC	850329	1575958	1575959
Formula	$[Pd(C_{34}H_{33}NP_2)(C_{17}H_{14}O)]$	$C_{34}H_{33}Cl_2NOP_2Pt$	$C_{68}H_{66}Cl_4N_2P_4Pd_2.2CH_2Cl_2$
FW	858.24	799.54	1559.56
T (K)	153	233	150(2)
Crystal system	Triclinic	Monoclinic	Triclinic
Space group	*P -1*	*P21/c*	*P -1*
a (Å)	10.087 (2)	9.9989(7)	9.291(2)
b (Å)	11.974 (2)	20.0285(18)	14.571(2)
c (Å)	17.473 (4)	17.9269(13)	15.196(3)
α (deg)	86.34 (3)	90	62.071(4)
β (deg)	81.27 (2)	119.840(4)	89.684(8)
γ (deg)	83.15 (3)	90	82.932(4)
V (Å^3)	2068.8 (7)	3114.1(4)	1800.6(6)
Z	2	4	1
ρ (g/cm^3)	1.378	1.705	1.438
μ (mm^{-1})	0.57	4.809	0.926
F(000)	888	1576	792
Crystal size (mm)	0.27 x 0.14 x 0.12	0.20 × 0.20 × 0.20	0.26 x 0.10 x 0.10
θ (deg)	1.0 to 27.5	2.2810 to 27.5437	3.04 to 27.48
Index ranges	$-12 \le h \le 13$	$-12 \le h \le 12$	$-12 \le h \le 12$
	$-14 \le k \le 15$	$-26 \le k \le 25$	$-16 \le k \le 18$
	$-22 \le l \le 22$	$-23 \le l \le 23$	$0 \le l \le 19$
Absorption correction	Multi-scan	Multi-scan	Multi-scan
Max. and min. transmission	1.000 and 0.837	1.0000 and 0.6055	0.9147 and 0.7968
GOF on F^2	1.582	1.142	1.556
$R1$, $R2$ [$I > 2\sigma(I)$]	0.0414, 0.0887	0.0312, 0.0836	0.0727, 0.1858
$R1$, $R2$ (all data)	0.0563, 0.0851	0.0339, 0.0912	0.0966, 0.1925
Largest diff. peak and hole (e.Å^{-3})	1.56 and -0.67	2.071 and -2.556	1.419 and -1.700

Table 17. Crystal data and structure refinement for silver and copper complexes.

Complex	**24**	**25**	**26**
CCDC	1575961	1575960	1575962
Formula	$C_{72}H_{66}N_2O_4P_4F_6Ag_2$	$C_{35.38}H_{35.75}Cl_{3.75}AgNP_2$	$C_{71.10}H_{70.65}Cl_{0.45}Cu_2N_2O_{3.10}P_4$
FW	1476.89	777.65	1269.66
T (K)	100(2)	123(2)	123(2)
Crystal system	Orthorhombic	Monoclinic	Monoclinic
Space group	*Pbcn*	*P21/c*	*P21/c*
a (Å)	13.723(5)	14.318(4)	17.184(5)
b (Å)	22.778(5)	14.345(5)	14.854(5)
c (Å)	20.929(5)	17.993(6)	24.265(8)
α (deg)	90.000(5)	90	90
β (deg)	90.000(5)	105.375(4)	94.731(5)
γ (deg)	90.000(5)	90	90
V (Å^3)	6542(3)	3563(2)	6173(3)
Z	4	2	4
ρ (g/cm^3)	1.499	1.45	1.366
μ (mm^{-1})	0.77	0.96	0.86
F(000)	3008	1583	2647
Crystal size (mm)	0.12 × 0.07 × 0.06	0.24 × 0.18 × 0.05	0.12 × 0.09 × 0.05
θ (deg)	1.73 to 27.50	3.00 to 27.50	3.00 to 27.50
Index ranges	$-17 \le h \le 17$	$-13 \le h \le 18$	$-20 \le h \le 19$
	$-29 \le k \le 29$	$-18 \le k \le 18$	$-17 \le k \le 17$
	$-27 \le l \le 27$	$-23 \le l \le 23$	$-28 \le l \le 28$
Absorption correction	Multi-scan	Multi-scan	Multi-scan
Max. and min. transmission	0.9541 and 0.9145	1.000 and 0.772	1.000 and 0.777
GOF on $F2$	1.631	1.106	1.376
$R1$, $R2$ [I > 2σ (I)]	0.1139, 0.2042	0.0503, 0.1210	0.1171, 0.1668
$R1$, $R2$ (all data)	0.1140, 0.2042	0.0552, 0.1238	0.1383, 0.1739
Largest diff. peak and hole (e.Å^{-3})	0.71 and -0.99	1.27 and -0.85	0.62 and -0.46

Table 18. Selected bond lengths (Å) and angles (degree) for **22**.

Bond Lengths (Å)	
Pd – P(1)	2.3068(10)
Pd– P(2)	2.3441(9)
Pd– C(41)	2.155(2)
Pd – C(42)	2.170(2)
Bond Angles (°)	
P(1) – Pd – P(2)	106.54(3)
P(1) – Pd – C(41)	99.11(7)
P(1) – Pd – C(42)	137.21(7)
P(2) – Pd – C(41)	154.31(7)
P(2) – Pd – C(42)	116.24(7)
C(41) – Pd – C(42)	38.09(9)

Table 19. Selected bond lengths (Å) and angles (degree) for **23**.

Bond Lengths (Å)	
Pt – P(1)	2.299(1)
Pt – P(2)	2.291(1)
Pt – Cl(1)	2.2960(7)
Pt – N	2.100(2)
Bond Angles (°)	
P(1) – Pt – P(2)	170.68(3)
P(1) – Pt – Cl(1)	96.53(3)
P(1) – Pt – N	85.18(9)
P(2) – Pt – Cl(1)	92.67(3)
P(2) – Pt – N	85.67(9)
Cl(1) – Pt – N	177.61(9)

Table 20. Selected bond lengths (Å) and angles (degree) for **24**.

Bond Lengths (Å)	
Ag(1) – P(1)	2.454(2)
Ag(1) – P(2)	2.434(2)
Ag(1*) – P(1*)	2.454(2)
Ag(1*) – P(2*)	2.434(2)
Ag(1*) – O(1*)	2.441(5)
Ag(1) – O(1)	2.441(5)
Ag(1*) – O(1)	2.466(5)
Ag(1) – O(1*)	2.466(5)
Bond Angles (°)	
P(1) – Ag(1) – P(2)	136.28(7)
P(1*) – Ag(1*) – P(2*)	136.28(7)
P(1) – Ag(1) – O(1*)	102.9(1)
P(1*) – Ag(1*) – O(1*)	102.9(1)
P(1) – Ag(1) – O(1)	103.4(1)
P(1*) – Ag(1*) – O(1)	103.4(1)
P(2) – Ag(1) – O(1)	107.3(1)
P(2) – Ag(1) – O(1*)	114.5(1)
P(2*) – Ag(1*) – O(1)	114.5(1)
P(2*) – Ag(1*) – O(1*)	107.3(1)
O(1) – Ag(1) – O(1*)	75.2(2)
O(1) – Ag(1*) – O(1*)	75.2(2)
Ag(1) – O(1) – Ag(1*)	104.4(2)
Ag(1) – O(1*) – Ag(1*)	104.4(2)

Table 21. Selected bond lengths (Å) and angles (degree) for **25**.

Bond Lengths (Å)	
Ag(1)– P(1)	2.493(1)
Ag(1*) – P(1*)	2.493(1)
Ag(1) – P(2)	2.463(1)
Ag(1*) – P(2*)	2.463(1)
Ag(1*) – Cl(1)	2.690(1)
Ag(1) – Cl(1*)	2.690(1)
Ag(1) – Cl(1)	2.726(1)
Ag(1*)–Cl(1*)	2.726(1)
Bond Angles (°)	
P(1) – Ag(1) – P(2)	132.89(3)
P(1*) – Ag(1*) – P(2*)	132.89(3)
P(1) – Ag(1) – Cl(1*)	104.34(3)
P(1) – Ag(1) – Cl(1)	99.57(3)
P(1*) – Ag(1*) – Cl(1)	99.57(3)
P(1*) – Ag(1*) – Cl(1*)	104.34(3)
P(2) – Ag(1) – Cl(1)	111.79(3)
P(2*) – Ag(1*) – Cl(1)	112.85(3)
P(2*) – Ag(1*) – Cl(1*)	111.79(3)
P(2) – Ag(1) – Cl(1*)	112.85(3)
Cl(1) – Ag(1) – Cl(1*)	84.02(3)
Cl(1) – Ag(1*) – Cl(1*)	84.02(3)
Ag(1) – Cl(1) – Ag(1*)	95.98(3)
Ag(1) – Cl(1*) – Ag(1*)	95.98(3)

Table 22. Selected bond lengths (Å) and angles (degree) for **26**.

Bond Lengths (Å)	
Cu(1) – P(1)	2.264(2)
Cu(1) – P(2)	2.242(2)
Cu(2) – P(3)	2.258(2)
Cu(2) – P(4)	2.272 (2)
Cu(1) – Cl(1)	2.414(6)
Cu(2) – Cl(1)	2.430(7)
Cu(1) – O(1)	2.055(5)
Cu(2) – O(2)	2.172(5)
Bond Angles (°)	
P(1) – Cu(1) – P(2)	125.41(8)
P(1) – Cu(1) – O(1)	105.6(1)
P(1) – Cu(1) – Cl(1)	94.2(2)
P(2) – Cu(1) – O(1)	101.8(1)
P(2) – Cu(1) – Cl(1)	118.9(2)
O(1) – Cu(1) – Cl(1)	110.2(2)
P(3) – Cu(2) – O(2)	111.2(1)
P(4) – Cu(2) – O(2)	93.6(1)
O(2) – Cu(2) – Cl(1)	103.6(2)
P(3) – Cu(2) – P(4)	122.84(8)
P(3) – Cu(2) – Cl(1)	108.3(2)
P(4) – Cu(2) – Cl(1)	114.8(2)

Table 23. Selected bond lengths (Å) and angles (degree) for **27**.

Bond Lengths (Å)	
Pd(1) – P(1)	2.327(2)
Pd(1) – P(2)	2.326(2)
Pd– Cl(1)	2.301(2)
Pd – Cl(2)	2.307(2)
Bond Angles (°)	
P(1) – Pd(1) – P(2)	173.25(6)
P(1) – Pd(1) – Cl(1)	89.88(7)
P(1) – Pd(1) – Cl(2)	90.39(6)
P(2) – Pd(1) – Cl(1)	89.58(7)
P(2) – Pd(1) – Cl(2)	90.05(6)
Cl(1) – Pd(1) – Cl(2)	179.07(7)

UV-Vis and Luminescence Studies of the Complexes and the Ligand

UV-Vis absorption spectra of complexes **23**–**27** and free ligand **3** were obtained (**Figure 59**). **3** had its absorption maximum at 257 nm with ε = 27437 $M^{-1}cm^{-1}$ for $\pi - \pi^*$ transition. Complexes **24**, **25**, and **26** had their absorption maxima significantly close to the free ligand, observed at 254, 256, and 259 nm with ε values of 55806, 50000, and 75399 $M^{-1}cm^{-1}$, respectively. Since these three complexes were dimers, they absorbed UV light to a greater extent than the ligand. Absorption maxima changed only a few nm upon complexation, most likely due to the fact that the conformation of the ligand and the resulting complexes of **24**, 2**5** and **26** were similar. The biggest extinction coefficient value belonged to the copper complex **26**. The two silver complexes had values close to each other. When **26** was in solid form, it was pale green and colorless when dissolved in

CH_2Cl_2. Complexes **23**, **24**, **25**, and ligand **3** were white both in solid state and in solution state. Complex is **27** was bright yellow, and its absorption spectrum had an additional peak at 332 nm with an ε value of 29183 $M^{-1}cm^{-1}$ (**25** was orange, but its UV-Vis spectrum was not measured). For all the other complexes (**23**–**26**), neither MLCT nor LMCT in the visible region of the spectrum were observed.

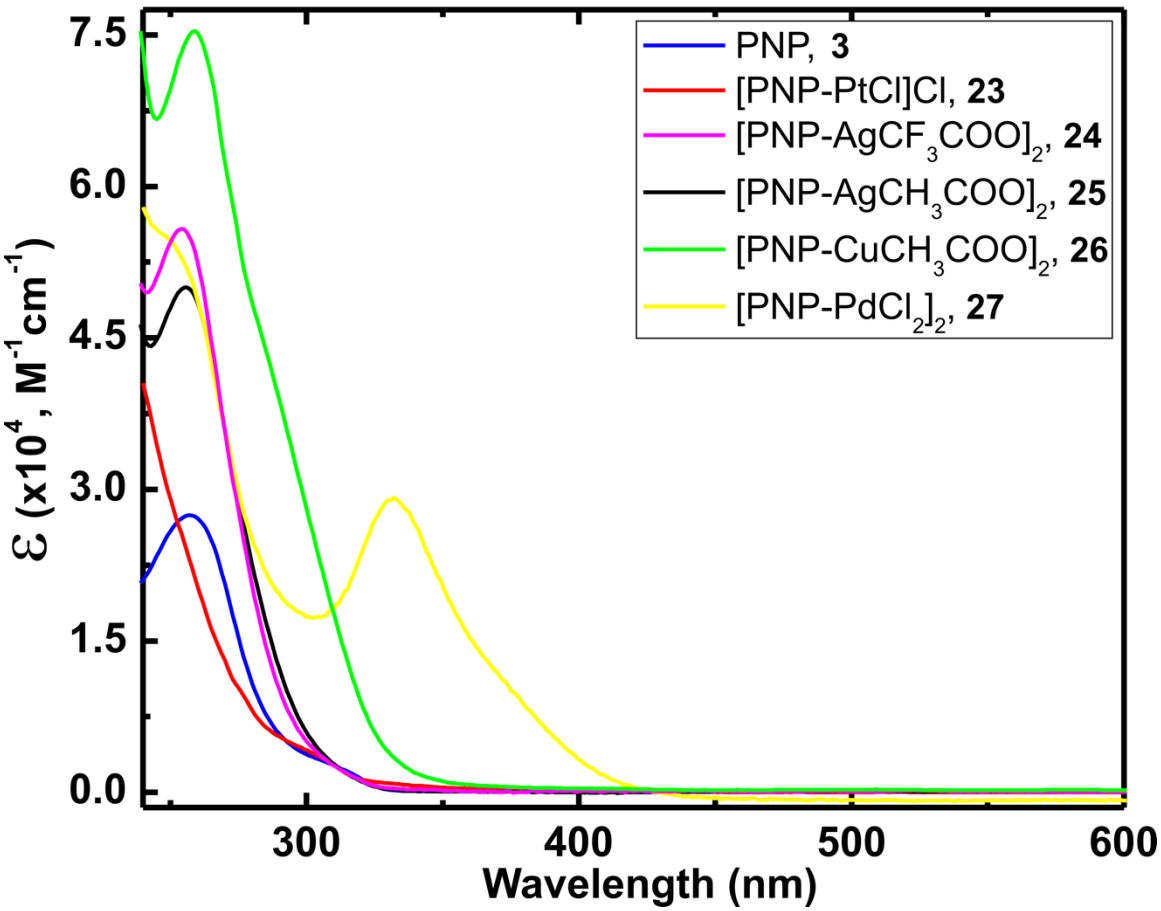

Figure 59. Absorption spectra of complexes **23**–**27** and the ligand **3**.

Complex **23** did not reveal any peak in the 235-800 nm range, but absorption was increasing toward the UV region. Solvent CH_2Cl_2 has the $\lambda_{cut-off}$ value of 235 nm. The only

solvent with a considerably low $\lambda_{cut-off}$ value was CH_3CN ($\lambda_{cut-off}$ = 190 nm). However, CH_3CN should not be used for measuring the absorption spectrum of **23**, because a *square planar* platinum complex of **23** had open coordination sites and CH_3CN could coordinate to the complex. During complexation of **23**, the conformation of ligand **3** changed drastically; this might cause the absorption maximum shifting to lower wavelengths.

Luminescence measurements of complexes **23**–**26** and the ligand **3** were obtained. No ^{3}MLCT phosphorescence was observed. Furthermore, emission spectra of the complexes were similar to that of the free ligand. First, room temperature measurements were performed (**Figure 60**). Subsequently, samples were cooled to 77 K (**Figure 61**). The emission spectra of ligand **3** indicated two peaks. The first one was around ~300 nm, which was the ligand fluorescence due to $\pi - \pi^*$ transition; the second peak was around 400 nm. The emission of the complexes coincided with either or both of those peaks. There were three possible causes for the formation of this peak in the ligand emission spectra, i.e., charge transfer, excimer formation, and ligand phosphorescence. Due to the fact that the concentrations of samples were in the range of 0.05 – 0.1 absorbance units, the excimer formation was the least likely to occur.

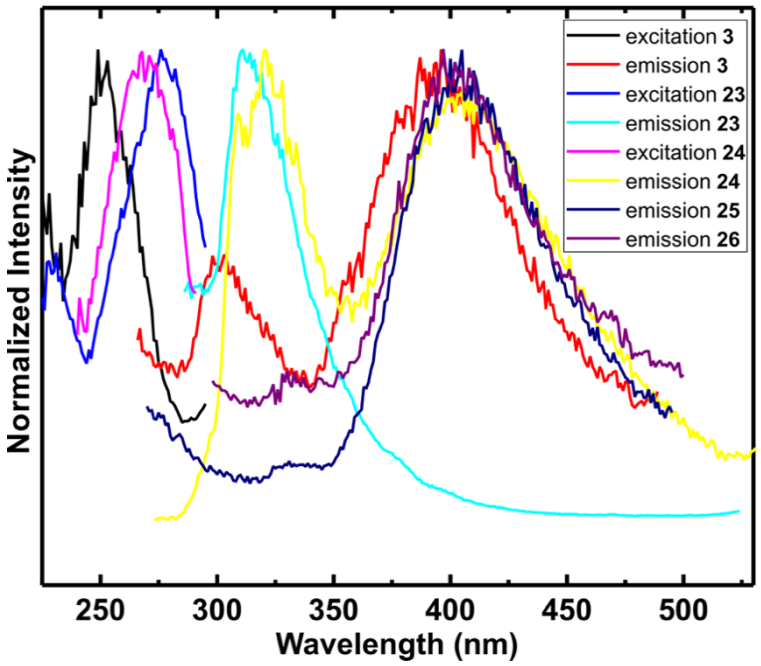

Figure 60. Excitation and emission spectra of the ligand and metal complexes at RT.

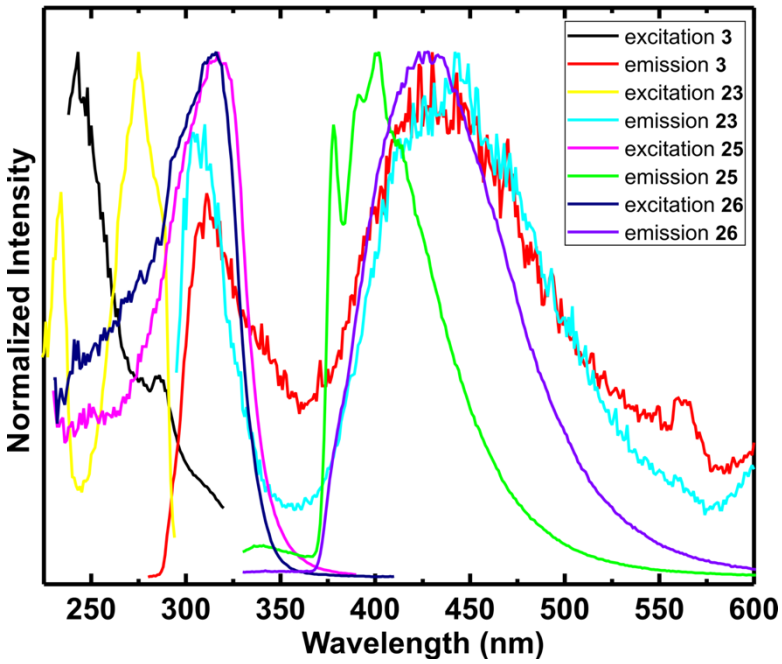

Figure 61. Excitation and emission spectra of the ligand and metal complexes at 77 K.

Solid samples of complexes **23**–**26** were tested with a simple UV lamp to detect if any phosphorescence would occur or not. Unfortunately, no phosphorescence was observed. Solid state fluorescence spectra of **25** and **26** were also measured. Spectra of **25** did not reveal any peak. However, spectra of **26** resulted in a ligand phosphorescence (**Figure 62**).

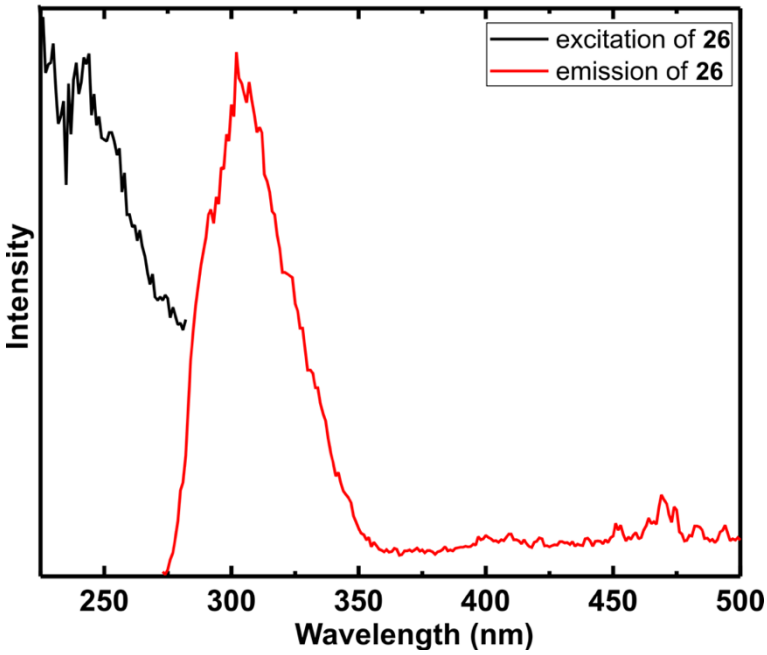

Figure 62. Solid state excitation and emission spectra of **26**.

Excitation and emission spectra of **3** were obtained in EEET (ethyl iodide/ether/ethanol/toluene, 2:2:1:1) solution to determine if the presence of iodine enhances any phosphorescence emission or not. Unfortunately, no change was observed. In order to determine if the emission around 400 nm was caused by a charge transfer coming from the ligand, the emission spectra of the free ligand were obtained in different solvents (which have different polarity); in other words, solvatochromism measurement

was carried out. The solvents used were: CH_2Cl_2, DMF, 2-MeTHF, EtOH and isobutanol. The peak maxima of the ligand emission varied with the changing solvent polarity; i.e., a positive solvatochromism was observed (**Figure 63**). This result proved that the peak at approximately 400 nm resulted from a charge transfer (ILCT). There were differences of a few nanometers between the peak maxima of the complexes. The reason for this variation could be the conformational differences upon complexation.

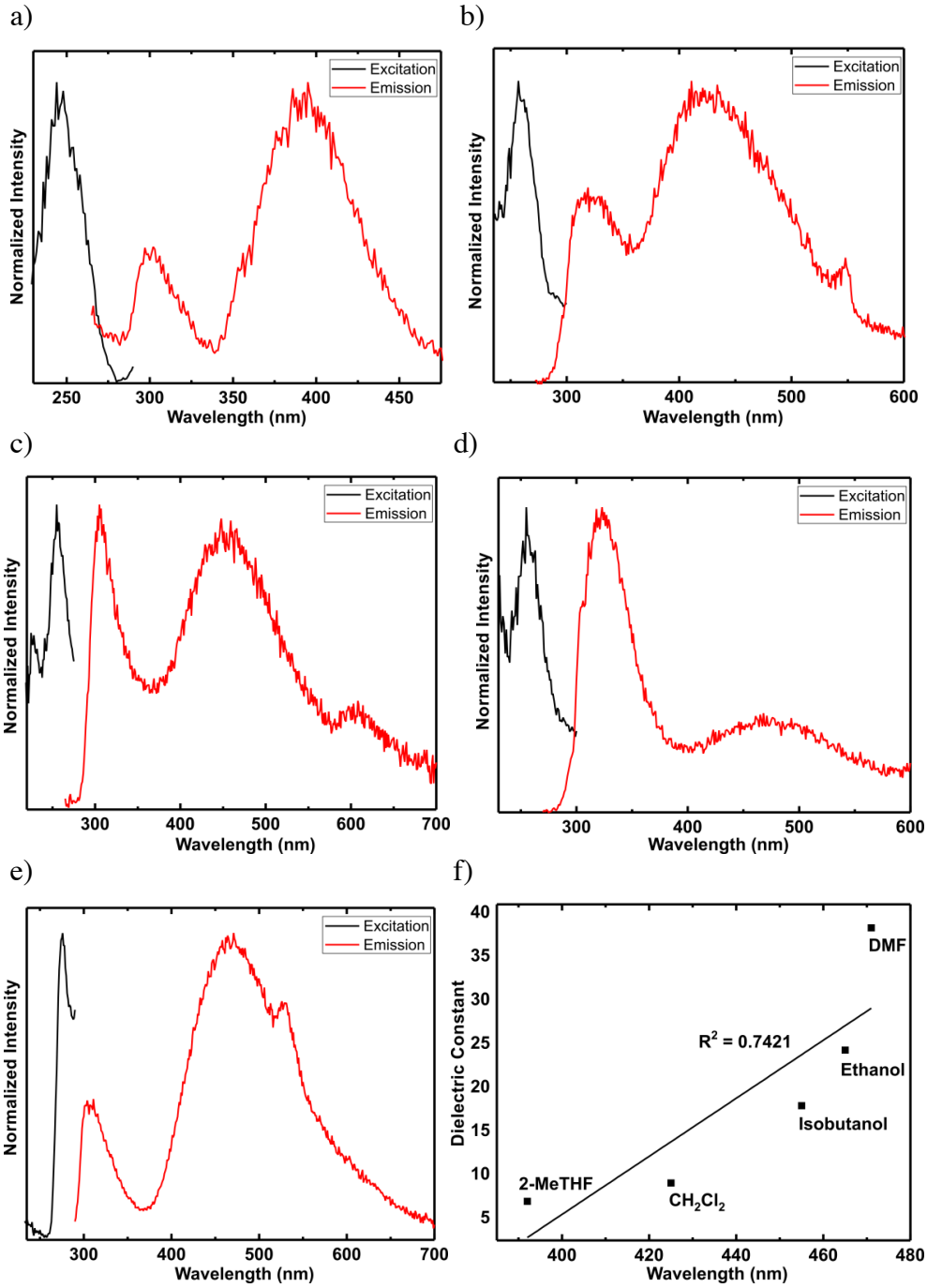

Figure 63. Excitation and emission spectra of ligand **3** in different solvents at RT (a-e). (f) dielectric constant of the solvent vs wavelength of emission.

CONCLUSIONS

In conclusion, the synthesis and characterization of the PNP complexes of copper, silver, palladium, and platinum were achieved; their absorption and luminescence spectra were obtained. The ligand fluorescence was observed for all complexes at approximately 300 nm due to π–π* transition. The peak at approximately 400 nm, however, was caused by a charge transfer from the ligand, as proved by the positive solvatochromism experiment. Neither a ^{3}MLCT nor a ^{3}LC phosphorescence was observed in the luminescence measurements of the complexes.

^{31}P{^{1}H} NMR spectra of the complexes were studied. ^{31}P{^{1}H} NMR chemical shift of PNP has changed upon complexation for all complexes. ^{31}P{^{1}H} NMR spectra of **22** had two singlets, **23** had platinum satellites, **26** and **27** resulted in one singlet. **24** and **25** were different at room temperature; i.e., **24** resulted in doublet of doublets while **25** resulted in a broad singlet. This result indicated that the counter anion had an effect on the strength of Ag–P bond. When the ^{31}P{^{1}H} NMR spectra of **25** were obtained at different temperatures, i.e., at room temperature, at -40 °C and at -80 °C, resolution differed. The measurement at -40 °C resulted in a doublet of doublets while the measurement at room temperature resulted in a singlet and the measurement at -80 °C resulted only in a doublet.

The complexes have different coordination modes, i.e. bidentate monomeric (**22**), tridentate monomeric (**23**), bidentate dimeric with bridge (**24**–**26**), and bidentate dimeric (**27**). The coordination number around the metal center was four for all structures, with either distorted *tetrahedral* or distorted *square planar* geometry; the only exception is **22**, with *trigonal planar* geometry involving a C=C (η^2) bond.

Appendix A: SNS Ligands[5]

The following SNS ligands (**41-44**) were synthesized and characterized by ^{1}H NMR and X-ray crystallography.

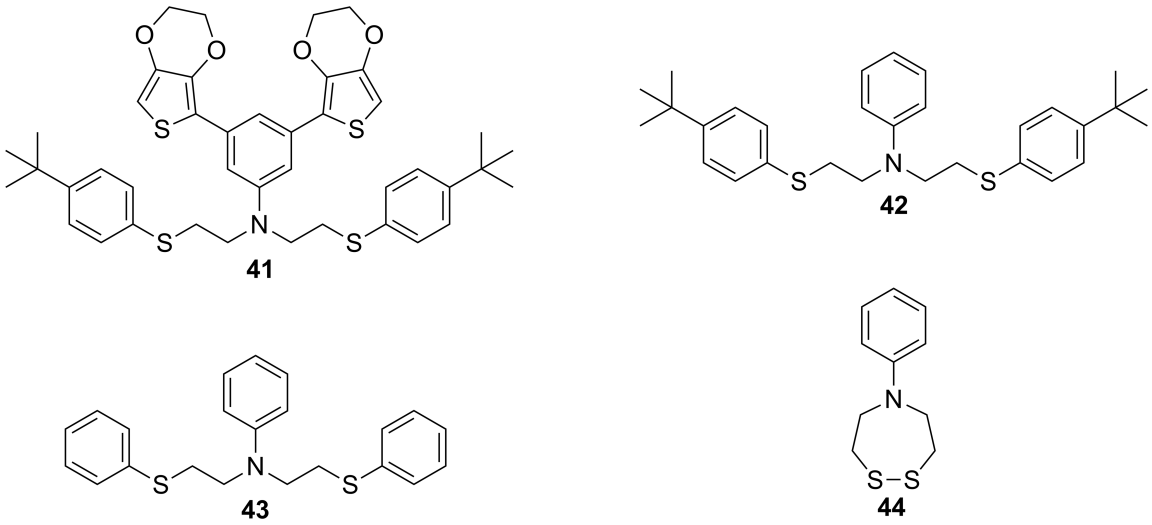

Figure A1. SNS ligands synthesized and characterized.

Syntheses

3,5-bis-EDOT-N,N-bis-[4-*tert*buthylthiophenylethyl]-aniline [41]. 4-tertbuthylthiophenol (0.02396 g) was dissolved in dry THF (~25 ml) and then cooled to 0°C. NaH (0.0035 g) powder was added into the solution in small portions under Ar. A gas evolution was observed. The mixture was stirred under Ar for an hour, and then 3,5-

[5] Compound **44** has been published as a journal article/structure report: Mitchell, L. A.; Mejía, M. L.; Keskin, S. G.; Holliday, B. J. 5-Phenyl-1,2,5-dithiazepane. *Acta Crystallogr Sect E* **2014,** 70(pt3), o285. Seyma Keskin carried out the synthesis, purification and characterization by ^{1}H NMR, and crystallization. The crystal was diffracted by Michelle L. Mejia; crystal data were completed by Lauren A. Mitchell. Experimental section of the article was written by Seyma Keskin. The rest of the article was written by Lauren Avery Mitchell. The principle investigator at the time of the work was Dr. Bradley J. Holliday.

bis-EDOT-N,N-bis-[2-chloroethyl]-aniline (0.0342 g) was dissolved in THF (~15 ml) in a vial and this solution was cannula transferred into the salt mixture. The reaction mixture was stirred at RT for overnight under Ar. The solvent was evaporated. The residue was extracted in between CH_2Cl_2 and H_2O. The organic phase was dried over $MgSO_4$, vacuum filtered, filtrate was evaporated. The residue was purified by a silica gel column in which the eluent was Hexanes:4/CH_2Cl_2:1. The yield was 65%. ^{1}H NMR (300 MHz, CD_2Cl_2): δ = 7.375 (s, 1H), 7.318 (s, 8H from thiophenol part), 6.943 (s, 2H, aromatic EDOT part), 4.241 (combined singlet, 8H, aliphatic EDOT part), 3.598 (t, *J* = 7.2 Hz, 4H), 3.142 (t, *J* = 7.2 Hz, 4H), 1.295 (s, 18H, tertbuthyl groups). ^{13}C{^{1}H} NMR (75 MHz, CD_2Cl_2): δ = 149.915, 147.381, 142.715, 138.724, 134.653, 132.589, 129.663, 126.478, 117.874, 113.139, 109.168, 97.646, 65.229, 64.954, 51.946, 34.702, 31.375, 30.052. LRMS (CI/CH_4): C_{42} $H_{47}NO_4S_4$ calculated for 758.079 and found to be 759.

N,N-bis-[4-*tert*buthylthiophenylethyl]-aniline [42]. 4-*tert*buthylthiophenol (1.906 g, 11.5 mmol) was dissolved in dry THF (~ 25 ml). NaH (0.275g, 11.5 mmol) powder was added into the solution in small portions under Ar. A gas evolution was observed. After all NaH has been added, the reaction mixture was refluxed for an hour. Afterwards the mixture was cooled down a little bit. A solution of N,N-bis-[2-chloroethyl]aniline (1g, 4.58 mmol) in some dry THF was added into the hot solution via a cannula and the mixture was refluxed for overnight. The solvent was evaporated. The residue was dissolved in CH_2Cl_2 and extracted between CH_2Cl_2 andH_2O. The organic phase was dried over $MgSO_4$, vacuum filtered, and the filtrate was evaporated. The residue was purified by a silica gel column in which the eluent was Hexanes:4/CH_2Cl_2:1. The yield was 95.53 %.

N,N-bis-[ethylphenylthioether]-aniline [43]. Thiophenol (0.2553 g, 2.317 mmol) was dissolved in dry THF (~25 ml). NaH (0.0585 g, 2.317 mmol) powder was

added into the solution in small portions under Ar. A gas evolution was observed. After all NaH has been added, the reaction mixture was refluxed for an hour. Then the mixture was cooled down little bit. A solution of N,N-bis[2-(p-tolylsulfonyl)ethyl]aniline (0.4187 g, 0.855 mmol) (0.4187g, 0.855 mmol) in dry THF was added into the hot solution via a cannula and the mixture was refluxed for overnight. The solvent was evaporated. The residue was dissolved CH_2Cl_2 and extracted between CH_2Cl_2 and H_2O. The organic phase was dried over $MgSO_4$, vacuum filtered, and the filtrate was evaporated to afford a white solid in quantitative yields.

5-Phenyl-1,2,5-dithiazepane [44]. $NaSH.H_2O$ (1.08 g, 14.78 mmol) was stirred in ethanol under positive pressure of Ar for an hour. N,N-bis-[2-chloroethyl]aniline (0.5124 g, 2.35 mmol) was dissolved in ethanol under Ar and then transferred into $NaSH.H_2O$. The reaction mixture was refluxed for 24 hours. Half of the solvent was pulled under Schlenk line and then degassed CH_2Cl_2 and degassed H_2O were added to extract the product under Ar. The organic phase was cannula transferred into a flask (with $MgSO_4$ in it) connected to the Schlenk line and then it was cannula filtered into another flask and dried under vacuum to obtain the product with an 83 % yield.[208]

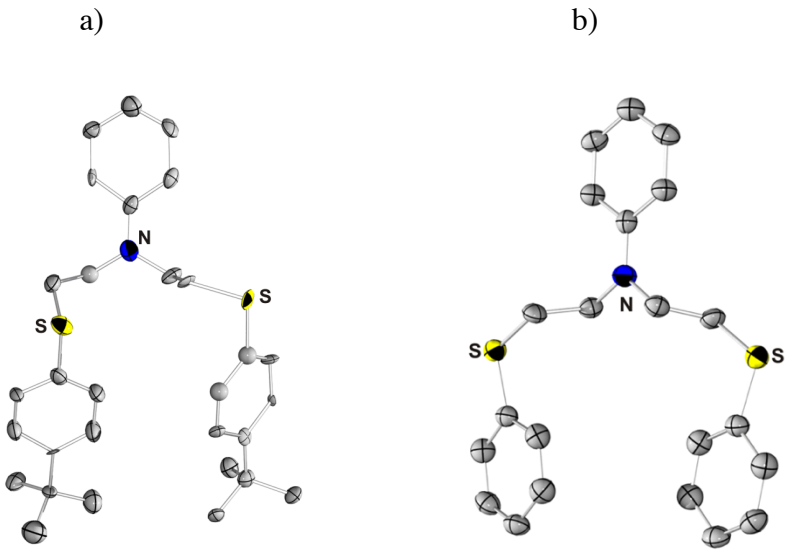

Figure A2. The crystal structure of (a) **42** (b) **43** showing the labeling of selected atoms. The hydrogen atoms were omitted for clarity and the displacement ellipsoids were scaled to the 50% probability level.

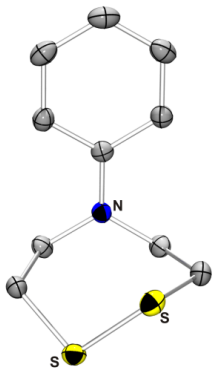

Figure A3. The crystal structure of **44** showing the labeling of selected atoms. The hydrogen atoms were omitted for clarity and the displacement ellipsoids were scaled to the 50% probability level.

Appendix B: Synthesis Attempts of Polymerizable and Nonpolymerizable Tridentate Ligands and Corresponding Metal Complexes

In the following syntheses scheme (**Scheme B1)**, the first step resulted in 17% yield and the second step produced mixture of multi substituted product in low yields. The proposed syntheses route is displayed with dashed arrows.

Scheme B1. Proposed syntheses scheme of a polymerizable PNP ligand.

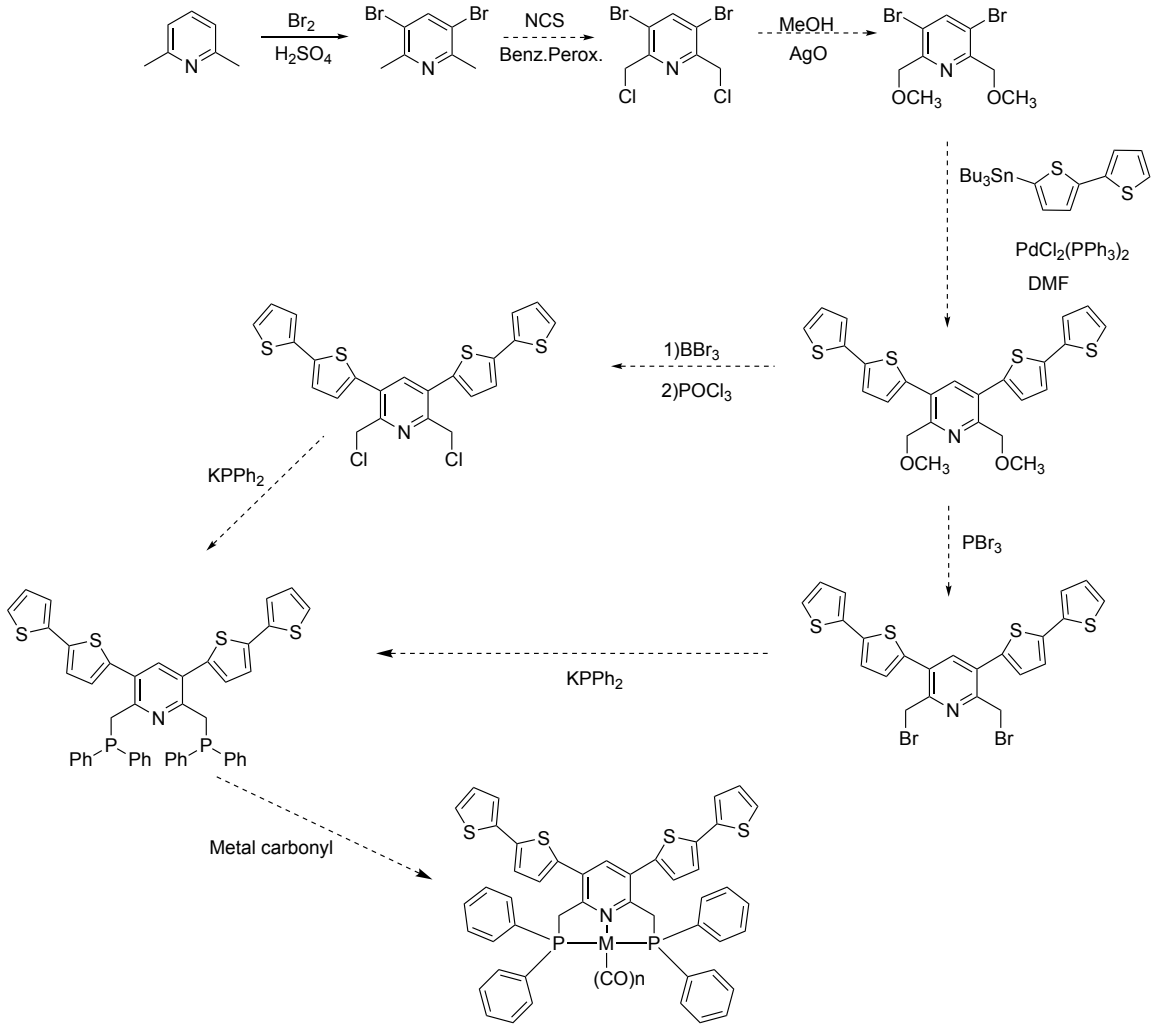

In **Scheme B2**, the first step could not be achieved.

Scheme B2. Proposed syntheses scheme of a polymerizable PNP ligand.

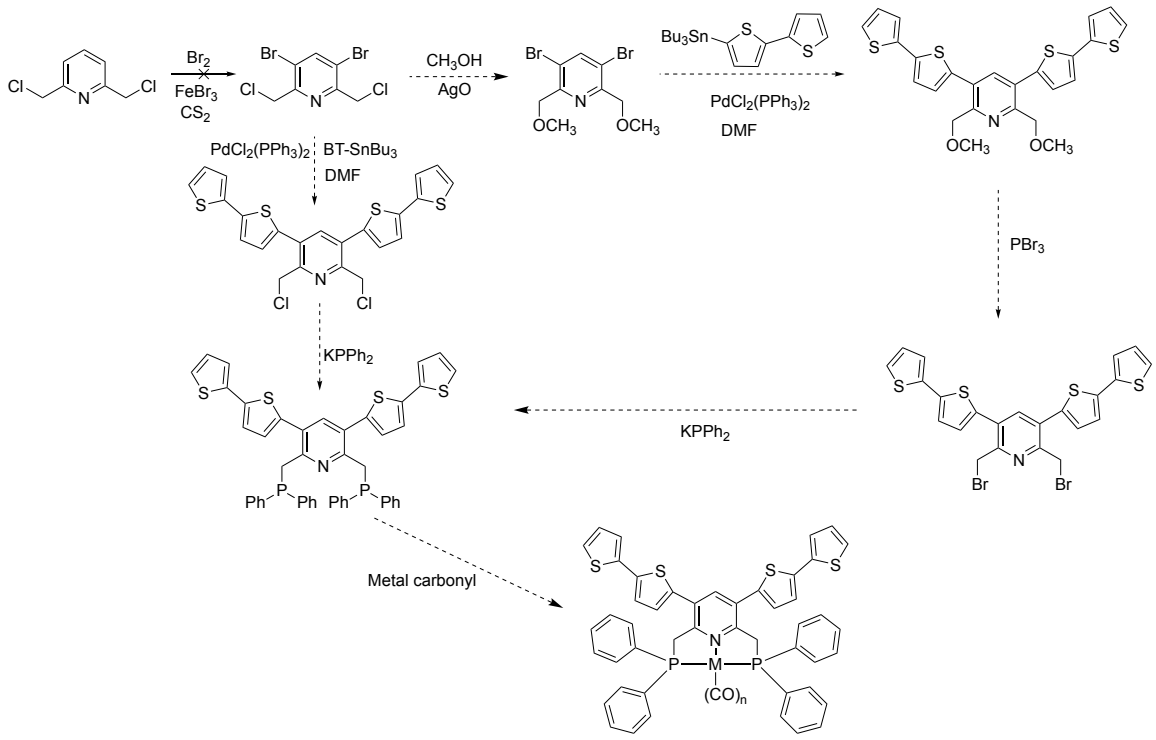

In **Scheme B3**, the first step (oxidation of the CH_3 groups to carboxylic acid) could not be achieved.

Scheme B3. Proposed syntheses scheme of a polymerizable PNP ligand.

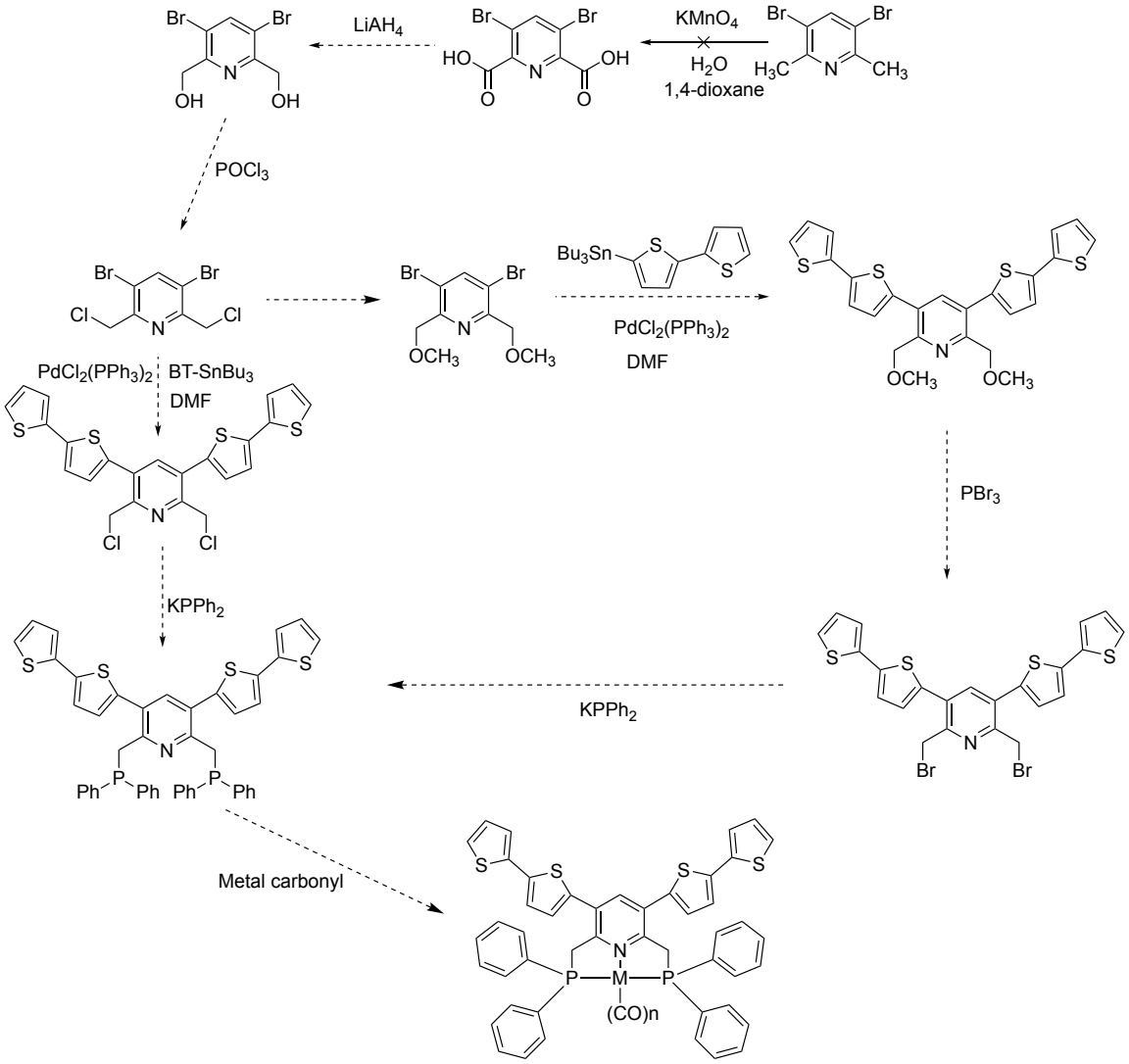

In **Scheme B4**, first two steps were succesful. However, instead of bromination of CH_3, bromination of the bithiophenes were observed.

Scheme B4. Proposed syntheses scheme of a polymerizable PNP ligand.

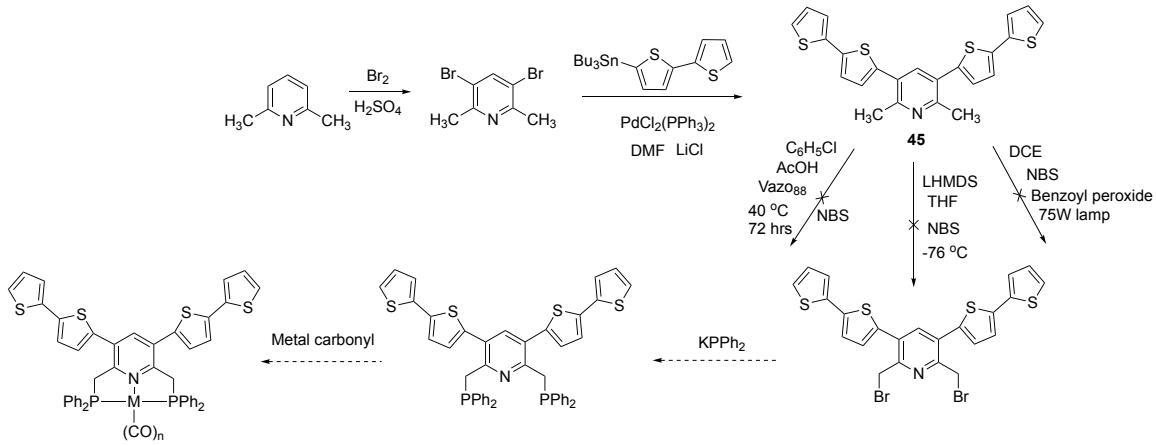

In **Scheme B5**, the second step could not be achieved.

Scheme B5. Proposed syntheses scheme of a polymerizable PNP ligand.

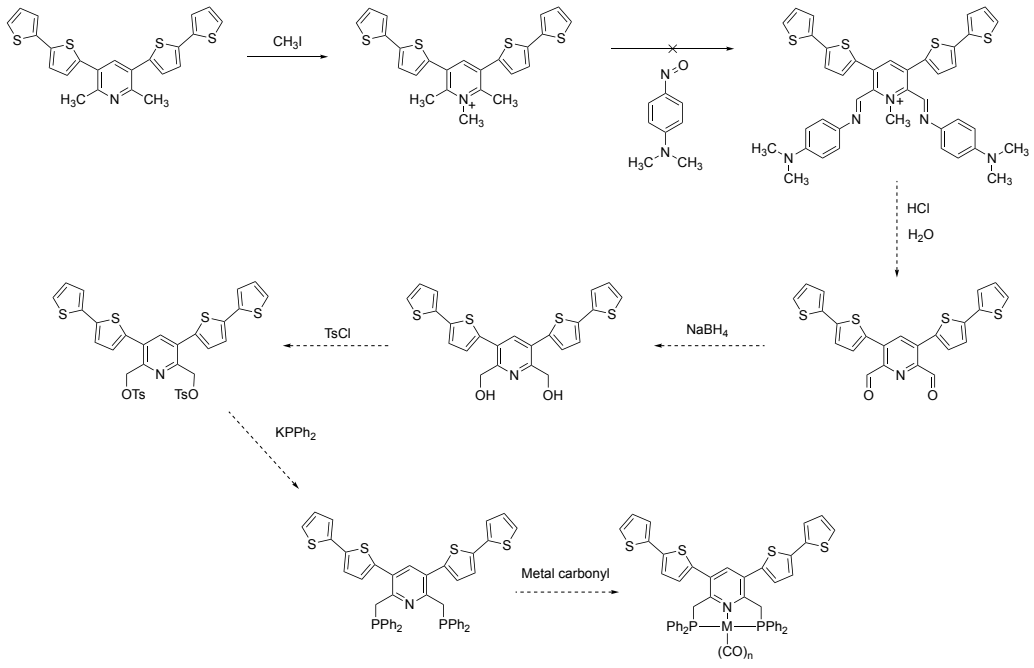

In **Scheme B6**, the second step could not be achieved.

Scheme B6. Attempts to functionalize CH_3 group of 2,6-luthidine and its derivatives.

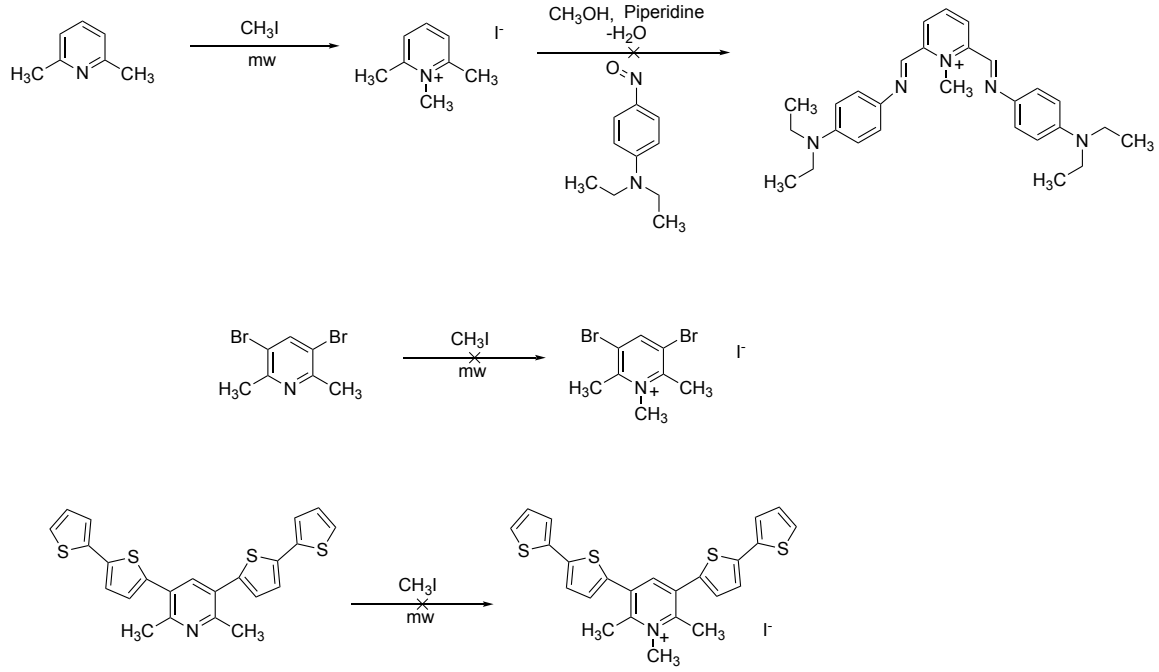

Scheme B7. Attempts to functionalize CH_3 group of 2,6-luthidine and its derivatives.

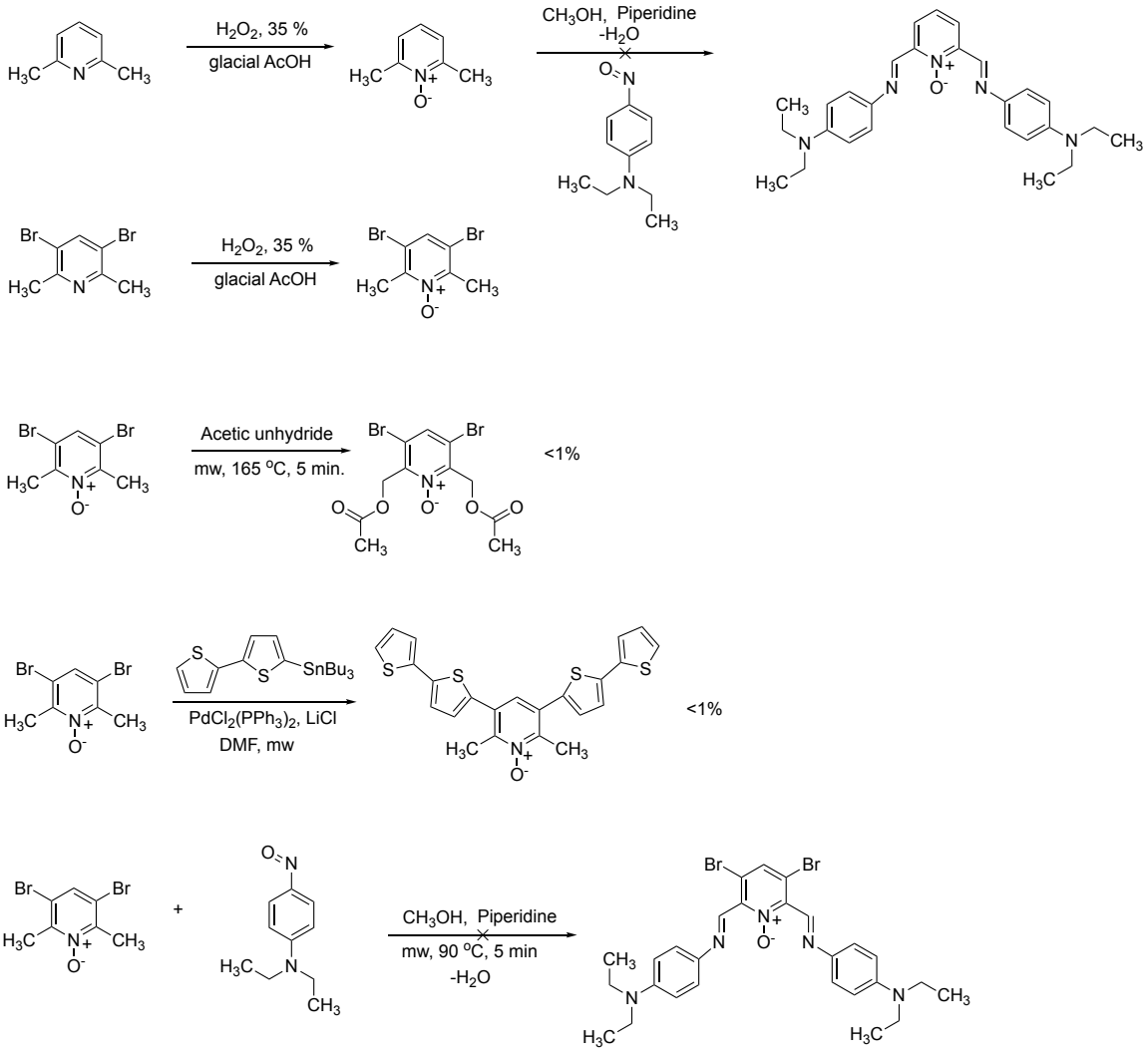

Scheme B8. CH_3 functionalization of 2,6-luthidine and related reactions.

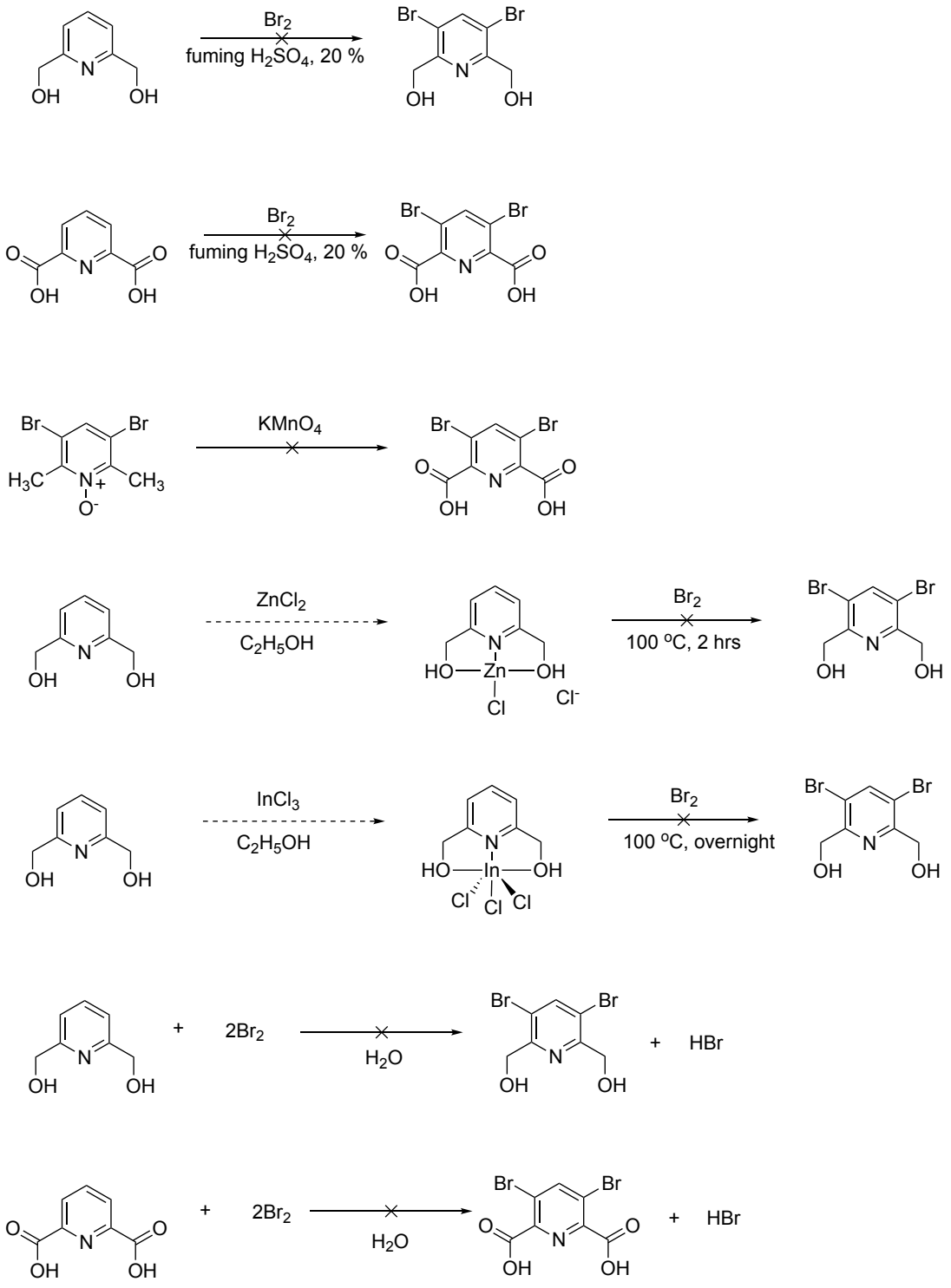

Scheme B9. Chelidamic acid reactions.

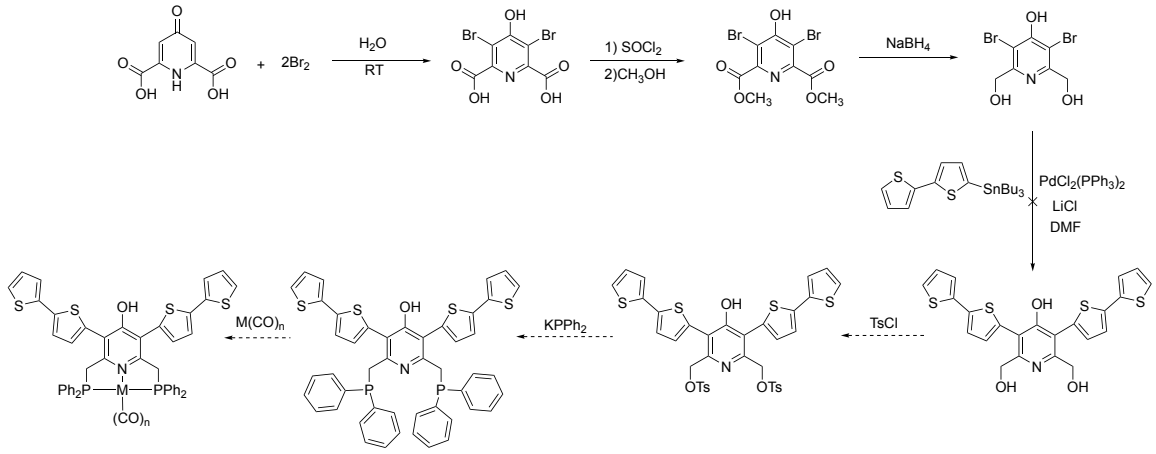

Scheme B10. Attempts to brominate the CH_3 groups of a 2,6-luthidine derivative.

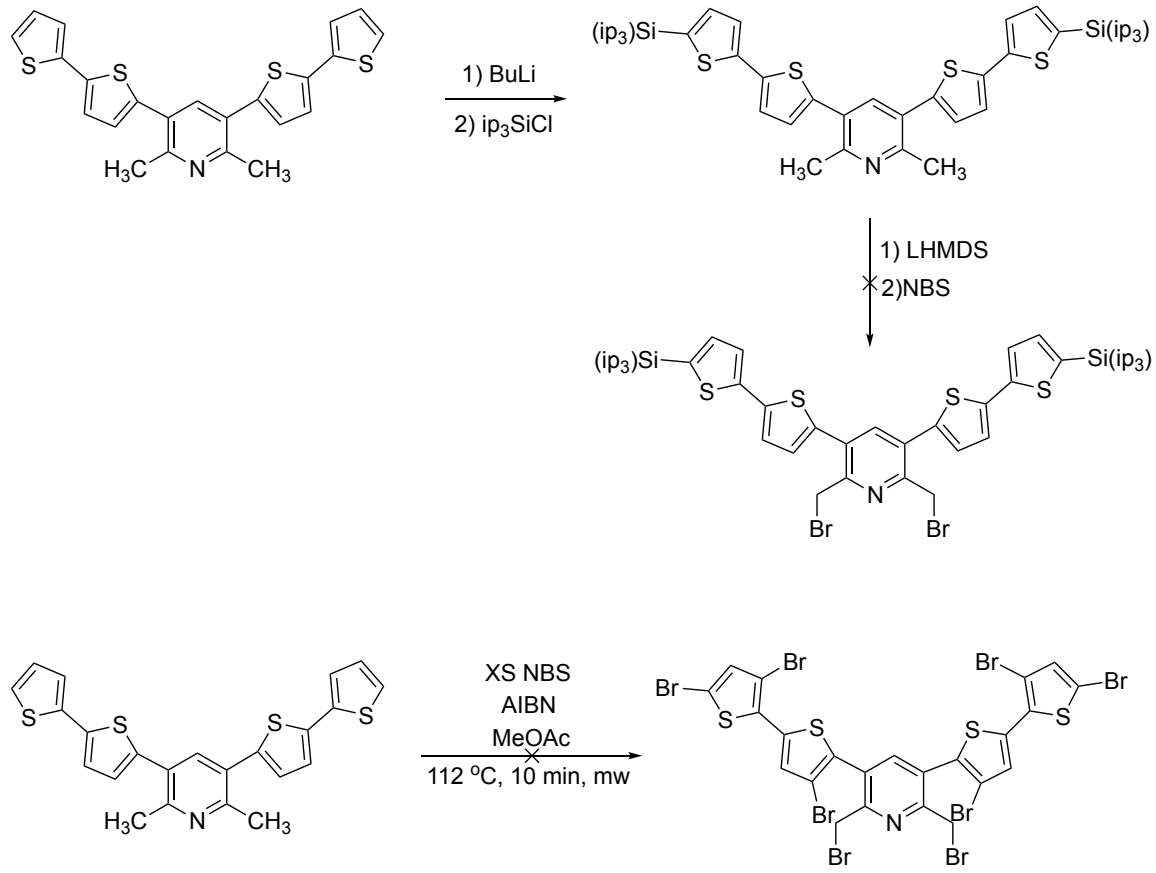

Scheme B11. Attempts to brominate the CH_3 groups of 2,6-luthidine derivatives.

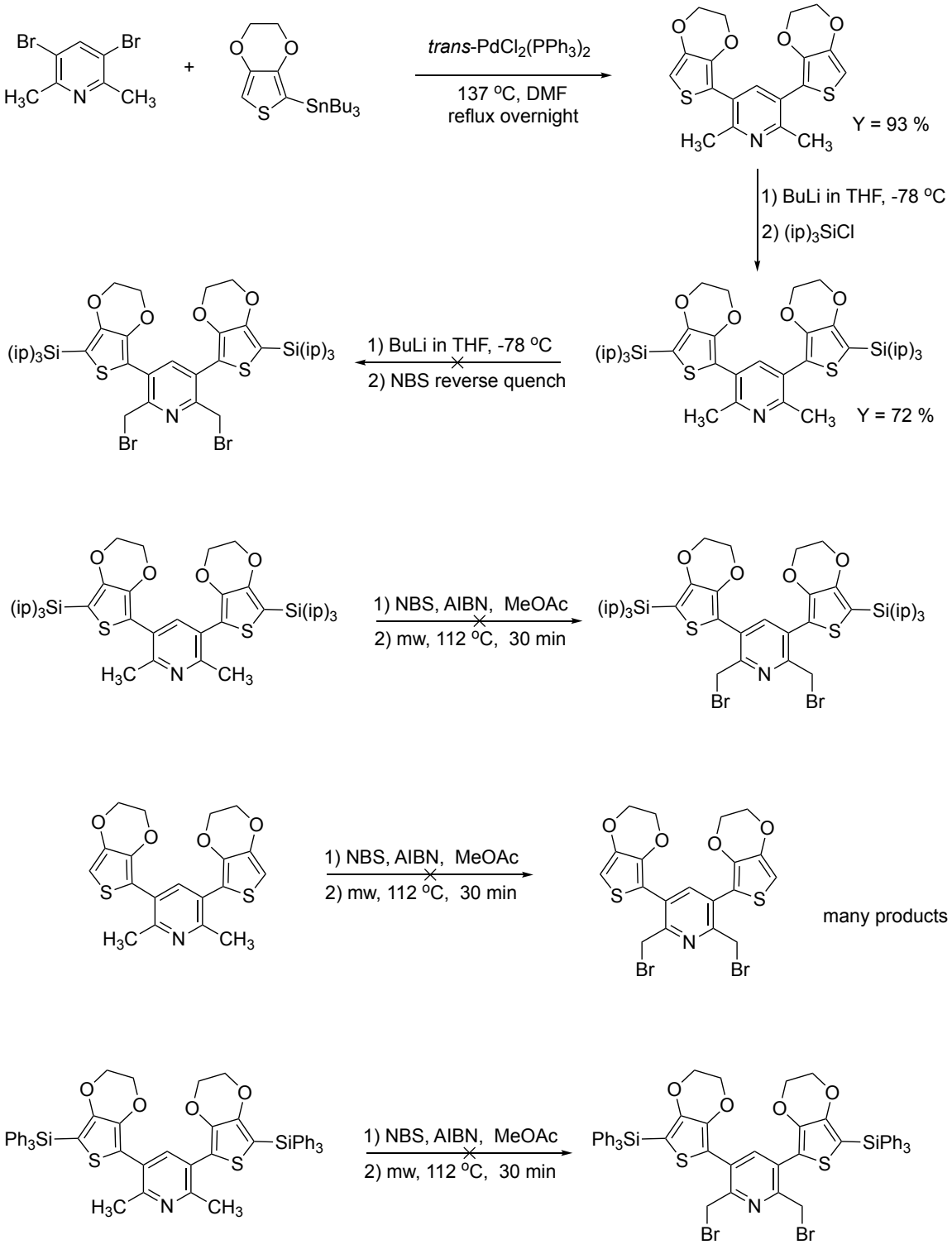

Scheme B12. Attempts to synthesize an NNN ligand.

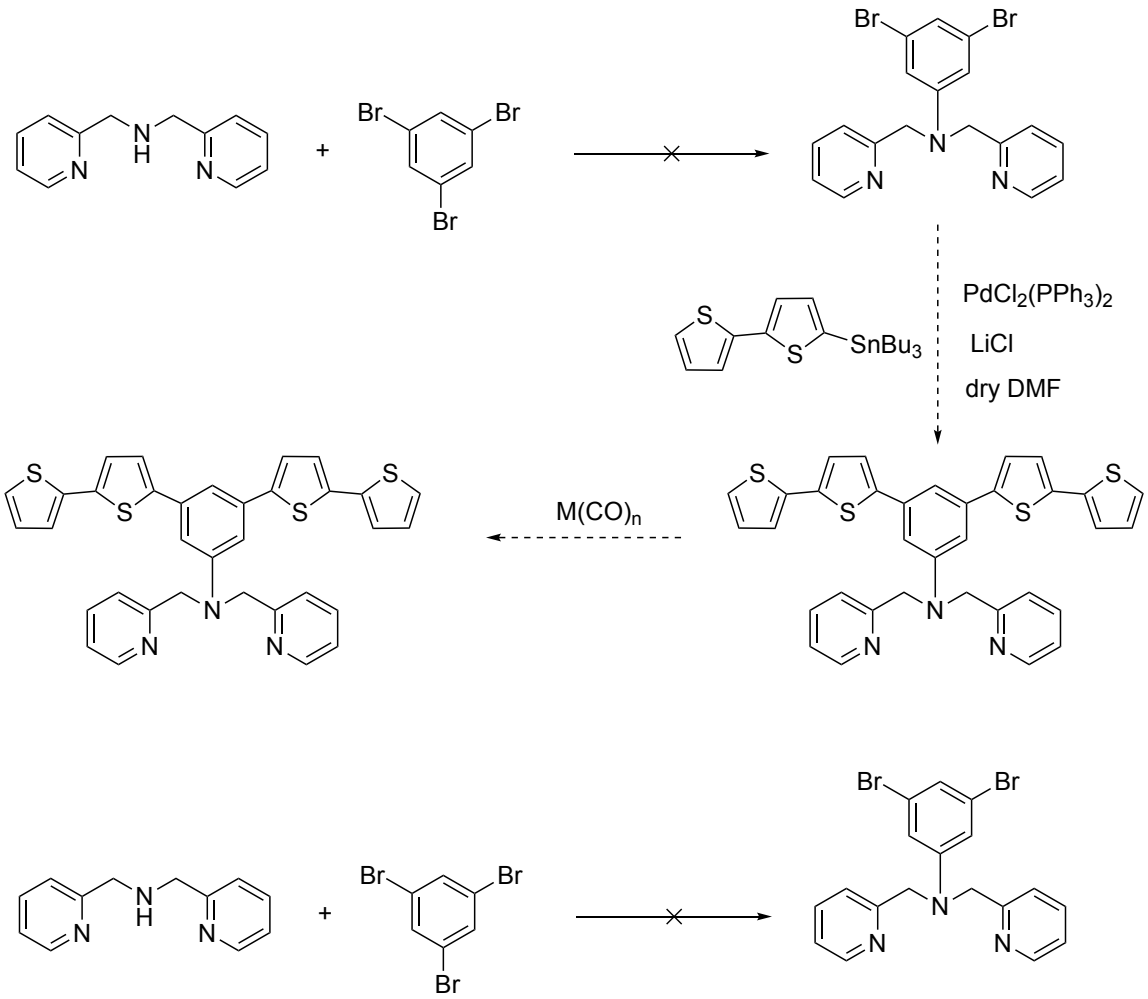

1) Cu powder, K_2CO_3, DMF reflux under Ar, 48hrs. (1g sm, 15mg product)
2) K_2CO_3, $CuSO_4.5H_2O$, 160 ^oC (no solvent).
3) KOH, $CuSO_4.5H_2O$, microwave 245 ^oC (no solvent).
4) Cu powder, K_2CO_3, DMF 173 ^oC, microwave.
5) KOH, $CuSO_4.5H_2O$, DMF 178 ^oC, microwave.
6) *t*-BuOK, DMSO, 150 ^oC, microwave.
7) *t*-BuOK, $Pd_2(dba)_3$, dry toluene, 150 ^oC, microwave.
8) *t*-BuOK, Pd-PPFA, dry toluene, 120 ^oC, microwave.

Scheme B13. Activation of an aryl amine in order to synthesize an NNN ligand (Buchwald aryl amination).

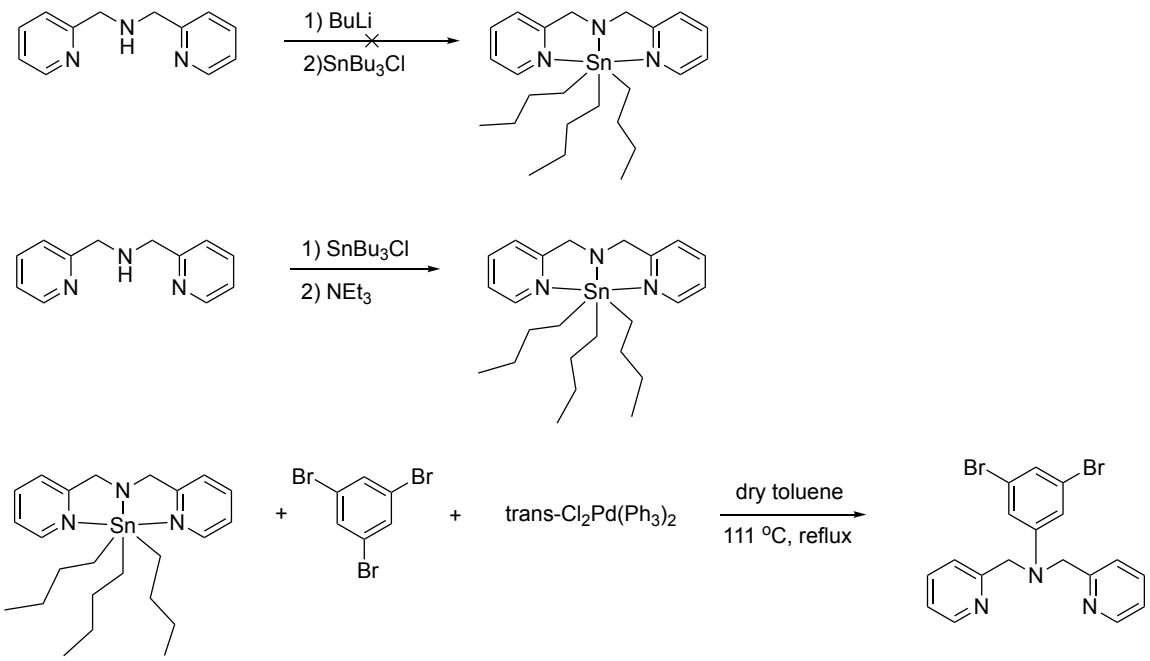

1) Did not work
2) $Cl_2Pd(o\text{-}tolyl_3P)_2$ was also tried, catalyst activated by turning green, but could not obtain the desired product
3) Same reaction was run in the microwave, but at 136 °C for 30 min. Did not work.

Scheme B14. Attempts to synthesize an NNN ligand.

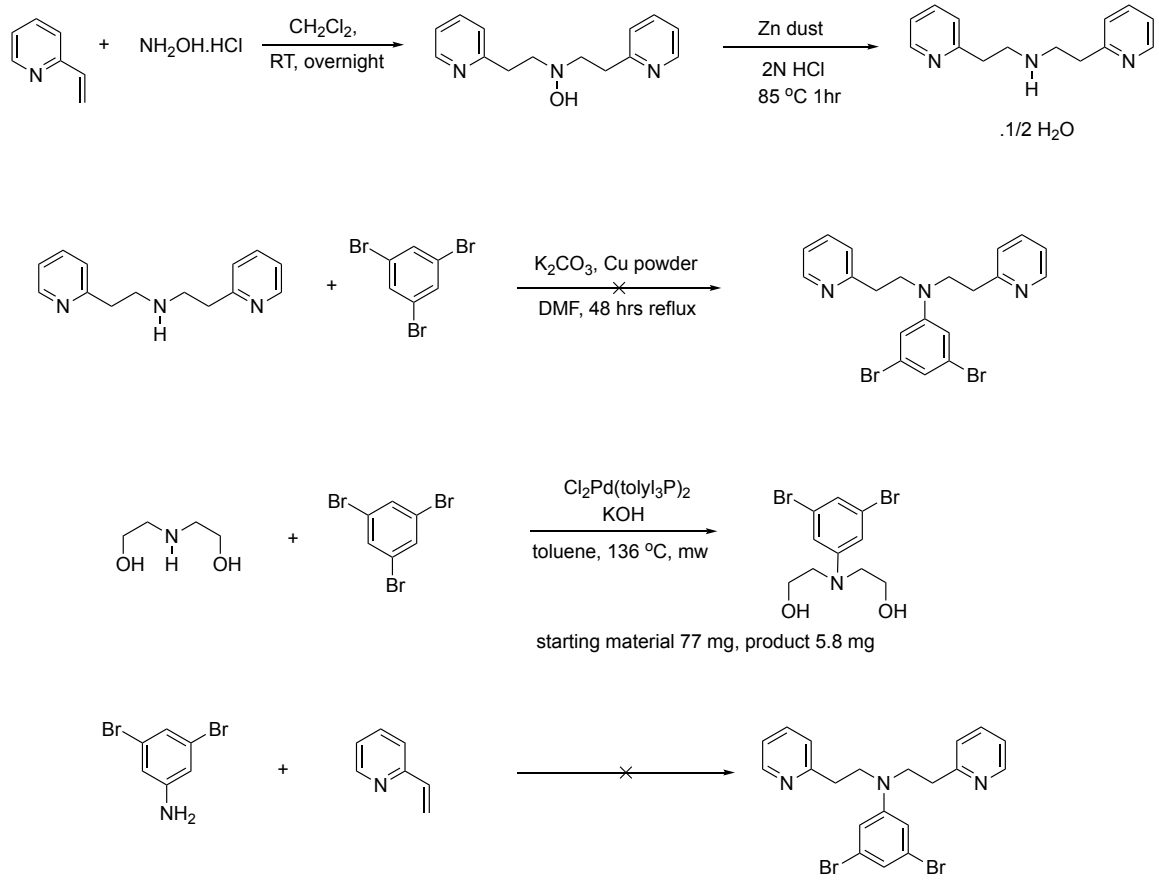

Scheme B15. Attempts to synthesize a carbazol based NNN ligand.

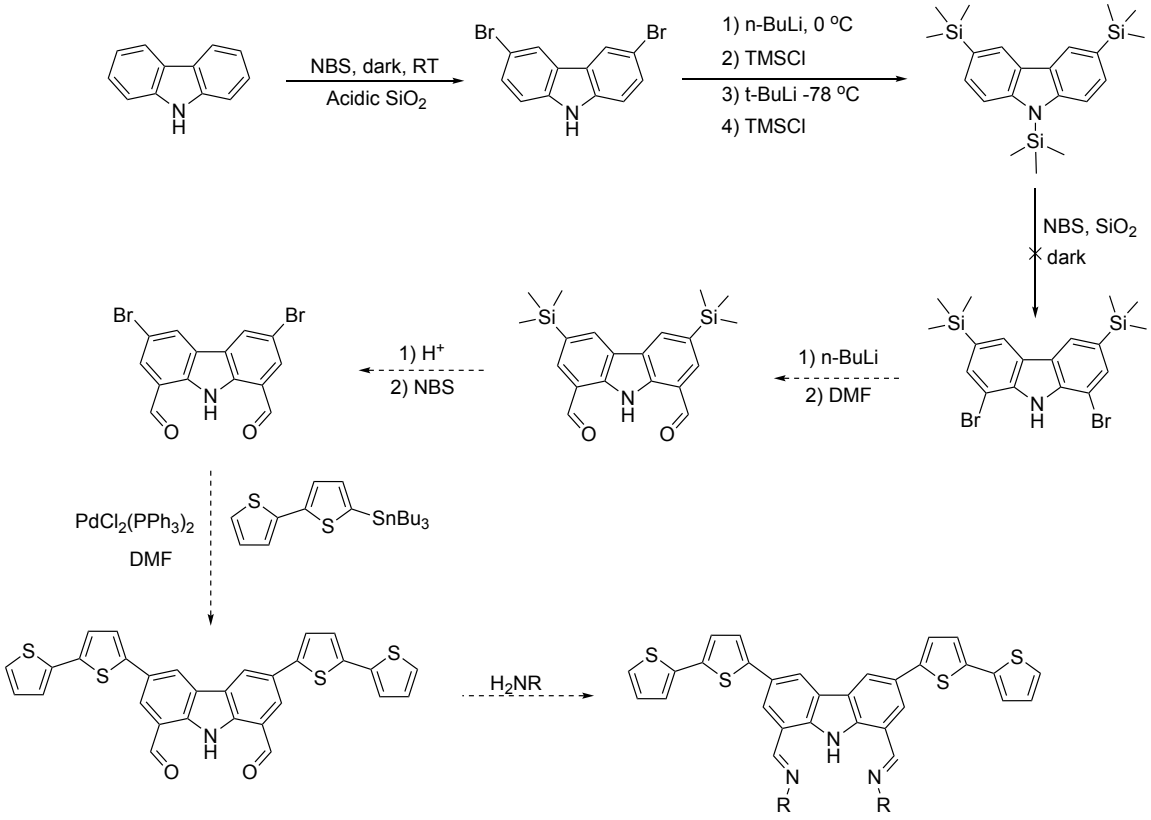

Scheme B16. Attempts to synthesize a carbazol based NNN ligand.

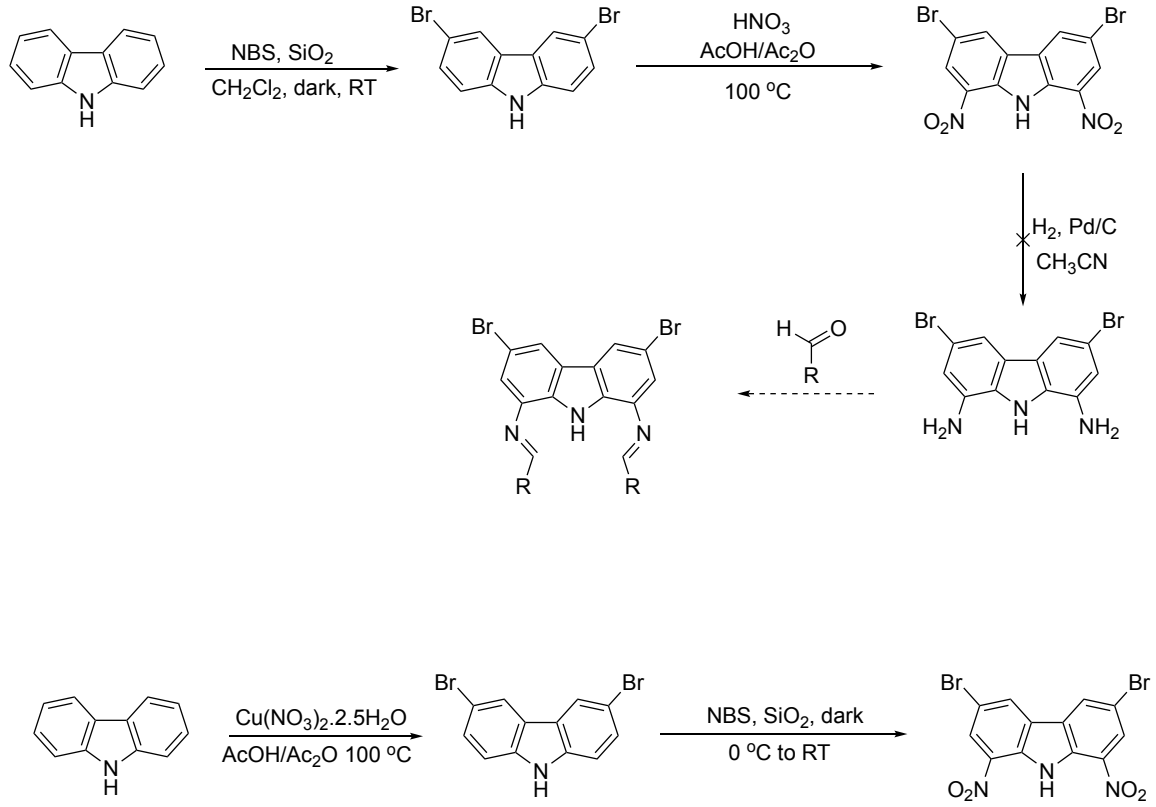

The synthesis of the following ligands in **Scheme 17** could not be achieved.

Scheme B17. Attempts to synthesize polymerizable tridentate ligands.

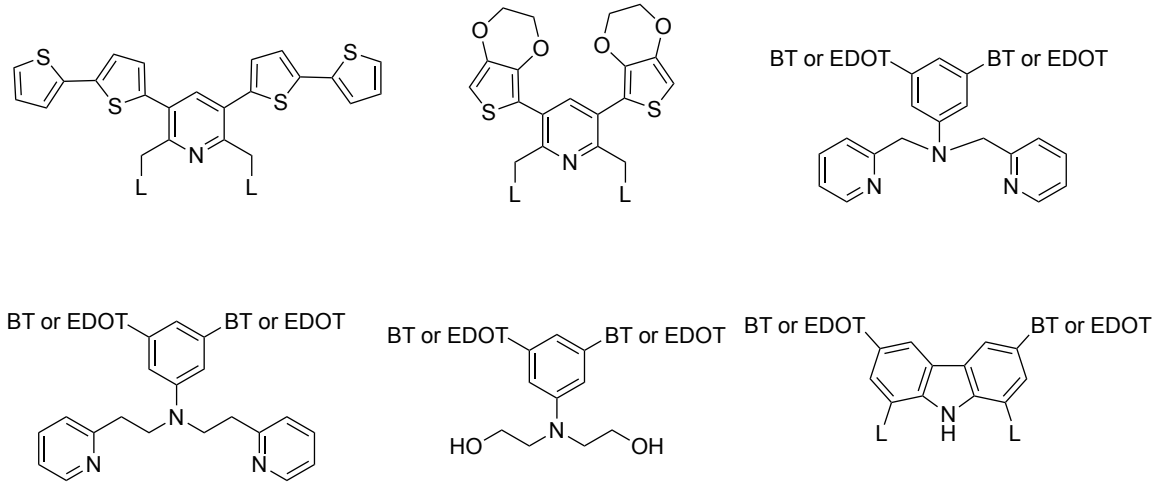

Scheme B18. Attempts to synthesize a tridentate ligand by epoxide reactions.

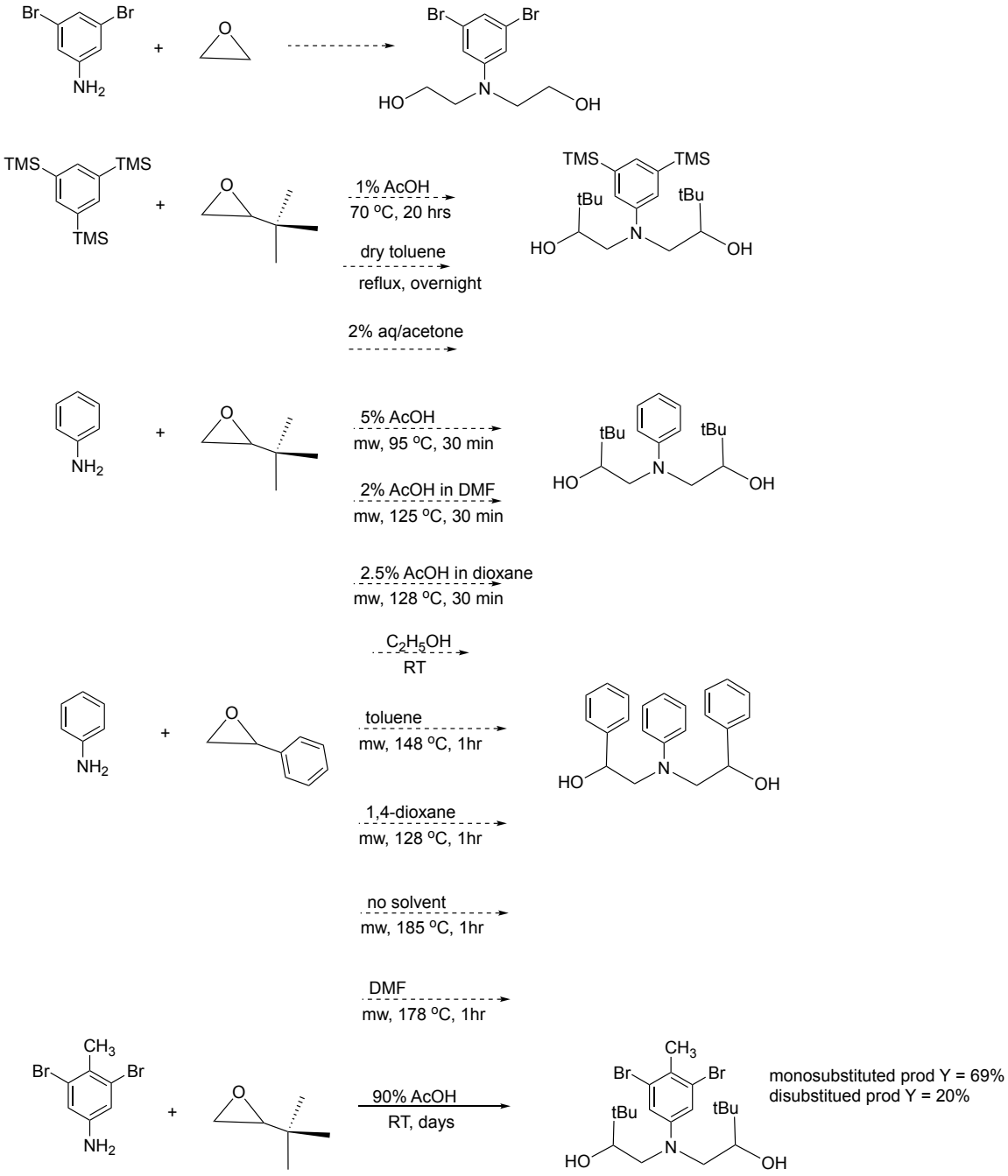

Scheme B19. Attempts to synthesize an aniline based ligand.

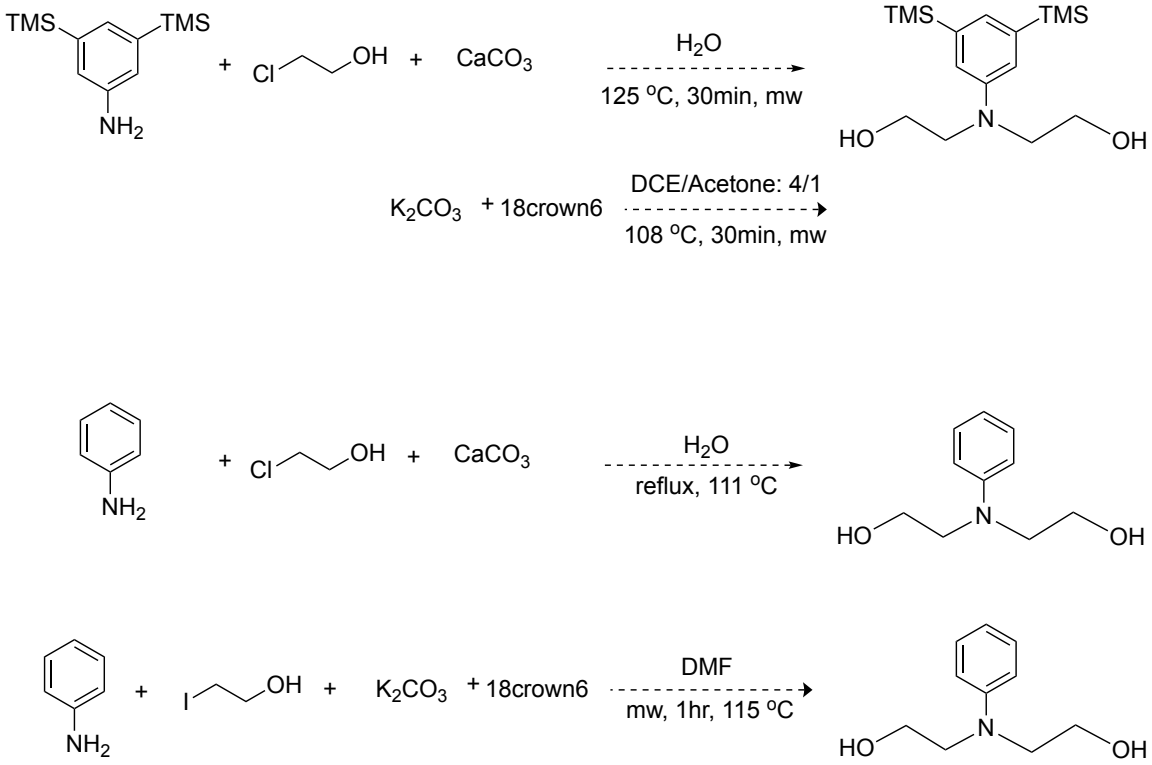

Scheme B20. Syntheses of a nonpolymerizable SNS ligand.

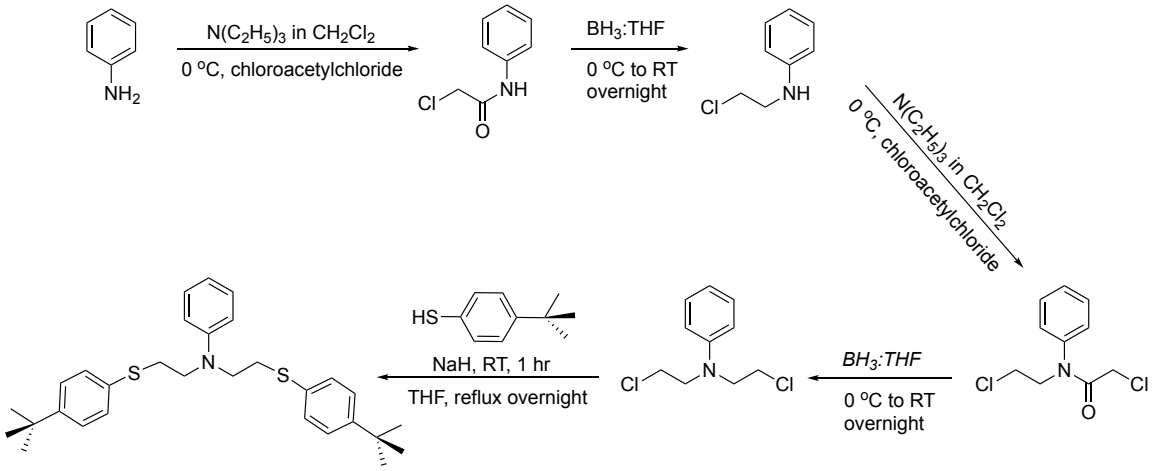

Scheme B21. Syntheses of a polymerizable SNS ligand and a related reaction.

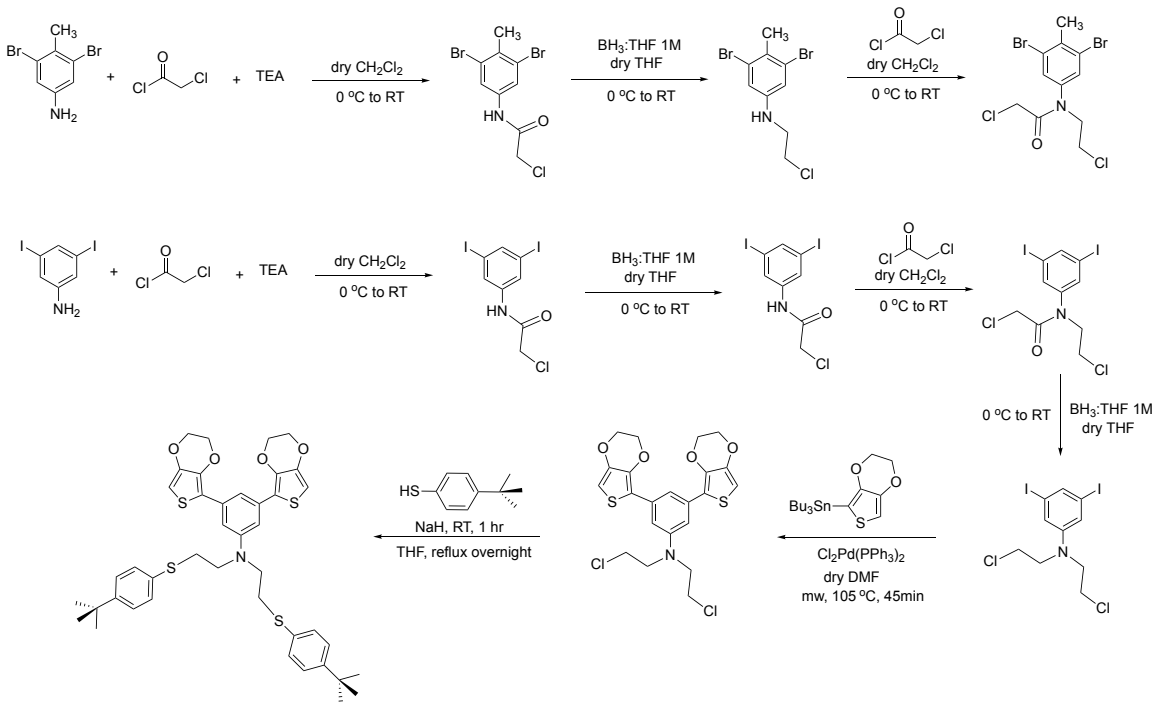

Scheme B22. Attempts to coordinate a metal to the nonpolymerizable SNS ligand.

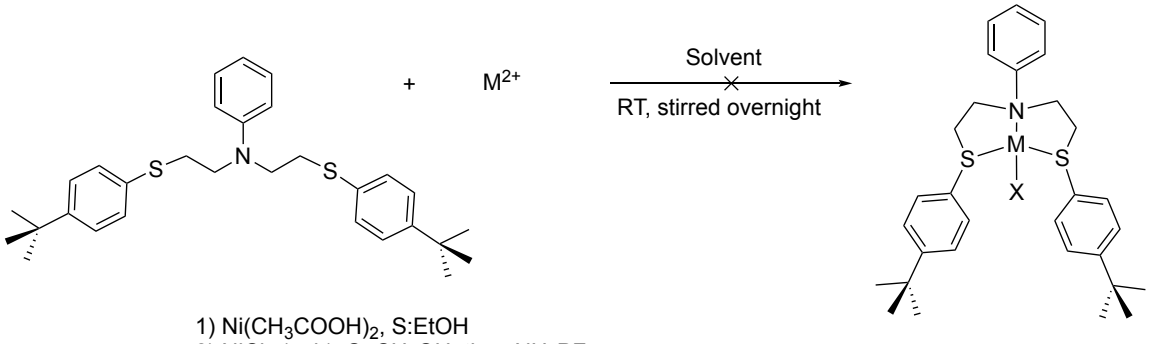

1) $Ni(CH_3COOH)_2$, S:EtOH
2) $NiCl_2$ (anh), S: CH_3OH, then NH_4PF_6
3) $Ni(NO_3)_2.6H_2O$, S:CH_3OH
4) $FeCl_2.4H_2O$, S:CH_3OH
5) $Co(NO_3)_2.6H_2O$, S:CH_3OH
6) $Cu(NO_3)_2$. 2 1/2 H_2O, S:CH_3OH
7) $MnCl_2$. $4H_2O$, S:CH_3OH
8) $Mn(CH_3COOH)_2.4H_2O$, S:CH_3OH, CH_2Cl_2 (1:1)
9) $Co(CH_3COOH)_2.4H_2O$, S:CH_3OH, CH_2Cl_2 (1:1)
10) $Cu_2(CH_3COOH)_4.2H_2O$, S:CH_3OH, CH_2Cl_2 (1:1)
11) $Ni(CH_3COOH)_2.4H_2O$, S:CH_3OH, CH_2Cl_2 (1:1)
12) $Cu(SO_3CF_3)_2$, S:CH_3OH, CH_2Cl_2 (1:1)
13) $Co(CH_3COOH)_2.4H_2O$, S:CH_3CN
14) $CoCl_2.6H_2O$, S:CH_3OH, CH_2Cl_2 (1:1)
15) $NiCl_2$ (anh), S: THF, H_2O, μw 75C, 30min
16) $Cu(SO_3CF_3)_2$, S:CH_2Cl_2, acetone, immediate color change
17) $Hg(CH_3COOH)_2$, S: CH_2Cl_2, Benzene, CH_3OH (layering)
18) $Pb(CH_3COOH)_2.3H_2O$: UV-Vis
19) $ZnClO_4.6H_2O$: UV-Vis
20) $Zn(CH_3COOH)_2.2H_2O$: UV-Vis
21) $SnCl_2.2H_2O$: UV-Vis

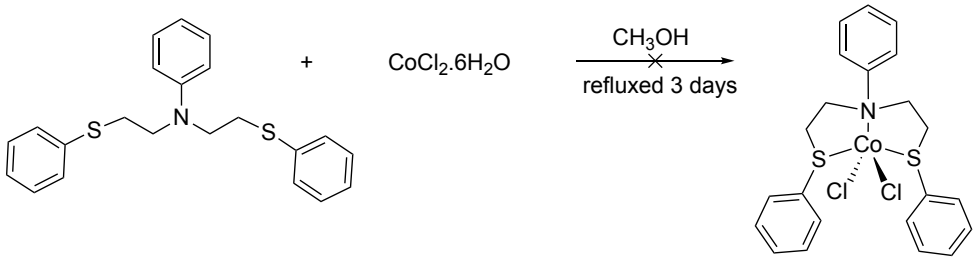

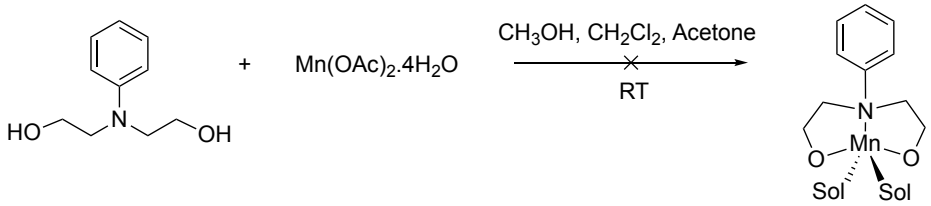

Scheme B23. Attempts to synthesize SNS ligands and corresponding metal coordinations.

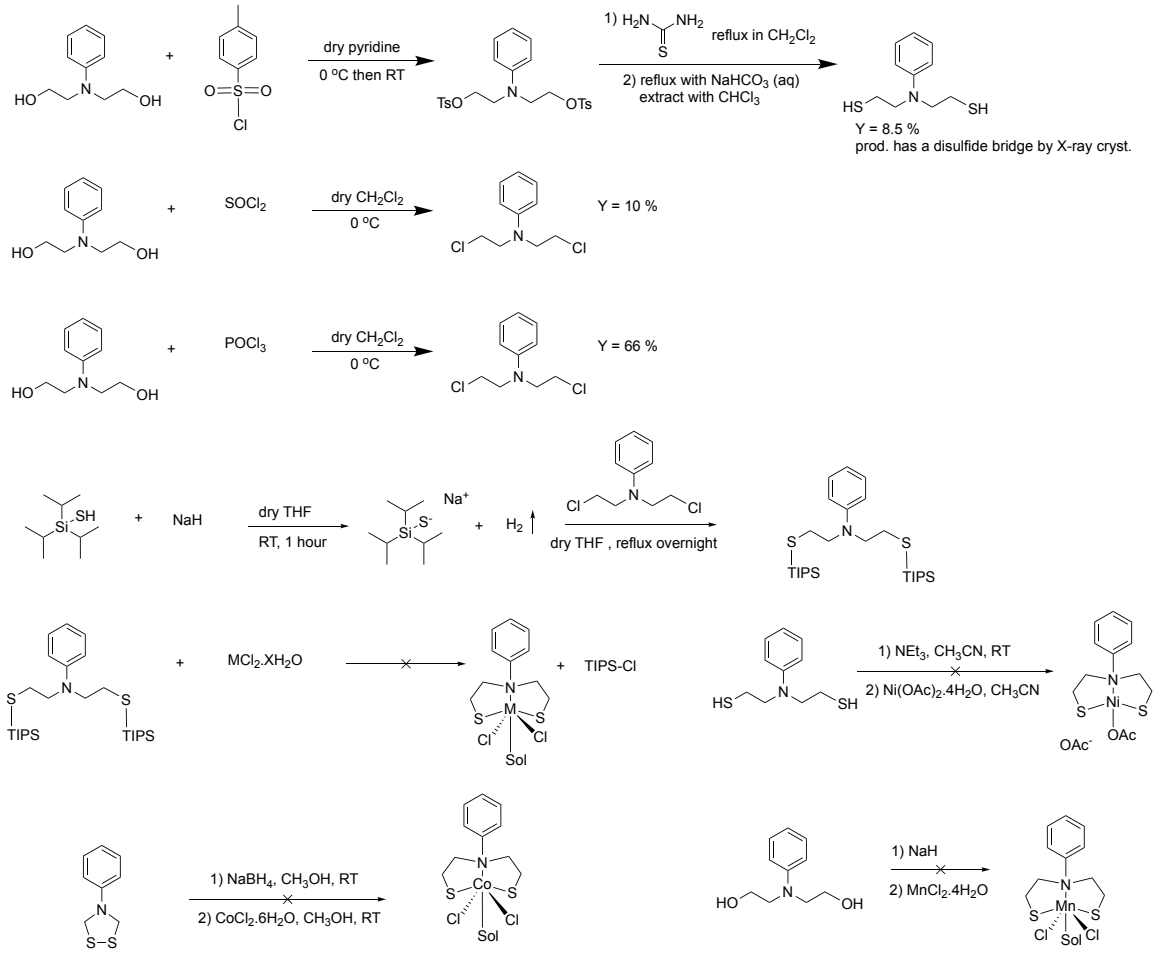

Scheme B24. Attempts to synthesize NNN tridentate ligands.

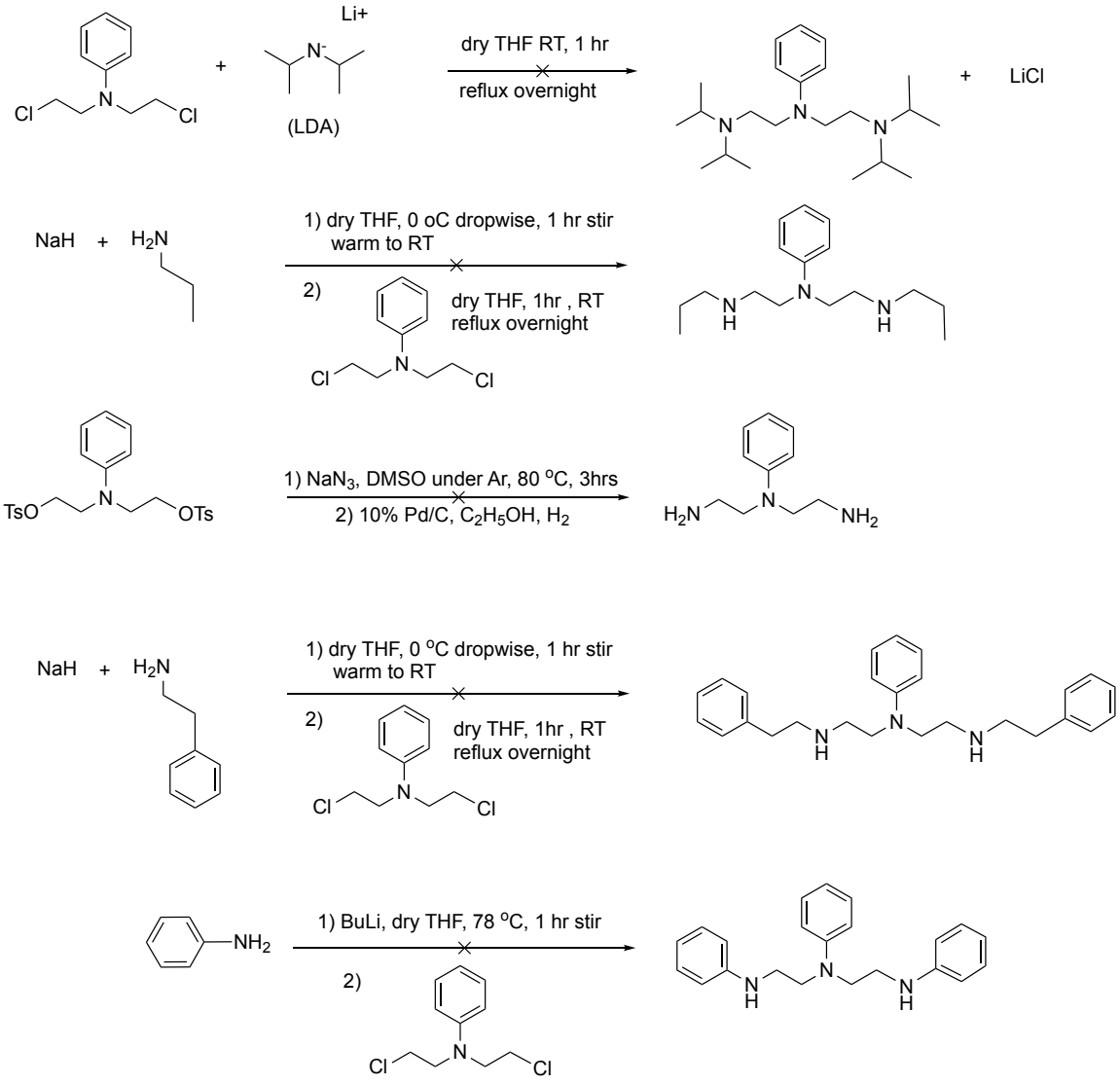

The synthesis of the compound with the yield 83 %, was not reproducible. The reaction resulted in the polymerization when it was repeated (**Scheme B25**).

Scheme B25. Attempts to synthesize tridentate ligands with three carbon chains.

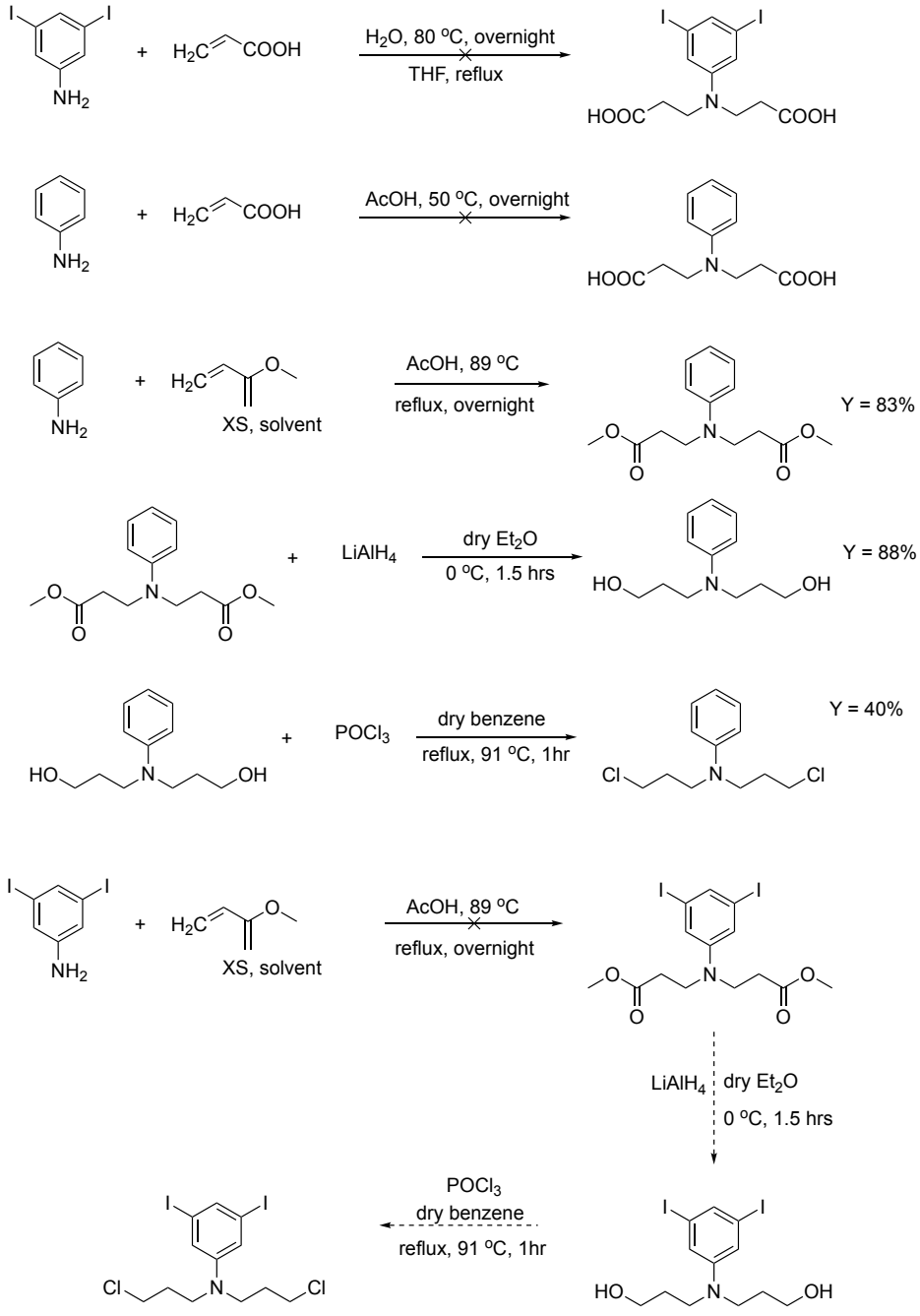

Scheme B26. Attempts of metal coordinations to the SNS and PNP ligands.

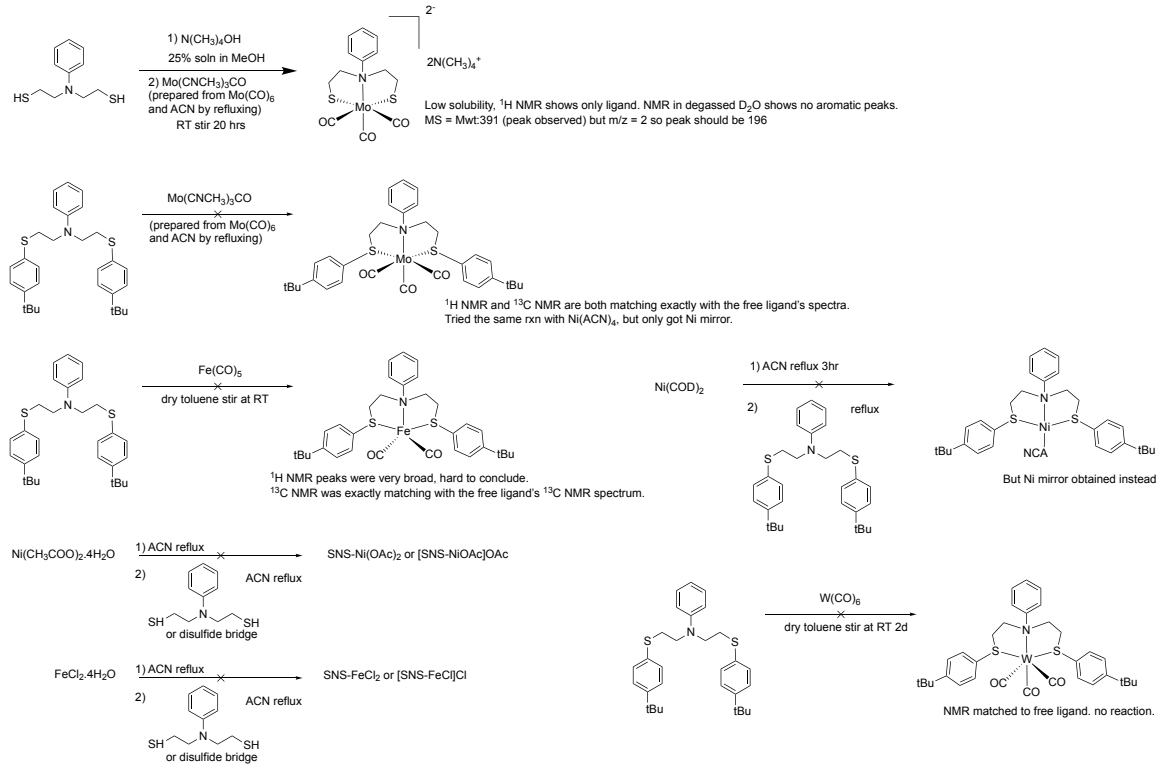

Scheme B27. Attempts to synthesize cyclic tridentate ligands.

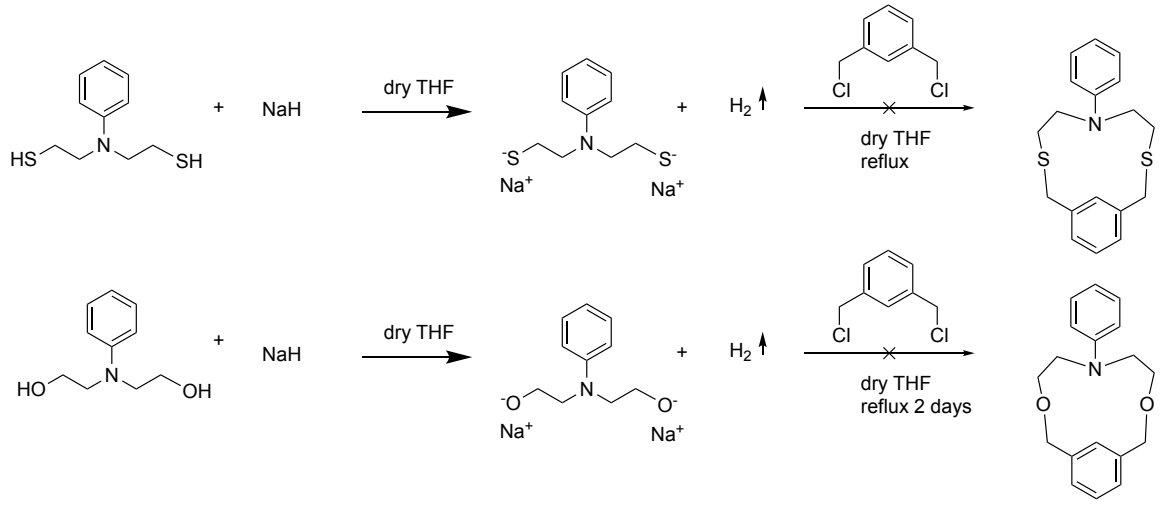

Scheme B28. Attempts of PNP-M coordination.

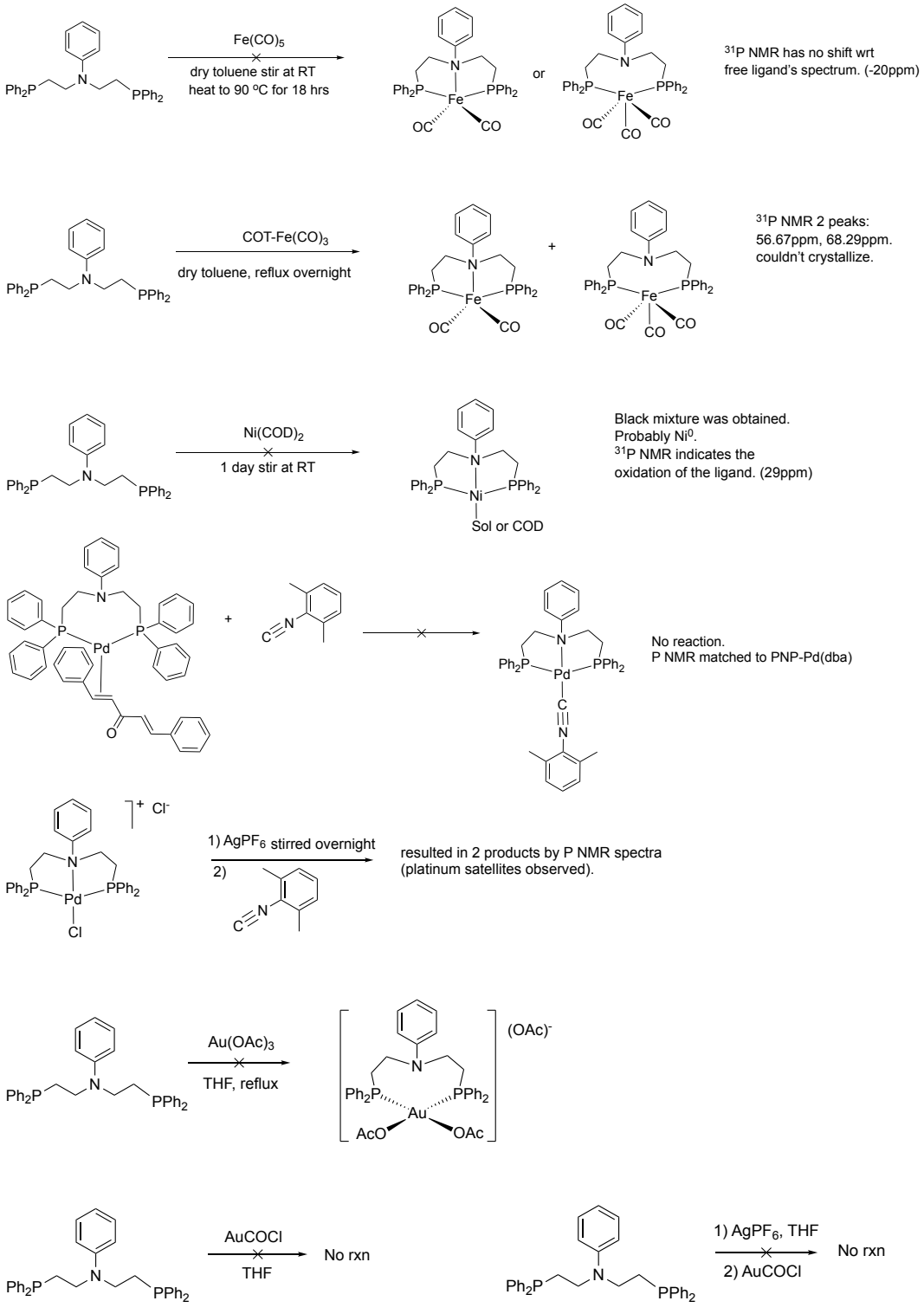

Scheme B29. Other attempts of PNP-M coordination.

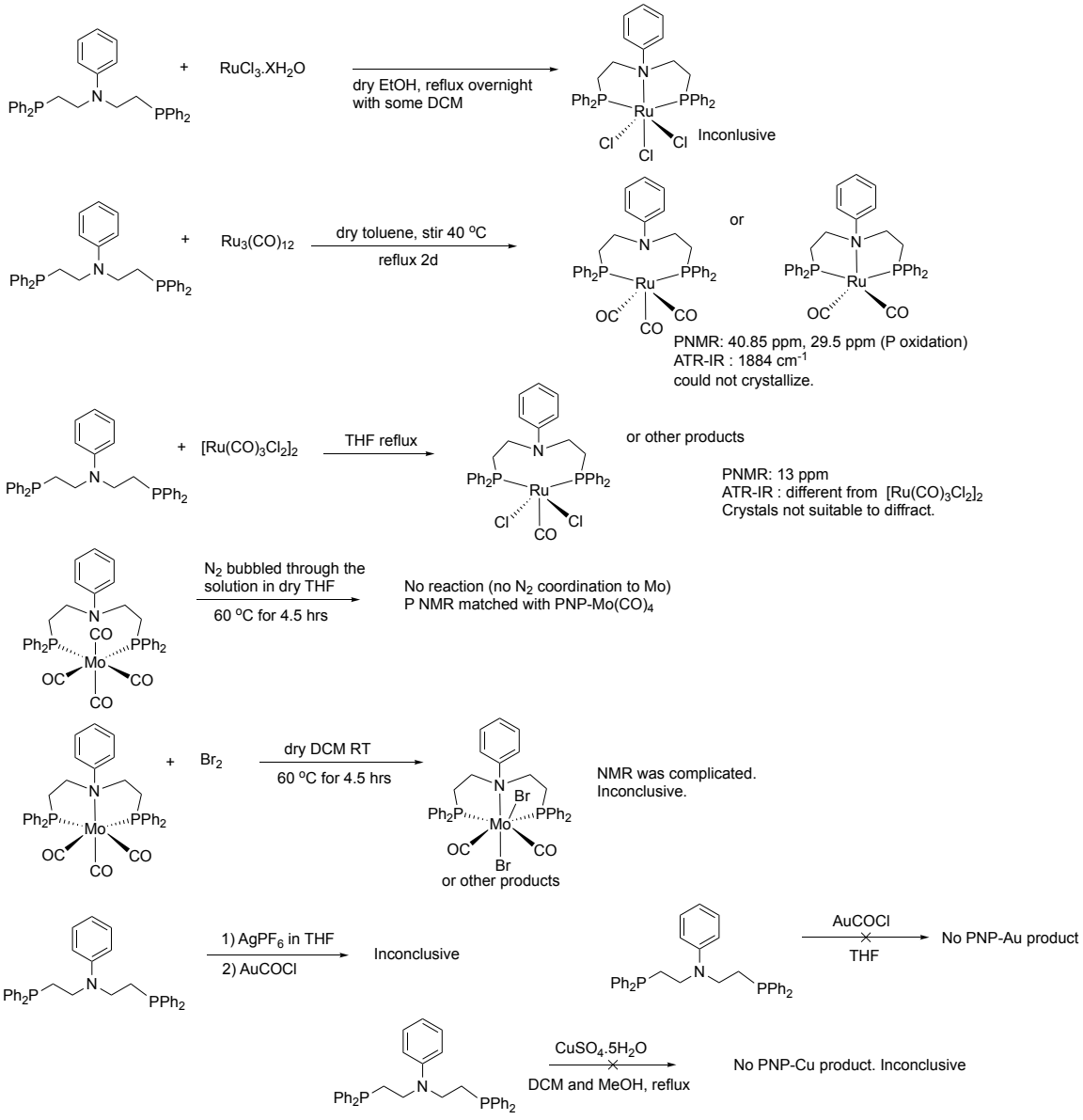

Scheme B30. Attempts to synthesize PNP-Mo(NO)$_2$.

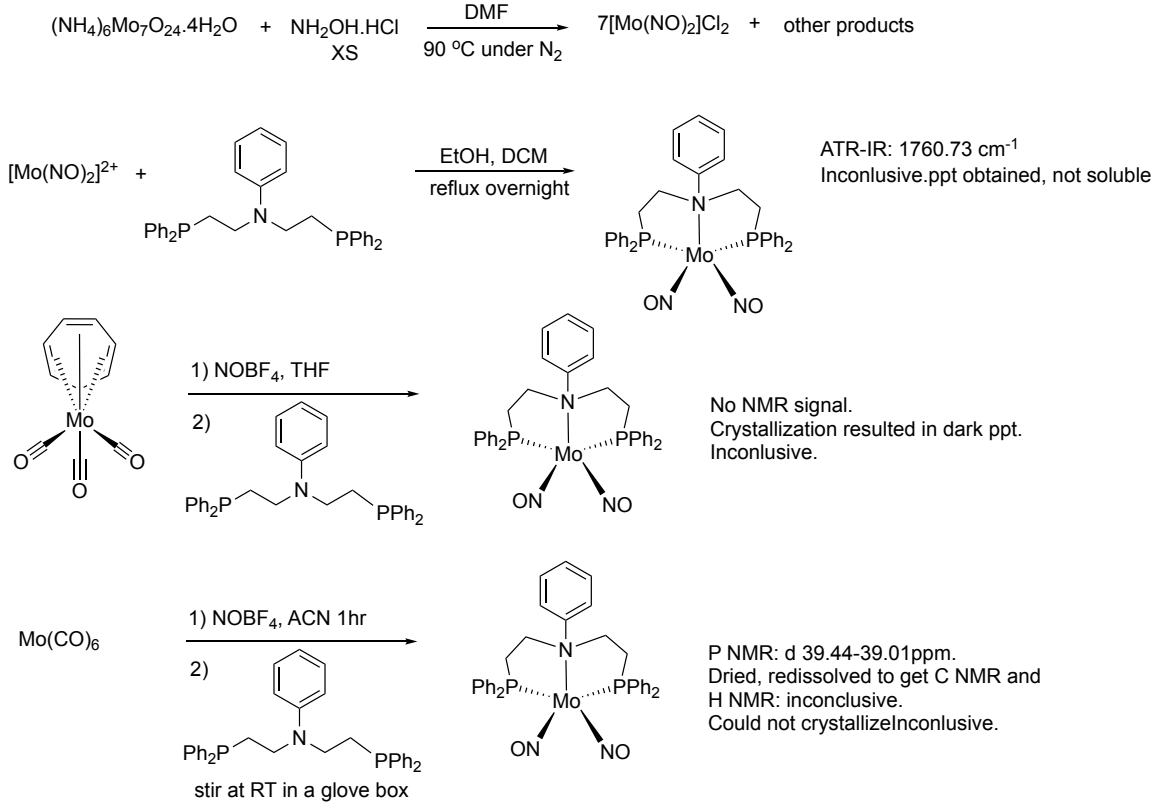

Scheme B31. Attempt to synthesize an SNS-Fe complex.

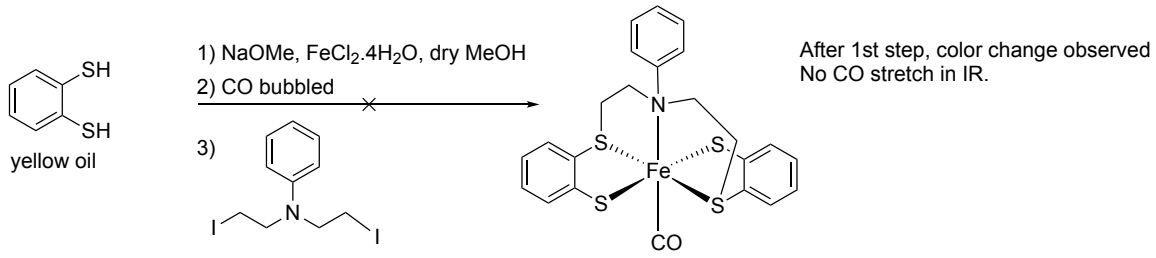

Scheme B32. Attempts to synthesize polymerizable NNN-metal complexes.

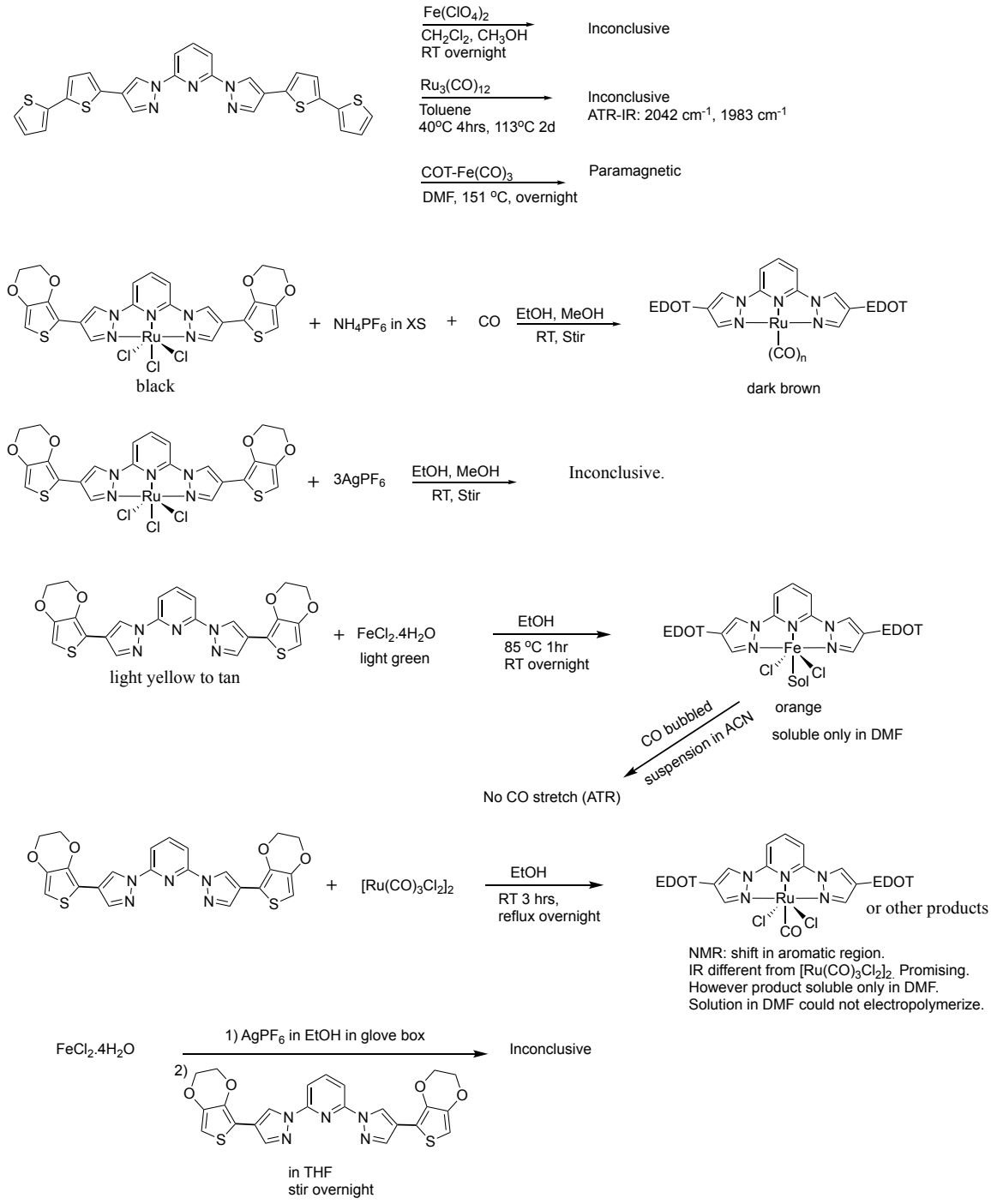

Scheme B33. Another synthesis trial.

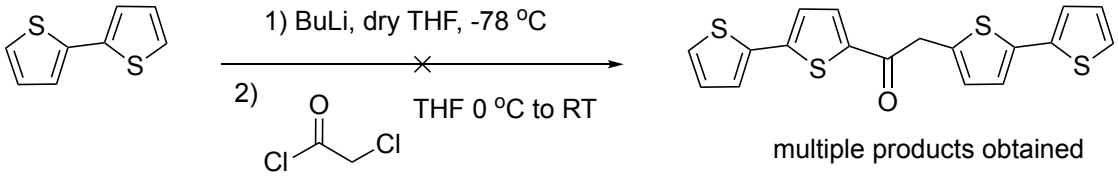

Scheme B34. Molybdenum carbonyl reagents used in Scheme 2, from top left clockwise: *fac*-CHT-$Mo(CO)_3$, NBD-$Mo(CO)_4$, *cis*-pip_2-$Mo(CO)_4$, $(ACN)_3Mo(CO)_3$.[209]

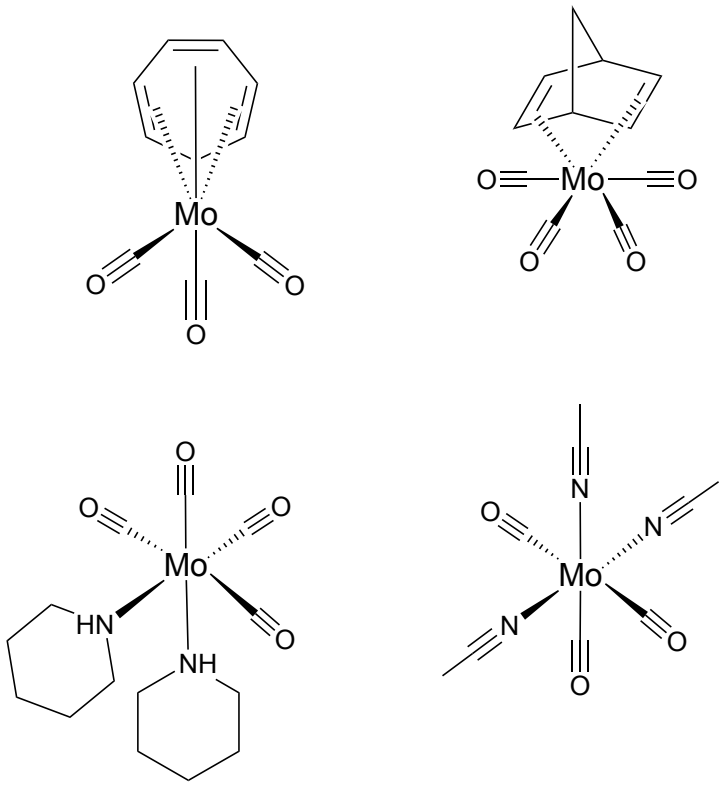

References

1. Chiang, C. K.; Fincher, C. R.; Park, Y. W.; Heeger, A. J.; Shirakawa, H.; Louis, E. J.; Gau, S. C.; Macdiarmid, A. G. Electrical Conductivity In Doped Polyacetylene. *Physical Review Letters* **1977,** *39* (17), 1098-1101.

2. Shirakawa, H.; Louis, E. J.; Macdiarmid, A. G.; Chiang, C. K.; Heeger, A. J. Synthesis of Electrically Conducting Organic Polymers-Halogen Derivatives of Polyacetylene, $(CH)_x$. *Journal of the Chemical Society-Chemical Communications* **1977,** (16), 578-580.

3. Holliday, B. J.; Swager, T. M. Conducting Metallopolymers: The Roles of Molecular Architecture and Redox Matching. *Chemical Communications* **2005,** (1), 23-36.

4. Wolf, M. O., Recent Advances in Conjugated Transition Metal-Containing Polymers and Materials. *Journal of Inorganic and Organometallic Polymers and Materials* **2006,** *16* (3), 189-199.

5. Wolf, M. O. Transition-Metal-Polythiophene Hybrid Materials. *Advanced Materials* **2001,** *13* (8), 545-553.

6. Balamurugan, A.; Reddy, M. L. P.; Jayakannan, M. Single Polymer Photosensitizer for Tb^{3+} and Eu^{3+} Ions: An Approach For White Light Emission Based on Carboxylic-Functionalized Poly(m-phenylenevinylene)s. *Journal of Physical Chemistry B* **2009,** *113*, 14128–14138.

7. Zhang, Y.; Xiong, Y.; Li, C.; Peng, J. Synthesis and Properties of Electrophosphorescent Conjugated Polymers Containing Iridium Complexes in Polymer Backbone. *Chemistry Letters* **2008,** *37* (742 - 743).

8. Man, K. Y. K.; Wong, H. L.; Chan, W. K.; Kwong, C. Y.; Djurisic, A. B. Efficient Photodetectors Fabricated from a Metal-Containing Conjugated Polymer by a Multilayer Deposition Process. *Chemistry of Materials* **2004,** *16* (3), 365-367.

9. Nguyen, M. T. Electronic Materials Based on Conducting Metallopolymers and Self-Assembly The University of Texas at Austin, 2014.

10. Roncali, J., Conjugated Poly(thiophenes): Synthesis, Functionalizatlon, and Applications. *Chemical Reviews* **1992,** *92*, 711-738.

11. Skotheim, T. A.; Reynolds, J. R., *Handbook of Conducting Polymers*. 3rd ed.; CRC Press: Boka Raton, 2007; Vol. I.

12. Yamamoto, T.; Saitoh, Y.; Anzai, K.; Fukumoto, H.; Yasuda, T.; Fujiwara, Y.; Choi, B. K.; Kubota, K.; Miyamae, T. Poly(1,10-phenanthroline-3,8-diyl) and Its Derivatives. Preparation, Optical and Electrochemical Properties, Solid Structure, and Their Metal Complexes. *Macromolecules* **2003,** *36* (18), 6722-6729.

13. Jaffe, H. H.; Miller, A. L. Fates of Electronic Excitation Energy. *Journal of Chemical Education* **1966,** *43* (9), 469-&.

14. Kasha, M. Characterization of Electronic Transitions in Complex Molecules. *Discussions of the Faraday Society* **1950,** *9*, 14 - 19.

15. Evans, R. C.; Douglas, P.; Winscom, C. J. Coordination Complexes Exhibiting Room-temperature Phosphorescence: Evaluation of Their Suitability as Triplet Emitters in Organic Light Emitting Diodes. *Coordination Chemistry Reviews* **2006,** *250* (15-16), 2093-2126.

16. Crosby, G. A. Spectroscopic Investigations of Excited-States of Transition-Metal Complexes. *Accounts of Chemical Research* **1975,** *8* (7), 231-238.

17. Yam, V. W. W., Molecular Design of Transition Metal Alkynyl Complexes as Building Blocks for Luminescent Metal-Based Materials: Structural and Photophysical Aspects. *Accounts of Chemical Research* **2002,** *35* (7), 555-563.

18. Holonyak, N. J., Lemelson-MIT Prize Winner. 2004.

19. Tang, C. W.; Vanslyke, S. A. Organic Electroluminescent Diodes. *Applied Physics Letters* **1987,** *51* (12), 913-915.

20. Gustafsson, G.; Cao, Y.; Treacy, G. M.; Klavetter, F.; Colaneri, N.; Heeger, A. J. Flexible Light-Emitting-Diodes Made from Soluble Conducting Polymers. *Nature* **1992,** *357* (6378), 477-479.

21. Mikami, A.; Nishita, Y.; Iida, Y. High Efficiency Phosphorescent Organic Light-Emitting Devices Coupled with Lateral Color-Conversion Layer. In *SID Symposium Digest of Technical Papers*, 2006; Vol. 37, pp 1376-1379.

22. Sun, C. Lewis-acidic Triarylboranes: Optoelectronic Applications and Unusual Reactivities. Queen's University, Kingston, Ontario, Canada, 2012.

23. Tang, C. W. 2-Layer Organic Photovoltaic Cell. *Applied Physics Letters* **1986,** *48* (2), 183-185.

24. Kraft, A.; Grimsdale, A. C.; Holmes, A. B. Electroluminescent Conjugated Polymers - Seeing Polymers in a New Light. *Angewandte Chemie-International Edition* **1998,** *37* (4), 402-428.

25. Shirota, Y.; Kageyama, H. Charge Carrier Transporting Molecular Materials and Their Applications in Devices. *Chemical Reviews* **2007,** *107* (4), 953-1010.

26. Babel, A.; Jenekhe, S. A., High Electron Mobility in Ladder Polymer Field-Effect Transistors. *Journal of the American Chemical Society* **2003,** *125* (45), 13656-13657.

27. Entwistle, C. D.; Marder, T. B., Applications of three-coordinate organoboron compounds and polymers in optoelectronics. *Chemistry of Materials* **2004,** *16* (23), 4574-4585.

28. Burroughes, J. H.; Bradley, D. D. C.; Brown, A. R.; Marks, R. N.; Mackay, K.; Friend, R. H.; Burns, P. L.; Holmes, A. B. Light-Emitting-Diodes Based on Conjugated Polymers. *Nature* **1990,** *347* (6293), 539-541.

29. Forster, T. *Discussions of the Farada Society* **1959,** *27*, 7 - 17.

30. Dexter, D. L., A Theory of Sensitized Luminescence in Solids. *Journal of chemical Physics* **1953,** *21*, 836 - 850.

31. Baldo, M. A.; Thompson, M. E.; Forrest, S. R. Phosphorescent Materials for Application to Organic Light Emitting Devices. *Pure and Applied Chemistry* **1999,** *71* (11), 2095-2106.

32. Kalinowski, J.; Fattori, V.; Cocchi, M.; Williams, J. A. G. Light-Emitting Devices Based on Organometallic Platinum Complexes as Emitters. *Coordination Chemistry Reviews* **2011,** *255* (21-22), 2401-2425.

33. Adachi, C.; Baldo, M. A.; Thompson, M. E.; Forrest, S. R. Nearly 100% Internal Phosphorescence Efficiency in an Organic Light-Emitting Device. *Journal of Applied Physics* **2001,** *90* (10), 5048-5051.

34. Greenham, N. C.; Friend, R. H.; Bradley, D. D. C. Angular-Dependence of the Emission from a Conjugated Polymer Light-Emitting Diode-Implications for Efficiency Calculations. *Advanced Materials* **1994,** *6* (6), 491-494.

35. Palz, W., *Power for the World - The Emergence of Electricity from the Sun*. Pan Stanford Publishing.: Belgium, 2010.

36. April 25, 1954: Bell Labs Demonstrates The First Practical Silicon Solar Cell. *APS News* **April 2009,** *18* (4).

37. Kietzke, T. Recent Advances in Organic Solar Cells. *Advances in OptoElectronics* **2007,** *2007*.

38. Guo, F. Q.; Kim, Y. G.; Reynolds, J. R.; Schanze, K. S. Platinum-Acetylide Polymer Based Solar Cells: Involvement of the Triplet State for Energy Conversion. *Chemical Communications* **2006,** (17), 1887-1889.

39. Wang, Q. W.; Wong, W. Y. New Low-Bandgap Polymetallaynes of Platinum Functionalized with a Triphenylamine-benzothiadiazole Donor-Acceptor Unit for Solar Cell Applications. *Polymer Chemistry* **2011,** *2* (2), 432-440.

40. Chao, Y. H.; Jheng, J. F.; Wu, J. S.; Wu, K. Y.; Peng, H. H.; Tsai, M. C.; Wang, C. L.; Hsiao, Y. N.; Lin, C. Y.; Hsu, C. S. Porphyrin-Incorporated 2D D-A Polymers with Over 8.5% Polymer Solar Cell Efficiency. *Advanced Materials* **2014,** *26* (30), 5205-5210.

41. Wang, P.; Liu, S. J.; Lin, Z. H.; Dong, X. C.; Zhao, Q.; Lin, W. P.; Yi, M. D.; Ye, S. H.; Zhu, C. X.; Huang, W. Design and Synthesis of Conjugated Polymers Containing Pt(II) Complexes in the Side-Chain and Their Application in Polymer Memory Devices. *Journal of Materials Chemistry* **2012,** *22* (19), 9576-9583.

42. Ling, Q. D.; Song, Y.; Teo, E. Y. H.; Lim, S. L.; Zhu, C. X.; Chan, D. S. H.; Kwong, D. L.; Kang, E. T.; Neoh, K. G. WORM-Type Memory Device Based on a Conjugated Copolymer Containing Europium Complex in the Main Chain. *Electrochemical and Solid State Letters* **2006,** *9* (8), G268-G271.

43. Choi, T. L.; Lee, K. H.; Joo, W. J.; Lee, S.; Lee, T. W.; Chae, M. Y. Synthesis and Nonvolatile Memory Behavior of Redox-Active Conjugated Polymer-Containing Ferrocene. *Journal of the American Chemical Society* **2007,** *129* (32), 9842.

44. Cotton, F. A.; Wilkinson, G. *Advanced Inorganic Chemistry*. 5th ed.; WILEY: New York, 1988.

45. Gutlich, P.; Goodwin, H. A., Spin Crossover - An Overall Perspective. *Spin Crossover in Transition Metal Compounds I* **2004,** *233*, 1-47.

46. Lin, W. P.; Liu, S. J.; Gong, T.; Zhao, Q.; Huang, W. Polymer-Based Resistive Memory Materials and Devices. *Advanced Materials* **2014,** *26* (4), 570-606.

47. Smith, R. C.; Tennyson, A. G.; Won, A. C.; Lippard, S. J. Conjugated Metallopolymers for Fluorescent turn-on Detection of Nitric Oxide. *Inorganic Chemistry* **2006,** *45* (23), 9367-9373.

48. Zhu, S. S.; Carroll, P. J.; Swager, T. M. Conducting Polymetallorotaxanes: A Supramolecular Approach to Transition Metal Ion Sensors. *Journal of the American Chemical Society* **1996,** *118* (36), 8713-8714.

49. Shioya, T.; Swager, T. M., A Reversible Resistivity-Based Nitric Oxide Sensor. *Chemical Communications* **2002,** (13), 1364-1365.

50. Holliday, B. J.; Stanford, T. B.; Swager, T. M., Chemoresistive Gas-Phase Nitric Oxide Sensing with Cobalt-Containing Conducting Metallopolymers. *Chemistry of Materials* **2006,** *18* (24), 5649-5651.

51. Edelman, K. R.; Stevenson, K. J.; Holliday, B. J. Conducting Metallopolymers as Precursors to Fabricate Palladium Nanoparticle/Polymer Hybrids for Oxygen Reduction. *Macromolecular Rapid Communications* **2012,** *33* (6-7), 610-615.

52. Kingsborough, R. P.; Swager, T. M. Electrocatalytic Conducting Polymers: Oxygen Reduction by a Polythiophene-Cobalt Salen Hybrid. *Chemistry of Materials* **2000,** *12* (4), 872.

53. Kostas, I. D., Synthesis of New Rhodium Complexes With a Hemilabile Nitrogen-Containing Bis(phosphinite) or Bis(phosphine) Ligand. Application to Hydroformylation of Styrene. *Journal of Organometallic Chemistry* **2001,** *626* (1-2), 221-226.

54. Singleton, J. T., The Uses of Pincer Complexes in Organic Synthesis. *Tetrahedron* **2003,** *59* (11), 1837-1857.

55. Zhao, C. Q.; Jennings, M. C.; Puddephatt, R. J., A Hemilabile Binucleating Pincer Ligand for Self-Assembly of Coordination Oligomers and Polymers. *Dalton Transactions* **2008,** (9), 1243-1250.

56. Adeloye, A. O.; Olomola, T. O.; Adebayo, A. I.; Ajibade, P. A., A High Molar Extinction Coefficient Bisterpyridyl Homoleptic Ru(II) Complex with trans-2-Methyl-2-butenoic Acid Functionality: Potential Dye for Dye-Sensitized Solar Cells. *International Journal of Molecular Sciences* **2012,** *13* (3), 3511-3526.

57. Berces, A., Ligand Effects in the Models and Mimics of Oxyhemocyanin and Oxytyrosinase. A Density Functional Study of Reversible Dioxygen Binding and Reversible O-O Bond Cleavage. *Inorganic Chemistry* **1997,** *36* (21), 4831-4837.

58. Pellei, M.; Papini, G.; Lobbia, G. G.; Santini, C. Chemistry and Relevant Biomimetic Applications of Group 6 Metals Systems Supported by Scorpionates. *Current Bioactive Compounds* **2009,** *5*, 321 - 352.

59. Lee, S. J.; Jung, J. H.; Seo, J.; Yoon, I.; Park, K. M.; Lindoy, L. F.; Lee, S. S. A Chromogenic Macrocycle Exhibiting Cation-Selective and Anion-Controlled Color Change: An approach to Understanding Structure-Color Relationships. *Organic Letters* **2006,** *8* (8), 1641-1643.

60. Milum, K. M.; Kim, Y. N.; Holliday, B. J. Pt- NCN Pincer Conducting Metallopolymers That Display Redox-Attenuated Metal-Ligand Interactions. *Chemistry of Materials* **2010,** *22* (8), 2414-2416.

61. Aguila, D.; Escribano, E.; Speed, S.; Talancon, D.; Yerman, L.; Alvarez, S. Calibrating The Coordination Chemistry Tool Chest: Metrics of Bi- and Tridentate Ligands. *Dalton Transactions* **2009,** (33), 6610-6625.

62. Trofimenko, S. Boron-Pyrazole Chemistry. *Journal of the American Chemical Society* **1966,** *88* (8), 1842 - 1844.

63. Moulton, C. J.; Shaw, B. L. Transition Metal-Carbon Bonds. 42. Complexes of Nickel, Palladium, Platinum, Rhodium and Iridium with Tridentate Ligand 2,6-Bis(di-t-buthylphosphino)methyl-phenyl. *Journal of the Chemical Society-Dalton Transactions* **1976,** (11), 1020-1024.

64. Albrecht, M.; Lindner, M. M. Cleavage of Unreactive Bonds with Pincer Metal Complexes. *Dalton Transactions* **2011,** *40* (35), 8733-8744.

65. Wolf, M. O.; Zhu, Y. B. Electropolymerization of Oligothienylferrocene Complexes. *Advanced Materials* **2000,** *12* (8), 599-601.

66. Zhu, S. S.; Swager, T. M. Design of Conducting Redox Polymers: A Polythiophene-Ru(bipy)$_3^{n+}$ Hybrid Material. *Advanced Materials* **1996,** *8* (6), 497.

67. Zhu, S. S.; Kingsborough, R. P.; Swager, T. M. Conducting Redox Polymers: Investigations of Polythiophene-Ru(bpy)$_3^{n+}$ Hybrid Materials. *Journal of Materials Chemistry* **1999,** *9* (9), 2123-2131.

68. Reddinger, J. L.; Reynolds, J. R. A Novel Polymeric Metallomacrocycle Sensor Capable of Dual-Ion Cocomplexation. *Chemistry of Materials* **1998,** *10* (1), 3-5.

69. Juris, A.; Balzani, V.; Barigelletti, F.; Campagna, S.; Belser, P.; Von Zelewsky, A. Ru(II) Polypyridine Complexes: Photophysics, Photochemistry, Electrochemistry, and Chemiluminescence. *Coordination Chemistry Reviews* **1988,** *84*, 85 - 277.

70. Campagna, S.; Puntoriero, F.; Nastasi, F.; Bergamini, G.; Balzani, V. Photochemistry and Photophysics of Coordination Compounds: Ruthenium. *Photochemistry and Photophysics of Coordination Compounds I* **2007,** *280*, 117-214.

71. Wong, C. T.; Chan, W. K. Yellow Light-Emitting Poly(phenylenevinylene) Incorporated with Pendant Ruthenium Bipyridine and Terpyridine Complexes. *Advanced Materials* **1999,** *11* (6), 455.

72. Chan, W. K. Metal Containing Polymers with Heterocyclic Rigid Main Chains. *Coordination Chemistry Reviews* **2007,** *251* (17-20), 2104-2118.

73. Knapp, R.; Schott, A.; Rehahn, M. A Novel Synthetic Strategy Toward Soluble, Well-Defined Ruthenium(II) Coordination Polymers. *Macromolecules* **1996,** *29* (1), 478-480.

74. Kelch, S.; Rehahn, M. High-Molecular-Weight Ruthenium(II) Coordination Polymers: Synthesis and Solution Properties. *Macromolecules* **1997,** *30* (20), 6185-6193.

75. Ng, P. K.; Gong, X.; Chan, S. H.; Lam, L. S. M.; Chan, W. K. The Role of Ruthenium and Rhenium Diimine Complexes in Conjugated Polymers That Exhibit Interesting Opto-electronic Properties. *Chemistry-a European Journal* **2001,** *7* (20), 4358-4367.

76. Fernandeztrujillo, M. J.; Basallote, M. G.; Valerga, P.; Puerta, M. C.; Hughes, D. L. Displacement of Tetrahydrofuran Ligands by Tripodal Phosphines-Crystal-Structure of $MoCl_3(N(CH_2CH_2PPH_2)_3).C_4H_8O$. *Journal of the Chemical Society-Dalton Transactions* **1991,** (11), 3149-3151.

77. Mendel, R. R.; Bittner, F., Cell Biology of Molybdenum. *Biochimica Et Biophysica Acta-Molecular Cell Research* **2006,** *1763* (7), 621-635.

78. Enemark, J. H.; Cooney, J. J. A. Synthetic Analogues and Reaction Systems Relevant to The Molybdenum and Tungsten Oxotransferases. *Chemical Reviews* **2004,** *104* (2), 1175-1200.

79. Maji, P.; Wang, W.; Greene, A. E.; Gimbert, Y. Studies Directed Toward The Synthesis of Chiral Tungsten and Molybdenum Carbonyl Complexes. *Journal of Organometallic Chemistry* **2008,** *693* (10), 1841-1849.

80. Hii, K. K. M.; Thornton-Pett, M.; Jutand, A.; Tooze, R. P. Syntheses and Properties of Palladium Complexes Containing Phosphorus-Nitrogen-Phosphorus Ligands with a Tunable Hemilabile Site. *Organometallics* **1999,** *18* (10), 1887-1896.

81. Welch, K. D.; Dougherty, W. G.; Kassel, W. S.; DuBois, D. L.; Bullock, R. M. Synthesis, Structures, and Reactions of Manganese Complexes Containing Diphosphine Ligands with Pendant Amines. *Organometallics* **2010,** *29* (20), 4532-4540.

82. Dong, Q.; Rose, M. J.; Wong, W.; Gray, H. B. Dual Coordination Modes of Ethylene-Linked NP2 Ligands in Cobalt(II) and Nickel(II) Iodides. *Inorganic Chemistry* **2011,** *50* (20), 10213-10224.

83. Michos, D.; Luo, X. L.; Crabtree, R. H. Synthesis and Characterization of Some Rhenium Complexes with The New Mixed Phosphorus Nitrogen Donor Ligand $NPH(CH_2CH_2PPH_2)_2$. *Journal of the Chemical Society-Dalton Transactions* **1992,** (10), 1735-1738.

84. Kostas, I. D.; Antonopoulou, G.; Potamitis, C.; Raptopoulou, C. P.; Psycharis, V. Platinum Complexes with A Methoxy-Amino Phosphine or A Nitrogen-Containing Bis(phosphine) Ligand. Synthesis, Characterization and Application to Hydrogenation of Trans-cinnamaldehyde. *Journal Of Organometallic Chemistry* **2017,** *828*, 133-141.

85. Hinrichsen, S.; Schnoor, A.-C.; Grund, K.; Flöser, B.; Schlimm, A.; Näther, C.; Krahmer, J.; Tuczek, F. Molybdenum Dinitrogen Complexes Facially Coordinated by Linear Tridentate PEP Ligands (E = N or P): Impact of The Central E Donor in Trans-Position to N2. *Dalton Transactions* **2016,** *45* (37), 14801-14813.

86. Siclovan, O. P.; Angelici, R. J. Tridentate Ligand Effects on Enthalpies of Protonation of (L-3)$M(CO)_3$ Complexes (M = W, Mo). *Inorganic Chemistry* **1998,** *37* (3), 432-444.

87. Hessler, A.; Kucken, S.; Stelzer, O.; Sheldrick, W. S. Water-Soluble Phosphanes. 7. Synthesis, Coordination Chemistry and Template Reactions of PH-functional Bis(phosphinoethyl)amines. *Journal of Organometallic Chemistry* **1998,** *553* (1-2), 39-52.

88. Ballester, N. M. S.; Elsegood, M. R. J.; Smith, M. B.; Brown, G. M. {N,N-bis(diphenylphosphino)methyl-aniline}tetracarbonylmolybdenum(0). *Acta Cryst. Section E-Structure Reports Online* **2007,** *63*, m719-m721.

89. Sherwood, R.; de Rivera, F. G.; Wan, J. H.; Zhang, Q.; White, A. J. P.; Rossell, O.; Hogarth, G.; Wilton-Ely, J. Multimetallic Complexes Based on a Diphosphine-Dithiocarbamate "Janus" Ligand. *Inorganic Chemistry* **2015,** *54* (9), 4222-4230.

90. Ainscough, E. W.; Brodie, A. M.; Buckley, P. D.; Burrell, A. K.; Kennedy, S. M. F.; Waters, J. M. Synthesis, Structure and Kinetics of Group 6 Metal Carbonyl Complexes Containing A New 'P2N' Mixed Donor Multidentate Ligand. *Journal of the Chemical Society-Dalton Transactions* **2000,** (16), 2663-2671.

91. Kubas, G. J.; Jarvinen, G. D.; Ryan, R. R. Stereochemical and Electronic Control of M-SO_2 Bonding Geometry In D_6 Molybdenum and Tungsten SO_2 Complexes - Novel Eta-1 - Eta-2 SO_2 Linkage Isomerization In $Mo(CO)_2(PPH_3)_2(CNR)(SO_2)$ and Structures of $Mo(CO)_3(P\text{-}I\text{-}PR_3)_2(SO_2)$ and $Mo(CO)_2(PY)(PPh_3)(mu\text{-}SO_2)_2$. *Journal of the American Chemical Society* **1983,** *105* (7), 1883-1891.

92. Finke, R. G.; Gaughan, G.; Pierpont, C.; Noordik, J. H. Heterobimetallic Oxidative Addition of CH_3I to The Polar RH-Mo Bond of $(C_5Me_5)RH(mu\text{-}PMe_2)_2Mo(CO)_4$. *Organometallics* **1983,** *2* (10), 1481-1483.

93. Fischer, E. O.; Wittmann, D.; Himmelreich, D.; Cai, R.; Ackermann, K.; Neugebauer, D. Transition-Metal Carbyne Complexes. 68. Synthesis and Structure of Novel Binuclear Biscarbyne Complexes of Chromium, Molybdenum, and Tungsten with Bridging Phenylthiohalogeno, Arylselenohalogeno, Halogenohalogeno, and Pseudohalogeno Ligands. *Chemische Berichte-Recueil* **1982,** *115* (9), 3152-3166.

94. Mayer, H. A.; Kaska, W. C. Stereochemical Control of Transition-Metal Complexes by Polyphosphine Ligands. *Chemical Reviews* **1994,** *94* (5), 1239-1272.

95. Owens, B. E.; Poli, R.; Rheingold, A. L. Conformational Preferences in 6-Coordinate, Octahedral Complexes of Molybdenum(III)-Synthesis and Structure of $MoX_3(DPPE)L$ X = Cl, Br, I, DPPE = Bis(diphenylphosphino)ethane, L = Tetrahydrofuran, Acetonitrile, Trimethylphosphine. *Inorganic Chemistry* **1989,** *28* (8), 1456-1462.

96. Higashi, T. ABSCOR. Rigaku Corporation: Tokyo, Japan., 2001.

97. Otwinowski, Z.; Minor, W. DENZO-SMN. (1997). Processing of X-ray Diffraction Data Collected in Oscillation Mode. In *Methods in Enzymology*, Carter, C. W. J.; Sweets, R. M., Eds. Academic Press: Vol. 276, pp 307 – 326.

98. Altomare, A.; Burla, M. C.; Camalli, M.; Cascarano, G. L.; Giacovazzo, C.; Guagliardi, A.; Moliterni, A. G. G.; Polidori, G.; Spagna, R., SIR97. A Program For Crystal Structure Solution. *Journal of Applied Crystallography* **1999,** *32*, 115 - 119.

99. Sheldrick, G. M. *SHELX 97, A Software Package For The Solution And Refinement of X-ray Data*, University of Göttingen: Göttingen, Germany, 1997.

100. Cromer, D. T.; Waber, J. T., International Tables for X-Ray Crystallography. Kynoch Press: Birmingham, 1992.

101. Shi, Y. L.; Gao, Y. C.; Shi, Q. Z.; Kershner, D. L.; Basolo, F. Oxygen Atom Transfer-Reactions to Metal-Carbonyls-Kinetics and Mechanism of CO Substitution-Reactions of $Cr(CO)_6$, $Mo(CO)_6$, $W(CO)_6$ In The Presence of $(CH_3)_3NO$. *Organometallics* **1987,** *6* (7), 1528-1531.

102. Blower, P. J.; Jeffery, J. C.; Miller, J. R.; Salek, S. N.; Schmaljohann, D.; Smith, R. J.; Went, M. J. Template Synthesis And Reactions of Tricarbonylmolybdenum Phosphadithiamacrocycle Complexes. *Inorganic Chemistry* **1997,** *36* (8), 1578-1582.

103. Crabtree, R. H. *The Organometallic Chemistry of the Transition Metals*. 3rd ed.; John Wiley and Sons: USA, 2001.

104. Manners, I. *Synthetic Metal-Containing Polymers*. Wiley-VCH: Weinheim, 2004.

105. Miller, T. M.; Ahmed, K. J.; Wrighton, M. S. Complexes of Rhenium Carbonyl Containing Ferrocenyl-Derived Ligands: Tunable Electron Density at Rhenium by Control of the Redox State of the Ferrocenyl Ligand. *Inorganic Chemistry* **1989,** *28*, 2347 - 2355.

106. Poverenov, E.; Gandelman, M.; Shimon, L. J. W.; Rozenberg, H.; Ben-David, Y.; Milstein, D. Pincer "Hemilabile" Effect. PCN Platinum(II) Complexes With Different Amine "Arm Length". *Organometallics* **2005,** *24* (6), 1082-1090.

107. Wolf, M. O.; Wrighton, M. S. Tunable Electron-Density At A Rhenium Carbonyl Complex Coordinated To The Conducting Polymer Poly-5,5'-(2-thienyl)-2,2'-Bithiazole. *Chemistry of Materials* **1994,** *6* (9), 1526-1533.

108. Weinberger, D. A.; Higgins, T. B.; Mirkin, C. A.; Stern, C. L.; Liable-Sands, L. M.; Rheingold, A. L. Terthienyl and Poly-terthienyl Ligands as Redox-Switchable Hemilabile Ligands for Oxidation-State-Dependent Molecular Uptake and Release. *Journal of the American Chemical Society* **2001,** *123* (11), 2503-2516.

109. Angell, S. E.; Rogers, C. W.; Zhang, Y.; Wolf, M. O.; Jones, W. E., Hemilabile Coordination Complexes For Sensing Applications. *Coordination Chemistry Reviews* **2006,** *250* (13-14), 1829-1841.

110. Allgeier, A. M.; Mirkin, C. A. Ligand Design For Electrochemically Controlling Stoichiometric and Catalytic Reactivit of Transition Metals. *Angewandte Chemie-International Edition* **1998,** *37* (7), 894-908.

111. Weinberger, D. A.; Higgins, T. B.; Mirkin, C. A.; Liable-Sands, L. M.; Rheingold, A. L. Terthienyl-Based Redox-Switchable Hemilabile Ligands: Transition Metal Polymeric Complexes with Electrochemically Tunable or Switchable Coordination Environments. *Angewandte Chemie-International Edition* **1999,** *38* (17), 2565-2568.

112. Higgins, T. B.; Mirkin, C. A. Model Coordination Complexes for Designing Poly(terthiophene)/Rh(I) Hybrid Materials with Electrochemically Tunable Reactivities. *Chemistry of Materials* **1998,** *10* (6), 1589-1595.

113. Boruah, J. J.; Kalita, D.; Das, S. P.; Paul, S.; Islam, N. S., Polymer-Anchored Peroxo Compounds of Vanadium(V) and Molybdenum(VI): Synthesis, Stability, and Their Activities with Alkaline Phosphatase and Catalase. *Inorganic Chemistry* **2011,** *50* (17), 8046-8062.

114. Moreno, J.; Iglesias, J.; Meleroa, J. A.; Sherringtonc, D. C. Synthesis and Characterisation of (Hydroxypropyl)-2-aminomethyl-pyridine Containing Hybrid Polymer–silica SBA-15 Materials Supporting Mo(VI) Centres and Their Use as Heterogeneous Catalysts for Oct-1-ene Epoxidation. *Journal of Materials Chemistry* **2011,** *21*, 6725 - 6735.

115. Maurya, M. R.; Kumar, M.; Kumar, U. Polymer-Anchored Vanadium(IV), Molybdenum(VI) and Copper(II) Complexes of Bidentate Ligand as Catalyst for the Liquid Phase Oxidation of Organic Substrates. *Journal of Molecular Catalysis a-Chemical* **2007,** *273* (1-2), 133-143.

116. Dolman, S. J.; Hultzsch, K. C.; Pezet, F.; Teng, X.; Hoveyda, A. H.; Schrock, R. R. Supported Chiral Mo-Based Complexes as Efficient Catalysts for Enantioselective Olefin Metathesis. *Journal of the American Chemical Society* **2004,** *126* (35), 10945-10953.

117. Shultz, G. V.; Zakharov, L. N.; Tyler, D. R., Transition-Metal-Containing Polymers by ADMET: Polymerization of *cis*-$Mo(CO)_4(Ph_2P(CH_2)_3CH{=}CH_2)_2$. *Macromolecules* **2008,** *41* (15), 5555-5558.

118. Chelebaeva, E.; Larionova, J.; Guari, Y.; Ferreira, R. A. S.; Carlos, L. D.; Paz, F. A. A.; Trifonov, A.; Guerin, C. Near-Infrared Luminescent and Magnetic Cyano-Bridged Coordination Polymers $Nd(phen)_n(DMF)_m[M(CN)_8]$ (M = Mo, W). *Inorganic Chemistry* **2011,** *50*, 9924 - 9926.

119. Matsumoto, T.; Chang, H. C.; Kobayashi, A.; Uosaki, K.; Kato, M. Metal-Dependent and Redox-Selective Coordination Behaviors of Metalloligand Mo-V(1,2-benzenedithiolato)(3) (-) with Cu-I/Ag-I Ions. *Inorganic Chemistry* **2011,** *50* (7), 2859-2869.

120. Zhang, J.; Meng, S.; Song, Y.; Zhou, Y.; Cao, Y.; Li, J.; Zhao, H.; Hu, J.; Wu, J.; Humphrey, M. G.; Zhang, C. Syntheses, Structural, Theoretical, and Nonlinear Optical Studies of Non-Interpenetrating Three-Dimensional Nest-Shaped-Cluster [$MoOS_3Cu_3$]-Based Coordination Polymers. *Crystal Growth and Design* **2011,** *11*, 100 - 109.

121. Das, B.; Srilatha, M.; Veeranjaneyulu, B.; Kanth, B. S. Molybdenum- and Tungsten-Based Coordination Polymers as Catalysts for an Efficient and Rapid Synthesis of Hexahydro-5-oxoquinoline-3-carboxylates and 1,4-Dihydropyridine-3,5-dicarboxylates). *Helvetica Chimica Acta* **2011,** *94* (885 - 891).

122. Kim, D. H.; Kang, B. S.; Lim, S. M.; Bark, K.; Kim, B. G.; Shiro, M.; Shim, Y.; Shin, S. C. Polyterthiophene-bearing Pendant Organomolybdenum Complexes: Electropolymerization of Erythro-[$Mo_2(\mu\text{-}C_5H_5)_2(CO)_4\{\mu\text{-}\eta_2\text{:}\eta_2\text{-}C(R)C[C_4HS(C_4H_3S\text{-}2)_2,5]\}$]. *Journal of the Chemical Society, Dalton Transactions* **1998**, 1893 - 1898.

123. Lytwak, L. A.; Stanley, J. M.; Mejia, M. L.; Holliday, B. J. Synthesis, Characterization, and Photophysical Properties of a Thiophene-functionalized Bis(pyrazolyl) Pyridine (BPP) Tricarbonyl Rhenium(I) Complex. *Dalton Transactions* **2010,** *39* (33), 7692-7699.

124. Milum, K. M.; Keskin, S.; Villa, M. I.; Mejia, M. L.; Holliday, B. J. Redox-Mediated Small Molecule Binding in Conducting Metallopolymers. *Abstracts of Papers of the American Chemical Society* **2009,** *238*.

125. *CrystalClear 1.40*, Rigaku Americas Corporation: The Woodlands, TX, 2008.

126. Zhu, S. S.; Swager, T. M., Conducting Polymetallorotaxanes: Metal Ion Mediated Enhancements in Conductivity and Charge Localization. *Journal of the American Chemical Society* **1997,** *119* (51), 12568-12577.

127. ten Brink, G. J.; Vis, J. M.; Arends, I.; Sheldon, R. A., Selenium Catalysed Oxidations with Aqueous Hydrogen Peroxide. Part 3: Oxidation of Carbonyl Compounds Under Mono/bi/triphasic Conditions. *Tetrahedron* **2002,** *58* (20), 3977-3983.

128. Berube, M.; Poirier, D., Synthesis of Simplified Hybrid Inhibitors of Type 1 17 Beta-hydroxysteroid Dehydrogenase via Cross-metathesis and Sonogashira Coupling Reactions. *Organic Letters* **2004,** *6* (18), 3127-3130.

129. Ball, C. R.; Wade, R. Synthesis of N,N-di-(2-chloroethyl)-3,5-$^3H_2$ Aniline of High Specific Activity. *Journal of the Chemical Society C-Organic* **1968,** (11), 1338.

130. Kvarnstrom, C.; Neugebauer, H.; Blomquist, S.; Ahonen, H. J.; Kankare, J.; Ivaska, A. In Situ Spectroelectrochemical Characterization of Poly(3,4-ethylenedioxythiophene). *Electrochimica Acta* **1999,** *44* (16), 2739-2750.

131. Zaban, A.; Zinigrad, E.; Aurbach, D., Impedance Spectroscopy of Li Electrodes .4. A General Simple Model of The Li-Solution Interphase in Polar Aprotic Systems. *Journal of Physical Chemistry* **1996,** *100* (8), 3089-3101.

132. Hilgers, F.; Bruns, W.; Fiedler, J.; Kaim, W., UV-Vis, HZ and EPR Spectroelectrochemical Study of The EC Redox Transition $(PR_3)_n(CO)_3(R'\text{-}pz)M^{+/0}$; M=Mo, W; R'-pz=N-alkylpyrazinium; R=Isopropyl, Cyclohexyl; n=1 or 2. *Journal of Organometallic Chemistry* **1996,** *511* (1-2), 273-280.

133. Castaneda, S. I.; Montero, I.; Ripalda, J. M.; Diaz, N.; Galan, L.; Rueda, F. X-ray Photoelectron Spectroscopy Study of Low-Temperature Molybdenum Oxidation Process. *Journal of Applied Physics* **1999,** *85* (12), 8415-8418.

134. Wang, P. G.; Cai, B. T.; Taniguchi, N. *Nitric Oxide Donors for Pharmaceutical and Biological Applications*. WILEY-VCH Verlag GmbH & Co KGaA: Weinheim, 2005.

135. Broomhead, J. A.; Young, C. G., Tris(2,2'-bipyridine)Ruthenium(II) Dichloride Hexahydrate. *Inorganic Syntheses* **1990,** *28*, 338-340.

136. Brandt, W. W.; Smith, G. F. Polysubstituted 1,10-Phenanthrolines and Bipyridines as Multiple Range Redox Indicators. *Analytical Chemistry* **1949,** *21*.

137. Burstall, F. H., Optical Activity Dependent on Coordinated Bivalent Ruthenium. *Journal of the Chemical Society* **1936**, 173 - 175.

138. Montalti, M.; Cedi, A.; Prodi, L.; Gandolfi, M. T. *Handbook of Photochemistry*. 3rd ed.; CRC press Taylor & Francis Group.: 6000 Broken Sound Prkway NW, Suite 200 Boca Raton FL, 2006.

139. Tokeltak.Ne; Hemingwa.Re; Bard, A. J. Electrogenerated Chemiluminescence .13. Electrochemical and Electrogenerated Chemiluminescence Studies of Ruthenium Chelates. *Journal of the American Chemical Society* **1973,** *95* (20), 6582-6589.

140. Saji, T.; Aoyagui, S. Polarographic Studies on Bipyridine Complexes .1. Correlation Between Reduction Potentials of Iron(II), Rruthenium(II) and Osmium(II) Complexes and Those of Free Ligands. *Journal of Electroanalytical Chemistry* **1975,** *58* (2), 401-410.

141. Vlcek, A. A. Ligand Based Redox Series. *Coordination Chemistry Review* **1982,** *43*, 39.

142. Dearmond, M. K.; Carlin, C. M. Multiple State Emission and Related Phenomena in Transition-Metal Complexes. *Coordination Chemistry Reviews* **1981,** *36* (3), 325-355.

143. Bard, A. J.; Fox, M. A. Artificial Photosynthesis-Solar Splitting of Water to Hydrogen and Oxygen. *Accounts of Chemical Research* **1995,** *28* (3), 141-145.

144. Hara, M.; Waraksa, C. C.; Lean, J. T.; Lewis, B. A.; Mallouk, T. E. Photocatalytic Water Oxidation in a Buffered Tris(2,2'-bipyridyl)ruthenium Complex-Colloidal IrO_2 System". *Journal of Physical Chemistrty* **2000,** *22* (A 104), 5275–5280.

145. Crosby, G. A., Luminescence as a Probe of Excited-State Properties. *Advances in Chemistry Series* **1976,** (150), 149-159.

146. Kober, E. M.; Meyer, T. J. Concerning The Absorption-Spectra of The Ions $M(bpy)_3^{2+}$ (M=Fe,Ru,Os, bpy=2,2'-Bipyridine). *Inorganic Chemistry* **1982,** *21* (11), 3967-3977.

147. Mandal, K.; Pearson, T. D. L.; Krug, W. P.; Demas, J. N. Singlet Energy Transfer from The Charge-Transfer Excited State of Tris(2,2'-bipyridine)ruthenium(II) to Laser Dyes. *Journal of the American Chemican Society* **1983,** *105*, pp 701–707.

148. Watts, R. J. Ruthenium Polypyridyls - A Case-Study. *Journal of Chemical Education* **1983,** *60* (10), 834-842.

149. Kalyanasundaram, K., Photophysics, Photochemistry and Solar-Energy Conversion with Tris(bupyridyl)ruthenium(II) and its Analogs. *Coordination Chemistry Reviews* **1982,** *46* (Oct), 159-244.

150. Seddon, E. A.; Seddon, K. R. *In The Chemistry of Ruthenium*, EIsevier, Amsterdam, 1984.

151. Demas, J. N., Photophysical Pathways in Metal-Complexes. *Journal of Chemical Education* **1983,** *60* (10), 803-808.

152. Fleischauer, P. D.; Fleischauer, P., Photoluminescence of Transition Metal Coordination Compounds. *Chemical Reviews* **1970,** *70* (2), 199.

153. Zhu, X. J.; Holliday, B. J. Electropolymerization of a Ruthenium(II) Bis(pyrazolyl)pyridine Complex to Form a Novel Ru-Containing Conducting Metallopolymer. *Macromolecular Rapid Communications* **2010,** *31* (9-10), 904-909.

154. Hjelm, J.; Handel, R. W.; Hagfeldt, A.; Constable, E. C.; Housecroft, C. E.; Forster, R. J. Conducting Polymers Containing In-Chain Metal Centers: Electropolymerization of Oligothienyl-Substituted {$M(tpy)_2$} Complexes and In Situ Conductivity Studies, M = Os(II), Ru(II). *Inorganic Chemistry* **2005,** *44* (4), 1073-1081.

155. Araki, K.; Endo, H.; Masuda, G.; Ogawa, T. Bridging Nanogap Electrodes by In Situ Electropolymerization of a Bis(terthiophenylphenanthroline)ruthenium Complex. *Chemistry-a European Journal* **2004,** *10* (13), 3331-3340.

156. Hjelm, J.; Constable, E. C.; Figgemeier, E.; Hagfeldt, A.; Handel, R.; Housecroft, C. E.; Mukhtar, E.; Schofield, E. A Rod-Like Polymer Containing {$Ru(terpy)_2$} Units Prepared by Electrochemical Coupling of Pendant Thienyl Moieties. *Chemical Communications* **2002,** (3), 284-285.

157. Jousselme, B.; Blanchard, P.; Ocafrain, M.; Allain, M.; Levillain, E.; Roncali, J. Electrogenerated Poly(thiophenes) Derivatized by Bipyridine Ligands and Metal Complexes. *Journal of Materials Chemistry* **2004,** *14* (3), 421-427.

158. Cameron, C. G.; Pickup, P. G. A Conjugated Polymer/Redox Polymer Hybrid with Electronic Communication Between Metal Centres. *Chemical Communications* **1997,** (3), 303-304.

159. Cameron, C. G.; Pickup, P. G. Electron Transport in a Conjugated Metallopolymer Containing Binuclear Osmium Centers with Strong Electronic Communication. *Journal of the American Chemical Society* **1999,** *121* (33), 7710-7711.

160. Cameron, C. G.; Pittman, T. J.; Pickup, P. G. Electron Transport in Ru and Os Polybenzimidazole-Based Metallopolymers. *Journal of Physical Chemistry B* **2001,** *105* (37), 8838-8844.

161. Cameron, C. G.; Pickup, P. G. Metal-Metal Interactions in a Novel Hybrid Metallopolymer. *Journal of the American Chemical Society* **1999,** *121* (50), 11773-11779.

162. MacLean, B. J.; Pickup, P. G. Electron Transport in Bithiophene-bithiazole Based Metallopolyniers. *Journal of Physical Chemistry B* **2002,** *106* (18), 4658-4662.

163. Peng, Z. H.; Yu, L. P. Synthesis of Conjugated Polymers Containing Ionic Transition Metal Complexes. *Journal of the American Chemical Society* **1996,** *118* (15), 3777-3778.

164. Peng, Z. H.; Gharavi, A. R.; Yu, L. P. Synthesis and Characterization of Photorefractive Polymers Containing Transition Metal Complexes as Photosensitizer. *Journal of the American Chemical Society* **1997,** *119* (20), 4622-4632.

165. Halcrow, M. A. The Synthesis and Coordination Chemistry of 2,6-Bis(pyrazolyl)pyridines and Related Ligands - Versatile Terpyridine Analogues. *Coordination Chemistry Reviews* **2005,** *249* (24), 2880-2908.

166. Jameson, D. L.; Goldsby, K. A. 2,6-BIS(N-pyrazolyl)pyridines-The Convenient Synthesis of a Family of Planar Tridentate N_3 Ligands that are Terpyridine Analogs. *Journal of Organic Chemistry* **1990,** *55* (17), 4992-4994.

167. Zoppellaro, G.; Baumgarten, M., One-Step Synthesis of Symmetrically Substituted 2,6-Bis(pyrazol-1-yl)pyridine Systems. *European Journal of Organic Chemistry* **2005,** (14), 2888-2892.

168. Stanley, J. M.; Zhu, X.; Yang, X.; Holliday, B. J. Europium Complexes of a Novel Ethylenedioxythiophene-Derivatized Bis(pyrazolyl)pyridine Ligand Exhibiting Efficient Lanthanide Sensitization. *Inorganic Chemistry* **2010,** *49* (5), 2035-2037.

169. Pavlishchuk, V. V.; Addison, A. W. Conversion Constants for Redox Potentials Measured versus Different Reference Electrodes in Acetonitrile Solutions at 25 °C. *Inorganica Chimica Acta* **2000,** *298* (1), 97-102.

170. Nakaramu, K. Synthesis, Luminescence Quantum Yields, and Lifetimes of Trischelated Ruthenium(II) Mixed-ligand Complexes Including 3,3′-Dimethyl-2,2′-bipyridyl. *Bulletin of the Chemical Society of Japan* **1982,** *55*, 2697-2705.

171. Armaroli, N.; Decola, L.; Balzani, V.; Sauvage, J. P.; Dietrichbuchecker, C. O.; Kern, J. M. Absorption and Luminescence Properties of 1,10-Phenanthroline, 2,9-Diphenyl-1,10-phenanthroline, 2,9-dianysil-1,10-phenanthroline and Their Protonated Forms in Dichloromethane Solution. *Journal of the Chemical Society-Faraday Transactions* **1992,** *88* (4), 553-556.

172. Bartecki, A.; Szoke, J.; Varsanyi, G.; Vizesy, M. *Absorption Spectra In The Ultraviolet And Visible Region*. Academic Press Inc.: New York, 1961; Vol. 2.

173. Stanley, J. M.; Chan, C. K.; Yang, X.; Jones, R. A.; Holliday, B. J. Synthesis, X-ray Crystal Structure and Photophysical Properties of Tris(dibenzoylmethanido)(1,10-phenanthroline)samarium(III). *Polyhedron* **2010,** *29* (12), 2511-2515.

174. De Silva, C. R.; Wang, R. Y.; Zheng, Z. P. Highly Luminescent Eu(III) Complexes with 2,4,6-Tri(2-pyridyl)-1,3,5-triazine Ligand: Synthesis, Structural Characterization, and Photoluminescence Studies. *Polyhedron* **2006,** *25* (17), 3449-3455.

175. Chen, X. Y.; Yang, X.; Holliday, B. J. Photoluminescent Europium-Containing Inner Sphere Conducting Metallopolymer. *Journal of the American Chemical Society* **2008,** *130* (5), 1546.

176. Crosby, G. A.; Elfring, W. H. Excited-States of Mixed-Ligand Chelates of Ruthenium(II) and Rhodium(III). *Journal of Physical Chemistry* **1976,** *80* (20), 2206-2211.

177. Rusak, D. A.; James, W. H.; Ferzola, M. J.; Stefanski, M. J. Investigation of Fluorescence Lifetime Quenching of $Ru(bpy)_3^{2+}$ by Oxygen Using a Pulsed Light-Emitting Diode. *Journal of Chemical Education* **2006,** *83* (12), 1857-1859.

178. Kretschmer, C. B.; Nowakowska, J.; Wiebe, R. Solubility of Oxygen and Nitrogen in Organic Solvents from -25 to 50 °C. *Industrial and Engineering Chemistry* **1946,** *38* (5), 506 - 509.

179. Farley, S. J.; Rochester, D. L.; Thompson, A. L.; Howard, J. A. K.; Williams, J. A. G. Controlling Emission Energy, Self-Quenching, and Excimer Formation in Highly Luminescent N Boolean and C Boolean and N-coordinated Platinum(II) Complexes. *Inorganic Chemistry* **2005,** *44* (26), 9690-9703.

180. Sacconi, L.; Morassi, R. 5-Coordination with Hybrid Ligands. 4. Cobalt(2) and Nickel(2) Complexes with Terdentate Ligands Containing Phosphorous and Nitrogen or Sulphur as Donor Atoms. *Journal of the Chemical Society a -Inorganic Physical Theoretical* **1968,** (12), 2997.

181. Morassi, R.; Sacconi, L. 5-Coordination with Hybrid Ligands. 6. Cobalt(II) and Nickel(II) Complexes with a Quadridentate Tripod Ligand Having a NOPP Donor Set. *Journal of the Chemical Society a -Inorganic Physical Theoretical* **1971,** (3), 492.

182. Garcia-Seijo, M. I.; Habtemariam, A.; Fernandez-Anca, D.; Parsons, S.; Garcia-Fernandez, M. E. Synthesis, Characterization, and Reactivity of Cationic Palladium(II) and Platinum(II) Iodo Complexes Containing a Linear or a Tripodal Aminophosphine. The X-ray Crystal Structures of $Pd\{HN(CH_2CH_2PPh_2)_2\}I$ I and $Pd\text{-}3\{N(CH_2CH_2PPh_2)_3\}_2I\text{-}4$ I-2. *Zeitschrift Fur Anorganische Und Allgemeine Chemie* **2002,** *628* (5), 1075-1084.

183. Janosi, L.; Kegl, T.; Hajba, L.; Berente, Z.; Kollar, L. Platinum Complexes of (R)-N,N-bis(2-(diphenylphosphino)ethyl)-1-phenyl-ethylamine: Their Synthesis and Characterisation. *Inorganica Chimica Acta* **2001,** *316* (1-2), 135-139.

184. Khan, M. M. T.; Paul, P.; Venkatasubramanian, K.; Purohit, S. Synthesis and Characterization of Dinuclear Cu(I) Complexes with 2 Bimetallic Hexadentate Ligands Having N_2P_4 Donor Sites - Crystal-Structure of Cu_2(BDPE)C_2.2DMF. *Inorganica Chimica Acta* **1991,** *183* (2), 229-237.

185. Muller, T. E.; Berger, M.; Grosche, M.; Herdtweck, E.; Schmidtchen, F. P. Palladium-Catalyzed Cyclization of 6-aminohex-1-yne. *Organometallics* **2001,** *20* (21), 4384-4393.

186. Liang, L. C., Metal Complexes of Chelating Diarylamido Phosphine Ligands. *Coordination Chemistry Reviews* **2006,** *250* (9-10), 1152-1177.

187. Zhang, J.-F.; Fu, W.-F.; Ganb, X.; Chenb, J.-H. Synthesis, Structures and Photophysical Properties of Luminescent Copper(I) and Platinum(II) Complexes with a Flexible Naphthyridine-Phosphine Ligand. *Dalton Transactions* **2008**, 3093–3100.

188. Yam, V. W. W.; Fung, W. K. M.; Wong, M. T. Synthesis, Photophysics, Electrochemistry, and Excited-state Redox Properties of Trinuclear Copper(I) Acetylides with Bis(diphenylphosphino)alkylamines and -Arylamines as Bridging Ligands. *Organometallics* **1997,** *16* (8), 1772-1778.

189. Harkins, S. B.; Peters, J. C. A Highly Emissive Cu_2N_2 Diamond Core Complex Supported by a PNP (-) Ligand. *Journal of the American Chemical Society* **2005,** *127* (7), 2030-2031.

190. Catalano, V. J.; Kar, H. M.; Bennett, B. L. Gold(I) and Silver(I) Metallocryptates Based on 2,9-Bis(diphenylphosphino)-1,8-naphthyridine. *Inorganic Chemistry* **2000,** *39* (1), 121-127.

191. Jin, Q.-H.; Cui, L.-N.; Li, Z.-F.; Jiang, Y.-H.; Wu, M.-H.; Gao, S.; Zhang, C.-L., Four Mono-/bi-nuclear Palladium(II) Complexes of Triphenylphosphine and Heterocyclic-N/NS Ligands: Synthesis, Structural Characterization and Luminescence Properties. *Polyhedron* **2012**, 472 - 477.

192. Kato, M. Luminescent Platinum Complexes Having Sensing Functionalities. *Bulletin of the Chemical Society of Japan* **2007,** *80* (2), 287-294.

193. Ramamurthy, V.; Schanze, K. Z. *Multimetallic and Macromolecular Inorganic Photochemistry*. M Dekker: New York, 1999.

194. Yam, V. W.-W.; Lo, K. K.-W.; Fung, W. K.-M.; Wang, C.-R., Design of Luminescent Polynuclear Copper(I) and Silver(I) Complexes with Chalcogenides and Acetylides as the Bridging Ligands. *Coordination Chemistry Reviews* **1998,** *171*, 17 - 41.

195. Ajjou, A. N.; Alper, H. A New, Efficient, and In Some Cases Highly Regioselective Water-Soluble Polymer Rhodium Catalyst for Olefin Hydroformylation. *Journal of the American Chemical Society* **1998,** *120* (7), 1466-1468.

196. Bianchini, C.; Farnetti, E.; Glendenning, L.; Graziani, M.; Nardin, G.; Peruzzini, M.; Rocchini, E.; Zanobini, F. Synthesis of the New Chiral Amonidiphosphine Ligands (R)-(alpha-methylbenzyl)bis(2-(diphenylphosphino)ethyl)amine and (S)-(alpha-methylbenzyl)bis(2-(diphenylphosphino)ethyl)amine and Their Use in the Enantioselective Reduction of Alpha,beta-unsaturated Ketones to Allylic Alcohols by Iridium Catalysis. *Organometallics* **1995,** *14* (3), 1489-1502.

197. Nuzzo, R. G.; Haynie, S. L.; Wilson, M. E.; Whitesides, G. M. Synthesis of Functional Chelating Diphosphines Containing the Bis 2-(diphenylphosphino)ethyl amino Moiety and the Use of These Materials in the Preparation of Water-Soluble Diphosphine Complexes of Transition-Metals. *Journal of Organic Chemistry* **1981,** *46* (14), 2861-2867.

198. *Inorganic Syntheses*. 1984; Vol. 26, p 345 - 346.

199. *Inorganic Syntheses*. 1990; Vol. 28, p 60 - 63.

200. Keskin, S. G.; Stanley, J. M.; Mejia, M. L.; Holliday, B. J. {N,N-bis2-(diphenylphosphanyl)ethyl-aniline}(eta$_2$-dibenzylideneacetone)palladium(0). *Acta Cryst. Section E-Structure Reports Online* **2011,** *67*, M1327-U248.

201. Besenyei, G.; Szalontai, G.; Parkanyi, L. Synthesis and Structure of Dinuclear Silver Complexes of N,N-bis(2-(diphenylphosphanyl)ethyl)phenylamine *Polyhedron* **2017,** *127*, 97-106.

202. Effendy; Nicola, C. D.; Fianchini, M.; Pettinari, C. S., Brian W.; Somers, N.; White, A. H. The Structural Definition of Adducts of Stoichiometry MX:dppx (1:1) M=CuI, AgI, X=simple anion, dppx=$Ph_2P(CH_2)_xPPh_2$, x=3–6. *Inorganica Chimica Acta* **2005,** *358*, 763-795.

203. Retboll, M. K.; Wenger, E.; Willis, A. C. A Palladium(0) Complex of Dibenzylideneacetone and a Chelating Diphosphine. *Acta Crystallographica Section E-Structure Reports Online* **2002,** *58*, M275-M277.

204. Goddard, R.; Hopp, G.; Jolly, P. W.; Kruger, C.; Mynott, R.; Wirtz, C. The Palladium-Catalyzed Intramolecular Cyclization of Alkadienyl-Substituted 1,3-Diketones. *Journal of Organometallic Chemistry* **1995,** *486* (1-2), 163-170.

205. Liang, L. C.; Lin, J. M.; Lee, W. Y., Benzene C-H Activation by Platinum(II) Complexes of Bis(2-diphenylphosphinophenyl)amide. *Chemical Communications* **2005,** (19), 2462-2464.

206. Di Nicola, C.; Effendy; Pettinari, C.; Skelton, B. W.; Somers, N.; White, A. H. The Structural Definition of Adducts of Stoichiometry AgX : dppf (1 : 1)((n)), X=Simple Anion, Dppf=Bis(diphenylphosphino)ferrocene. *Inorganica Chimica Acta* **2005,** *358* (3), 695-706.

207. Bowmaker, G. A.; Effendy; Hanna, J. V.; Healy, P. C.; King, S. P.; Pettinari, C.; Skelton, B. W.; White, A. H. Solution and Mechanochemical Syntheses, and Spectroscopic and Structural Studies in the Silver(I) (Bi-)carbonate: Triphenylphosphine System. *Dalton Transactions* **2011,** *40* (27), 7210-7218.

208. Mitchell, L. A.; Mejía, M. L.; Keskin, S. G.; Holliday, B. J. 5-Phenyl-1,2,5-di-thia-zepane. *Acta Crystallographica Section E-Structure Reports Online* **2014**, *70 (pt3)*, o285.

209. Keskin, G. S.; Stanley, J. M.; Cowley, A. H. Synthesis, Characterization and Theoretical Investigations of Molybdenum Carbonyl Complexes with Phosphorus/Nitrogen/Phosphorus Ligand as Bidentate and Tridentate Modes. *Polyhedron* **2017,** *138*, 206-217.